Adaptive Baseband Processing Techniques for Cognitive Radio Systems

Adaptive Baseband Processing Techniques for Cognitive Radio Systems

PROEFSCHRIFT

Ter verkrijging van de graad van doctor
Aan de Technische Universiteit Delft,
Op gezag van de Rector Magnificus Prof. Dr. Ir. J. T. Fokkema,
Voorzitter van het College voor Promoties,
In het openbaar te verdedigen op dinsdag 1 December 2009 om 12.30 uur
door

Ibrahim BUDIARJO

Master of Science in Communications Engineering
Technische Universitaet Muenchen, Duitsland

geboren te Bandung, Jawa Barat, Indonesien.

Dit proefschrift is goedgekeurd door de promotor :

Prof. dr. ir. L. P. Ligthart

Copromotor :

Dr. H. Nikookar

Samenstelling promotiecommissie:

Rector Magnificus	voorzitter
Prof. dr. ir. L. P. Ligthart	Technische Universiteit Delft, promotor
Dr. H. Nikookar	Technische Universiteit Delft, copromotor
Prof. dr. R. Prasad	Aalborg Universitet
Prof. dr. ir. E. R. Fledderus	Technische universiteit Eindhoven
Prof. dr. ir. I. G. M. M. Niemegeers	Technische Universiteit Delft
Prof. dr. ir. S. M. Heemstra De Groot	Technische Universiteit Delft
Prof. dr. ir. W. C. van Etten	Universiteit Twente

This research has been supported by the AAF project in the framework of the Freeband programme sponsored by the Dutch Ministry of Economic Affairs.
Work presented in this thesis has been performed at the International Research Centre for Telecommunications and Radar of Delft University of Technology

Copyright © 2009 by Ibrahim Budiarjo

All rights reserved. No part of the material protected by this copyright notice may be reproduced or utilized in any form or by any means, electronic or mechanical, including photocopying, recording or by any information storage and retrieval system, without the prior permission of the author.

Cover: The illustration of cognitivity with the brain that has the learning capability, collecting and analyzing information i.e. link budget, spectrum occupancy, radio propagation and the target QoS to decide the proper radio parameter values to be used by the Cognitive Radio system. The background is an example of a view from a terminal, and taken from the pictures collection of Apple Macbook.

ISBN 978-90-9024753-3

Printed in The Netherlands

To the memory of My Father, and to My Mother, Brother and My Fiancee

Thesis Summary

Adaptive Baseband Processing Techniques for Cognitive Radio Systems

Cognitive Radio is a new paradigm in the wireless communications. It puts the intelligence and awareness dimension to the radio communication system. A Cognitive Radio system will be aware of the changing condition in its environment. The awareness in this thesis is related to the spectrum and the channel stipulation. By intelligent learning and understanding from the environment, a Cognitive Radio device will adapt its transmission parameters to the changing environment. The objective of a Cognitive Radio system is to have a reliable communication and efficient spectrum utilization.

Although most of the spectral ranges are already licensed, studies and measurements have shown that most of the time the spectrum is not fully occupied, and even some bands are rarely occupied. The congestions happen because of the existing poor spectrum access technique. This condition raises the opportunity to rent or to access the spectrum while the licensed user is in idle condition or by having the Cognitive Radio side by side with the licensed users band occupying the spectrum holes. In this way, the spectrum is utilized in a more efficient way. The challenging problem is to settle a “win-win” co-existence between the Cognitive Radio, which is the rental system, with the legacy licensed system. Spectrum pooling has been proposed in the literature as a technique of sharing the spectrum with the licensed system by using the Orthogonal Frequency Division Multiplexing (OFDM) as modulation technique. Some of the OFDM carriers located in the licensed user’s band will be deactivated in order not to interfere the legacy system access. Due to this flexibility, the OFDM is considered as a proper modulation technique to be applied to a Cognitive Radio system. Deactivation of more carriers adjacent to the licensed user’s band, as well as windowing and several signal processing techniques could reduce the interference contribution of the OFDM based Cognitive Radio system to the licensed users signal. These techniques are studied and presented in this dissertation. The spectrum pooling technique could only work upon the reception of the accurate spectrum occupancy information. The spectrum occupancy information is derived from a spectrum sensing module. Spectrum sensing necessitates such a sophisticated module and requires a proper attention. This thesis does not focus on the spectrum sensing module, but rather it is assumed that the spectrum

occupancy information is available and accurate. The work on spectrum sensing is conducted by out partner at the Twente University*.

Following the objective of Cognitive Radio to have reliable communications, the observation or emphasis of the technique is not only on the licensed users side but also on the rental user. Besides assuring the reliable communications of the licensed system, the target Quality of Service (QoS) of the Cognitive Radio system should be attained. The practical parameters to be observed are the Bit Error Rate (BER) and the bit rate of the system. The application of OFDM with spectrum shaping for the purpose of reducing the interference contribution to the licensed system can be achieved with the cost of self QoS degradation. Results from literature have shown that application of adaptive bit loading could enhance the BER of an OFDM system. By adaptive bit loading, the bits are allocated to each of the OFDM carrier intelligently according to the channel condition by setting the target BER and bit rate of the overall system. In this work, we propose to combine the adaptive bit loading with the spectrum shaping to preserve the Cognitive Radio system's QoS. The impact of this combination on the OFDM Peak to Average Power Ratio (PAPR) growth is evaluated through simulations.

There is a growing interest in replacing the Fourier transform in OFDM with wavelet basis functions. The technique is termed as the Wavelet Packet Multicarrier Modulation (WPMCM). Investigations reported in literature have presented the evaluation of WPMCM and compared the results with OFDM. Following the successful application of a frequency selective wavelet in the Ultra Wide Band system, in this dissertation we evaluate the suitability of the frequency selective wavelet in WPMCM combined with the spectrum pooling concept to be applied to the Cognitive Radio system. As the efficient spectrum utilization is one of the major objectives of Cognitive Radio, it is reasonable to include Multiple Input Multiple Output (MIMO) to the Cogntive Radio system. This subject is studied in this thesis and the performance of MIMO in the OFDM and WPMCM based Cogntive Radio system is evaluated.

Channel estimation is the crucial module in every OFDM system. We propose an effective channel estimation scheme based on optimum pilot patterns of conventional OFDM using virtual pilots and apply it to Cognitive Radio systems. The virtual pilots are derived from the combination of the linear interpolation/extrapolation between two real pilots with the so called decision directed method. Without loss of generality we use the Wiener filter as the channel estimation technique due to its efficient and straightforward method in utilizing the channel correlation property according to the distance between pilots and data. First we adopt the Single Input Single Output (SISO) OFDM based Cognitive Radio system, and then we expand the scheme to the MIMO application.

* This thesis is part of the Work Package 3 (WP3) Dutch Adaptive Adhoc Freeband (AAF) project. The WP3 will produce 3 PhD theses, one on Spectrum Sensing, one on Baseband Processing (this thesis) and the third one is on the mapping of the Spectrum Sensing and Baseband Processing into a heterogeneous architecture.

Beside OFDM and WPMCM based Cognitive Radio system, recently Transform Domain Communication System (TDCS) and Wavelet Domain Communication System (WDCS) have been introduced as promising modulation techniques for Cognitive Radio application. TDCS and WDCS have bit rate limitations. As an effort to enhance the bit rate of TDCS and WDCS, we propose to add an extra embedded symbol to TDCS and WDCS. We analyze the impact of the embedded symbol on the conventional TDCS and WDCS data detection. The impact of the embedded symbol on the data detection in a multi-user environment, which is inherently supported by the conventional TDCS and WDCS, is observed. In addition, we also evaluate the performance of the TDCS with an embedded symbol in the MIMO system.

As a sort of verification platform for Cognitive Radio we proposed a practical Demonstrator that involved a spectrum scanning module and baseband processing transceiver module. The spectrum sensing is employed by the Universal Software Defined Radio Peripheral (USRP) while the baseband processing transceiver module is applied to an FPGA Development board. The current made Cognitive Radio verification platform is simple and still has a limited feature. While further developments are required in this field, details of this effort are also provided in this thesis.

Contents

Thesis Summary **i**

1 Introduction **1**

1.1 Research Background 1
1.2 Research Motivation 3
1.3 Scope and Novelties of the Dissertation 4
1.4 Outline of the Thesis 4

2 OFDM Based Cognitive Radio **7**

2.1 Introduction 7
2.2 Spectrum Pooling with OFDM 10
2.3 OFDM Sidelobes Reduction Techniques 16
2.3.1 Sidelobe Suppression by Cancellation Carriers Insertion 16
2.3.2 Sidelobe Suppression by Subcarrier Weighting 18
2.3.3 Sidelobe Suppression by Multiple Choice Sequence 18
2.3.4 Sidelobe Suppression by Adaptive Symbol Transition 19
2.3.5 Sidelobe Suppression by Frequency Domain Additive Signal 20
2.3.6 Sidelobe Suppression by Constellation Expansion 21
2.4 Frequency Hopping 22
2.4.1 Evaluation Using GSM 900 MHz Channel Model 22
2.5 Conclusions 24

3 Baseband Processing for OFDM Based Cognitive Radio **25**

3.1 Introduction 25
3.2 Combined Spectrum Pooling, Windowing, Adaptive Bit Loading and Sidelobes Cancellation Carriers 26
3.2.1 Modulation Detection by Signaling and Blind Detection 28
3.2.2 Adaptive Bit Loading 32
3.2.2.1 Chow Algorithm 33
3.2.2.2 Fischer Huber Algorithm 33
3.2.2.3 Simple Blockwise Loading Algorithm (SBLA) 35
3.2.2.4 Subband Bit Loading based on Fischer-Huber Algorithm 37
3.2.3 Spectrum Pooling and Sidelobes Cancellation Carriers Insertions 37
3.2.4 Combined Adaptive Bit Loading with Spectrum Pooling and Sidelobes Cancellation Carriers Simulation Results and Analysis 41
3.3 Wavelet Packet Modulation by Frequency Selective Wavelet for Cognitive Radio 49
3.3.1 Generation of Wavelet Packet Sub-Carriers Bases 51

3.3.2 Generation of Wavelet Packet Dual Bases 53
3.3.3 Design of Best Wavelet Packet Bases for WP-MCM 54
3.3.3.1 Paraunitary Condition 54
3.3.3.2 Compact Support 55
3.3.3.3 Regularity 55
3.3.4 Wavelet Families 56
3.3.4.1 Daubechies 56
3.3.4.2 Coiflet 56
3.3.4.3 Symlet 56
3.3.4.4 Frequency Selective Wavelet 56
3.3.5 Performance Evaluation and Analysis 62
3.4 Conclusions 75

4. Channel Estimation for OFDM Based Cognitive Radio 77

4.1 Introduction 77
4.2 Wiener Filter Channel Estimation 78
4.3 Pilot Pattern for Frequency Hopping OFDM Based Cognitive Radio 84
4.4 Combined Optimum Pilot Pattern and Virtual Pilots for OFDM Based Cognitive Radio 88
4.4.1 Performance Evaluation and Analysis 96
4.5 MIMO OFDM Based Cognitive Radio Optimum Pilot Pattern with Virtual Pilots Concept 106
4.5.1 Performance Evaluation and Analysis 114
4.6 Training and Pilot Pattern for OFDM Based Cognitive Radio Synchronization and PAPR Reduction 124
4.6.1 Synchronization for OFDM Based Cognitive Radio System 124
4.6.2 Peak to Average Power Ratio Reduction for OFDM Based Cognitive Radio Channel Estimation 126
4.7 Conclusions 127

5. Single Carrier Cognitive Radio System 129

5.1 Introduction 129
5.2 Transform Domain Communication System (TDCS) with Embedded Symbol 130
5.2.1 Multi User TDCS with Extra Embedded Symbol Detection Analysis 137
5.3 Wavelet Domain Communication System (WDCS) with Embedded Symbol 140
5.4 MIMO Application to Single Carrier Cognitive Radio System 142
5.5 Performance Evaluation and Analysis 145
5.5.1 TDCS Evaluation 145
5.5.2 WDCS Evaluation 157
5.6 Conclusions 159

6. AAF Project Cognitive Radio Demonstrator in IRCTR TU Delft 161

6.1 Introduction 161
6.2 The Hardware Requirements for Baseband Transmission 162

6.3 Spectrum Scanner Module 169
6.4 Cognitive Radio Nodes Demonstrator Design 170
6.5 Conclusions 179

7. Conclusions and Recommendations 181

7.1 Conclusions 181
7.2 Recommendations for Future Work 185

Appendix A - OFDM based Cognitive Radio Frame Design for Frequency Hopping Scenario 187

Appendix B – Training Symbol Repetition Period Mathematical Proof by Zeros Insertion 190

Appendix C - Single User CCSK Detection in TDCS with Embedded Symbol 192

Appendix D - The Power to Mean Sidelobe Power Ratio (PMR) of TDCS basis function 193

Appendix E – Multi User CCSK Detection in TDCS with Embedded Symbol 195

Appendix F – V-BLAST Algorithm 197

Appendix G – Future Work in Wavelet Packet Multicarrier Modulation Based Cognitive Radio 199

Bibliography 201

List of Abbreviations 212

List of Symbols 214

Publications by the Author 216

Samenvatting 221

Acknowledgements 225

Curriculum Vitae 227

Chapter 1

Introduction

1.1 Research Background

The growing demand on wireless communications systems to provide high data rates and the introduction of new communication applications, e.g. Long Term Evaluation (LTE), IEEE 802.11N and the Ultra Wide Band standard have made the spectrum become congested. This condition has brought the need for a flexible and efficient use of the spectrum resource. The regional spectrum allocation policy counteracts the free mobility of radio communication equipment. The vast majority of the available spectral resources have already been licensed, so it appears that there is little or no room to add any new services, unless some of the existing licenses are discontinued. The old spectrum licensing policies need therefore to be revised. New spectral ranges that are suitable for future radio transmission remain interesting to be made available to the public even if spectrum parts are already licensed.

Furthermore, recent studies and measurements have shown that vast portions of the licensed spectra are rarely used, and congestions often happen due to inflexible spectrum utilization and regulations instead of the non availability of the spectrum.

In order to utilize the unused spectrum efficiently in dynamically changing environments, a new communication technique is required. It should adapt to the rapidly changing environment condition while coexist with the existing legacy systems by ensuring minimal or tolerable interference to the legacy user's communication. This technology is named as Cognitive Radio. The idea of Cognitive Radio has been initially introduced by Joseph Mitola in his Doctoral Thesis [1]. Mitola described how a Cognitive Radio could enhance the flexibility of wireless services through a radio knowledge representation language. This concept was further expanded in Mitola's dissertation.

Simon Haykin gave in his paper [2] the solid definition of Cognitive Radio as an intelligent wireless communication system that is aware of its surrounding environment (i.e., outside world), and uses the methodology of understanding-by-building to learn form the environment and adapt its internal states to statistical variations in the incoming radio frequency (RF) stimuli by making corresponding changes in certain operating parameters (e.g., transmit-power, carrier-frequency, and modulation strategy) in real-time, with primary

objectives of highly reliable communications and efficient utilization of the radio spectrum. This definition delivers six keywords related to Cognitive Radio, they are : awareness, intelligence, learning, adaptivity, reliability, and efficiency. Fette in [3] relates the awareness scope of a Cognitive Radio system to the transmitted waveform, radio frequency (RF) spectrum, communication network, geography, locally available services, user needs, situation and security policy. In adition to the previoiusly mentioned capabilities, the Cognitive Radio is equipped with reconfigurability. The reconfigurability provides the adaptation of the radio interface to accommodate variations in the development of new interface standards, incorporation of new applications, services, and updates in software technology, and exploitation of flexible heterogeneous services provided by radio networks [4]. The term cognition itself includes language and communication aspects [5]. The Cognitive Radio's language includes the set of signs and symbols that permits different internal constituents of the radio to communicate with each other [2], [5]. In summary the main Cognitive Radio tasks include :

- radio-scene analysis which encompasses estimation of interference impact from temperature of the radio environment and detection of spectrum holes.
- channel identification which encloses the channel state information (CSI) estimation and channel capacity prediction for use at the transmitter site.
- Transmit power control and dynamic spectrum management.

By including the interaction with RF environment then three tasks can be distinguished and form a cognitive cycle as depicted in Figure 1.1 [6]. The radio scene analysis will receive stimuli from the radio environment and further identify the spectrum holes and CSI.

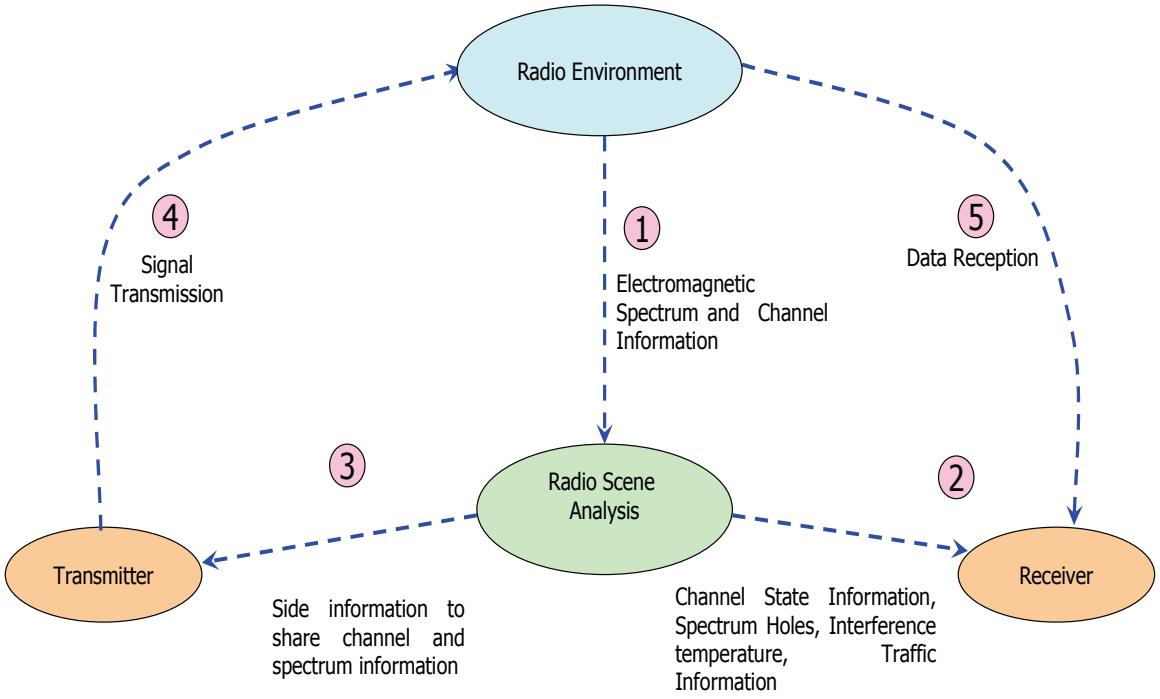

Figure 1.1: Cognitive Radio signal transmission cycle [6]

In the radio scene analysis block the spectrum and channel information will be evaluated (line (1) in Figure 1.1) , the analysis will be distributed to the Transmitter and Receiver (lines (2) and (3)) and accordingly the Transmitter and Receiver will decide their transmission and reception technique in interaction with the environment condition (line(4) and (5)).

In this dissertation the scope of "cognition" is limited to have the co-existence between the Cognitive Radio based rental (unlicensed) users (RUs) and the licensed users (LUs) by means of reducing the mutual interference between them, while obtaining reliable communications for RUs. The spectrum owners who are the LUs allow portions of their spectrum to be utilized for certain periods of time by RUs which apply the Cognitive Radio system in their transmissions. The underlying mechanism is based on utilizing the actual spectrum occupancy condition knowing that the allocated spectrum is not occupied most of the time. In fact, some portions of the spectrum are rarely used [7]. The LUs are ordinary mobile terminals and their associated base stations. They do not possess much intelligence. The RUs, on the other hand, should possess the intelligence to sense the spectrum and use whatever resources are available when they need them. At the same time, the RUs should adjust its spectrum usage when an LU begins transmission. The RU access should be done in such a way that the neighboring LUs will not be aware of the RU existence.

1.2 Research Motivation

As one of the Cognitive Radio objectives is to obtain efficient utilization of the radio spectrum, and the focus of our Adaptive Ad-hoc Freeband (AAF) project is on identification of free resources in the frequency domain, we limit our observation to the spectrum. The scope of the spectrum utilization is focused on the co-existence between the Cognitive Radio based RUs and the legacy LUs. Successful co-existence between RU access and the neighboring LUs can be accomplished by assuring that the neighboring LUs will not be interrupted or intervened when a RU wants to get an access to the spectrum hole adjacent to the LU's band. This stringent requirement can be technically interpreted as an overlay demand within an opportunistic RU access mode. The part of the RU spectral energy which is located at the neighboring occupied LU band should therefore be as low as possible. It must not interrupt the LU transmission. The mutual interference between the RU and LU should also be reduced. The mutual interference reduction is a way of preserving reliable communications for both users. This shaping can be interpreted as sidelobe suppression technique in frequency domain.

In the RU perspective reliable communications is not connected to an interference avoidance aspect, but also to the quality of service in terms of target bit rate and maximum allowable bit error rate (BER). Due to priority onLU access, the RU resources will be limited and may still affect the LU achievable bitrate, meaning that this resource limitation could also have impact on the LU BER performance.

For these reasons, we investigated some novel baseband signal processing techniques for Cognitive Radio system to suppress the LU sidelobes, to increase the LU bit rate that subsequently enhance the spectral utilization efficiency, to counteract fading of the channel to improve the system BER and to handle the OFDM challenges (e.g peak to average power ratio (PAPR) and synchronization) in the application of a Cognitive Radio system.

Further, the goal of our AAF project i.e., research and demonstration of a Cognitive Radio system, which continuously adapts its communications scheme to the available resources, will be incorporated in this thesis by describing our development of the Cognitive Radio baseband processing and the AAF demonstrator platform.

1.3 Scope and Novelties of this Dissertation

In correspondence to the motivation of the research, the following novelties and primary results are delivered in this thesis :

- Non Contiguous Orthogonal Frequency Division Multiplexing (NC-OFDM) is considered as a feasible modulation technique to be applied in Cognitive Radio systems. A problem arises if the non contiguity delivers inadequate target quality of service (QoS) e.g. bit rate. Frequency hopping is then considered as an alternative. The system will hop to a frequency range that could provide the Cognitive Radio with the desired QoS. With respect to this issue this dissertation contributes to an OFDM based Cognitive Radio frame design with full active carriers according to the Bluetooth time division duplex (TDD) for frequent frequency hopping in the 900 MHz channel model (Chapter 2, Section 2.4).
- A combination of spectrum pooling, windowing, adaptive bit loading and sidelobes cancellation carriers is proposed. Spectrum pooling, windowing and sidelobes cancellation carriers are incorporated for the purpose of sidelobes reduction (mutual interference reduction between RUs and LUs). Adaptive bit loading is applied to preserve the Cognitive Radio based RUs target bit rate and BER (Chapter 3, Section 3.2).
- Signal spectrum shaping by a frequency selective wavelet in multicarrier wavelet packet modulation and a single carrier wavelet domain communication system (WDCS) is introduced (Chapter 3, Section 3.3 and Chapter 5, Section 5.3).
- An optimum pilot allocation strategy for OFDM based Cognitive Radio channel estimation has been worked out. For that purpose the virtual pilot concept is set up in order to simplify the filtering process in the channel estimation (Chapter 4). Their application in MIMO system is also evaluated.
- Use of an embedded symbol for higher rate single carrier transform domain communication system (TDCS) and WDCS based Cognitive Radio is motivated. Results have shown that by increasing the constellation size of the embedded symbol, the TDCS signal to noise ratio (SNR) per bit will increase and further will enhance the legacy data source detection from the cyclic code shift keying data mapping (Chapter 5, Section 5.2).

1.4 Outline of the Thesis

The organization of this thesis is as follows :

Chapter 2 provides the insight into the modulation techniques feasible for the Cognitive Radio system. The spectrum can be accessed in overlay mode or underlay mode. In overlay mode the signal power is above the noise level while in underlay mode the condition is opposite. OFDM is the proper multicarrier modulation mode for overlay spectrum access Cognitive Radio system, while TDCS is the single carrier approach. The underlay spectrum access Cognitive Radio system can be applied in systems using the Ultra Wideband Technique. Due to its higher rate and better performance, the OFDM flexibility and the various degrees of freedom in modifying its parameters to achieve the successful coexistence between the RU, which is a Cognitive Radio system and the LU, several OFDM based Cognitive Radio modulation techniques are analyzed and discussed in this chapter. As several techniques in suppressing mutual interference between RU and LU are introduced in this chapter, we come up with the idea to combine some of the available mutual interference suppression techniques to get lower sidelobes (as low as possible), and present them in chapter 3.

Chapter 3 introduces the novel combination of spectrum pooling, windowing, adaptive bit loading and sidelobes cancellation carriers to be applied in an OFDM based Cognitive Radio system for the purpose of attaining significant mutual interference reduction between RU and LU while the target quality of service is maintained. An alternative approach by replacing the Fourier-based transformation in OFDM with wavelet packet modulation has been investigated. The optimization problem and its use in the Cognitive Radio application are described. As in this chapter OFDM is considered as the promising modulation technique for the Cognitive Radio system, the critical component in OFDM, which is the channel estimation, should be observed in the cognitive radio context. This issue is studied in the following chapter.

Chapter 4 proposes a novel pilot allocation technique for OFDM-based Cognitive Radio channel estimation as an effort to counteract the channel fading to obtain a reliable quality of communications. Pilot patterns that can cope with the LU existence are suggested in this chapter. The virtual pilot concept is utilized to aid the channel estimation process. Further, the application is examined in a MIMO system. The MIMO OFDM based Cognitive Radio performance evaluation through simulations reveals its higher BER gain compared to the application of adaptive bit loading into the SISO OFDM based Cognitive Radio system. Training and pilot designs to resolve other common challenges like synchronization and high peak to average power ratio in the context of Cognitive Radio are drawn. The multicarrier modulation for Cognitive Radio and its critical component have been discussed in this and the two previous chapters. The single carrier modulation approach can also

be used for Cognitive Radio. Therefore, in the following chapter the single carrier technique is discussed and an optimization technique to this approach is explained.

Chapter 5 describes the efforts in optimizing and enhancing the utilization of the single carrier modulation termed as TDCS for the Cognitive Radio system. The novel contribution of the chapter is the application of an embedded symbol to the single carrier TDCS based Cognitive Radio system. The embedded symbol adds extra transmitted source bits that can be used as an extra data or side information. Further, its impact to the sister technique WDCS and their extended application in a MIMO system are evaluated. The baseband processing for Cognitive Radio has been discussed and described in chapters 2 till 5. As the implementation aspect of algorithms is also important, in chapter 6 the implementation efforts of the developed baseband processing in a demonstrator platform will be described.

Chapter 6 deals with the implementation of the Cognitive Radio baseband processing into a demonstrator platform which includes control programming of the field programmable gate array (FPGA) on the selected evaluation board P25M[*] and universal software radio platform (USRP[†]) .

Chapter 7 summarizes all main results of the thesis, draws overall conclusions and gives some recommendations for future work.

[*] P25M is a development board produced by Innovative Integration equipped with FPGA and DSP module, 4 channels 25 MSamples/sec A/D and 4 channels 50 MSamples/sec D/A.
(http://www.innovative-dsp.com/products.php?product=P25M)

[†] USRP is a software radio device with low capacity FPGA and 4 input and 4 output channels; it is controlled by a computer through the USB connection.(http://www.ettus.com)

Chapter 2

OFDM Based Cognitive Radio

2.1 Introduction

In this thesis we assume that the spectrum can be accessed in overlay mode or underlay mode. In overlay mode the signal power is above the noise level while in underlay mode the signal power will be below the noise level. In the context of Cognitive Radio the overlay mode spectrum access is applied side by side (adjacent) to the legacy system, utilizing a spectrum hole. In underlay mode the signal will overlap with the legacy system, therefore the technique should be robust to interference by removing the impact of the legacy system signal from the own signal in order to detect its own signal correctly. Ultra Wide Band is a suitable technique for underlay spectrum access [8]. Ultra Wide Band is a good technique for short range high rate and long range low rate communications. In our AAF project we consider long range and high rate communications; therefore the overlay access mode is the preferable option.

In the overlay mode Orthogonal Frequency Division Multiplexing (OFDM) is considered as the proper multicarrier modulation technique, and the Transform Domain Communications System (TDCS) as the single carrier modulation suitable for Cognitive Radio systems. The reason is that both OFDM and TDCS have the capability in notching a part of their spectrum energy located at the LU band in order to guarantee the co-existence with the legacy LU. TDCS has been initially introduced in [9]. TDCS relies on the cross correlation property of its basis function in detecting its transmitted data. OFDM provides a higher rate and a better performance compared to the TDCS, while TDCS gives simplicity in shaping its spectrum energy.

In this chapter we focus our attention on OFDM, while TDCS will be presented in detail in chapter 5, where we discuss its performance and compare it with the OFDM.

Orthogonal frequency division multiplexing (OFDM) is a multicarrier modulation technique that splits its total transmit bandwidth into a number of orthogonal subcarriers such that each subcarrier can transmit independent data from each other. The subcarriers orthogonality is attained by setting the frequency spacing between two carriers equal to the inverse of its symbol duration. As the number of subcarriers increases for a certain fixed bandwidth the symbol duration increases. In this way, a high rate data stream is divided into a number of

lower data streams. Due to the long symbol duration, the inter symbol interference (ISI) impact from the multipath delay channel is reduced. Further, the insertion of a guard interval (GI) at the beginning of each OFDM symbol will remove the ISI impact completely, as long as the GI duration is longer than the maximum multipath delay [10].

A simple common OFDM scheme is depicted in Figure 2.1, while the OFDM subsystem with the spectrum sensing module is in Figure 2.2.

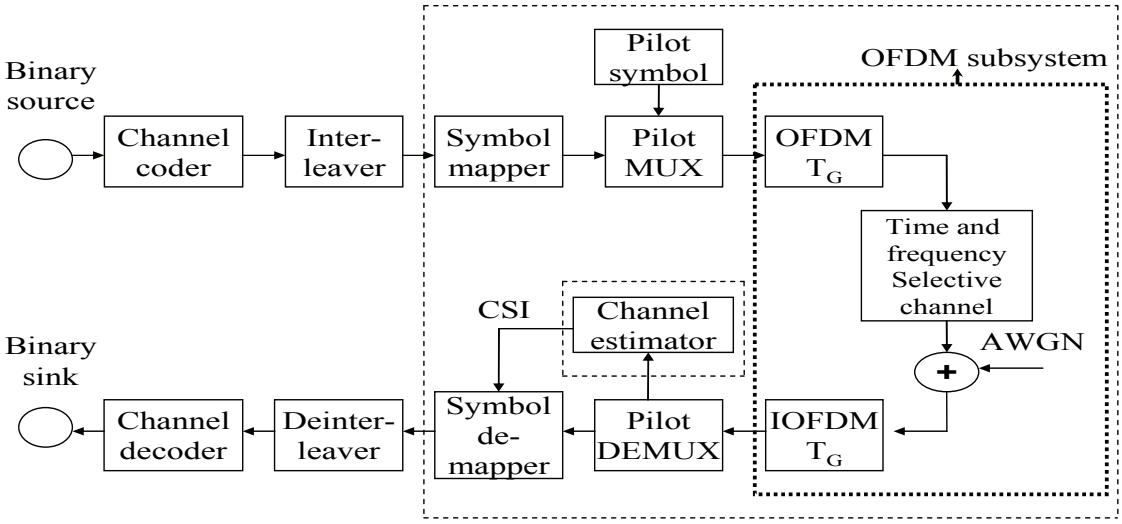

Figure 2.1 : OFDM system model

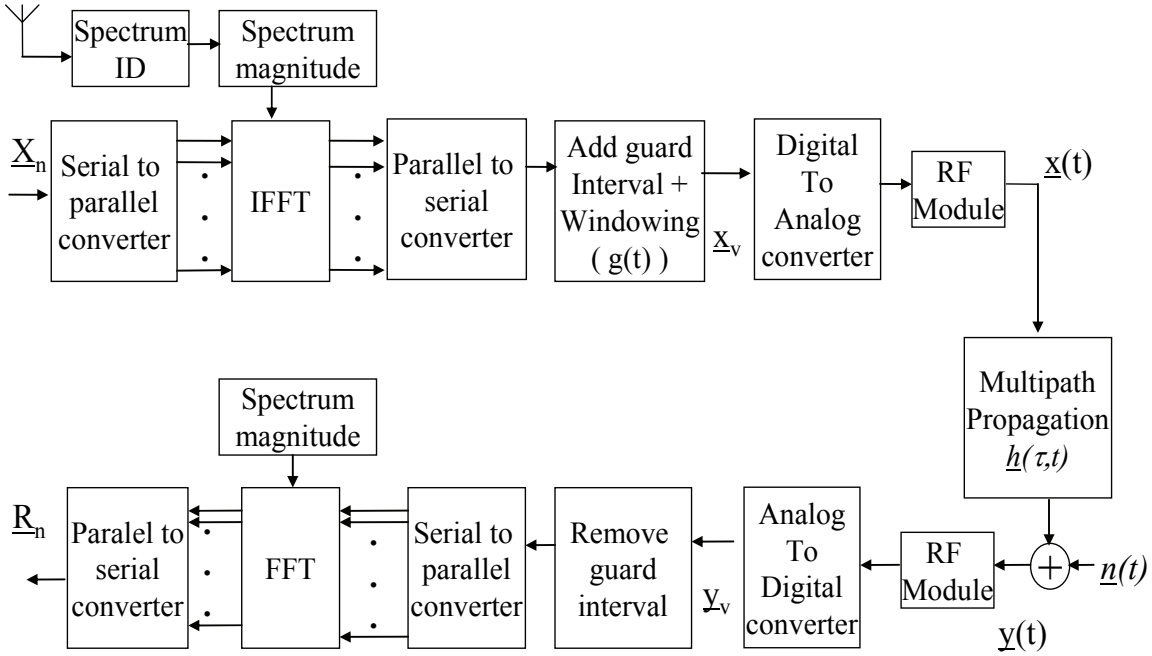

Figure 2.2 : OFDM subsystem description with spectrum sensing module

In the scope of cognitive radio for assuring the co-existence between the RU and LU , the feasibility of OFDM in achieving this cognitive radio goal can be observed from its power spectral density (PSD) equation :

$$\left|X(f)\right|^2 = \frac{1}{N_{FFT}} \left| \sum_{n=1}^{N_{FFT}} \sqrt{p_n} X_n \int_{-(1+\alpha)T_u}^{(1+\alpha)T_u} g(t) e^{-j2\pi(f - f_n)t} dt \right|^2 \qquad (2.1)$$

$$\text{subject to} \quad \left|X(f_{LU})\right|^2 < P_{Threshold} \quad , \quad \text{and} \quad \sum_{n=1}^{N_{FFT}} p_n = P_T$$

where $X(f)$ is the OFDM spectrum, N_{FFT} is the number of FFT points which refers to the possible number of total subcarriers, X_n and p_n are the modulated data and the allocated power on carrier n respectively, $g(t)$ is the window function, α is the window roll off factor, and T_u is the useful OFDM symbol duration. f_n is the frequency of carrier n, and P_T is the total transmitted power, f_{LU} is a frequency within the LU band, and $P_{Threshold}$ is the level of interference power that is still tolerable by the LU.

In order to allow a RU to co-exist with LU, its PSD at the location of any frequency of the LU should be zero or negligible. The direct interpretation of this statement would be de-activating of subcarriers at those frequency locations of the LUs. This technique is known as *Spectrum Pooling* [11]. The details about this technique will be explained in the following section. The coexistence effort will depend on the spectrum information accuracy provided by the spectrum sensing module. Another advantage of OFDM is the use of an FFT module that can also be utilized in sensing the spectrum.

Spectrum sensing is another critical research issue and requires a proper attention. In this dissertation we will not explore the techniques applied in spectrum scanner module. This topic is investigated in detail separately by another PhD candidate in our AAF project. We assume that the spectrum information is available and accurately estimated. A special approach is required to gather spectrum information from all available cognitive radio devices in order to have a really accurate spectrum occupancy information. This is especially the case when the LU's geographical position is close to one RU so that the LU is easily detected by the corresponding RU. In case the LU is far from the other RUs, those RUs would probably not detect the LU presence. The simple approach could then be applying the logical 'OR' operation to the spectrum information vector of all RU transceivers. In our AAF project the spectrum info is planned to be distributed to all RU (Cognitive Radio) transceivers through a dedicated control channel. Research has been conducted on use of the Ultra Wide Band technology as a possible technique for applying such a common control channel [12].

Although the subcarriers of the OFDM based Cognitive Radio located in the LU band are de-activated, due to the OFDM window properties, part of its spectrum, which is termed as sidelobes, will be smeared into the LU band. This is the reason why the term $P_{Threshold}$ is included in (2.1), as a reference for the cognitive radio system designer in shaping the

spectrum of the RU signal in such a way that the part of its spectrum in the LU band is considered to be negligible.

The PSD equation described in eq. (2.1) shows that the OFDM side-lobe power is determined by the allocated power on each subcarrier, the constellation size of X_n, the composition of the X_n values, the window roll off factor α, and the window form $g(t)$. The larger the X_n constellation size, the higher the possibility of large side-lobe power occurrence. A large side-lobe refers to a higher interference to the licensed system.

Another aspect that determines the side-lobe amplitude is the distance between the arbitrary frequency point f in the LU band and the carrier position f_n. The side-lobe of the carriers adjacent to the LU band has a major role in interfering the LU. De-activating some of these carriers will lower the side-lobe magnitude. In the application of adaptive bit loading, the constellation size of carriers especially the ones close to the LU band should be taken into account in such a way that the $|X(f_{LU})|^2$ be constrained to a threshold $P_{Threshold}$.

In the following sections some available techniques in reducing the OFDM sidelobes for cognitive radio application will get attention. The sidelobe reduction outcome of all techniques can be explained by relating them to eq. (2.1).

A novel research output with respect to OFDM based cognitive radio subject will be given in Section 2.4 of this chapter, where hopping is applied to the cognitive radio system in case the number of available carriers for cognitive radio transmission is not sufficient to attain the target BER and bit rate. For the purpose of the hopping, the OFDM frame will be designed according to the Bluetooth time division duplex (TDD) frame since Bluetooth also uses this hopping mechanism for its transmission.

2.2 Spectrum Pooling with OFDM

Spectrum pooling has been proposed in [12] and [13] as a strategy where public access is enabled to these bands without giving significant interference to the actual license owners. Spectrum pooling enables public access to spectral ranges of licensed frequency bands which are seldom used by overlaying a secondary rental user (RU) to an existing licensed user (LU). The LUs are radio systems authenticated to operate under licensed spectral bands. The RUs are intelligent CR systems that actively scan the landscape of frequency usage and opportunistically utilize the available and unused resources. The RU relinquishes control over the resources (here spectrum) as and when the LU starts using them. To identify and utilize the unused bands, the frequency bands of various radio systems (including licensed and rental users) are combined to obtain a common spectral pool. Cohabitation of LU and RU systems is actualized by shaping the transmission waveform of the RU in a way that it utilizes the unoccupied time-frequency gaps of the LU.

The pioneering work on the subject was conducted by Jondral et al [12] who devised a spectrum pooling scheme using multi-carrier modulation (MCM). According to this scheme

the individual OFDM sub-carriers occupied by the LU and adjacent to LU are de-activated. Figure 2.3 illustrates a typical scenario of spectrum pooling.

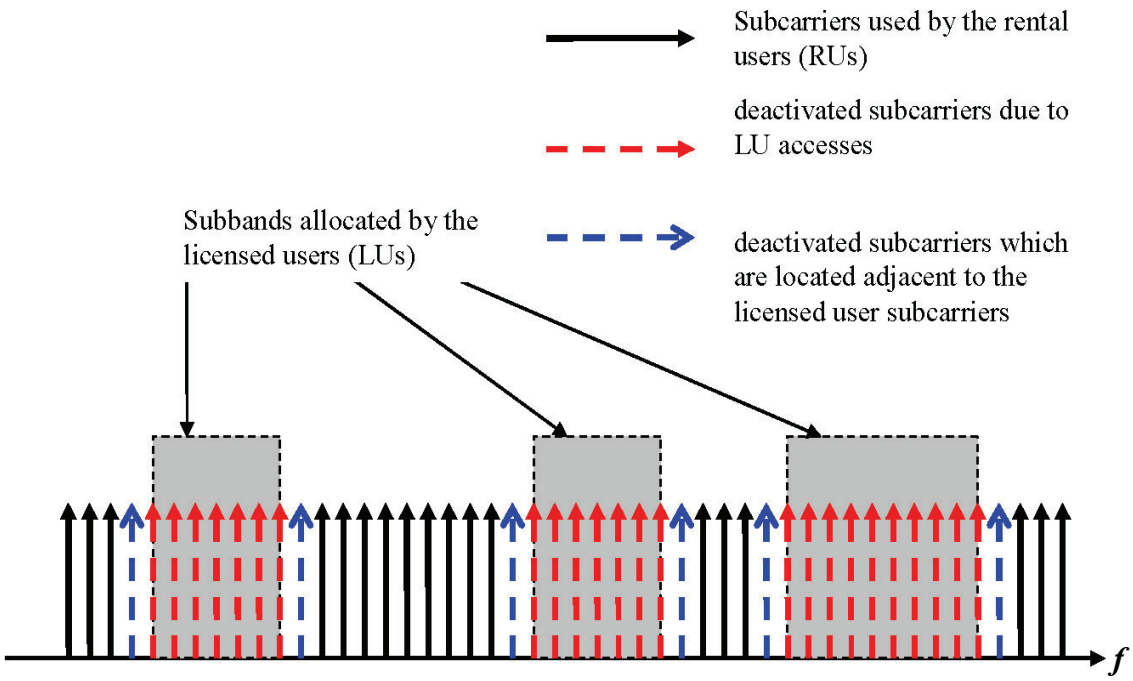

Figure 2.3 : Illustration of spectrum pooling block diagram

Further, in [12] and [13] the extension of each OFDM block with long cyclic prefix and suffix samples and the application of some windowing to reduce the side-lobes of the subcarrier channels is proposed. Obviously, this solution occurs at the expense of bandwidth loss because an excessive time has to be allocated to cyclic extensions which otherwise could be used for data transmission. The interference reduction method is extended by combining the windowing technique with de-activating of subcarriers located adjacent to the LU's band which provides a kind of shield to the LUs. One commonly used window is the raised cosine window [12],

$$g(t)=\begin{cases}\dfrac{1}{T_u} & 0\le|t|\le\dfrac{T_u(1-\alpha)}{2}\\ \dfrac{1}{2T_u}\left\{1+\cos\left[\dfrac{\pi}{\alpha T_u}\left(|t|-\dfrac{T_u(1-\alpha)}{2}\right)\right]\right\} & \dfrac{T_u(1-\alpha)}{2}\le|t|\le\dfrac{T_u(1+\alpha)}{2}\\ 0 & \text{Otherwise}\end{cases} \tag{2.2}$$

where $g(t)$ is the window function, α is the roll-off factor, and T_u is the useful OFDM symbol interval (without guard interval). The sketches of the raised cosine window with different

values of roll off factor (α) are depicted in Figure 2.4, while the spectra of an OFDM carrier with the respective windows are given in Figure 2.5. Increasing the α will reduce the sidelobes with the expense of longer symbol duration.

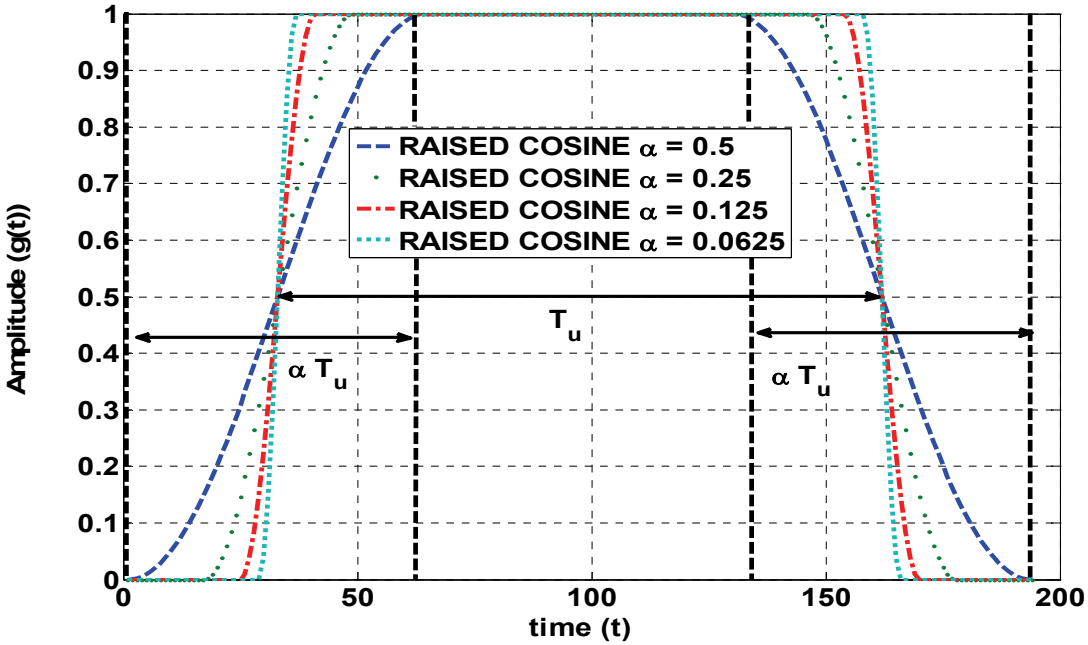

Figure 2.4: Raised cosine window with different roll-off factor (α)

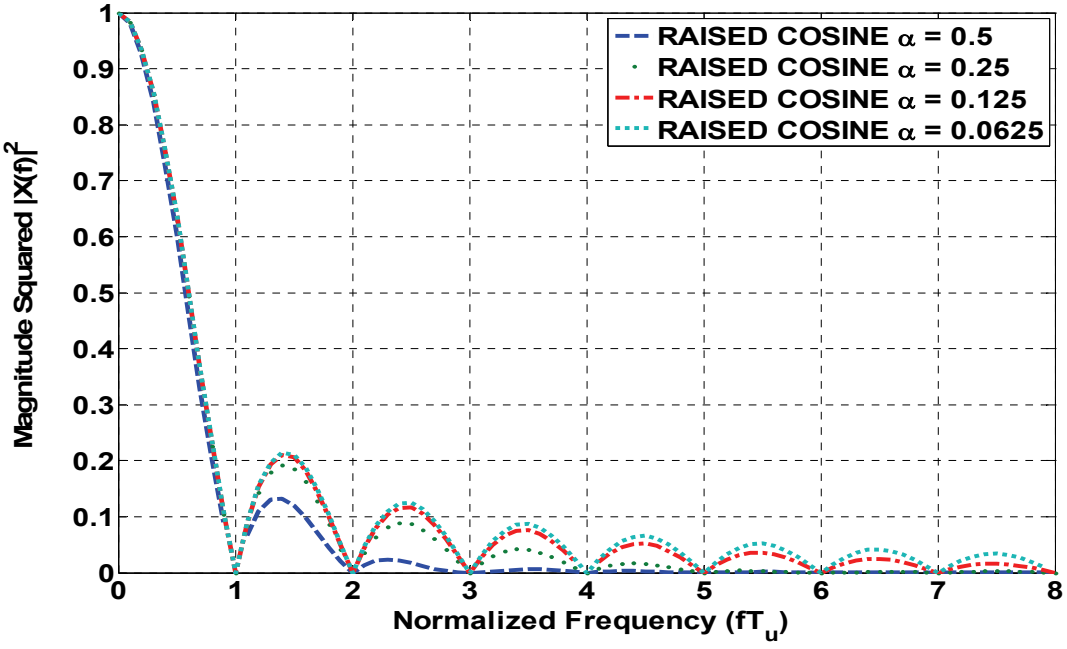

Figure 2.5: OFDM carrier spectrum with raised cosine window with different roll-off factor (α)

Other available forms are Bartlett [14],

$$g(t)=\begin{cases}\dfrac{1}{T_u}, & 0\le|t|\le\dfrac{T_u(1-\alpha)}{2}\\ \dfrac{1}{2T_u}-\dfrac{1}{T_u}\left[\dfrac{|t|}{\alpha T_u}-\dfrac{1}{2\alpha}\right], & \dfrac{T_u(1-\alpha)}{2}\le|t|\le\dfrac{T_u(1+\alpha)}{2}\\ 0 & \text{Otherwise}\end{cases} \tag{2.3}$$

Better than Raised Cosine (BTRC) [15],

$$g(t)=\begin{cases}\dfrac{1}{T_u}, & 0\le|t|\le\dfrac{T_u(1-\alpha)}{2}\\ \dfrac{1}{T_u}e^{\left(-2\ln 2/\alpha T_U\right)\left[|t|-(T_U(1-\alpha)/2)\right]}, & \dfrac{T_u(1-\alpha)}{2}\le|t|\le\dfrac{T_u}{2}\\ \dfrac{1}{T_u}\left[1-e^{\left(\frac{-2\ln 2}{\alpha T_u}\right)\left[\frac{T_u(1-\alpha)}{2}-|t|\right]}\right], & \dfrac{T_u}{2}\le|t|\le\dfrac{T_u(1+\alpha)}{2}\\ 0 & \text{Otherwise}\end{cases} \tag{2.4}$$

and Flipped Inverse Hyperbolic Secant (farchsech) [16] window,

$$g(t)=\begin{cases}\dfrac{1}{T_u}, & 0\le|t|\le\dfrac{T_u(1-\alpha)}{2}\\ \dfrac{1}{T_u}\left[1-\dfrac{1}{\alpha T_u\gamma}\operatorname{arcsech}\left(\dfrac{1}{\alpha T_u}\left(\dfrac{T_u(1+\alpha)}{2}-|t|\right)\right)\right], & \dfrac{T_u(1-\alpha)}{2}\le|t|\le\dfrac{T_u}{2}\\ \dfrac{1}{T_u}\left[\dfrac{1}{\alpha T_u\gamma}\operatorname{arcsech}\left(\dfrac{1}{\alpha T_u}\left(|t|-\dfrac{T_u(1-\alpha)}{2}\right)\right)\right], & \dfrac{T_u}{2}\le|t|\le\dfrac{T_u(1+\alpha)}{2}\\ 0 & \text{Otherwise}\end{cases} \tag{2.5}$$

where $\gamma=2\ln(\sqrt{3}+2)/(\alpha T_u)$. The shape of the window in the region of $\frac{T_u(1-\alpha)}{2}\le|t|\le\frac{T_u(1+\alpha)}{2}$ determines how rapidly the OFDM spectrum falls to zero. The PSD will hit zero on the frequencies in the interval of *1/ T_u*. From these windows we learn that the farchsech window provides the lowest sidelobes (Figure 2.6). The Figures show the window forms including their respective spectrum on an OFDM carrier.

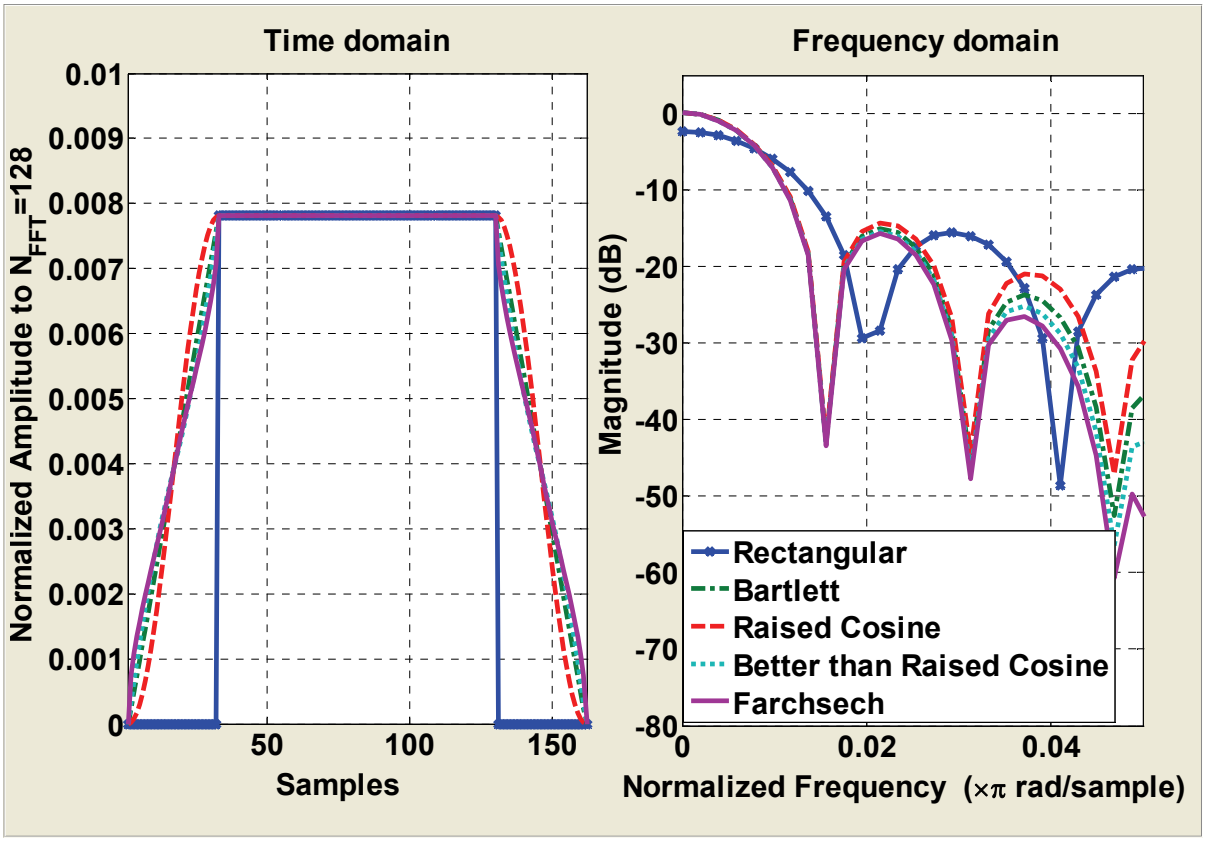

Figure 2.6: The sketches of different windows with their respective spectrum

According to [17] the duration of the OFDM signal should be $2T_u$ in order to complete a total of $2N_{FFT}$ samples to preserve the orthogonality, and zeros are added in the region outside the window $g(t)$. If the duration of the OFDM signal is only T_u $(1+\alpha)$ then the window will affect the transmitted signal, and as a consequence an error floor will be formed. Figure 2.7(a) shows an example of a Bartlett window with an OFDM signal duration $T_u(1+\alpha)$ which affects the transmitted signal. To avoid the error floor, the applied window must not influence the signal during its effective period [18]. To fulfill this requirement, the window forms are expanded, so that the new T_u becomes $2T_u$, and α is restricted in the range of $0 \le \alpha \le \frac{\left(1-\frac{T_{GI}}{T_u}\right)}{2}$, where T_{GI} is the guard interval duration. The orthogonality is preserved since the PSD hits zeros in the $1/(2T_u)$ interval at the expense of a longer duration of the OFDM signal $(2T_u(\alpha+1))$. The solution is that the window is truncated to fit the $2T_u$ OFDM duration, as depicted in Figure 2.7(b) [6]. The orthogonality is preserved by applying the rectangular receiver filter with T_u duration, that is implemented by the DFT [18]. In this way, there is more freedom to shape the window in the $T_u(1-\alpha) \le |t| \le T_u$ region as long as its PSD at the symbol boundaries remains low, e.g Gaussian window or half sine window [19].

By referring to eq. (2.1) the de-activating carriers adjacent to the licensed band will provide flexible guard bands that will make the PSD sidelobes of the RU's OFDM signal at the licensed band lower. In OFDM bits errors are typically concentrated in a set of severely faded subcarriers. This is due to the channel propagation condition. For this reason, it is possible that the quality of service may not be maintained. Meanwhile, the carriers resource is limited due to de-activation of the RU carriers. Furthermore, the long OFDM symbol duration due to the windowing reduces the OFDM transmission bit rate. Having adaptive OFDM in CR is thus a solution. The heavily faded and noisy subcarriers are excluded from transmission to improve the overall bit error rate (BER) of the system, and the loss of throughput is counteracted by applying higher order modulation modes to the subcarriers which have better signal to noise ratios (SNR) or BER.

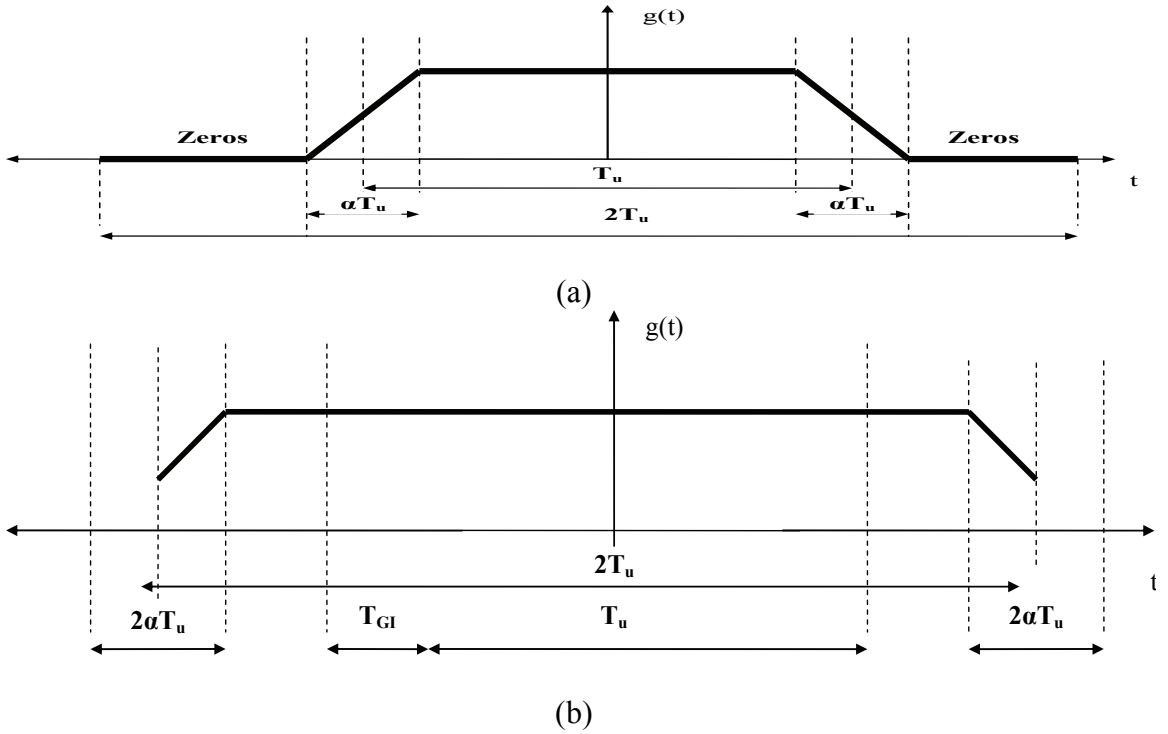

Figure 2.7: (a) Window design influencing the transmitted signal (b) Window design not influencing the transmitted signal [6]

Recently in [20] overlapped OFDM symbol transmission with long symbol duration (known as offset OFDM) has been introduced to counteract the throughput loss. The scheme is described in Figure 2.8. The delay between one OFDM symbol and another is designed in such a way that no inter symbol interference occurs, which means that the next OFDM symbol should start after the end of the useful data part of the previous OFDM symbol. If zeros are inserted at the prefix and suffix points (outside the T_{GI} and T_U area in Figure 2.7(b)), the useful data of the next OFDM symbol should start after the last useful data of the previous OFDM symbol. With this technique the accumulated symbol duration will be shorter compared to non offset OFDM, hence, the bit rate loss can be reduced.

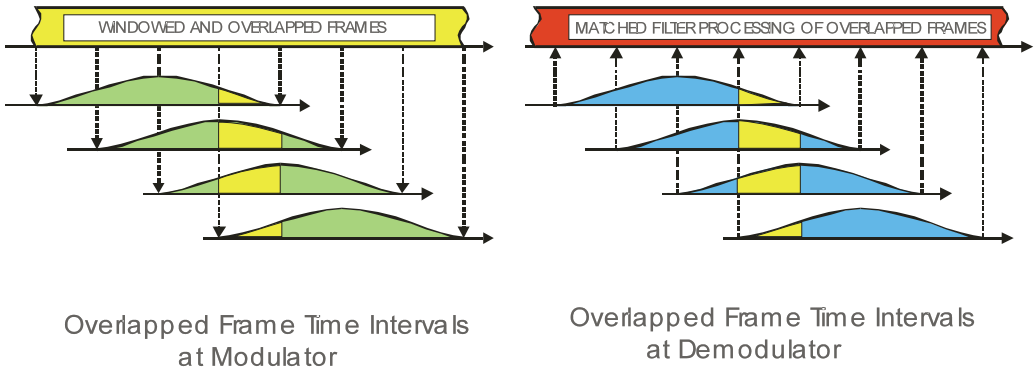

Figure 2.8: Overlapped OFDM symbol with zero ISI; technique applied at the transmitter site (left) and at the receiver site (right)

2.3 OFDM Sidelobes Reduction Techniques

In this section a sidelobes reduction technique by manipulating the composition of X_n in (2.1) is described. The results in [21]-[33] show that a significant sidelobe reduction gain can be obtained.

2.3.1 Sidelobe Suppression by Cancellation Carriers Insertion

In [21]-[23] instead of having de-activated carriers adjacent to the LU band, these carriers are used to cancel out the sidelobes on the LU band. The concept is to find the proper amplitude of the cancellation carriers in such a way that the resulting sidelobes be as low as possible. The optimization can be formulated as :

$$|X(f)|^2 = \frac{1}{N_{FFT}} \left| \sum_{\substack{n=1 \\ n \neq cc}}^{N_{FFT}} \sqrt{p_n}(X_n) \int_{-(1+\alpha)T_u}^{(1+\alpha)T_u} g(t) e^{-j2\pi(f-f_n)t} dt + \sum_{\substack{cc=cc1 \\ cc \neq n}}^{ccN} \sqrt{p_{cc}}(Xc_{cc}) \int_{-(1+\alpha)T_u}^{(1+\alpha)T_u} g(t) e^{-j2\pi(f-f_{cc})t} dt \right|^2$$

$$\text{subject to } |X(f_{LU})|^2 < P_{Threshold,} \quad \text{and} \quad \sum_{n=1}^{N_{FFT}} p_n = P_T \tag{2.6}$$

where ccN is the total number of sidelobes cancellation carriers, and Xc_{cc} is the symbol on the cancellation carrier position in the range $cc1,\ldots,ccN$. The power constraint for all subcarriers including the cancellation carriers remains, meaning that no extra energy is added. The possible high power required by the cancellation carriers can be compensated from the unused power due to the carriers de-activation.

We introduce an alternative optimization approach by simplifying it to a set of *ccN* linear equations to solve *ccN* cancellation carrier amplitude values. Figure 2.9 provides a simple example of how the cancellation carriers with this new approach work. The spectrum is derived from 9 subcarriers (including the cancellation carriers) and uses a rectangular window which produces a spectrum derived from a sum of sinc functions. One cancellation carrier is located at the left edge of the RU band adjacent to the LU band and another one is at the right edge. They are indicated by the dark vertical arrows. If we take a look at the OFDM spectrum with carriers de-activation (one carrier at the left and one carrier at the right edge) denoted by the solid curve, we can see that the maximum sidelobe occurs at a frequency point half of the carrier spacing from the de-activated carrier which, in Figure 2.9 is indicated by the coordinate position (X:-4.5,Y:-0.1564). The cancellation carriers can be weighted in such a way that the sum of their spectra will make the OFDM spectrum zero at that particular coordinate position (e.g. by having a cancellation carrier spectrum coordinate (X_{c1}=X_{c2}=-4.5, Y_{c1}=0.1477, Y_{c2}=0.0087)).

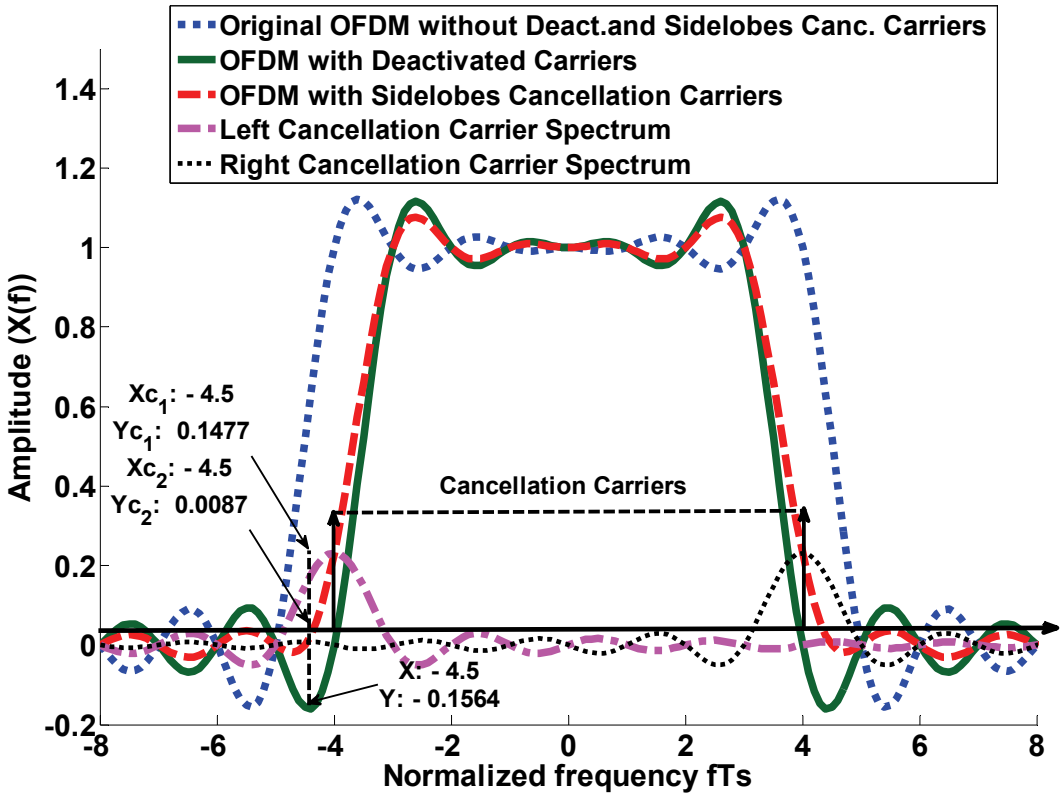

Figure 2.9: The OFDM spectrum amplitude with the effect of de-activated carriers or cancellation carriers

The same technique is also applied to the sidelobes reduction on the right side. The resulting spectrum derived from using the cancellation carriers technique is depicted by the dashed lines. The sidelobes are lower than the sidelobe of the OFDM with the de-activated carriers.

The cancellation carriers can be combined with windowing [24]-[25]. Different windows provide different sidelobe levels. Combining a window that gives very low sidelobes (e.g. the farchsech window) with the cancellation carriers technique will lead to a very significant sidelobe (interference) reduction in the LU band. The results in [24] have shown that the combination of 2 cancellation carriers on each side adjacent to the LU band and raised cosine window with roll off factor (α) 0.2 gives more than 30 dB sidelobes reduction compared to the conventional OFDM.

2.3.2 Sidelobe Suppression by Subcarrier Weighting

Subcarrier weighting is introduced in [26]-[27]. The weighting can be seen as varying the allocation power p_n on each carrier m which, according to (2.1), will affect the spectrum amplitude. By selecting the appropriate weight for each of the carriers the desired low sidelobes can be obtained. The sidelobe reduction by means of carriers weighting is attained at the expense of the bit error rate (BER) versus signal to noise ratio (SNR) degradation [28], since the weighting will give unequal amounts of transmission power on each of the OFDM carriers. The weighting method was originally used in [28] to counteract the high peak to average power ratio (PAPR) problem in OFDM.

2.3.3 Sidelobe Suppression by using Multiple Choice Sequence

In principle multiple choice technique is applied by mapping an OFDM symbol into several sequences and choose the one which gives the smallest sidelobe to be transmitted. In [29] several multiple choice sequence techniques are introduced. Among the techniques are the symbol constellation approach, the interleaving approach and the phase approach. The symbol constellation approach is applied by mapping the symbol X_n in eq. (2.1) which is derived from one of the symbols set of QAM or PSK mapping into a different value $X'_n(l)$ which is still derived from one of the symbols set of QAM or PSK mapping. The index l ranges from $l=1,2,\ldots,L$, where L is the number of possible alternative values. This means that the bits can be mapped into L possible symbols. By putting the N_{FFT} symbols of $X'_n(l)$ into (2.1), and observing from all L possible PSDs, the one with the lowest sidelobe is then chosen for transmission. An example of simple mapping from X_n into $X'_n(l)$ is given in [29]. The CS points of QAM or PSK are numbered as $0,1,\ldots,CS-1$, hence the symbol X_n is assigned to the number I_n ($I_n \in \{0,1,\ldots,CS-1\}$) according to its point position, where CS is the constellation size. The $X'_n(l)$ will be the symbol value on the new number $I_n(l)$ which is derived from the addition of the assigned number I_n with the random number $D_n(l)$ which has L different possible values [29],

$$I_n(l) = I_n + D_n(l) \ . \tag{2.7}$$

By transmitting the information about the set index information l, the receiver can decode the received signal and reconstruct the original X_n symbol.

By means of the interleaving approach, the N_{FFT} X_n symbols are interleaved by L different interleaver rules,

$$\boldsymbol{X'}(l) = \boldsymbol{\Pi}(l)\boldsymbol{X}, \tag{2.8}$$

where $\boldsymbol{\Pi}(l)$ is the permutation matrix that will do the interleaving, $\boldsymbol{X}$ is the symbol vector, and $\boldsymbol{X'}$ is the symbol vector after interleaving. The matrix $\boldsymbol{\Pi}(l)$ has L different possible matrix values and will be available at the transmitter and receiver. Among L different possible OFDM spectra using a set of symbols $\boldsymbol{X'}(l)$, the one with the lowest sidelobes is chosen for transmission. The receiver will use the de-interleaver permutation matrix $\boldsymbol{\Pi}^{-1}(l)$ to recover the transmitted data upon receiving the side information index l.

In the phase approach each phase of symbol X_n is shifted by a random phase $\theta_n(l)$ with L different possible values. The phase shifted symbol $X'_n(l)$ becomes [29],

$$X'_n(l) = X_n e^{j\theta_n(l)} \tag{2.9}$$

where $\theta_n(l)$ is in the range of between 0-2π. In the vector notation, the phase shifted signal $\boldsymbol{X'}(l)$ is derived from a point to point multiplication between the original signal $\boldsymbol{X}$ and the complex number vector derived from $e^{j\boldsymbol{\theta}(l)}$. As in the constellation and interleaver approach also, in the phase approach, with L possible sets for vector $\boldsymbol{\theta}(l)$, the one that produces the lowest sidelobes is chosen and applied to the symbol vector $\boldsymbol{X}$. The index information l is transmitted so that the receiver can reconstruct the symbol vector $\boldsymbol{X}$. Apart from the random shift, a random amplitude shift can also be applied, but in such cases the BER performance will be affected. Another approach is to only apply the multiple choice sequence technique to the carriers adjacent to the LU band, since these carriers mostly affect the sidelobes magnitude [29].

2.3.4 Sidelobe Suppression by Adaptive Symbol Transition

Sidelobes Suppression by using a time domain approach has been introduced in [30]. A time domain symbol transition is inserted between two OFDM symbol, and a symbol transition value is obtained in such a way that the signal spectrum or the Fourier transform of the two consecutive time domain OFDM symbol (including the symbol transition) will have low sidelobes. The objective is to minimize the spectrum resulting from two consecutive time domain OFDM symbols without symbol transition added by the spectrum contributed from the symbol transition onto the LU band [30]. If the OFDM based cognitive radio signal contribution on the LU is described as :

$$\boldsymbol{I} = \boldsymbol{F}_{LU}\begin{bmatrix} \boldsymbol{y}^{m} \\ \boldsymbol{a}^{m} \\ \boldsymbol{y}^{m+1} \end{bmatrix} \tag{2.10}$$

where $\boldsymbol{I}$ is the signal part of the cognitive radio signal in LU band, $\boldsymbol{F_{LU}}$ is the Fourier transformation matrix for the signal in LU band, $\boldsymbol{y}^m$ is the mth time domain OFDM symbol including the guard interval, $\boldsymbol{a}^m$ is the additive symbol transition, and $\boldsymbol{y}^{m+1}$ is the next OFDM symbol, then the optimization problem will be to find that vector $\boldsymbol{a}^m$ in making $\boldsymbol{I}$ as small as possible. The symbol transition scheme is depicted in Figure 2.10.

The symbol transition will not introduce any inter symbol interference (ISI) but the transmission duration becomes longer, which means that the bit rate is reduced. The search for the time domain symbol transition values is characterized as a linear least squares problem with a quadratic inequality constraint [30].

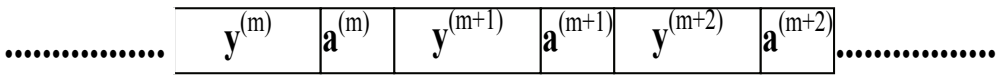

Figure 2.10: Adaptive symbol transition scheme

2.3.5 Sidelobe Suppression by Frequency Domain Additive Signal

In [31] sidelobe suppression for OFDM based cognitive radio can be achieved by mapping the data symbol using QPSK modulation mode and add the frequency domain symbol vector $\boldsymbol{X}$ with random values vector $\boldsymbol{d}$ in such a way that the resulting PSD in the LU region become as small as possible. The optimization problem is described by

$$|X(f)|^2 = \frac{1}{N_{FFT}} \left| \sum_{n=1}^{N_{FFT}} \sqrt{p_n}(X_n + d_n) \int_{-(1+\alpha)T_u}^{(1+\alpha)T_u} g(t) e^{-j2\pi(f-f_n)t} dt \right|^2 , \quad (2.11)$$

$$\text{subject to} \quad |X(f_{LU})|^2 < P_{Threshold}, \quad \text{and} \quad \sum_{n=1}^{N_{FFT}} p_n = P_T$$

where d_n is the additive signal on subcarrier n. In order not to destroy the cognitive radio BER performance and keep the total allocated power constant, the value of d_n is restricted to a circle with magnitude $| d_n | \leq 0.7$ [24]. In this way, according to the QPSK gray mapping, the value of $X'_n = X_n + d_n$ will not give a decision error at the receiver, except in a severely noisy and/or faded channel. Simulation results in [31] have shown about 15 dB sidelobes reduction could be achieved with the cost of 2.8 dB SNR degradation in case the upper limit value of $| d_n |$ is 0.7.

2.3.6 Sidelobe Suppression by Constellation Expansion

A most recent technique in OFDM sidelobe suppression has been proposed in [32], where the M-PSK modulation mapping is expanded to 2xM-PSK mapping in order to have lower OFDM sidelobe. The original symbol after M-PSK mapping which is located at point *a* of *M* available PSK symbol points is transformed into two possible new points a_1 and a_2 where the location of a_1 and a_2 must not in the same region. The purpose is to have random selection of points so there will be sidelobe pattern difference compared to the previous sidelobe using the *a* point. By combining all possible new OFDM symbol set on the 2x M-PSK points through all OFDM carriers, the one set which gives the smallest sidelobes will be chosen for transmission. No additional information is required by the receiver for data detection, since the receiver has the knowledge of all possible a_1 and a_2 positions. Therefore, the receiver can detect the data by calculating the minimum Euclidean distance between the received symbol and the reference points on 2xM-PSK mapping, and accordingly translates the result to the M PSK mapping. Figure 2.11 shows an example on how the points from QPSK are expanded to 8-PSK mapping. In this way there are two possibilities of mapping a data symbol, and accordingly the constellation expansion will add extra randomness to X_n in eq. (2.1) with various possible sidelobes magnitude. The one which gives the smallest sidelobes will be chosen to be transmitted. Simulation results in [32] have shown that the sidelobes suppression technique by the constellation expansion from QPSK to 8-PSK gives only a slight BER degradation. With this Constellation Expansion technique about 9 dB sidelobes suppression can be attained [32].

The work has been extended in [33] by combining the constellation expansion technique with the cancellation carriers inserted on the carriers adjacent to the LU band. Extra sidelobes reduction has been achieved without having high magnitudes for cancellation carriers, due to prior sidelobes reduction by the constellation expansion technique. According to [33] the combination between constellation expansion and one sidelobes cancellation carrier on each side adjacent to LU band gives around 16 dB sidelobes reduction.

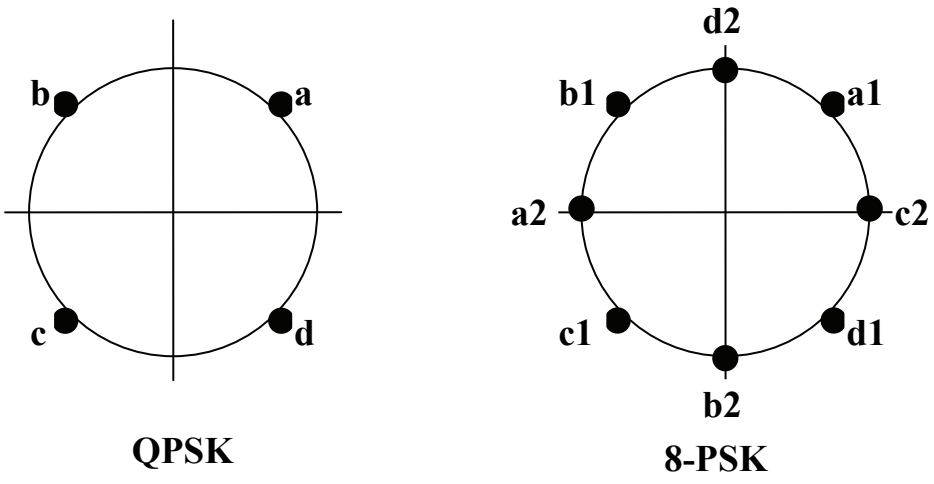

Figure 2.11: Constellation Expansion from QPSK to 8-PSK mapping

2.4 Frequency Hopping

Despite the application of spectrum pooling by carriers de-activation in the LU band and sidelobes reduction by different techniques (windowing, additional carriers de-activation, cancellation carriers, multiple choice on the transmitted data sequence, additive signal in time or frequency domain, constellation expansion and combinations between them), a problem arises if too many carriers need to be de-activated, as there will be not enough resources to transmit data to fulfil the target bitrate. In [34] frequency hopping is proposed to deal with too many carriers de-activation in a selected band. While frequency hopping is a proper solution, another techniques (i.e. Ultra Wide Band), could be an alternative due to its signal power property below noise level hence it can be overlapped with the LU signal itself. In this thesis, because of the demand for a Cognitive Radio service which provides high rate transmission at long distance, we put our attention to the frequency hopping scheme.

2. 4. 1 Evaluation Using GSM 900 MHz Channel Model

We have evaluated the proposed frequency hopping technique with TDD Bluetooth frame design in simulations. The details about the OFDM frame design for frequency hopping scenario and the hopping mechanism are available in Appendix A. The evaluations were presented in [35]. The propagation models in this dissertation are taken from the ETSI GSM model at 900 MHz [36]. The power delay profile for the rural area model is given in Table 2.1, and for the urban area model is given in Table 2.2. There are 2 alternative taps setting in each model. The coherence bandwidth for the rural area model of the first alternative taps setting is 1.6 MHz while the second alternative is 1.2 MHz. In the case of the urban area model, the coherence bandwidth of the first alternative is 155 kHz while the second alternative is 159 kHz.

Table 2.1: Propagation model for Rural Area GSM in 900 MHz [36]

Tap Number	**Relative Time (μs)**		**Average relative power (dB)**	
	(1)	(2)	(1)	(2)
1	0.0	0.0	0.0	0.0
2	0.1	0.2	-4.0	-2.0
3	0.2	0.4	-8.0	-10.0
4	0,3	0.6	-12.0	-20.0
5	0.4	-	-16.0	-
6	0.5	-	-20.0	-

The first alternative of the two area model suggests that the sampling time of the OFDM signal should be 0.1 μs while for the second alternative 0.2 μs sampling time is sufficient in order to have a sample spaced channel model and good channel estimation result. The worst condition of the propagation model is found in the urban area propagation model where the maximum delay (τ_{max}) is 5 μs and we have a non constant tap spacing.

Since the frame duration must not exceed 366 μs, Table 2.3 shows the choices of OFDM parameters that fulfils the 366 μs frame duration constraint. The guard interval (GI) must exceed the worst case scenario in the urban area channel model with a maximum delay of 5 μs.

Table 2.2: Propagation model for Urban Area GSM in 900 MHz [36]

Tap Number	**Relative Time (µs)**		**Average relative power (dB)**	
	(1)	(2)	(1)	(2)
1	0.0	0.0	-4.0	-4.0
2	0.1	0.2	-3.0	-3.0
3	0.3	0.4	0.0	0.0
4	0.5	0.6	-2.6	-2.0
5	0.8	0.8	-3.0	-3.0
6	1.1	1.2	-5.0	-5.0
7	1.3	1.4	-7.0	-7.0
8	1.7	1.8	-5.0	-5.0
9	2.3	2.4	-6.5	-6.0
10	3.1	3.0	-8.6	-9.0
11	3.2	3.2	-11.0	-11.0
12	5.0	5.0	-10.0	-10.0

As depicted in Figure 2.1, the OFDM system requires a channel estimator module to remove the effect of fading on the received signal. In order to aid the channel estimation process pilots or trainings need to be inserted to the OFDM frame. The details about frame design including the pilots or the training pattern, analysis and performance evaluations will be described in detail in chapter 4.

Table 2.3: OFDM frame design according to TDD Bluetooth frame.

N_{FFT}	T_S (µs)	Δf (kHz)	# OFDM symbols	T_G/ T_S
1024	204.8	4.9	1	1/32
512	102.4	9.7	3	1/16
256	51.2	19.5	6	1/8
128	25.6	39	11	1/4

2.5 Conclusions

In this chapter we discussed how OFDM can be considered as the proper technique for the Cognitive Radio system in realizing the co-existence between the LU and RU. OFDM has the capability to notch part of its spectrum which is occupied by the LU. This is carried out by de-activating some of its carriers which fall in the LU band.

By sidelobes reduction techniques some part of the OFDM based Cognitive Radio signal which are still smearing out into the LU band due to the OFDM power spectrum density property, can be suppressed.

If too many OFDM carriers must be de-activated due to the LU access, the Cognitive Radio system target data rate and quality of service (QoS) can not be attained. In this situation the frequency hopping technique can be applied. Although Ultra Wide Band could be considered as an alternative technology, frequency hopping is preferable in satisfying the Cognitive Radio service demand in accommodating long range high data rate transmissions. As the spectrum scanning module finds a proper band that can accommodate the target data rate and QoS, the frontend part of the cognitive radio device will set its carrier frequency to that proper band. An example of the Bluetooth TDD frequency hopping mechanism has been presented. An OFDM frame according to the Bluetooth TDD slot has been proposed.

Chapter 3

Baseband Processing for OFDM-Based Cognitive Radio

3.1 Introduction

Cognitive Radio according to reference [2] is an intelligent communication system with the capability of changing its transmission parameters according to the environment condition with the objectives to attain highly reliable communications and efficient utilization of the radio spectrum.

The application of Cognitive Radio in this research work is focused on the spectrum utilization efficiency by operating the Cognitive Radio system as rental user (RU) to co-exist with the licensed user (LU). OFDM has been described in chapter 2 as the proper candidate to realize this co-existing aim by de-activating some of its carriers at the LU positions and applying sidelobes suppression techniques.

In this chapter beside the co-existence between LU and RU, the effort to obtain reliable communications for the RU system itself is established. Section 3.2 will key out the combination of spectrum pooling, windowing, adaptive bit loading and sidelobes cancellation carriers. The purpose of the combination is to obtain the desired target data rate while the required BER remains. Part of the RU spectrum in the LU band will be seen as interference by the LU. This interference should be suppressed to a level which can be considered negligible or tolerable by the LU.

Section 3.3 describes an alternative technique by replacing the Fourier transform in OFDM with wavelet basis function that forms a wavelet packet multi carrier modulation (WPMCM) technique. In this chapter a frequency selective wavelet to replace the Fourier transform in OFDM to form WPMCM is applied[§]. The WPMCM is combined with the spectrum pooling

[§] Initially at the IRCTR Madan K. Lakshmanan and H. Nikookar used a frequency selective wavelet basis function for single carrier ultra wideband (UWB) modulation and applied pulse position modulation (PPM) as data mapping technique. The work on WPMCM explained in this thesis was conducted in collaboration with Madan K. Lakshmanan.

concept to have co-existence between the LU and RU. The particular reason why the frequency selective wavelet is interesting to be applied in WPMCM is due to parameters in designing the wavelet basis function such as frequency selectivity, regularity order, transition bandwidth, and filter length that can be set in such a way that the target QoS will be achieved. Conclusions on this chapter are summarized in Section 3.4.

3.2 Combined Spectrum Pooling, Windowing, Adaptive Bit Loading and Sidelobes Cancellation Carriers

Conventionally, the modulation scheme in OFDM is constant over all data subcarriers for a given mode. A critical situation that may occur in OFDM within this mode is when bit errors are concentrated in a set of severely faded subcarriers, while in the rest of the OFDM spectrum often no bit errors are observed. Such event raises the idea of having adaptive OFDM, where subcarriers that will exhibit high bit error probability are excluded from transmission. It will improve the overall BER with a potential slight loss in system throughput. The potential loss in throughput due to the exclusion of faded subcarriers is counteracted by employing higher order modulation modes on subcarriers which have a very small BER. The data should be concentrated more on the sub channels with higher frequency response gain, hence a higher SNR, and noisy sub channels should carry little or no data.

In transmitting such a preferred OFDM symbol, the transmitter needs to estimate the expected channel condition at that time. The channel prediction may use the knowledge of the past channel quality estimation. Such adaptive system can only operate efficiently in slow varying channel conditions. If the communications between two stations is bidirectional and the channel can be considered reciprocal (important for using Time Division Duplex (TDD) and Frequency Division Duplex (FDD)), T_x/R_x station can estimate the channel quality based on the received OFDM symbols and adapt the parameters of the local transmitter to this estimation. This approach is named *open loop adaptation*, since there is no feedback between the receiver of a given OFDM symbol and the choice of the modulation parameters. For the case of a non-reciprocal channel, the stations cannot determine the parameters for the next OFDM symbol's transmission from the received symbols; the receiver has then to estimate the channel quality and this perceived channel quality information has to be used in the transmitter for the inverse link. This approach is called *closed loop adaptation*. The two cases are described in Figure 3.1. The solid lines represent the data transmission, while the dashed lines represent the inherent side information about the signal mode i.e. modulation, coding parameters. The BER in each subcarrier is determined by the fluctuations of the current frequency-domain channel transfer function H_n with the aid of channel transfer function estimation provided by information extracted from the transfer of the pilot symbols. More accurate measures of the channel transfer function can be gained by means of decision-directed or time-domain training sequence based techniques. Another crucial thing to be considered is the delay between the channel quality estimation and the actual transmission of the OFDM symbol in relation to the maximum channel Doppler frequency. It will influence the adaptive system's performance. This delay in the closed-loop adaptive system is generally

longer than for an open-loop adaptive system, hence the Doppler frequency of the channel is more critical in the closed-loop adaptive system.

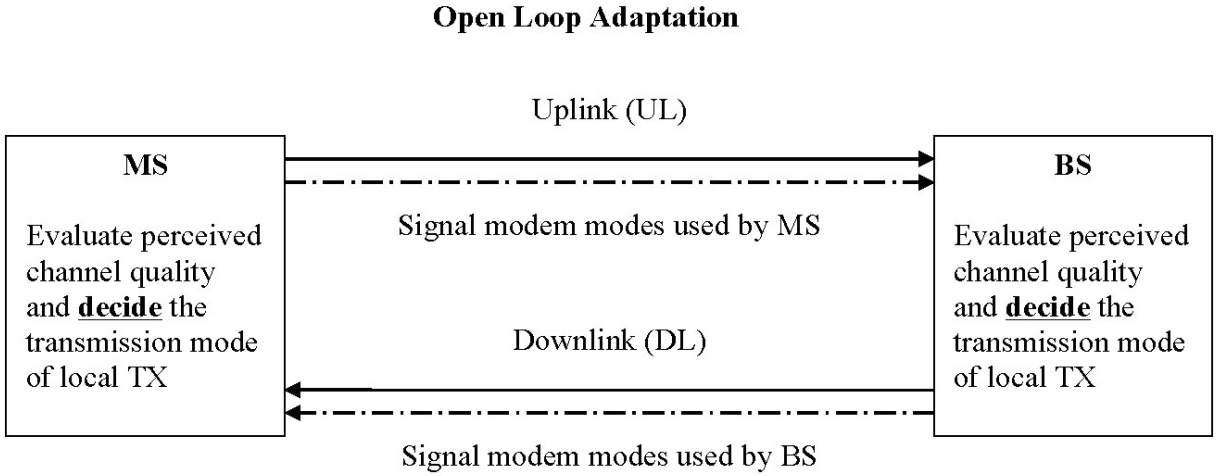

(a)

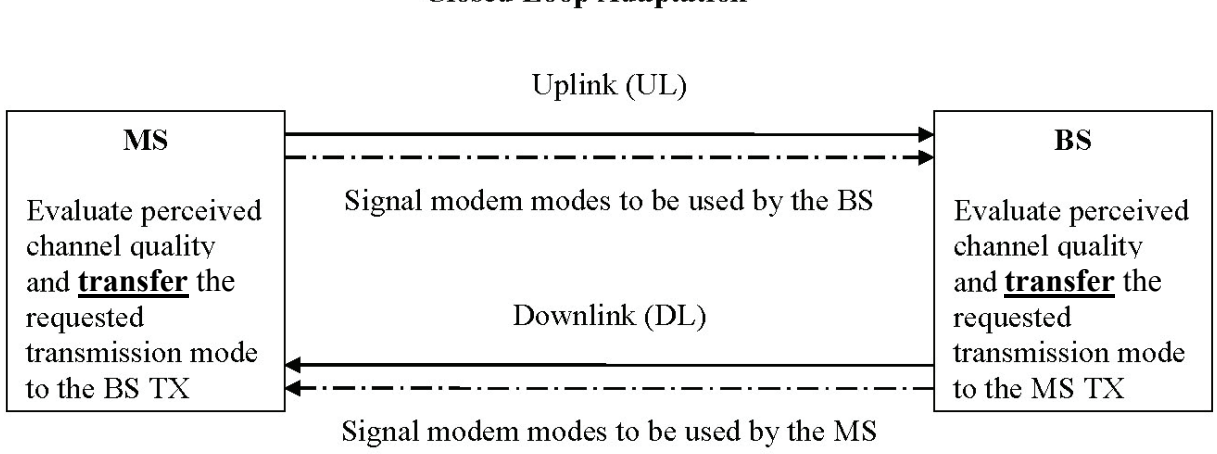

(b)

Figure 3.1: Signaling scenarios in adaptive modems [37] for (a) Open Loop Adaptation and (b) Closed Loop Adaptation

Based on the channel fading information derived from the channel estimation process in OFDM, the constellation size of each sub-carrier is determined. In order to demodulate the transmitted data properly, the information of modulation mode in each carrier is required by the receiver. This information can be derived by estimating it blindly [38],[39], or from the transmitted signalling symbols [38].

The next subsection will describe how the signaling and blind estimation for the purpose of modulation detection are applied including their pros and cons, followed by another subsection discussing several available adaptive bit loading algorithms.

3.2.1 Modulation Detection by Signaling and Blind Detection

If the channel quality estimation and parameter adaptation have been performed at the transmitter of a particular link, then according to the open loop adaptation, the resulting set of parameters has to be communicated to the receiver in order to successfully demodulate and decode the OFDM symbol.

In the closed loop case, the receiver determines the requested parameter set to be used by the remote transmitter, the same amount of information has to become available in the remote transmitter for the inverse link. If the signaling information is corrupted then the receiver can not correctly decode the OFDM symbol corresponding to the incorrect signaling information. Adaptive OFDM systems have to react to the frequency-selective nature of the channel, by adapting the parameters across the subcarriers. The resulting signaling overhead can become significantly higher, and can be prohibitive. In order to overcome these limitations, efficient and reliable signaling techniques have to be employed for practical implementation in adaptive OFDM systems.

If some flexibility in choosing the transmission parameters is sacrificed within an adaptation scheme, the amount of signaling can be reduced. Alternatively, blind parameter detection schemes can be devised, which require little or no signaling information. With respect to the effects of transmission parameter adaptation in OFDM systems the following issues should be considered: data buffering and latency due to varying data throughput, effects of co-channel interference, and bandwidth efficiency.

For example in order to keep the system complexity low, the modulation mode is varied on sub-band to sub-band basis. The total set of OFDM subcarriers are split into blocks of adjacent subcarriers which means divided into several sub-bands. The same modulation scheme is employed for all subcarriers in a sub-band. This will simplify the task of signaling. The simplest way of signaling the modulation mode employed in a sub-band is to replace one data symbol by an MPSK symbol, where M is the number of possible modulation modes, hence the reception of each of the constellation points directly signals a particular modulation mode in the current sub-band. For four modulation modes and assuming perfect phase recovery, the probability of a signaling error $p_s(\gamma)$, when employing one signaling symbol, is the symbol error probability of QPSK. The expression for the modulation mode signaling error probability according to [37] is

$$p_s(\gamma) = 1 - \left(1 - Q\left(\sqrt{\gamma}\right)\right)^2 \tag{3.1}$$

where $Q(.)$ is the probability Gaussian Function $Q(x) = \frac{1}{\sqrt{2\pi}} \int_{x}^{\infty} e^{-\frac{t^2}{2}} dt$. The signaling error probability can be reduced by employing multiple signaling symbols and maximum ratio combining of the received signaling symbols $R_{s,n}$ in order to generate the decision variable R'_s prior to the decision [37], i.e.

$$R'_s = \sum_{n=1}^{N_s} R_{s,n} \hat{H}^*_{s,n} \tag{3.2}$$

where N_s is the number of signaling symbols per sub-band, the quantities of $R_{s,n}$ are the received symbols in the signaling subcarriers and $\hat{H}_{s,n}$ represents the estimated values of the frequency-domain channel transfer function (CTF) at the signaling subcarriers. With the assumption of perfect channel estimation and constant values of the channel transfer function across the groups of signaling subcarriers, the signaling error probability for N_s signaling symbols can be expressed as [37]:

$$p'_s(\gamma, N_s) = 1 - \left(1 - Q\left(\sqrt{N_s \gamma}\right)\right)^2 \tag{3.3}$$

The signaling symbols for a given sub-band can be interleaved across the entire OFDM symbol bandwidth, to benefit from frequency diversity in fading wideband channels.

Another way of signaling is by transmitting the signaling symbols from QAM mapping as shown in Figure 3.2. where the allowable constellation size is restricted to the set of {0, 2,4,16 and 64}. The inner rectangle which is the decision area for the so called 0 modulation mode (no symbol is transmitted) can be made smaller up to a distance of about $\frac{3d}{4}$ from the other reference symbols; d is the distance between the outer points and the no symbol point (zero). This is due to the fact that a decision error (e.g no symbol transmitted but either BPSK or another modulation mode is decided) is just caused by noise (no contribution from channel fading). By this technique the signalling error probability can be reduced since the minimum Euclidean distance between the signalling points is high; this distance equals according to Figure 3.2 to $7\sqrt{2}$ (distance between no data is transmitted (0) and other modulation modes).

Blind detection algorithms estimate the employed modulation mode directly from the received data symbols, therefore avoiding any loss of data capacity due to signaling subcarriers. There are two algorithms for this blind detection. One is based on SNR estimation and the other one is based on incorporating error correction coding. By SNR estimation, the receiver has no *a priori* knowledge of the modulation mode employed in a particular received sub-band but estimates this parameter by finding the closest distance between the received data symbols after the fading removal ($R_n/\hat{H}_n$) in that sub-band to all possible value of $\hat{R}_{n,m}$ in the chosen modulation modes M for each subcarrier index n in the current sub-band. The index m defines the index of possible points on the constellation map, and ranges from $1,\ldots, M$. The error

energy e_m between the ideal constellation phasor positions and the received phasors is calculated for each modulation mode via [40]

$$e_m = \sum_n \left(\frac{R_n}{\hat{H}_n} - \hat{R}_{n,m} \right)^2 , \tag{3.4}$$

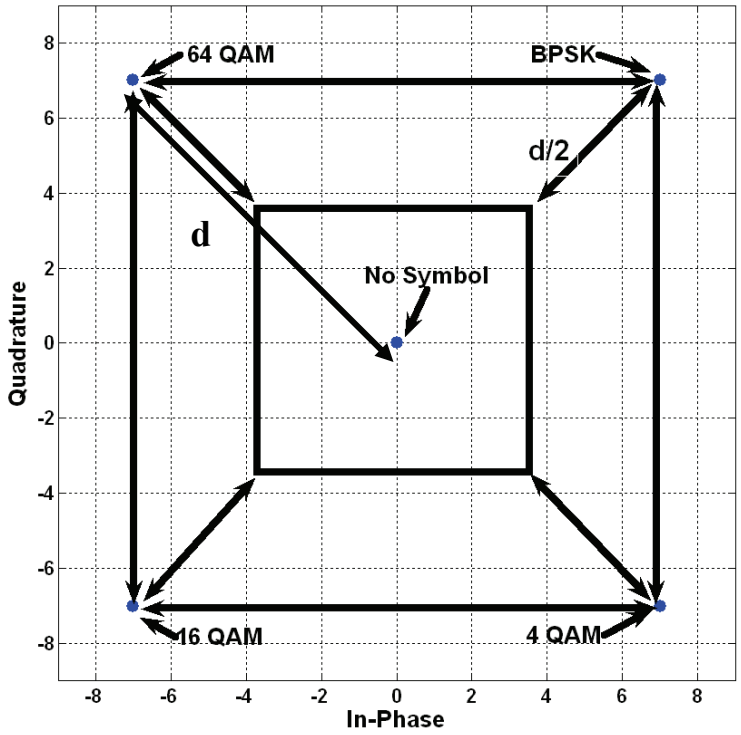

Figure 3.2: An example of signaling symbol points for adaptive bit loading with allowable M= {0, 2, 4, 16, and 64}

The modulation mode M_m, which minimizes e_m, is then chosen for the demodulation of the sub-band. It is mentioned in [40] that there are two ways to conduct blind modulation detection. They are pattern recognition and decision theoretic approaches. The pattern recognition approach needs a relatively large number of samples available to make a decision. This requires a large memory during computations. Therefore signaling is considered to be a better alternative than the pattern recognition approach. There are three methods known for use in the decision theoretic approach.

The first one is based on the average Euclidean distance, which is calculated as [40] :

$$e_m = \frac{\sum_s \left| R_s - \hat{R}_{s,m} \right|^2}{S} \qquad m = BPSK, QPSK, \ldots \quad \text{etc}$$

(3.5)

R_s is the received sample on index sample s, $\hat{R}$ is the hypothesis of the received sample, m is the index of the modulation, and S is the number of samples used for averaging. The scheme which minimizes the average Euclidean distance e is chosen for demodulation.

The second method is based on the *Kullback-Leibler (K-L)* distance algorithm. The K-L distance is defined as the distance between any two probability distribution functions, f and g. In the method, f is the probability distribution of errors from the received symbols, and g is the distribution for the approximate model. The distance between the two distributions is a measure of dissimilarity between them. It should be noted that the directed distance from f to g is not the same as that from g to f. The K-L distance can be expressed as [40] :

$$I(f,g) = I(p,\pi) = \sum_{i=1}^{L} p_i \log\left(\frac{p_i}{\pi_i}\right) \tag{3.6}$$

where p_i is the ith true probability outcome, π_1 to π_L correspond to elements of the approximating probability distribution. L is the number of possible modulation modes. Both, Σp_i and $\Sigma \pi_i$ are equal to 1. f and g correspond to p_i and π_i, respectively. The notation $I(f, g)$ according to information theory is the mutual information between random variables f and g and in this context is referred as the information lost when g is used to approximate f.

Since in adaptive modulation, different modulation schemes are used between specific SNR bounds for the purpose of optimum performance, the probability density function (PDF) approximation can be used to determine the SNR and then the modulation scheme can be estimated at the transmitter. Assuming that for a set of K SNRs, the probability distributions of errors, i.e the PDFs $g_1, \ldots, g_K$ for K SNRs, are known, therefore K can be seen as the number of samples (data for which their modulation modes have to be determined) to be observed. The distribution of the errors of received noisy symbols (i.e. model f) can now be calculated and allow us to estimate the K-L distances to all approximating PDFs g_1 to g_K. By minimizing the K-L distance, the resulted SNR and transmitted modulation scheme can be obtained.

The third method uses the mean-squared-error (MSE) between the elements f and g, calculated from [40] :

$$MSE_k = \sum_{i=1}^{L} \left(p_i - \pi_{k,i}\right)^2, \qquad 1 \le k \le K \tag{3.7}$$

By using this method, only a simple measure of the distance and not a weighted directed distance is obtained. This is why K-L distance is well suited for SNR estimation. Two sets of distributions may have the same MSE, but may result from different SNRs.

3.2.2 Adaptive Bit Loading

Adaptive bit loading is an intelligent bit allocation technique. The allocation is applied based on the channel condition. More bits are allocated to the good channel and less bits to the bad channel. Each bit loading algorithm has its own optimization criterion. The common required information by the bit loading algorithms are the channel state information (H), the noise variance (σ_n^2) and interference variance (σ_I^2) that refers to the signal to interference plus noise ratio (SINR) on each carrier. This information can be acquired by sending periodic training pilot symbols in an OFDM frame. When a channel estimation module produces the channel estimates, the estimated noise ($\hat{N}_{n,l}$) and interference ($\hat{I}_{n,l}$) on carrier n of OFDM symbol l can be derived by subtracting the received signal ($Y_{n,l}$) on carrier n of OFDM symbol l from the multiplication of the channel transfer function estimate ($\hat{H}_{n,l}$) and the pilot ($X^P_{n,l}$) at that same position, i.e.

$$\begin{aligned}\hat{N}_{n,l}+\hat{I}_{n,l} &= Y_{n,l} - (\hat{H}_{n,l}X^P_{n,l}) = ((H_{n,l}X^P_{n,l}) + N_{n,l} + I_{n,l}) - (\hat{H}_{n,l}X^P_{n,l}) \\ &= \underbrace{(H_{n,l} - \hat{H}_{n,l})}_{\Delta_{n,l}} X^P_{n,l} + N_{n,l} + I_{n,l} \\ &= \Delta_{n,l}X^P_{n,l} + N_{n,l} + I_{n,l}\end{aligned} \tag{3.8}$$

where $H_{n,l}$ is the actual channel state, $\Delta_{n,l}$ is the channel estimate mismatch error, $N_{n,l}$ and $I_{n,l}$ are the original noise and interference term on carrier n of OFDM symbol l. In this way the multiplication of the channel mismatch error $\Delta_{n,l}$ and pilot $X^P_{n,l}$ is treated as another source of noise/interference. The noise and interference variances can be calculated from the collection of the estimated noise and interference terms on carrier n of all training symbols in an OFDM frame. If the channel states are perfectly estimated at the receiver, the value of $\Delta_{n,l}$ will be zero.

The bit loading can be applied carrier-wise or group-wise. In the carrier-wise bit loading the bits are allocated to a particular carrier according to the estimated channel state, noise and interference variance for that carrier. In the group-wise bit loading the carriers are grouped where each group consists of L carriers. The grouping can be based on the index numbering of the carriers or derived from the sorting of the channel state gains (from the lowest up to the highest one). The carriers with low channel state gain will be grouped with other carriers with low channel state gains, while a carrier with high channel state gain will be grouped with other carriers having similar channel gains. The bits to each group will be allocated according

to the average estimated channel state, noise and interference variance for that group. In the following sub sections some existing bit loading algorithms will be overviewed and evaluated.

3.2.2.1 Chow Algorithm

This algorithm focuses on the rate distribution knowing the capacity of the subcarriers. The goal is not to send as many bits as possible, but to send a fixed data rate most reliably by maximizing the performance margin. The optimization problem can be described as follows [41]:

$$\max \quad \gamma_{m\arg in} \quad subject \quad to \quad \sum_{n=1}^{N_c} R_n = R_{t\arg et}, \quad \sum_{n=1}^{N_c} p_n = P_{budget}, \tag{3.9}$$

where γ_{margin} is the system performance margin (in dB) that defines the maximum allowable noise quantity on the system, R_n is the number of allocated bits in subcarrier n, R_{target} is the targeted total number of bits per OFDM symbol, p_n is the power allocation on subcarrier n, and P_{budget} is the total allocated power per OFDM symbol. Chow algorithm tries to maximize the allowable amount of noise while it still can achieve the targeted bit error rate (BER). For each subcarrier the bits are allocated based on the following equation [41]:

$$R_n = \log_2\left[1 + \frac{SNR_n}{\Gamma + \gamma_{m\arg in}}\right], \tag{3.10}$$

SNR_n is the SNR in subcarrier n (in dB). Γ is the SNR gap (in dB) which is a constant which estimates the difference between the channel capacity and the actual capacity usage by the transmission scheme is defined as: $\Gamma = (Q^{-1}(SER/4))^2/3$ where SER is the expected symbol error rate, and $Q(x)$ is the Gaussian probability function. γ_{margin} is updated iteratively until the total number of bits per OFDM symbol satisfies the target rate. R_n is quantized to R_{Qn} according to the allowable constellation size of the modulation (i.e., 2 bits for 4-QAM, 4 bits for 16-QAM, 6 bits for 64-QAM, and 8 bits for 256-QAM). The complete algorithm is given in [41].

3.2.2.2 Fischer Huber Algorithm

This algorithm tries to guarantee that all subcarriers have the same SNR, considering that the overall error rate is dominated by the subcarrier with highest error rate. The rate and power are distributed in such a way that the error probability on each subcarrier is minimized. In a

QAM modulated system the optimization problem is minimizing the probability of symbol error on subcarrier n (i.e., p_n), which is defined as [42]:

$$p_n = K_n Q\left(\sqrt{\frac{d_n}{2\sigma_n^2}}\right) \tag{3.11}$$

where p_n is the probability of error on subcarrier n, K_n is the number of nearest neighbors, d_n is the minimum distance between constellation points, and $\sigma^2{}_n$ is the variance of the noise on subcarrier n. The minimum BER is achieved when all subcarriers have the same error probability. The number of bits per subcarrier per symbol R_n can have any real value. The optimum bit distribution which maximizes the SNR under the condition that it is constant for all subcarriers equals [43] :

$$R_n = \frac{1}{K}\left[R_T + \log_2\left(\prod_{k=0}^{K-1}\frac{\sigma_k^2}{|H_k|^2}\right) - K\log_2\left(\frac{\sigma_n^2}{|H_n|^2}\right)\right], \tag{3.12}$$

where R_T is the target rate, K is the number of active carriers, $\sigma^2{}_n$ is the noise variance on subcarrier n, and H_n is the channel gain on subcarrier n.

If R_n becomes negative for any n, the n-th subcarrier is excluded and the algorithm is applied again over a reduced K subcarriers set. This is done iteratively until all remaining subcarriers have a positive rate.

R_n is also quantified into R_{Qn} as described in the Chow algorithm. After all the subcarriers have their allocated bits according to eq. (3.12), but if the target rate is still not obtained, then addition or subtraction of bits is conducted based on the difference between R_n and R_{Qn} until the total rate reaches the targeted bit rate.

The set of quantified rates must be chosen such that it minimizes the mean square error between the optimum rate distribution R_n and the quantized distribution R_{Qn}, with the constraint that $\Sigma_n R_{Qn} = R_{target}$. Because of the quantization procedure, the SNR is no longer constant at the different subcarriers, as obtained for the continuous distribution of R_n. A constant SNR can be guaranteed by adapting the power for the remaining subcarriers [43]:

$$p_n = C\frac{\sigma_n^2}{|H_n|^2}2^{R_{Qn}}, \quad n \in D \tag{3.13}$$

where D is the subset of active subcarriers, C is a power constant such that $\Sigma_n p_n = P_T$ is satisfied (P_T equals the total transmitted power). If the noise is white, i.e., $\sigma^2{}_n = \sigma^2$ for any n,

the algorithm depends on the channel gains $|H_n|$ only. If the transmitter knows the channel coefficients, the algorithm can be performed without requiring knowledge of the noise level at the receiver.

3.2.2.3 Simple Blockwise Loading Algorithm (SBLA)

The given number of N_c subcarriers is divided into n_B blocks of b adjacent subcarriers. For block i, the algorithm determines a modulation level m_i, such that at a given bandwidth efficiency E (in units [bit/subcarrier]), code rate R and given number of blocks n_B the following equation is satisfied [44]:

$$\frac{R}{n_B}\sum_{i=0}^{n_B-1} m_i = R.m = E\,. \tag{3.14}$$

where $m = \frac{1}{n_B}\sum_{i=0}^{n_B-1} m_i$. One key property of the SBLA is assigning the same modulation level to adjacent subcarriers within one block. Due to the observation that in general the channel gains and consequently the SNRs of neighboring subcarriers are (highly) correlated, no noticeable performance degradations are expected by introducing a block of subcarriers, which are smaller than the coherence bandwidth of the channel.

A second key property of SBLA is the low computational complexity, which is mainly based on the usage of a predetermined SNR grid. The SNR grid contains a list of differences of the SNR thresholds, required to switch between the modulation levels m_i of the supported QAM modulation alphabets for a specific block.

The choice of modulation level m_i for a specific block of subcarriers is based on the (mean) SNR for this block i.e., SNR_i. The predetermined SNR grid (containing fixed interval sizes for each modulation level m_i) is used, as given for example in Figure 3.3. The absolute position on the SNR axis, i.e. the absolute SNR threshold for each desired bandwidth efficiency E is determined by shifting the grid according to the average modulation level m and the mean SNR (SNR_{mean}) for the given channel. (i.e. the mean SNR over all subcarriers). After first allocation of bits per subcarrier which has been performed by usage of an SNR grid without any iteration, it might be necessary to add or subtract bits in order to meet the desired bandwidth efficiency E (i.e. data rate). The detailed steps of this method are as follows [44]:

- Initialization of the total number of subcarriers (N_c), the number of subcarriers (b) per cluster, the average number of bits per subcarrier (m) over all subcarriers, and the inverval sizes for the predetermined SNR grid according to the targeted bit error rate BER_{target}. The total number of bits to be distributed by the algorithm in one OFDM symbol then follows as $R_{target} = mN_c$.

- Determine the SNR for each block of subcarriers (SNR_i) and the mean SNR (SNR_{mean}) over all subcarriers.
- Shift the SNR grid according to the average number of bits per subcarrier m and SNR_{mean}.
- Assign a modulation scheme (number of bits m_i) to each subcarrier block i according to the position of SNR_i in the SNR grid.
- Calculate the total number of allocated bits as $R_{total} = \Sigma_i \, m_i.b$
- As long as $R_{total} \neq R_{target}$, add or subtract bits as in the Fischer algorithm and increase or decrease R_{total} accordingly.
- Perform a scaling of the transmit power (equal for all subcarriers), depending on the number of unused subcarriers.

Determination of the SNR grid is done by applying the OFDM transmission technique, the frequency selective radio channel is transformed into K frequency non selective channels. Thus, K parallel AWGN channels with different SNRs result. Therefore K can be seen as the number of SNR level or the number of modulation modes applied on this adaptive bit loading technique. With the aim to obtain the same BER_{target} on all subcarriers, the BER curves for the AWGN channel can be used to derive the SNR grid. An example of the SNR grid is shown in Figure 3.4.

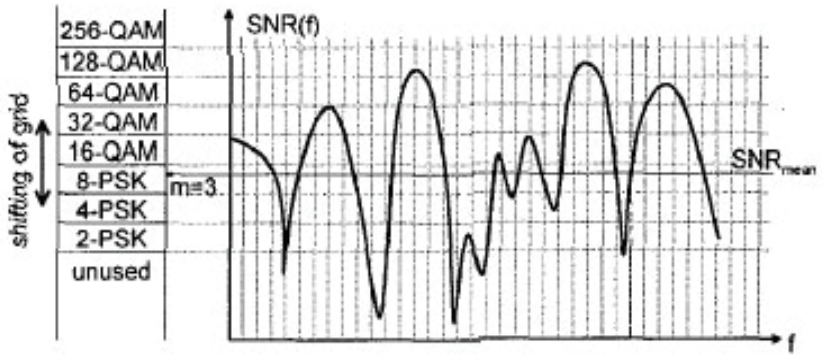

Figure 3.3 : Allocation of modulation schemes. The grid is shifted according to the average number of bits per subcarrier (m=3 as example) and the mean SNR [44]

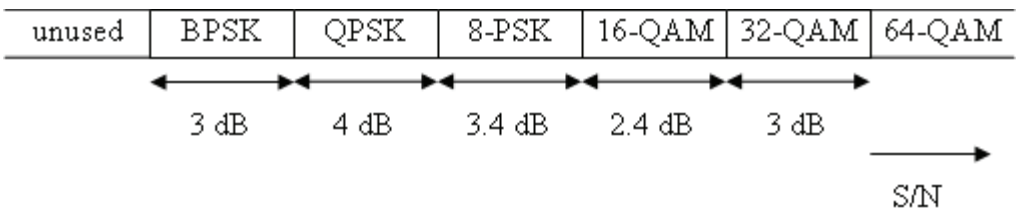

Figure 3.4 : An example of SNR gap for applying the simple block wise loading algorithm [45]

3.2.2.4 Subband Bit Loading based on Fischer-Huber Algorithm

Equation (3.14) can be modified in order to have the bit allocation per subband. As given in [46] the equation becomes:

$$R_i = \frac{R_{TOT}}{N'_B} + \frac{1}{N'_B}\cdot\log_2\left(\frac{\left(|H_i|^2\right)^{N'_B}}{\prod_{k\in\psi}|H_k|^2}\right) \tag{3.15}$$

where H_i denotes the channel gain of the i-th subband, which is the average value of the channel gains of the subcarriers affiliated to that subband. ψ contains the set of indices of the active subbands (subcarriers with non-negative values for R_i), N'_B is the number of active groups in the set. The grouping of subcarriers can be based on their indices (successive subband grouping) or based on the order of the channel gain (sorted subband grouping).

3.2.3 Spectrum Pooling and Sidelobes Cancellation Carriers Insertions

In previous chapter the windowing design was described. The window according Figure 2.7 (b) is applied in order to reduce the bit rate loss. The scheme can be seen as having overlapped OFDM. Figure 3.5(a) depicts the overlapping time domain OFDM signal (with duration $2T_u(\alpha+1)$) with overlap length $2\alpha T_u$.

Another overlapped OFDM scheme is depicted in Figure 3.5 (b). The overlap length is arranged in such a way that the useful signal in the area of T_{GI} and T_u of one OFDM symbol will not be overlapped with the useful signal of the following OFDM symbol. For this reason, the value of the signals outside the T_{GI} and T_u areas of the OFDM symbol (see Figure 3.5(b)) are filled with zeros.

Another approach to reduce the long symbol duration is by applying the sidelobes cancellation carriers technique proposed in [21]-[23] which can avoid the long symbol duration due to windowing. The sidelobes cancellation carriers are carriers that will cancel the peak sidelobes at some optimization points in the LU band. The principle of sidelobes carriers de-activation is described in Figure 3.6. By looking at the optimization area, we can choose the number of side-lobe peaks that we want to nullify. Accordingly, the number of peaks to be nullified will determine the number of sidelobes cancellation carriers required.

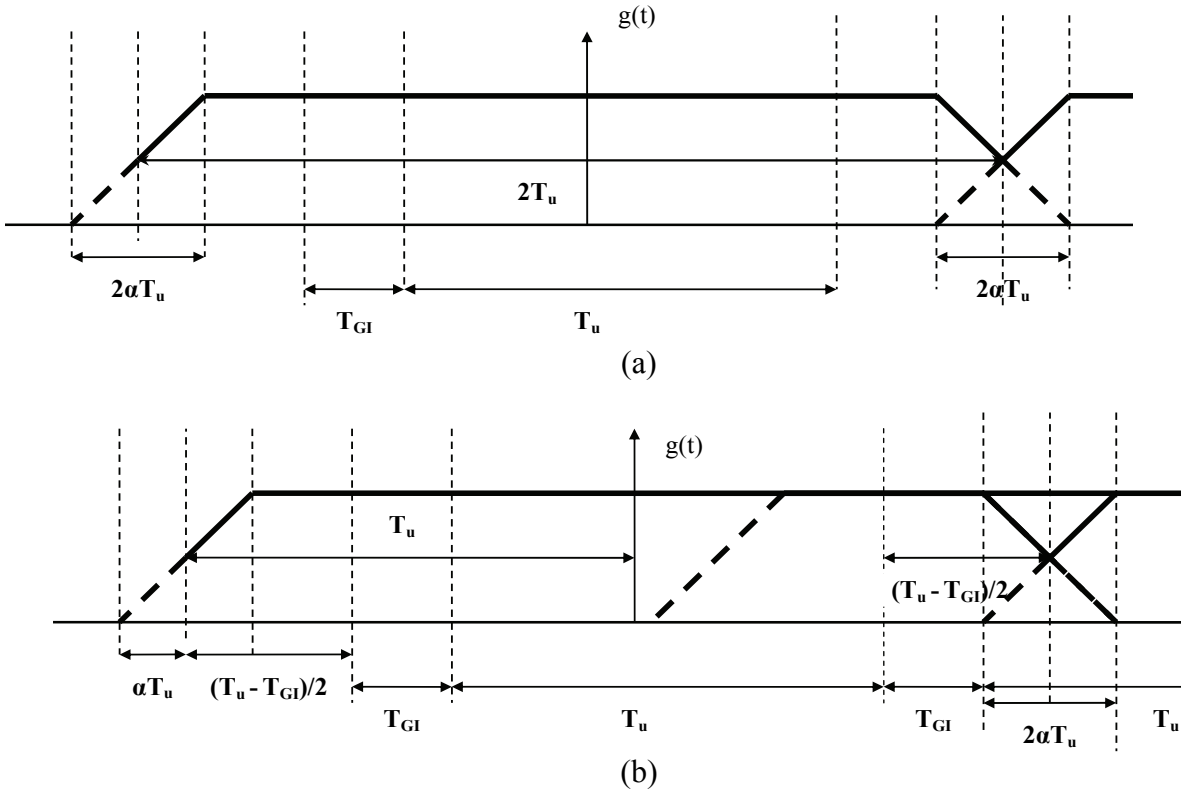

Figure 3.5 : Window design (a) without influence to the transmitted signal in the period of $0 \le |t| \le \frac{T_u}{2}(1-\alpha)$ with shorter overlap period and (b) with longer overlap period

In [21] and [22] the optimum number of cancellation carriers is found by observing the resulting sidelobes from the OFDM power spectrum density with cancellation carriers through simulations. The results revealed that more than 2 cancellation carriers on each border side with respect to the LU band will not add significantly to the sidelobes reduction. The sidelobes cancellation carriers will be used in the replacement scheme of de-activated carriers. Choosing l peak points to be nullified requires a set of l linear equations that involves l variables. The example in Figure 3.6 shows the problem of determining the amplitude of the 4 cancellation carriers (Xc_{cc1}, Xc_{cc2}, Xc_{cc3}, Xc_{cc4}). The amplitude value of these 4 cancellation carriers will be obtained by solving 4 linear equations according to the general optimization equation in eq. (3.16) for each frequency of the sidelobe peak i (i.e., $f_o(i)$),

$$\sum_{cc=cc1}^{N_o} \left[Xc_{cc} G_{cc}(f_o(i) - f_{cc}) \right] + X_{dd}(f_o(i)) = 0 \quad , \quad i = 1,...,N_o \tag{3.16}$$

where N_o is the number of optimization points (in our case is 4), f_{cc} is the frequency location of the cancellation carrier cc, $G_{cc}(f)$ is the window spectrum ($G(f)$ is derived from the Fourier

transform of the window function $g(t)$) of the the cancellation carriers cc on frequency f (if rectangular window is used, $G_{cc}(f)$ will be a sinc function), and $X_{dd}(f_o(i))$ is the OFDM spectrum without cancellation carriers (i.e. OFDM spectrum by replacing the cancellation carriers with de-activated carriers) on the side-lobe peak i .

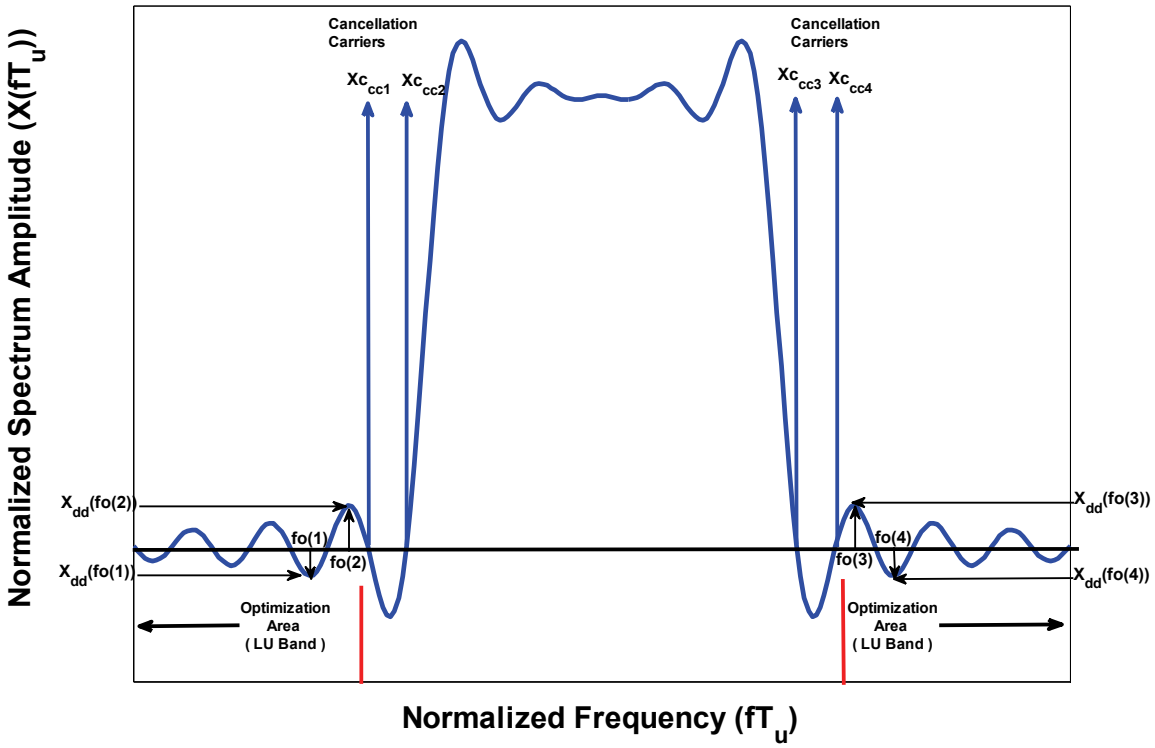

Figure 3.6: Cancellation carriers technique by determining the side-lobe peak points to be eliminated in the optimization area

Due to carriers de-activation in the LU band there will be some unused power that can be allocated to the cancellation carriers in case high cancellation carriers amplitudes occur. The remaining power can be allocated to the data signal in order to have a better data detection at the receiver. The optimization problem in eq. (3.16) takes all cancellation carriers into account. In case the distance between the cancellation carriers at one edge and the side-lobe peak points at the other edge is large, then the influence of the cancellation carriers side-lobes at that side-lobe peak point can be neglected (e.g. $X_{c1}(f_o(3)\text{-}f_{c1}) \approx X_{c2}(f_o(3)\text{-}f_{c2}) \approx X_{c3}(f_o(2)\text{-}f_{c3}) \approx X_{c4}(f_o(2)\text{-}f_{c4}) \approx 0$). Therefore, the optimization can be separated by solving the equations with variables involving the subset of cancellation carriers at one edge, and then solving the equations with variables involving the second subset of cancellation carriers at the other edge. The side-lobes reduction by the cancellation carriers can be seen in Figure 3.7. The spectrum is derived from a rectangular windowed OFDM spectrum with 16 FFT points, 9 active carriers located in the middle that makes 4 carriers on the left and 3 carriers on the right are

de-activated. Each active carrier is allocated with a BPSK symbol. Two cancellation carriers are located at the left edge, and two are at the right edge. The peaks at the optimization points are eliminated, thus lower side-lobes are achieved.

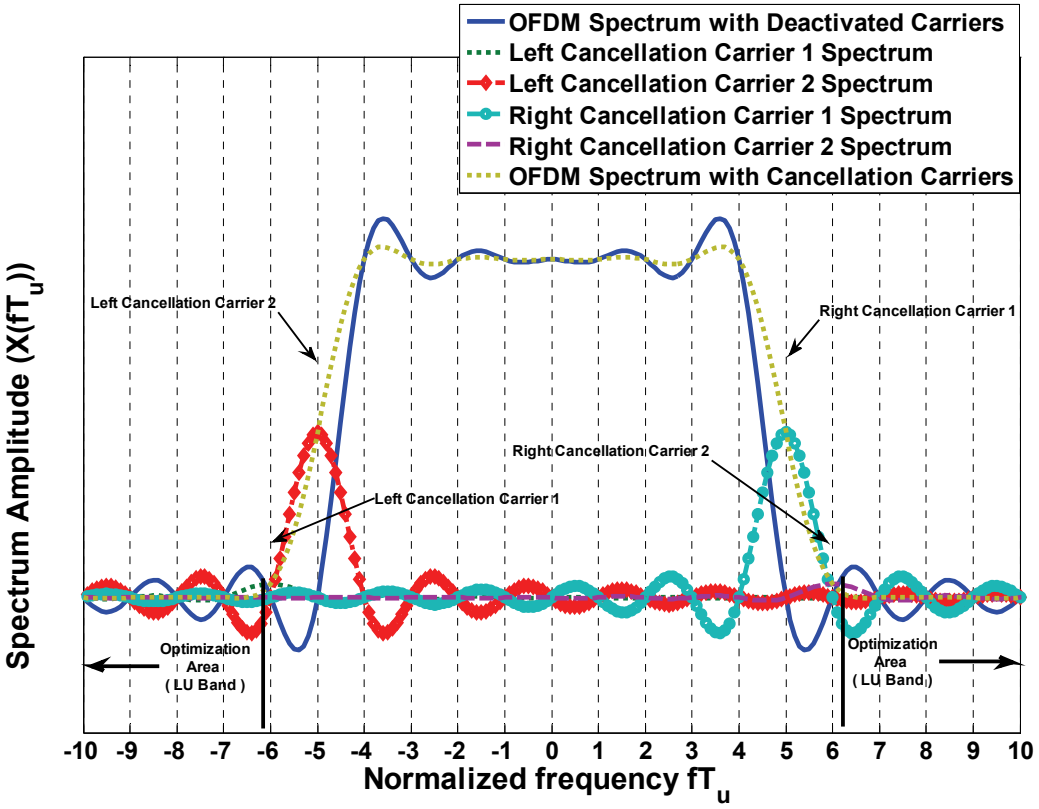

Figure 3.7: The rectangular windowed OFDM spectra with sidelobe suppression by using two cancellation carriers on each edge

Fig. 3.8 depicts the comparison between the side-lobes of a combined rectangular windowed OFDM with de-activated carriers, cancellation carriers, and cancellation carriers combined with de-activated carriers and other kind of windows. The OFDM parameters in Figure 3.8 are the same as the ones in Figure 3.7. The duration of the other windows (non-rectangular) is $2T_u(\alpha+1)$, hence the spectrum is orthogonal in the frequency period of $1/(2T_u)$ and the useful signal is not deteriorated by the window. The sidelobe of the combined T_u duration rectangular window with the sidelobes cancellation carriers in the optimization area is considerably lower than for the other form of windows. By observing the outcomes of having lower side-lobes and shorter symbol duration, the combination of OFDM with de-activation of carriers in the LU band and sidelobes cancellation carriers located adjacent to LU band is a promising modulation technique to be applied in Cognitive Radio.

Without the sidelobes cancellation carriers, the application of combined adaptive bit loading and spectrum pooling is restricted by the allowable side-lobes power ($P_{Threshold}$) in the LU

band. Inserting the sidelobes cancellation carriers will ease the application of adaptive bit loading since each sidelobes cancellation carrier will make sure that the OFDM based CR sidelobes will be reduced. Hence the adaptive bit loading algorithm can be optimally utilized. Therefore, the sidelobes increase in the LU band due to the allocated bits will be counteracted by the insertion of cancellation carriers.

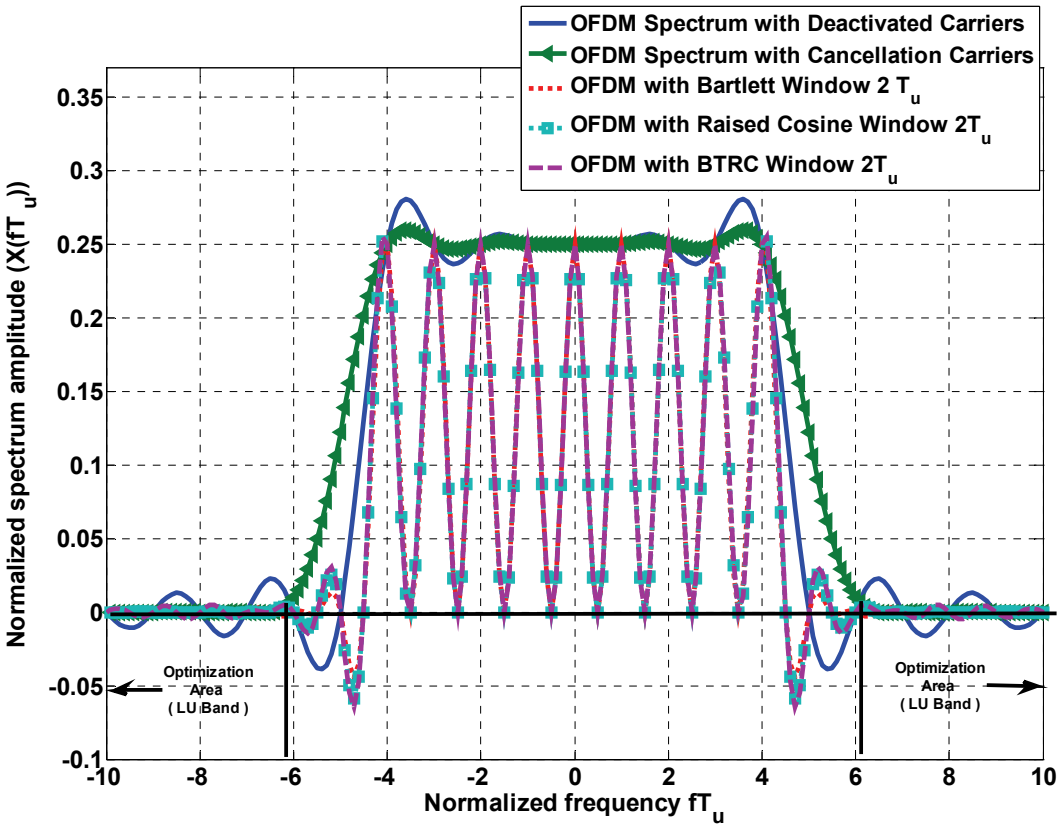

Figure 3.8: Spectrum side-lobe comparisons between rectangular windowed OFDM with de-activated carriers, cancellation carriers, and, cancellation carriers combined with different kind of windows ($\alpha = 0.25$) and de-activated carriers

3.2.4 Combined Adaptive Bit Loading with Spectrum Pooling and Sidelobes Cancellation Carriers Simulation Results and Analysis

In the initial work we applied combined adaptive bit loading with Spectrum Pooling. The spectrum pooling was applied carefully in such a way that the mutual interference between the LU and the Cognitive Radio system is very low (negligible). The simulation parameters are given in Table 3.1. We hereby assume perfect synchronization between transmitter and receiver, and the receiver can detect the modulation mode on each carrier correctly.

Figure 3.9 shows the performance comparison between several adaptive bit loading schemes and the Better Than Raised Cosine (BTRC) window with $\alpha = 21/128$, under the condition of perfect channel estimates. It is shown that the Fischer algorithm is superior to other bit loading algorithms. At a BER=10^{-2}, around 5 dB gain is then achieved [47], [48]. Since the window shape will not affect the BER performance of the OFDM system (see Figure 3.5(a)), it can be assumed that the the gain remains for other window forms such as Raised Cosine and Bartlett.

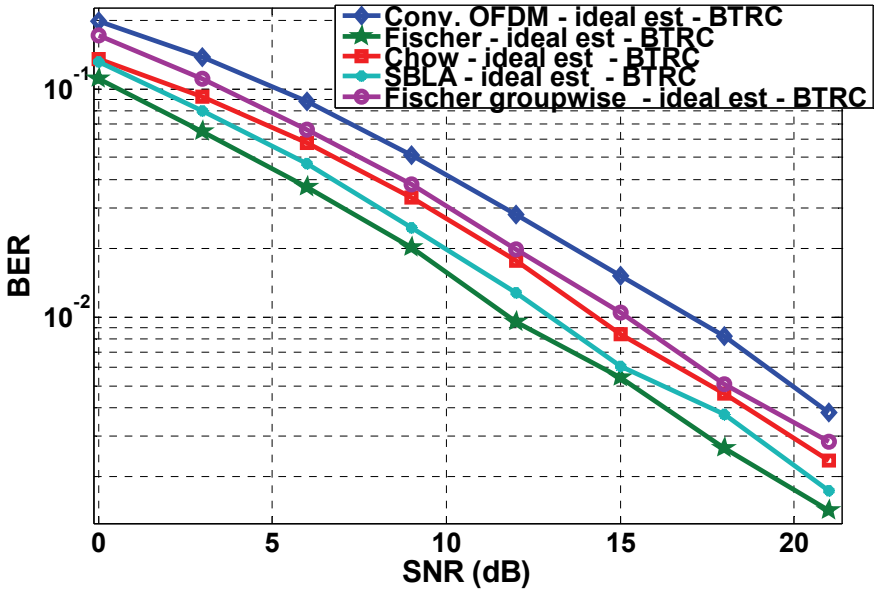

Figure 3.9 : BER vs SNR (dB) comparisons of Adaptive Bit Loading algorithms using Better Than Raised Cosine Window form according the design in Figure 2.3(b) with $\alpha = 21/128$ (T_{GI}/T_u) and allowable modulation modes : BPSK, 4-QAM,16-QAM, 64-QAM, and 256-QAM

In the case of an imperfect channel estimate after Wiener filtering, the adaptive bit loading performance will degrade. The results show that the SNR degradation of the Fischer algorithm with Wiener filtering is about 7 dB at a BER of 10^{-2} compared to the case with perfect channel knowledge as depicted in Figure 3.10 [47]. With respect to the CR sidelobes, its impact to the CR BER will be manifested if the guard band between LU and CR is not really implemented; hence, the I term in eq. (3.10) will exist and should be treated as extra noise that (according to the available bit loading algorithm) will be counteracted by reducing the bit allocations on the carriers contaminated by those interferences for the purpose of maintaining the targeted BER.

Table 3.1: Simulation Parameters

OFDM Parameters		Channel Parameters	
Carr. freq.	5.5 GHz	Max. channel delay	5 μs
# of carriers	256	# of Taps	11
Carr. spacing	31.25 kHz	Taps distance	0.5 μs
Guard time	5.25 μs	#. of Paths	12
Bit Rate	3 Mbps	Veh. speed	100 Km/hr
Chn. coding	OFF	Fading Model	Rayleigh

An imperfect channel estimate denotes an imperfect frequency shift recovery by the channel estimation module due to the Doppler effect, resulting into an intercarrier interference (ICI) effect. The higher the sidelobes the larger the ICI which will degrade the BER performance. By decreasing the sidelobes the impact of ICI will be reduced. The phenomenon can be analyzed from the received signal on subcarrier k (Y_k) of an OFDM symbol after fading removal by utilizing the estimated channel transfer functions (CTFs):

$$
\begin{aligned}
Y_k &= \sum_{n=1}^{N_{FFT}} \frac{X_n H_n e^{j2\pi f_s t}}{\hat{H}_n e^{j2\pi \hat{f}_s t}} \int_{-(1+\alpha)T_u}^{(1+\alpha)T_u} g(t) e^{-j2\pi(f_k - f_n)t}\, dt \\
&= \sum_{n=1}^{N_{FFT}} X_n A_n e^{j2\pi \Delta f_s t} \int_{-(1+\alpha)T_u}^{(1+\alpha)T_u} g(t) e^{-j2\pi(f_k - f_n)t}\, dt \\
&= \sum_{n=1}^{N_{FFT}} X_n A_n \int_{-(1+\alpha)T_u}^{(1+\alpha)T_u} g(t) e^{-j2\pi(f_k - f_n - \Delta f_s)t}\, dt \\
&= \underbrace{X_k A_k \int_{-(1+\alpha)T_u}^{(1+\alpha)T_u} g(t) e^{j2\pi \Delta f_s t}\, dt}_{Desired\ \ Signal} + \underbrace{\sum_{\substack{n=1 \\ n \neq k}}^{N_{FFT}} X_n A_n \int_{-(1+\alpha)T_u}^{(1+\alpha)T_u} g(t) e^{-j2\pi(f_k - f_n - \Delta f_s)t}\, dt}_{ICI\ \ Term}
\end{aligned}
\tag{3.17}
$$

where $g(t)$ is the window function, N_{FFT} is the number of FFT points (number of subcarrier), H_n, $\hat{H}_n$, and f_n are the CTF, estimated CTF and frequency of subcarrier n respectively , f_s is the carrier frequency shift due to the channel fading (can be seen as Doppler effect), $\hat{f}_s$ is the estimated carrier frequency shift, $\Delta f_s = f_s - \hat{f}_s$, and $A_n = H_n / \hat{H}_n$. The first term in eq. (3.17) is the desired signal while the second term is the ICI contribution. By observing eq. (3.17) we

can see that the window function $g(t)$ plays a role in determining the ICI quantity. Therefore by proper selection of a window $g(t)$ with low sidelobes, the ICI effect can be minimized.

The BER results of the OFDM-based CR system employing combined adaptive bit loading, spectrum pooling and cancellation carriers will have the same tendency as shown in Figure 3.9, where carrier-wise bit loading using the Fischer-Huber algorithm outperforms the other algorithms since the useful signal will not be affected by the window or by the sidelobes cancellation carriers. The carriers close to the border with the LU band would be the most interfered carriers by the LU access due to the LU signal side-lobes, but this condition will be anticipated by adaptive bit loading algorithm and by taking into account the interference term as described in eq. (3.10). The bits allocated to these carriers (close to the border with the LU band) will be small, and a small constellation size is more robust against interference and noise.

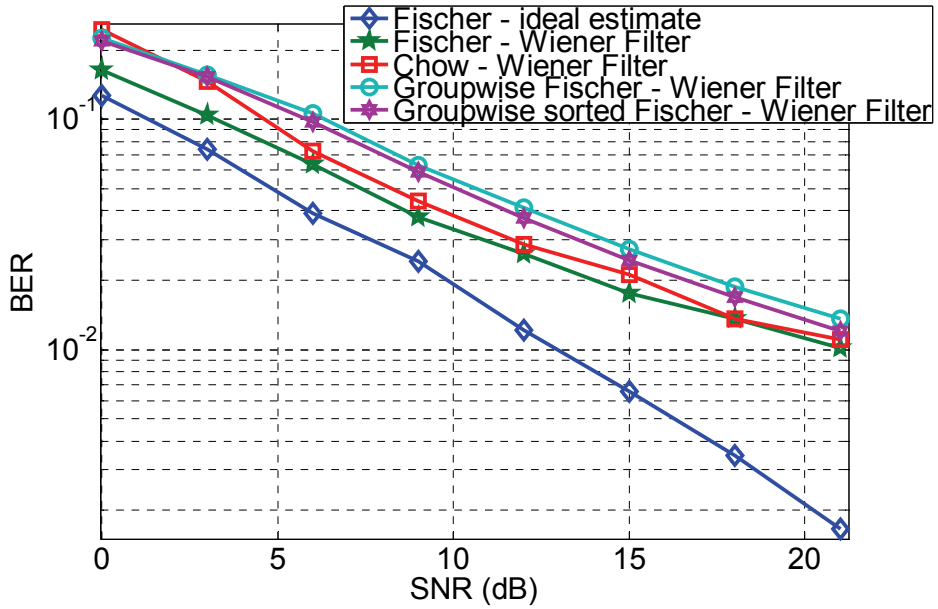

Figure 3.10: BER vs SNR (dB) for Adaptive OFDM after a Rect Wiener Filter Channel Estimation; allowable modulation modes: BPSK, 4-QAM,16-QAM, 64-QAM, and 256-QAM

An important issue in applying combined adaptive bit loading with spectrum pooling and cancellation carriers into an OFDM-based CR is the interference quantity (sidelobes) that the CR system will cause to the neighboring LU band. We have discussed that the adaptive bit loading will take care of the constellation size of carriers located at the border with the LU by considering the LU sidelobes quantity on those carriers. The worst condition is when the interference by the LU to the OFDM based CR carriers at the border stays undetected; further also, if the sidelobes contributions of all OFDM-based CR carriers on one reference peak in the LU band have the same phase, and each of them has maximum symbol values that will add together constructively and so making a high sidelobe peak.

In order to further explain the impact of adaptive CR, we start from a normalized spectrum amplitude example of an OFDM-based CR with 256 carriers. 36 carriers in the middle (carriers 111 -146) are occupied by the licensed user. Totally 40 carriers are de-activated, that means carriers 1-108 and 149-256 are active carriers. If 2 sidelobes cancellation carriers are inserted on each side of the border with the LU band then they will be located on carriers 109,110, 147 and 148. If only 1 sidelobe cancellation carrier is inserted then only carriers 109 and 148 are used. As shown in Figure 3.8 the maximum sidelobe peak will normally occur within a normalized frequency distance of 0.5 to the closest sidelobes cancellation carrier on the LU band. (e.g on position 110.5 for the 2 sidelobes cancellation carriers insertion and on position 109.5 for the 1 sidelobe cancellation carrier insertion). The worst case will be if all the carriers will apply 256 QAM. The 256 QAM modulation gives a high error vector magnitude (EVM) compared to the lower constellation sizes and as a consequence gives the highest impacts on the BER performance [49]. This is an important reason why this constellation size is not used in any practical standard. However, in this chapter we only try to observe the impact of such worst case situation on our OFDM based CR signal. Putting $fT_u=110.5$ and also $fT_u=109.5$ into eq. (2.1) and having $g(t)$ as rectangular window, then the maximum peak will occur if the odd numbered carriers produce a negative symbol QAM point with the highest amplitude (in 256 QAM this is the symbol on the $-15 - j15$ point) while the even numbered carriers produce a positive symbol QAM point with the highest amplitude (in 256 QAM this is the symbol on the $15 + j15$ point). The sidelobes in the region of $fT_u=109.5$ untill $fT_u=147.5$ for the OFDM with de-activated carriers, 1 sidelobe cancellation carrier and 2 sidelobes cancellation carriers cases are depicted in Figure 3.11. The roll-off factor $\alpha=0.2$.

As a consequence of applying the adaptive bit loading, there is the possibility that the sidelobes cancellation carriers require high power as can be seen in Figure 3.11. This power requirement can be compensated as the unused power due to carriers de-activation in the LU band can be allocated to those sidelobes cancellation carriers. Further, by combining the sidelobes cancellation carriers with time domain windowing as suggested in [22] and [23] (e.g Raised Cosine, BTRC, or farcsech), the amplitude of the sidelobes cancellation carriers can be further reduced. Figure 3.11 depicts the impact of the raised cosine window in avoiding high amplitude of sidelobes cancellation carriers compared to sidelobes cancellation carriers combined with rectangular window. The results in [24] have shown that the combination of 2 cancellation carriers on each side adjacent to the LU band and a raised cosine window with a roll-off factor $\alpha=0.2$ gives more than 30 dB sidelobes reduction compared to the conventional OFDM. In comparison with our observation in the worst case scenario, the combination between 2 sidelobes cancellation carriers on each side adjacent to the LU band and the raised cosine window with the same roll-off factor value gives a sidelobes reduction more than 30 dB, even more than 40 dB compared to the rectangular window with carriers de-activation as depicted in Figure 3.11(b).

With respect to the peak to average power ratio (PAPR) problem in OFDM, the sidelobes cancellation carriers contribution to the PAPR growth is described as given in eq. (3.18),

$$PAPR\left(x\left[k\right]\right)=\frac{\max_k\left(\left|\frac{1}{\sqrt{N_{FFT}}}\left(\sum_{\substack{n=0\\n\neq cc}}^{N_{FFT}-1}X_n e^{j\frac{2\pi kn}{N_{FFT}}}+\sum_{cc=cc1}^{N_{cc}}Xc_{cc}e^{j\frac{2\pi kcc}{N_{FFT}}}\right)\right|^2\right)}{E_x\left[\left|\frac{1}{\sqrt{N_{FFT}}}\sum_{n=0}^{N_{FFT}-1}X_n e^{j\frac{2\pi kn}{N_{FFT}}}\right|^2\right]}$$
$$=\frac{\max_k\left(\left|\frac{1}{\sqrt{N_{FFT}}}\left(\sum_{\substack{n=0\\n\neq cc}}^{N_{FFT}-1}X_n e^{j\frac{2\pi kn}{N_{FFT}}}+\sum_{cc=cc1}^{N_{cc}}Xc_{cc}e^{j\frac{2\pi kc}{N_{FFT}}}\right)\right|^2\right)}{E_x\left[\left|\frac{1}{\sqrt{N_{FFT}}}\sum_{n=0}^{N_{FFT}-1}X_n e^{j\frac{2\pi kn}{N_{FFT}}}\right|^2\right]} \tag{3.18}$$

where $x(k)$ is the time domain OFDM signal for the k th sample, Xc_{cc} is the symbol value on the sidelobes cancellation carriers position cc, E_x is the averaging operator, $cc1$ is the first sidelobes cancellation carrier, N_{cc} is the total number of sidelobes cancellation carriers being inserted, while the rest of the symbols have been explained before (in eq. (2.1)). By observing eq. (3.18) we guess that the sidelobes cancellation carriers will not give a significant additional PAPR growth. [The peak power in the time domain signal is the result of accumulated coherent phase of the multiplication between the frequency domain OFDM symbol (X_n) and the factor $e^{j\frac{2\pi kn}{N_{FFT}}}$ $\left(x_k=\frac{1}{N_{FFT}}\sum_{n=0}^{N_{FFT}}X_n e^{j2\pi nk}\right)$]. We predict that less than 2 % peak power contribution comes from the sidelobes cancellation carriers (assuming N_{FFT}=256, N_{cc}=4). It is possible that this 2% contribution raises a higher PAPR. The evaluation in [23], based on simulations, shows that the sidelobes cancellation carriers give only a slight PAPR increase.

To check this juncture we have simulated random symbols from a 256 QAM constellation mapping (in order to demonstrate the effect of adaptive bit loading) applied in combination with sidelobes cancellation carriers and windowing. The OFDM parameters remain the same with the parameters used in producing Figure 3.11. The complementary cumulative distribution function (CCDF) graphs of the PAPR for adaptive OFDM with de-activation carrier and rectangular window, with addition 2 cancellation carriers on each edge, or 2 cancellation carriers combined with raised cosine windows are given in Figure 3.12. The Figure indicates an insignificant impact by the sidelobes cancellation carriers and its combination with low sidelobes time domain windowing, in this case the Raised Cosine window was used to the PAPR growth.

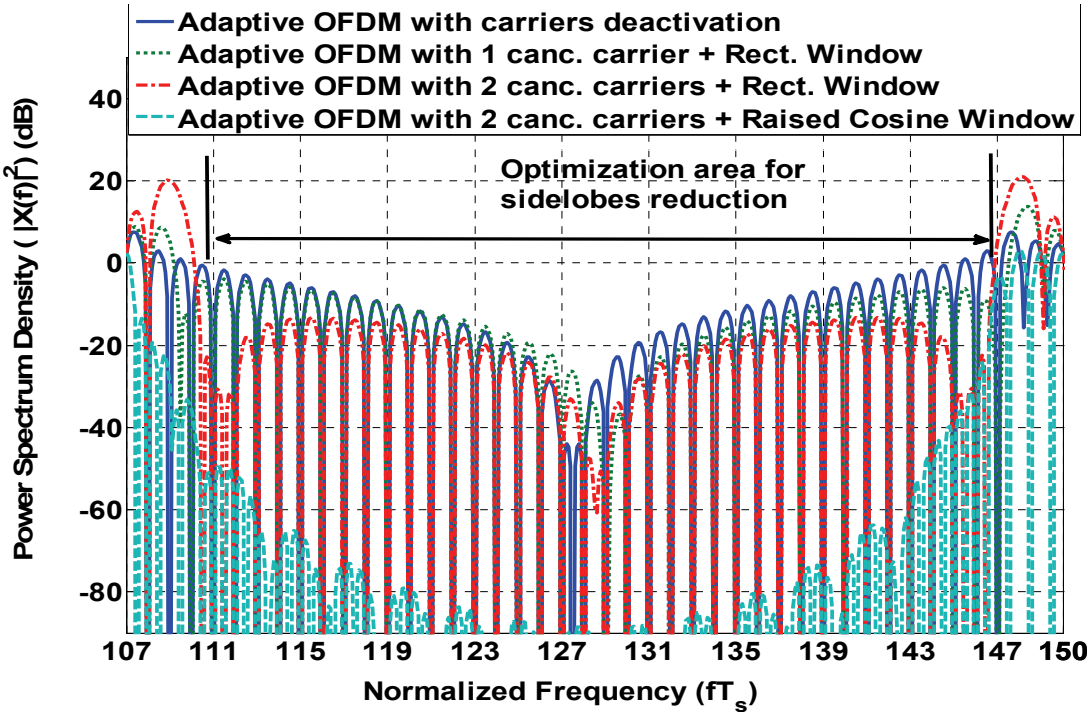

(a)

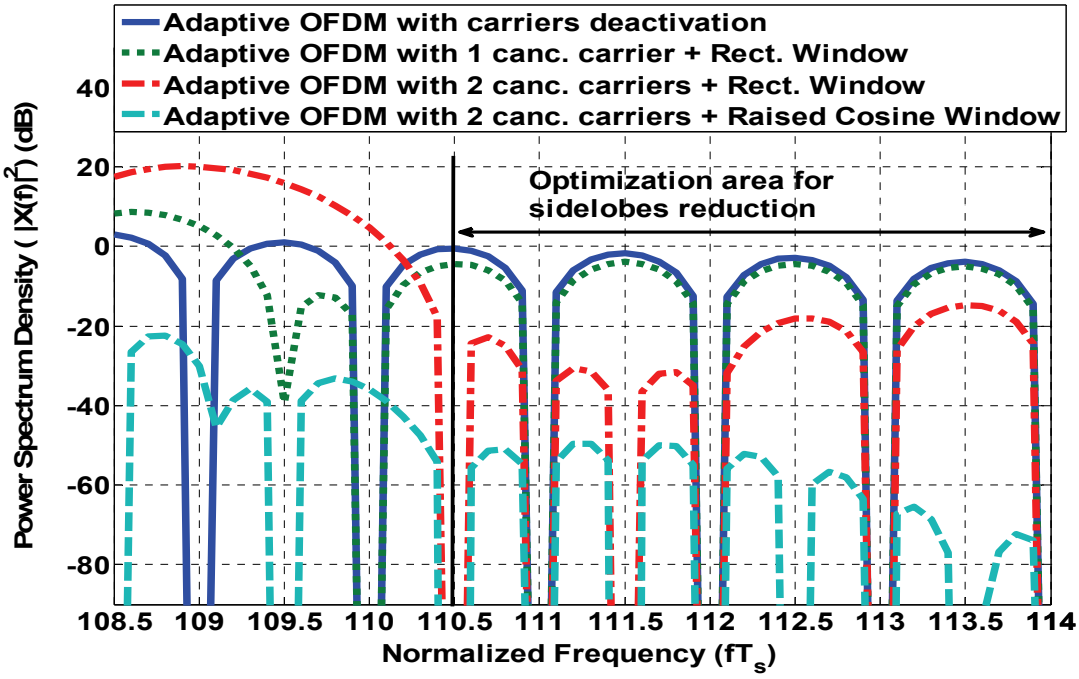

(b)

Figure 3.11 : Spectrum sidelobe comparison between the rectangular windowed OFDM with de-activated carriers; 1 sidelobe cancellation carrier, 2 sidelobes cancellation carriers at the border with the LU band and 2 sidelobes cancellation carriers with a raised cosine windowed OFDM in combination with adaptive bit loading in the worst case scenario with $\alpha=0.2$, (a) the complete optimization area and (b) left part of the optimization area

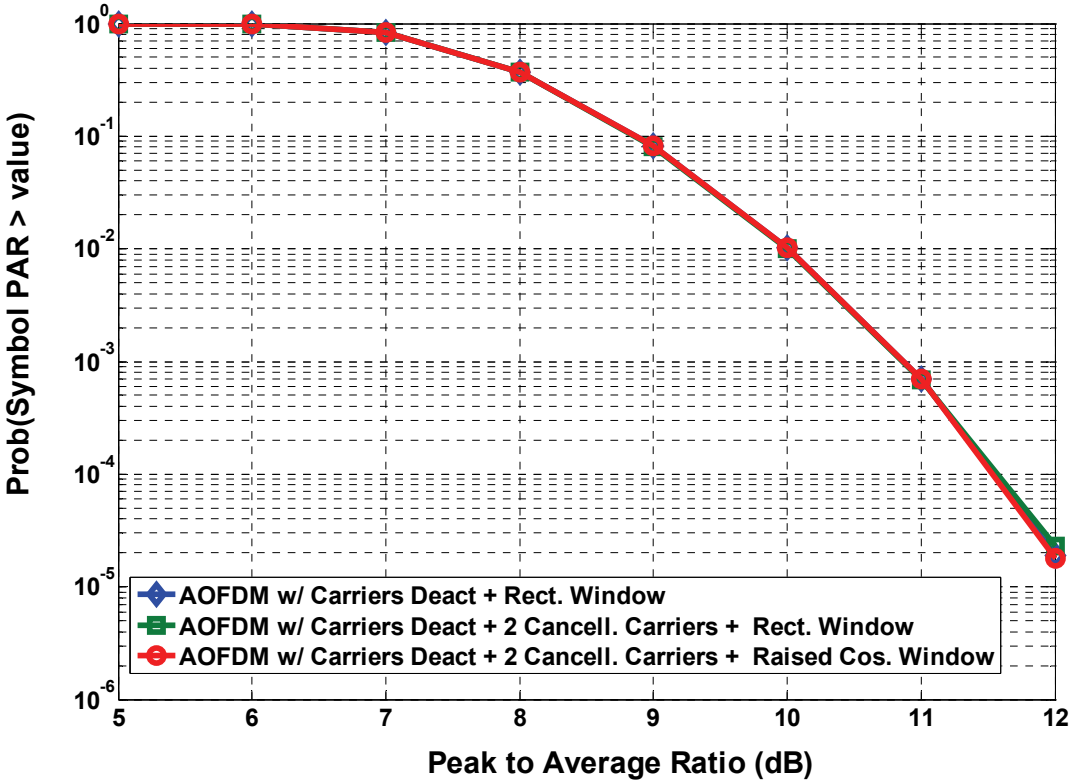

Figure 3.12 : PAPR CCDF comparison of a) Adaptive OFDM with a carriers de-activation and Rectangular window; b) combination of Adaptive OFDM with a carriers de-activation and 2 cancellation carriers adjacent to the LU band and using a Rectangular window, and c) combination of Adaptive OFDM with a carriers de-activation and 2 cancellation carriers adjacent to the LU band and using a Raised Cosine window

It has been discussed in section 2.2 that in order to have a window that will not influence (deteriorate) the bit rate, the useful signal duration should be $2T_u$; a longer signal will reduce therefore the transmission bit rate. The windowing strategy according to Figure 3.5 (b) tries to reduce the total OFDM frame duration as low as possible, therefore this window would be a promising alternative to attain the targeted bit rate.

PAPR is a common problem in every OFDM system, therefore, the current available conventional OFDM-PAPR reduction techniques can be applied in the Cognitive Radio context. According to the analysis, the OFDM based CR bit rate and sidelobes reduction capability will be the trade-off optimization problem in the CR system.

3.3 Wavelet Packet Modulation by Frequency Selective Wavelet for Cognitive Radio[**]

The Fourier transform in OFDM uses Cosine and Sinusoidal waveforms as its transformation function. These Cosine and Sine can be replaced by wavelet basis function. Hence a new modulation technique termed as wavelet packet multi carrier modulation (WP-MCM) is formed. In this way, there is a degree of freedom in shaping the spectrum of the wavelet based OFDM. In the context of Cognitive Radio, the spectrum shaping is crucial. The Cognitive Radio spectrum should be shaped in such a way that it will not disturb the legacy system signal. The co-existence between the Cognitive Radio and the legacy system should be preserved. The flexibility in shaping the wavelet-based OFDM spectrum makes wavelet based OFDM interesting to be explored further.

The two fundamental tasks of the WP-MCM cognitive system are – 1. Radio spectrum analysis to gather intelligence on spectrum holes and occupied bands, and 2. WP-MCM based adaptive data transmission on idle bands. At the transmitting end, an incoming high-rate serial data stream is split into M lower-rate parallel streams. The data in each parallel branch is then upsampled by M and used to modulate M subcarriers. Meanwhile, the spectrum estimator gauges the channel and performs a radio scene analysis to estimate LU frequency bands and detect spectrum holes. Based on the spectrum estimates, the cognitive modules dynamically de-activate those sub-channels of the WP-MCM system that lie in and around the spectrum of the LU. The idea is to dynamically sculpt the CR transmission signal so that it has no or very little time-frequency components competing with the LU. In this way the CR can seamlessly blend with the LU operation. The sub-carriers are then modulated and scaled to the desired energy level to obtain the WP-MCM transmission signal. The transmitted signal in the discrete domain, $y[k]$, is composed of successive modulated symbols, each of which is constructed as the sum of M sub-carriers, $\varphi_m[k]$, individually modulated. It can be expressed in the discrete domain as:

$$y[k] = \sum_{s} \sum_{m=0}^{M-1} (a_{s,m} \varphi_m[k - sM]) \tag{3.19}$$

where $a_{s,m}$ is a constellation encoded sth data symbol modulating the mth waveform. To reduce the error probability, the sub-carriers are made orthogonal. The orthogonality of the subcarriers is defined as [50]:

$$< \varphi_m[k], \varphi_n[k] >= \delta[m - n] \tag{3.20}$$

[**] This work is the result of collaboration with M.K. Lakshmanan. The theoretical content of this section is selected from the papers [6], [62], [65] and the paper from M. K. Lakshmanan and H. Nikookar, "Optimum Wavelet Packet Construction for Multicarrier Based Cognitive Radio system", published in *Proc. Int. Symp. on Wireless Personal and Multimedia Communications (WPMC)*, Finland, Sept. 2008.

where, $<\cdot>$ represents an inner product operation and $\delta[\cdot]$ is the dirac-delta function. In OFDM, the discrete functions $\varphi_m[k]$ are complex basis functions $g[k]e^{\frac{j2\pi mk}{M}}$ limited in the time domain by the window function $g[k]$. In the WP-MCM scheme, the subcarrier waveforms are obtained by successively decomposing a couple of elementary paraunitary filters [50]-[52]. The nature of the subcarriers therefore depends on the properties of the underlying filters used; therefore filters with suitable properties have to be developed. More on this will be presented in the following subsection. The steps to generate the WP-MCM transmission signal are elucidated in Figure 3.13.

To detect the transmitted data, the received signal $r[k]$ is de-convolved with a receiver sub-carrier waveforms, $\tilde{\varphi}_m[k]$. The sub-channels $\tilde{\varphi}_m[k]$ are the duals of $\varphi_m[k]$ and their orthogonality can be expressed as

$$<\varphi_m[k],\tilde{\varphi}_n[k]>=\delta[m-n] \tag{3.21}$$

The estimate of each subchannel $\hat{a}_{s,m}$ is derived from

$$\hat{a}_{s,m}=(r[k]*\tilde{\varphi}_m[k-sM])\downarrow_M \tag{3.22}$$

Here the down arrow represents decimation by M while * is the convolution operation. These estimates are then de-mapped and parallel to serial converted to identify the transmitted data.

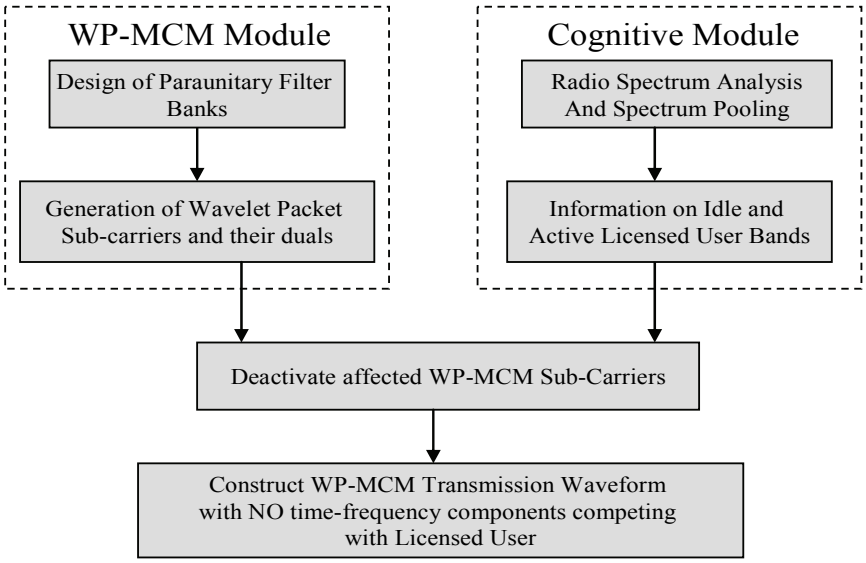

Figure 3:13: Fundamental Blocks of WP-MCM based Cognitive Radio system

3.3.1 Generation of Wavelet Packet Sub-Carrier Bases

The subcarrier signal waveforms in traditional MCM implementations, such as OFDM, are sine / cosine basis functions. In WP-MCM the sub-carrier waveforms are derived from poly-channel tree structures built by cascading multiple two-channel filter banks like the one shown in Figure 3.14.

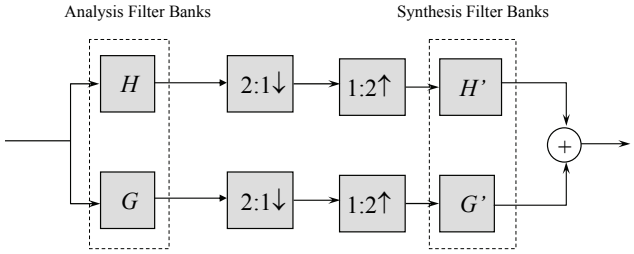

Figure 3.14: Two channel filter bank analysis with analysis filters *H* and *G* (low and high pass, respectively) and synthesis filters *H*'and *G*' (low and high pass, respectively)

A two-channel filter bank consists of a set of 4 perfect reconstruction filters (2 high pass and 2 low pass) which allow the decomposition and reconstruction of a signal without amplitude or phase or aliasing distortion [53]. The two-channel filter bank has the property of splitting the signal into two lower resolution versions – namely the coarse (low pass) and the detail (high pass). When the decomposition into coarse and detail components is continued iteratively, it leads to the generation of wavelet packet bases. When the perfect reconstruction filters used satisfy an additional property known as the para-unitary condition (explained later in section 3.3.3), they lead to wavelet packet bases with impulse responses that are mutually orthogonal to one-another and to their duals [53]-[55].

The wavelet packet sub-carriers (to be used at the transmitter end) are generated through a multi-channel filterbank consisting of cascaded two-channel filters applying the synthesis filters (*H*' and *G*'). This represents an inverse discrete wavelet packet transformation (IDWPT) and consists of binary interpolation (up-sampling) by 2, filtering and recombination at each level. The number of iterations *J* determines the number of subcarriers *M* generated and the relationship is given as $M \le 2^J$ .The time domain representation of the wavelet packet bases $\psi_i[k]$ is obtained through a simple convolution rule.

$$\begin{aligned} &\psi_i[k] = w(k) * w(k/2) * .... * w(k/2^{J-2}) * w(k/2^{J-1}); \\ &\text{where}, 0 \le i \le 2^J - 1 \\ &\text{and}, w(k) = \begin{cases} h'(k), \text{for lowpass branches} \\ g'(k), \text{for highpass branches} \end{cases} \end{aligned} \tag{3.23}$$

Here *h'* and *g'* stand for the impulse responses of the low and high pass synthesis filters, respectively.

3.3.2 Generation of Wavelet Packet Dual Bases

The wavelet packet duals (to be used at the receiver end) are obtained from multi-channel filter bank analysis too, though the processes are reversed. The duals are obtained from the analysis filters (*H* and *G*) through the analysis procedure which consists of filtering, decimation (down sampling) by 2 and decomposition at each stage. This process is called discrete wavelet packet transformation (DWPT). First the signal is passed through a half-band high and low pass filter. The half-band low pass filter removes all frequencies that are above half of the highest frequency, while the half-band high pass filter removes all frequencies that are below half of the highest frequency of the signal. Such a half-band filtering halves the resolution, but leaves the scale unchanged. The signal is then sub-sampled by two since half of the number of samples is redundant, according to the Nyquist's rule. This decomposition halves the time resolution since only half the number of samples then comes to characterize the entire signal. Conversely, it doubles the frequency resolution, since the frequency band of the signal spans only half the previous frequency band effectively reducing the uncertainty by half. This procedure is iteratively repeated till the desired degree of resolution. The duals $\tilde{\psi}_i[k]$ are derived from:

$$\begin{aligned} &\tilde{\psi}_i[k] = f(k) * f(2k) * .... * f(2^{J-2}k) * f(2^{J-1}k); \\ &\text{where}, 0 \le i \le 2^J - 1 \\ &\text{and}, f(k) = \begin{cases} h(k), \text{for lowpass branches} \\ g(k), \text{for highpass branches} \end{cases} \end{aligned} \tag{3.24}$$

In (3.24) *h* and *g* denote the impulse responses of the low and high pass analysis filters, respectively. Figure 3.15 illustrates the derivation of 8 wavelet packet bases and their duals from a cascaded level-3 tree structure. Accordingly by following the rules of obtaining the wavelet packet subcarrier bases in (3.23) and the duals according to (3.24), the Mallat reconstruction and decomposition filterbanks [56] are depicted in Figure 3.16.

Due to the convolution process between the parallel data stream with the filter bank, the resulting output of the time domain signal per WP-MCM symbol will be longer than the number of the subcarriers. Therefore during the transmission, the WP-MCM symbols will overlap. The overlapping distance should be designed in such a way that the total number of samples in one WP-MCM frame will be equal to the multiplication between the number of subcarriers and the number of WP-MCM symbol per frame.

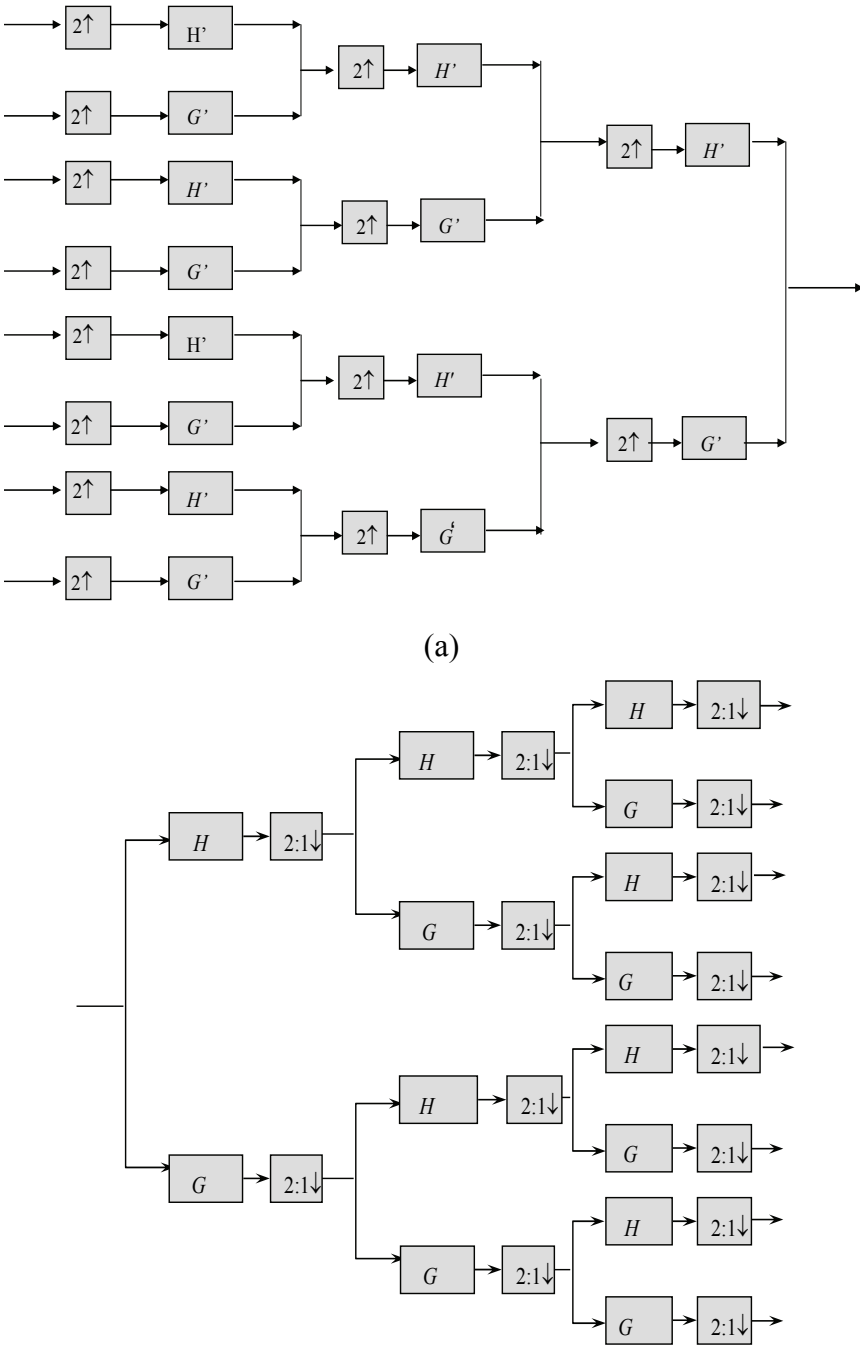

(a)

(b)

Figure 3.15 Generation of wavelets. (a) A level-3 tree gives 8 wavelet packet bases for the transmitter and their (b) duals for the receiver. The up arrows represent interpolation by 2, the down arrows represent decimation by 2. *H'* and *G',* denote the frequency responses of the low and high pass reconstruction filters, while *H* and *G* denote the frequency responses of the low and high pass decomposition filters, respectively

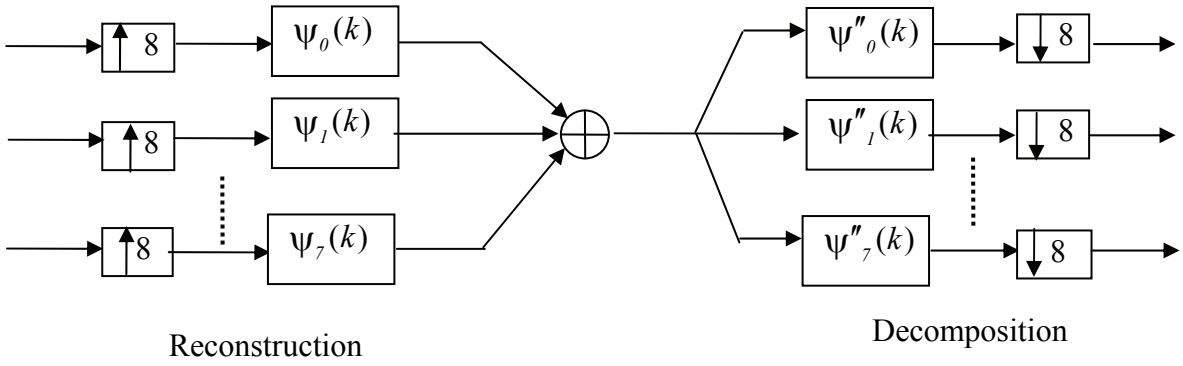

Figure 3.16: An Mallat representation of 8-subcarriers Reconstruction and Decomposition filter banks

3.3.3 Design of Best Wavelet Packet Bases For WP-MCM

The attributes of a multicarrier modulation system greatly depends on the set of waveforms used. The property of the waveforms in turn depends on underlying filter banks used. Many considerations go into the design of a wavelet system including properties such as orthogonality, compact support, symmetry, and smoothness. Here we shall discuss a few important ones.

3.3.3.1 Para-unitary Condition

A rational transfer function $A(z)$ is said to be para-unitary when it obeys the relation $\tilde{A}(z)A(z)=1$. Here $\tilde{A}(z)$ is the para-conjugate of $A(z)$ and is given as $\tilde{A}(z)=A^{\dagger}(z^{-1})$ where the superscript † denotes the conjugation of the coefficients.

The paraunitary condition is essential for many reasons. Firstly, it is a prerequisite for generating orthonormal wavelets [53]. Second, it automatically ensures perfect reconstruction of the decomposed signal [53], i.e. the original signal can be reconstructed without amplitude or phase or aliasing distortion, if the filter banks used satisfy the paraunitary condition. Only para-unitary filters are considered in the thesis and for such solution pairs the high pass and low pass filters share the relationship [53]-[55]:

$$g[L-1-n]=(-1)^n h[n] \tag{3.25}$$

where L is the length of the filters. Further, para-unitary filters automatically satisfy the perfect reconstruction criterion [55] with the decomposition and reconstruction filters being

the complex conjugate time reversed versions of one another i.e.

$$h'[n]=h^{\dagger}[-n] \quad \text{and} \quad g'[n]=g^{\dagger}[-n] \tag{3.26}$$

Filters satisfying this condition are commonly used in signal processing, and are known as the Quadrature Mirror Filters (QMF). A nice aspect of these relations is that it is enough to design a single filter, either the low or high pass filter alone.

3.3.3.2 Compact support

This property ensures that the wavelet is of finite duration and the filter banks used to derive the wavelets have a finite number of non-zero coefficients [57].
Paraunitary and compact support properties are necessary and sufficient conditions for the wavelets to be realized. However, they may not always guarantee the generation of smooth, regular and well shaped wavelets. Quite often the wavelets can be irregular or even fractal shaped [58]. Therefore to ensure smoothness or regularity of the wavelets the additional property of regularity is important.

3.3.3.3 Regularity

This property is a measure of smoothness of the wavelet. The regularity condition requires that the wavelet be locally smooth and concentrated in both time and frequency domain. It is normally quantified by the number of times a wavelet is continuously differentiable. The simplest regularity condition is the "flatness" constraint which is stated on the low pass filter. A LPF is said to satisfy K^{th} order flatness if its transfer function $H(z)$ contains K zeroes located at the Nyquist frequency ($z=-1$ or $\omega=\pi$). Parameter K is called the regularity order and for a filter of length L it satisfies the relation $0 \le K \le L/2$.

Wavelets are defined by the wavelet function $\psi(t)$ (i.e. the mother wavelet) and scaling function $\varphi(t)$ (also called father wavelet) in the time domain. Another way to determine the regularity of the wavelets is in terms of the number of vanishing moments of the wavelet and scaling functions [57] and it uses the dual vanishing moments to determine the convergence rate of the multiresolution projections. The l^{th} moments of the wavelet and scaling functions, $m_w(l)$ and $m_s(l)$, respectively, are defined in continuous time domain by:

$$m_w(l)=\int t^l \psi(t)dt \quad \text{and} \quad m_s(l)=\int t^l \varphi(t)dt \tag{3.27}$$

3.3.4 Wavelet Families

In this work we shall largely deal with the Daubechies family and its variants.

3.3.4.1 Daubechies

The Daubechies wavelets are a family of orthonormal wavelets with compact support and highest degree of smoothness. It was derived by Ingrid Daubechies [54] who used all degrees of freedom K to generate a wavelet family of maximum regularity for a given filter length L, or to generate the minimum L for a given regularity [57]. This she did by imposing the maximum number of zero moments to the wavelet function in the vanishing moments' condition (equation (3.27)).

3.3.4.2 Coiflet

Coiflets wavelets are a variation of the Daubechies wavelets. They are so named because it was derived by I. Daubechies at the recommendation of R. Coifman who suggested the construction of orthonormal wavelet basis with vanishing moment conditions for both wavelet and scaling functions (unlike Daubechies wavelets where only the wavelet functions have zero moments). The wavelet function has $2L$ moments equal to 0 and the scaling function has $2L$-1 moments equal to 0.

3.3.4.3 Symlet

The symlet family of wavelets is another variant of the Daubechies family which are *nearly-symmetrical* (as opposed to being symmetrical). These modifications were also proposed by I. Daubechies and the properties of the two wavelet families are similar.

3.3.4.4 Frequency Selective Wavelet

Choosing the right wavelet is a delicate and some times even an overwhelming task. In theory any time and frequency limited function can be utilized. However in practice, the wavelet bases cannot be arbitrarily chosen and instead have to satisfy a number of specific requirements. In general the choices to make concern with the system of representation (continuous or discrete), properties of the wavelets desired (orthogonality/ bi-orthogonality, regularity/smoothness, frequency selectivity), the application in hand and the context of use [58]. A framework that accounts for these requirements must first be defined and the wavelet should be selected in a principle approach through optimization of the wavelet design parameters.

With regard to the applicability to WP-MCM systems, the desirable properties may be listed as follows:

- The wavelet bases must be time-limited.

- The bases must be well confined in frequency.
- The wavelet packet bases and their duals must be orthogonal (or at least linearly independent) to each other to enable perfect reconstruction.
- The bases must be orthogonal (or at least linearly independent) to each other in order to have a unique demodulation capability.
- The bases must enable the system to handle channel effects and other distortions.
- The system must be easily realizable and must permit application of fast algorithms.

And in the filter bank domain the objective of the design procedure translates to a construction of filters with the characteristics that they:

- have finite impulse response (FIR)
- are maximally frequency selective
- allow orthonormal expansion and perfect reconstruction of discrete-time signals
- satisfy the para-unitary condition
- satisfy a desired flatness/regularity condition

Amongst these properties the para-unitary and regularity properties are mandatory to the design of the filter banks. In addition to these properties the criterion that needs specific focus is the property of frequency selectivity.

In an ideal scenario the filter banks used to generate the wavelets have zero transition bands B, i.e. zero difference at the transition between pass and stop band frequencies (refer Figure 3.17). Under such an ideal scenario the wavelet packet bases derived from a level-i decomposition have confined spectral footprints with bandwidth $(1/2^i)$ times that of the Nyquist frequency. However, available wavelet families are derived from filter banks that have a wide transition band and hence the resultant wavelet sub-carriers have a dispersed spectrum with footprints spilling into neighboring regions. The wider the transition bandwidth the greater the dispersion of the carrier's spectral footprint and therefore the greater the difficulty in isolating those sub-carriers that fall in the region of the licensed user. This greatly reduces the efficiency of the system. It is therefore important to design filter banks that have narrow transition bands.

The design procedure comprises of defining a low pass FIR filter, satisfying the regularity, para-unitary and frequency selectivity conditions, expressed in the form of an impulse response $h(n)$ or a transfer function $H(z)$ or a difference equation. For a filter of length L this means essentially solving L unknown filter coefficients from L linear equations. Of these L linear equations, $L/2$ equations come from the para-unitary constraint, K equations come from the regularity or flatness constraint and the remaining $L/2 - K$ conditions offer the room for flexibility to establish the desired wavelet property such as frequency selectivity. The larger the value of $L/2$-K, the greater the degree of freedom for frequency selectivity and the greater the loss in regularity. There is therefore a trade-off between frequency selectivity and regularity. Wavelets such as the Daubechies family are maximally flat with regularity order $K=L/2$ and hence they are not frequency selective.

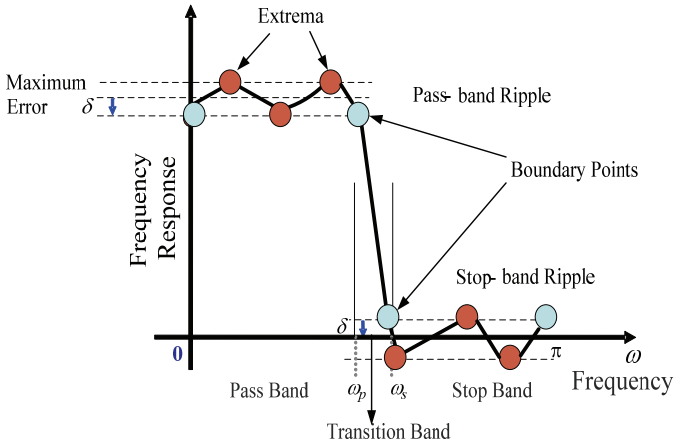

Figure 3.17: Filter Characteristics in frequency. In the figure ω_p and ω_s, denote pass and stop band frequencies, respectively, [0, ω_p] is called the pass-band, [ω_s,π] is called the stop-band and [ω_p, ω_s] is the transition band. δ is the tolerance or ripple

To implement frequency selective filters, the design parameters are stated in the frequency domain in terms of the desired magnitude response of the LPF as shown in Figure 3.17. In the figure ω_p and ω_s, denote pass and stop band frequencies, respectively, [0, ω_p] is called the pass-band, [ω_s,π] is called the stop-band and [ω_p, ω_s] is the transition band. δ is the maximum value of the tolerance or ripple. The design goal is to generate the filter with a desired transition band even while the maximum error δ in the pass/stop-band is minimized.

The fundamental theory on the design of frequency selective filter banks was developed by Rioul and Duhamel [59]-[60]. They devised the procedure to design maximally frequency selective filter banks under a given set of constraints using the Remez exchange algorithm. The Remez exchange algorithm is an optimization algorithm that is commonly used in the design of FIR filters. It is popular because of its flexibility and computational efficiency. It is known also as the Parks-McClellan algorithm; it works by converting the filter design problem into a problem of polynomial approximation [61]. The algorithm is an application of the Chebyshev alternation theorem that constructs the polynomial of best approximation to a desired function under a set of constraints. Through a minimax approximation the scheme seeks to arrive at a l^{th} order approximation polynomial function $C(x)$ that best approximates a desired filter polynomial function $B(x)$ (in our case the LPF $H(z)$ that satisfies the design specifications) in the given interval such that the absolute maximum error is minimized. The error is defined here as the weighted difference between the desired filter polynomial function and the approximation polynomial function and is given by

$$E(x) = W(x)(B(x) - C(x)) \tag{3.28}$$

$E(x)$ and $W(x)$ are respectively the error and weighting polynomial functions. All polynomial functions are of the form $\sum_{i=0}^{l} p_i x^i$, with coefficients p_i; the degree of the polynomial function equals l. Chebyshev proved that such a polynomial $C(x)$ exists and that it is unique [61]. He also gave the criteria for a polynomial to be a minimax polynomial. The algorithm states that in the interval of consideration, the necessary and sufficient condition that $C(x)$ is a unique mini-max polynomial solution of degree l is that there are at least $(l + 2)$ points at which the error function $E(x)$ attains the absolute maximum value δ with alternating sign, i.e.

$$E(x_i) = -E(x_{i+1}) = \pm \max_{x \in I} \{|E(x)|\} = (-1)^i \delta \tag{3.29}$$

for $x_1 < x_2 < \ldots < x_{l+2}$ in the desired interval I. Parks and McClellan proved that this approach could be used to derive a filter of a given length with minimal ripple. The right set of extremal points x_i is arrived through an iterative procedure. In each iteration an interpolation problem is solved and the reference set of extremal points is updated. Rioul and Duhamel deduced that $L/2-K+1$ extremal points in the pass-band are necessary and sufficient to characterize a unique and optimal solution [59].

The procedure starts by choosing an arbitrary set of $L/2-K+1$ points in the given interval. These $L/2-K+1$ points help to form $L/2-K+1$ linear equations. The filter coefficients are obtained by solving the $L/2-K+1$ linear equations in a way that the error at the $L/2-K+1$ points is equal in magnitude and alternating in sign. It cannot be guaranteed after the first step that the solution satisfies the minimax condition for the error function. It means that the magnitude of the error need not be the absolute maximum magnitude in the interval of consideration. In order to find the minimax solution, the second step of the algorithm seeks new set of $L/2-K+1$ points that approach the $L/2-K+1$ points of the minimax solution. The new set is determined by locating those points where the slope of the error function $E(x)$ is zero. Once these points are identified, the old set of $L/2-K+1$ points is exchanged with the new points. This process is iteratively performed till the desired set of points (that satisfy the minimax solution) is obtained. The algorithm has converged when the set of extremal points remains unchanged. Once the right set of extremal points is identified, the optimum error and filter can be obtained. The exact details of how these equations are solved to obtain the low pass filter $H(z)$ using the modified Remez exchange algorithm can be found in [59]-[60]. A flow chart of the algorithm is shown in Figure 3.18. From the low pass filter $H(z)$, the high pass filter $G(z)$ and the reconstruction filters ($H'(z)$ and $G'(z)$) can be obtained by applying eqs. (3.27) and (3.28).

As mentioned earlier, in the construction of maximally frequency selective filter banks three design parameters have a role to play namely, the length of the filter L, the regularity order K, and the transition bandwidth B. All three parameters affect the system performance. As an example we here derive a frequency selective filter bank using the following specifications –

length of filter L = 30, regularity order K = 12, degree of freedom $N = L/2 - K = 3$, transition bandwidth B= 0.1.

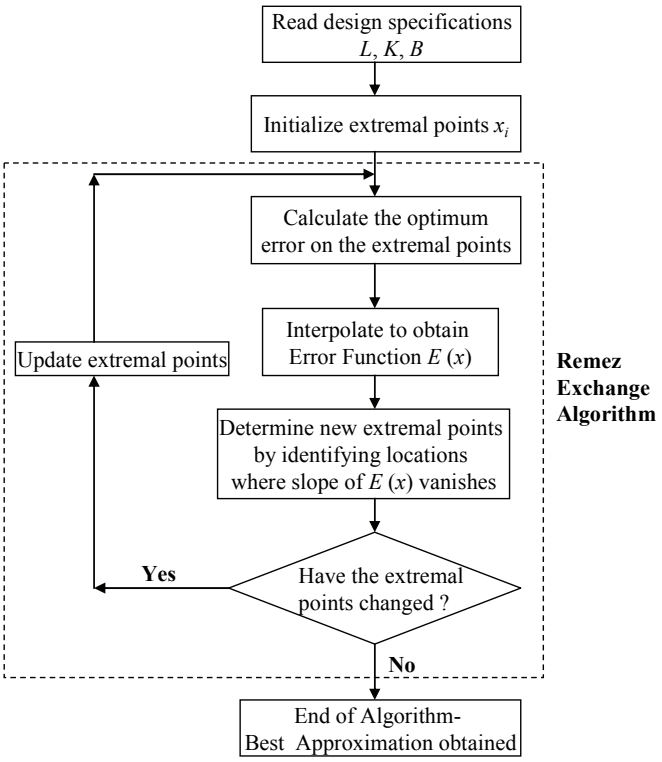

Figure 3.18: Flowchart of the Remez exchange algorithm

Out of all combinations the LPF transfer function is so chosen that all zeros lie inside the unit circle. Such choice makes the LPF a minimum phase filter and hence ensures stability. Figure 3.19(a) shows the distribution of the zeros in the complex plane of the chosen minimum phase LPF $H(z)$ solution. An FIR filter of length 30 has 29 zeros and for regularity order K = 12, the zero located at z = -1 has a multiplicity of 13. The other zeros are located on or inside the unit circle. For both K = 12 and K = 13, the zero located at z = -1 has a multiplicity of 13. This is because when $L/2 - K$ is odd, the optimal solution for regularity order $K + 1$ have the same number of alternations as the optimal solution for regularity order K, [62]. Fig. 3.19(b) shows the frequency response of the minimum phase LP-HP filter pair.

And Figure 3.20 (a) shows the wavelet packet sub-band pulses derived from a 3-stage cascading of maximally frequency selective wavelets (with specifications length L=30, regularity K=12 and transition band B=0.1) and their corresponding 8-channel spectrum (Figure 3.20 (b)). More on the frequency selective wavelets is explained in the next section.

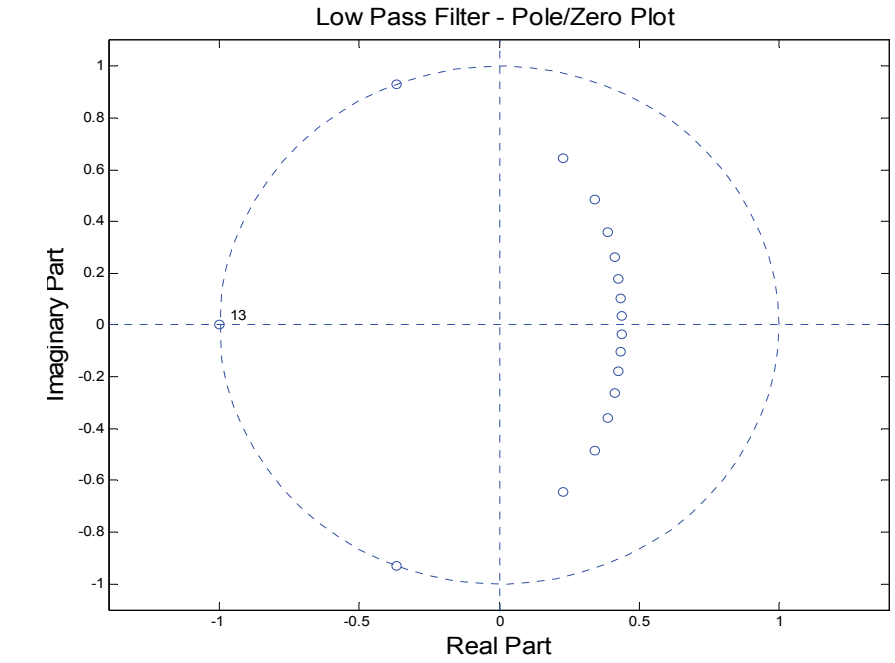

(a)

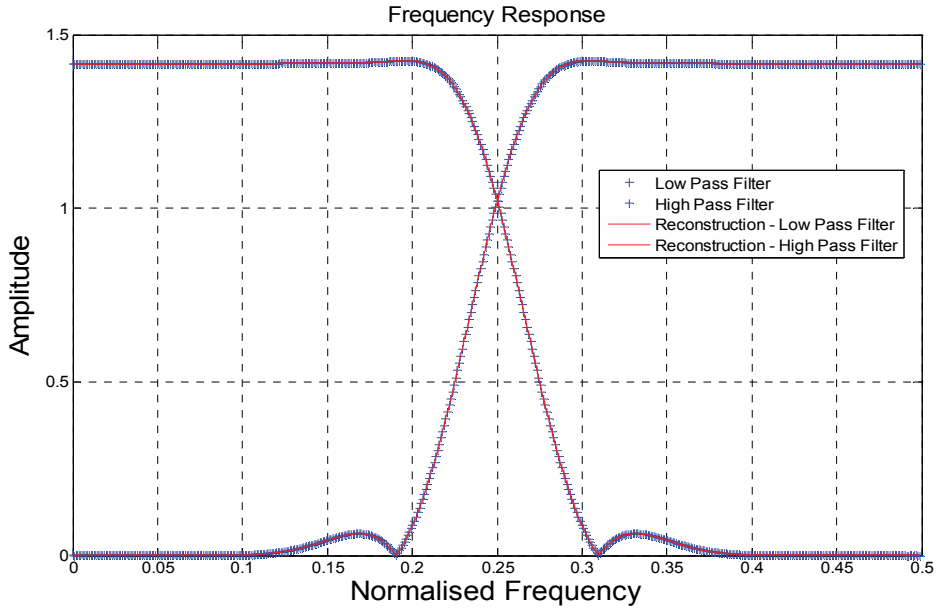

(b)

Figure 3.19: (a) Distribution of the zeros in the complex plane of the chosen minimum phase LPF $H(z)$ solution. For regularity order $K = 12$, the zero located at z = -1 has a multiplicity of 13. The other zeros are located on or inside the unit circle; (b) Frequency response of the maximally frequency selective para-unitary filter pair where the curve that gives the pass band on the low frequency range is the low pass filter while the one that gives the pass band on the high frequency range is the high pass filter.

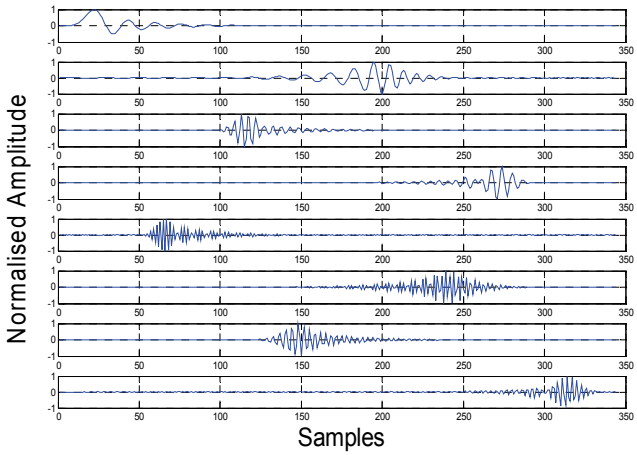

(a)

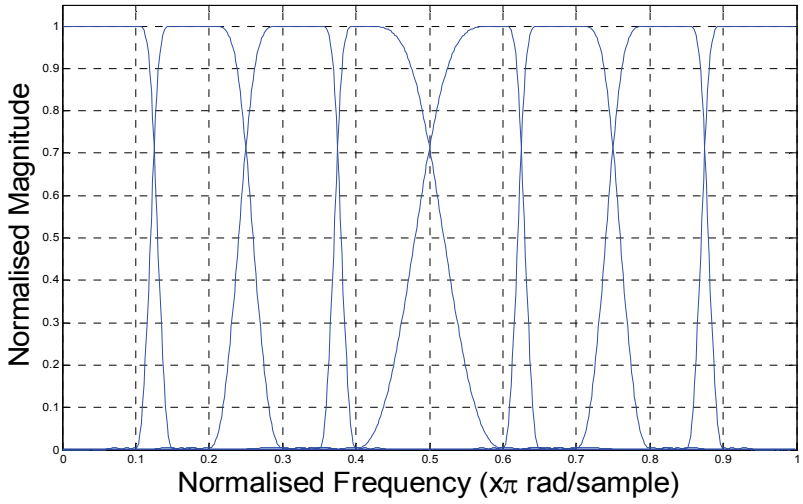

(b)

Figure 3.20: Wavelet Packet bases for MCM carriers (eight carriers). (a) Sub-band pulses in time domain. (b) Spectra of carriers. The wavelet packet bases are derived from maximally frequency selective para-unitary filter banks with specifications L=30, K=12, B=0.1

3.3.5 Performance Evaluation and Anaysis

We start out evaluation on the WPMCM performance for a CR system operating with 128 equally spaced carriers. The LU bandwidth is considered to be comparable to 32 carriers ($1/4^{th}$) of the CR system and located in the middle of the CR spectral band (Figure 3.21). The 128 wavelet packet carriers are derived from a level-7 cascaded tree. To simplify the evaluation of the system performance, the channel is assumed to be affected by Additive

White Gaussian Noise (AWGN) with no distortions such as intersymbol interference (ISI) or inter carrier interference (ICI). The modulation scheme used is Quadrature Phase Shift Keying (QPSK). Lastly, the cognitive modules at the transmitter and receiver are taken to be always aware of the transmission signal characteristics, including details of the active and de-activated carriers. The synchronization between transmitter and receiver is assumed to be perfect.

The frequency ordering of wavelet packet carriers is not in a succession but rather in binary Gray code order. This is because the output of any 2-channel analysis is the result of low/high pass filtering followed by down sampling. Down sampling generates two new filter results with half the number of elements. In addition to this it also results in mirroring of the high pass components. This switches the order of low and high pass components in a subsequent decomposition. When the wavelet packet algorithm is recursively applied, the frequency ordering of the resultant carriers follows the Gray code sequence [59]. This factor must be considered during the identification of affected carriers.

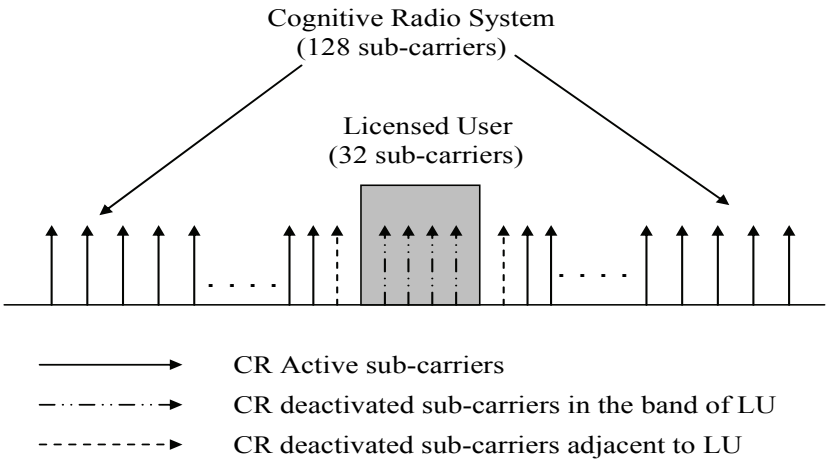

Figure 3.21: Cognitive Radio (CR) and Licensed User (LU) Characteristics

The length of the filter has a direct impact on the system performance, i.e. the longer the filter length the greater the possibility to configure the other filter parameters, K and B, to arrive at the optimal combination. However, it is important that the filter length is kept within practically realizable limits. The key in the approach is to identify the best combination of L, K and B such that the transition band is less and the ripples are tolerable. During the simulation studies we considered a set of about 700 permutations of L, K and B to arrive at the optimum combination. The ranges of L were between 20 and 50; B varied from 0.05 and 0.15 while K was in the region L/2-6 to L/2. From the set considered the best performance was obtained for the combination L=50, K=19, B=0.1. In the following simulations we shall use these specifications to derive the filter banks and wavelet packets.

We next have evaluated the performance of wavelet packet modulation with a frequency selective filter within a cognitive radio context and have compared the results with OFDM-based cognitive radio. The comparisons are presented in [63]. Figure 3.22 gives the BER performance curves of the WP-MCM based CR system in the scenarios: absence of LU (only AWGN), presence of LU without any carrier de-activation and presence of LU with carrier de-activation. From the plots it is quite clear that the presence of LU affects the CR performance. When the CR transmission characteristics are communicated around, the LU with carriers in and around the region of interference removed, and the CR system recuperates. Best results are obtained when 40 or more of the CR carriers are removed. When 44 carriers are removed seamless co-existence with LU is possible with a performance almost matching the AWGN case (when LU is not present).

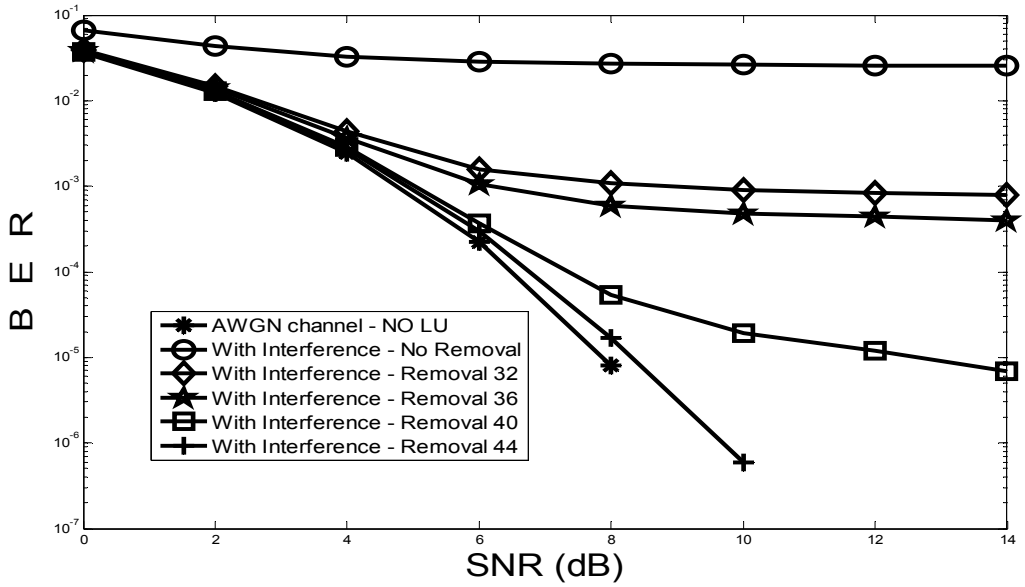

Figure 3.22: Performance of WP-MCM based CR system with frequency selective wavelet in the presence of LU. The carriers of CR in the region of the LU are removed to improve system performance and promote co-existence of CR and LU

It is highly imperative that the CR access to free/idle bands of LU does not cause any harmful effects on the LU communication. To gauge this effect, we present in Figure 3.23 the performance of the LU system under CR. The relevant BER curves are for operation of the LU under the conditions: absence of CR (AWGN channel), presence of CR without any carrier de-activation and presence of CR with carrier de-activation. As in the earlier case, the de-activation of CR carriers is indeed necessary to prevent any loss in LU performance. For the scenario considered here, a noticeable improvement in the performance is obtained when 40 or more of the CR carriers are removed.

It will be interesting to see how the WP-MCM construction matches with traditional OFDM implementations. For fairness of comparison both the OFDM and WP-MCM scheme use the same set of transmission parameters.

As illustrated in Figure 3.24, the performance of both the OFDM and WP-MCM based CR systems worsens (WP-MCM marginally more tolerant than OFDM) in the presence of LU and perform better when their carriers in and around the LU spectral bands are removed. For OFDM the best results are obtained when 36 or more carriers are removed while for WP-MCM the number is about 40 carriers. The advantage of WP-MCM is that once its transmission signal is steered away from the LU bands, it comfortably outperforms its OFDM counterpart. For example, for a given BER of 10^{-4} with 44 carrier removals, WP-MCM gives a gain of about 2 dB in comparison to OFDM.

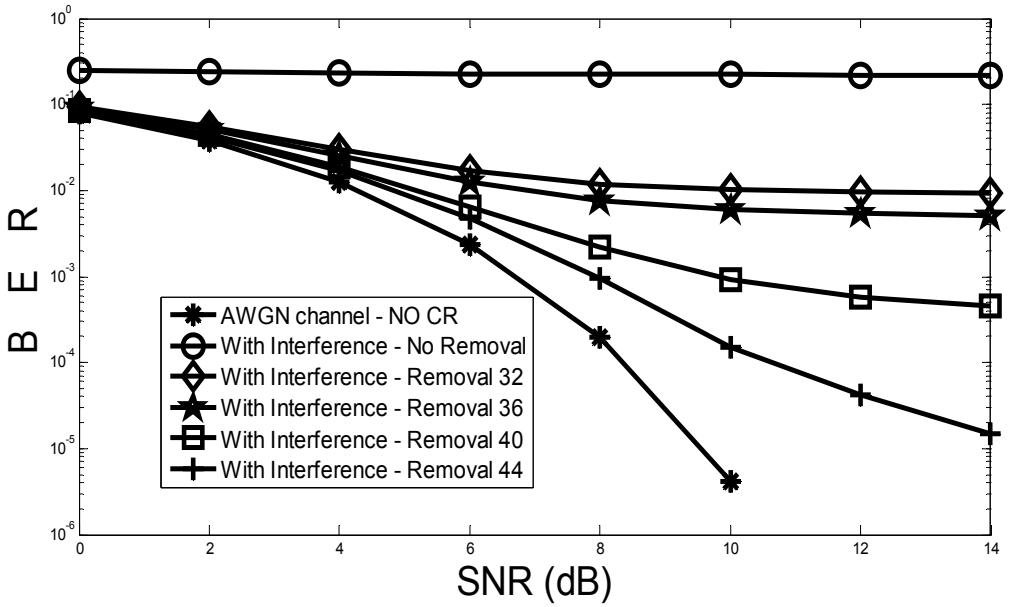

Figure 3.23: BER performance of LU in the presence of the WP-MCM based CR system. The carriers of CR in the region of the LU are removed to enable RU co-existence with LU

The LU performance worsens in the presence of both WP-MCM and OFDM CR systems and (as in the previous case), removal of CR carriers brings relief (Figure 3.25). OFDM needs a lower number of carriers to be removed in comparison to WP-MCM to restore the system performance to the levels of AWGN.

Figure 3.26 depicts the effect of removal of carriers on the system performance. The SNR is fixed at 8 dB. From the plots we may note that though OFDM requires less carrier removals, WP-MCM based CR gives a better SNR gain. Another point to note is that removing the carriers does promote co-habitation of the CR and LU systems but this has a saturation point beyond which removing anymore carriers has no more benefit.

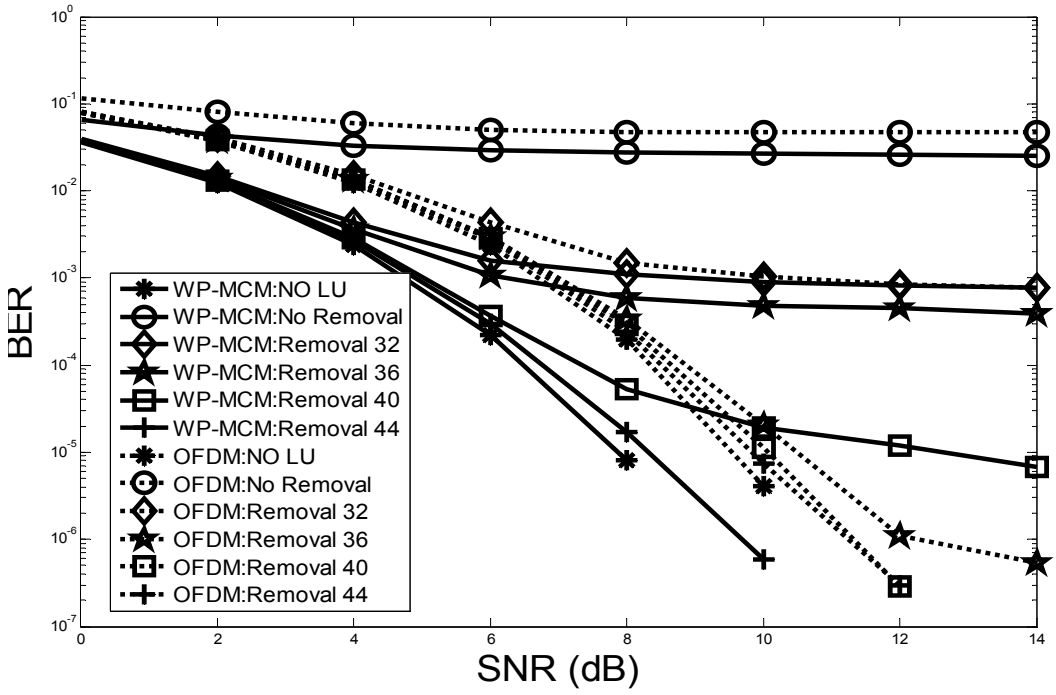

Figure 3.24: BER performance comparison of OFDM and WP-MCM based CR systems in the presence of LU

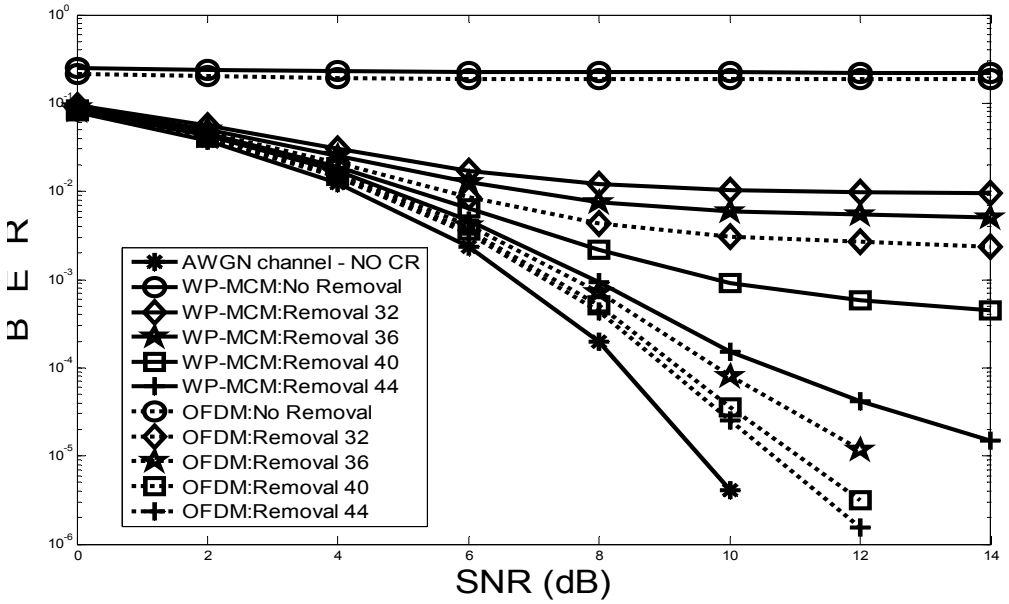

Figure 3.25: Influence of WP-MCM and OFDM based CR systems on the operation of LU

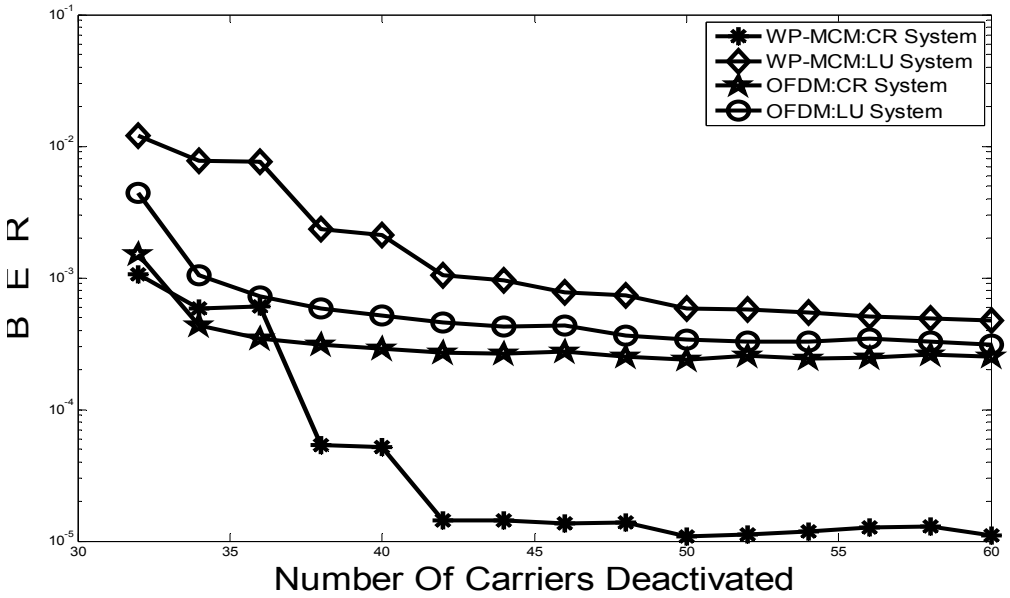

Figure 3.26: OFDM versus WP-MCM based CR: Number of carriers de-activated and their effect on system performance. The BER curves are plotted for a SNR of 8 dB

The use of another kind of wavelet basis function to WP-MCM has been evaluated and compared with the frequency selective wavelet. Here we equate the performance improvements brought by a maximally frequency selective filter bank with a few known wavelets. The wavelets considered are Daubechies-15, Coiflet-5 and Symlet-15. For the fairness of comparison, all filter banks are taken to be of the same length (L=30). Table 3.2 depicts the considered wavelets characteristic.

Table 3.2: Filter Bank Characteristics

Name	Orthonormal	Length	Regularity
Daubechies	Yes	30	15
Coiflet	Yes	30	15
Symlet	Yes	30	15
Frequency Selective	Yes	30	12

The system performance has a direct correlation to the frequency selectivity of the filter bank used to derive the carriers. This effect is exemplified in Figure 3.27 (a), where the frequency responses of the wavelet families has been plotted, and in Figure 3.27(b) which shows the corresponding MCM spectra of the lowest 4 carriers. The Daubechies-15 and Symlet-15 responses almost match and hence the responses of Symlet-15 are not visible. The BER performance curves of the CR and LU systems have been plotted in Figures 3.28(a) and 3.28(b), respectively. The maximally frequency selective filter banks have the narrowest

transition band and hence they clearly outperform the other wavelet families while Coiflet-5 is much worse because of its very wide transition band.

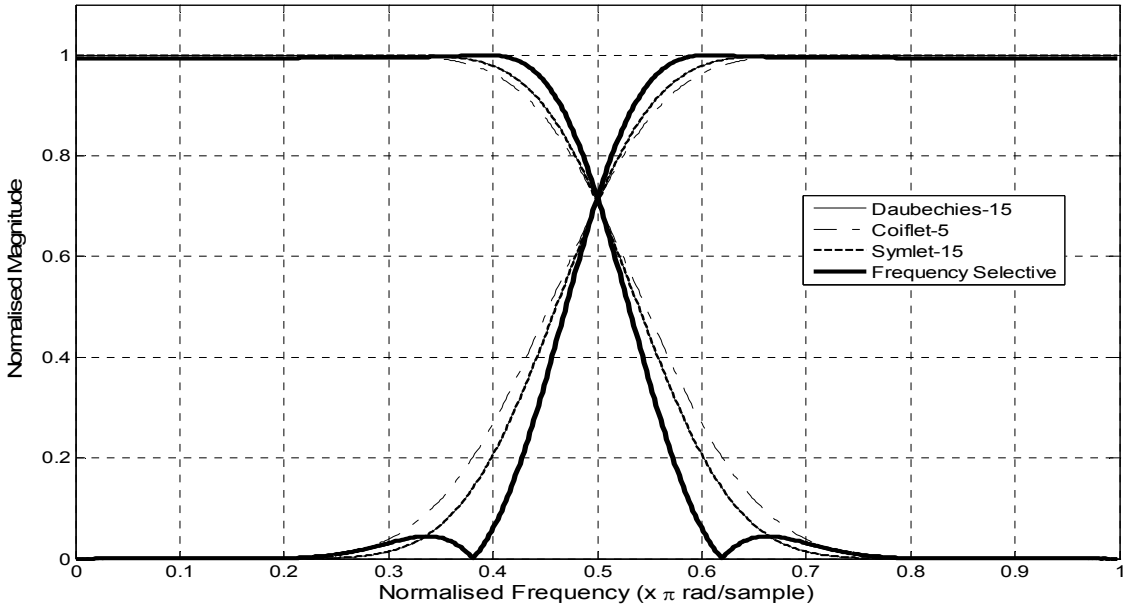

(a)

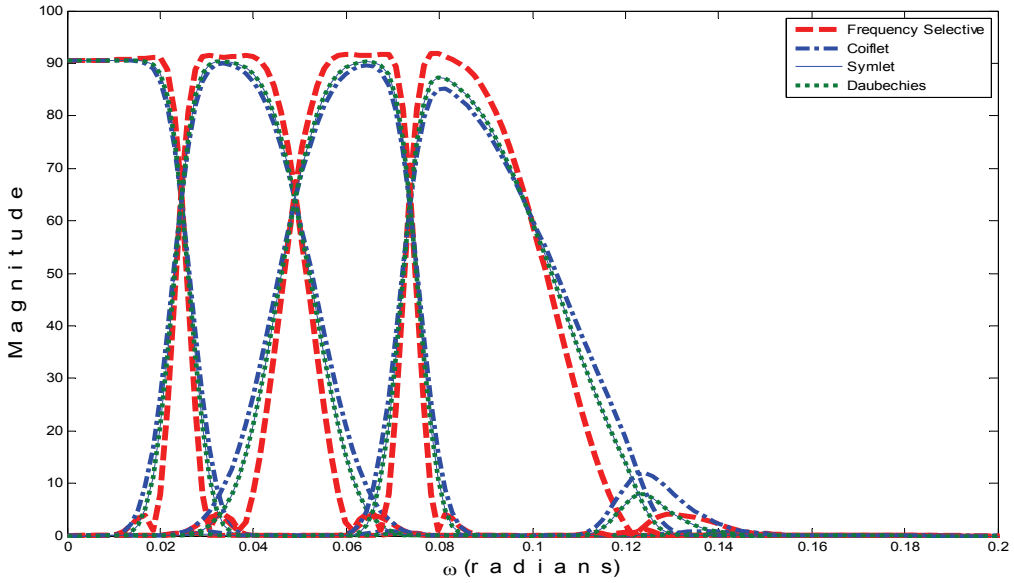

(b)

Figure 3.27: (a) Frequency responses of the LPF-HPF pairs of various wavelets. (b) Wavelet Packet bases as MCM carriers (only first 4 carriers shown).The wavelets considered are Daubechies-15, Symlet-15, Coiflet-5, Maximally Frequency Selective wavelet with L=30, K=12, B=0.1.

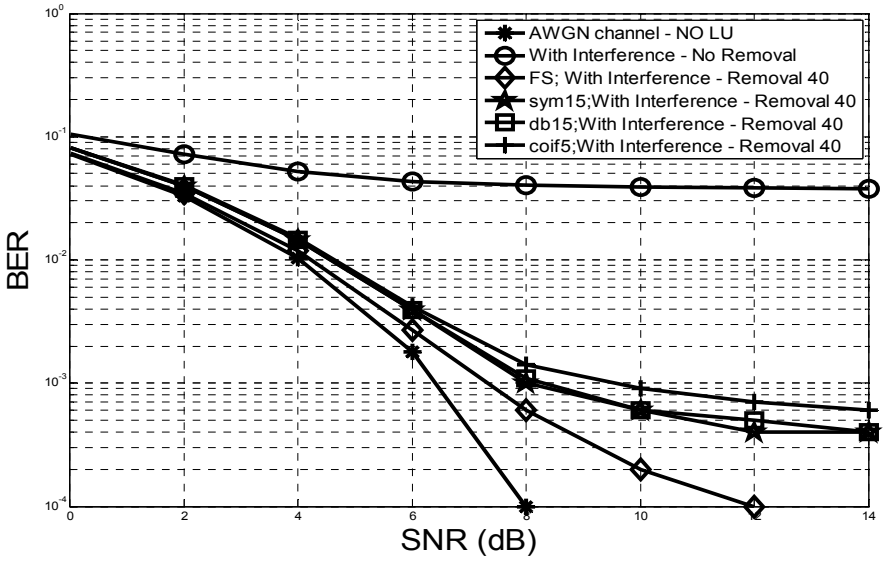

(a)

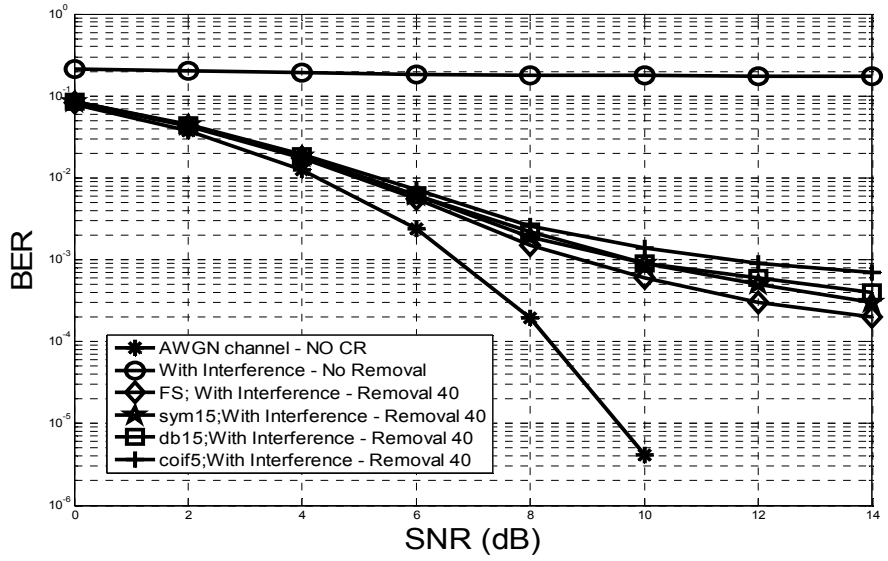

(b)

Figure 3.28: Comparison of different wavelets: (a) BER performance of the WP-MCM based CR system in the presence of LU. (b) BER performance of LU in the presence of the WP-MCM based CR system. The carriers of CR in the region of the LU are removed to enable it to co-exist with LU. FS denotes the maximally frequency selective wavelet, db denotes Daubechies, sym – symlet, coif stands for coiflet

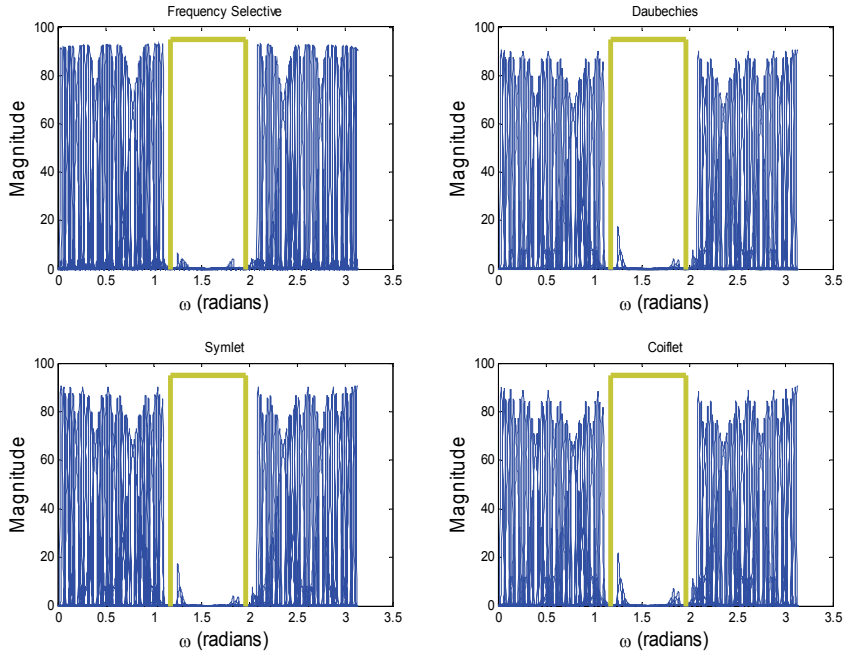

Figure 3.29: Comparison of the spectrum of different WP-MCM based CR system with carrier removals in the region of the LU. The rectangle marks the LU spectral footprint

Figure 3.29 shows spectrum comparisons of different WP-MCM based CR systems with carrier removals in the region of the LU. The frequency selective wavelets ensure a neat separation of the CR and LU footprints while all other wavelets have residual infringing components. To validate this further we refer to Figure 3.30 which depicts the effect of removal of carriers on the system performance. The SNR is fixed at 8 dB. From the plots we note that the usage of maximally frequency selective filters requires less carrier removals and gives a better SNR gain.

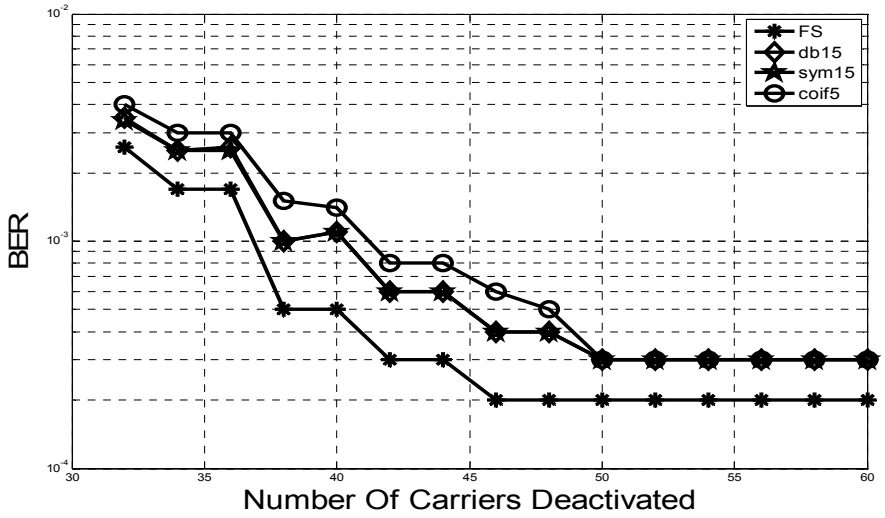

Figure 3.30: BER performance of different wavelets: Number of carriers de-activated and their effect on system performance at 8 dB SNR. FS denotes the maximally frequency selective wavelet, db denotes Daubechies, sym – symlet, coif stands for coiflet.

As the objective of cognitive radio is to obtain efficient spectrum utilization, it is logical that adding MIMO to the system will fulfil this goal even further. By applying the Vertical Bell Labs Space Time (V-BLAST) architecture at the receiver the BER of the system will be enhanced due to channel diversity exploitation [64]-[65].

We have evaluated the performance of the CR system under various WP-MCM-MIMO configurations [66]. The WP-MCM-MIMO Architecture is depicted in Figure 3.31. The WP-MCM-MIMO system operates under a LU with 40 of its 128 carriers (in and around the region of LU) are de-activated. We also consider AWGN as the channel model. The data symbols are derived from BPSK mapping. In the fading channel model with Doppler effects the impact of multipath delay cannot be counteracted by the use of a cyclic prefix like in OFDM. This is due to the overlapping transmission between consecutive WP-MCM symbols. Hence both inter-symbol interference (ISI) and inter–symbols inter-carriers interference (ISCI) will occur. The fading in WP-MCM has to be cancelled by a time-domain equalization scheme [50]. At the moment we have not deeply investigated the time domain equalization for WP-MCM. The use of MIMO in AWGN channel will not give a diversity gain from the channel but the performance gain will be derived from the increasing number of receive antennas. This increasing number will give extra redundancy and the effect of code repetition, so that the data detection at the receiver will be improved. The results in Figure 3.32 show that for all combination of transmit and receive antennas, as long as the number of receive antennas is increased, the BER performance will be improved.

The carriers are derived from maximally frequency selective filters with L=30, K=12 and B=0.1. To better understand the operation, we classify the MIMO configurations as follows:

a) First we consider the case with the same number of antennas in both the transmitter and receiver ends (Figure 3.32a). The formations considered are 1x1, 2x2, 3x3 and 4x4. The pattern of the BER curves is un-ambiguous. With increase in the number of transmit-receive pairs, the BER improves. This is due to the array gain in the AWGN channel.
b) Effect of receiver antennas – Increasing the number of receiver antennas significantly improves the system performance. This is illustrated in Figure 3.32b where the number of transmit antennas is kept constant at 2 while increasing the number of receive antennas to 3, 4, 5 and 6 respectively. For a BER of 10^{-4} the improvements with respect to the 2x2 configuration are 2 dB for 2x3, 3dB for 2x4, 4dB for 2x5 and 5dB for 2x6.
c) Figure 3.32c shows the curves for a few other MIMO transmit-receive antenna combinations. In all MIMO configurations the performance of the CR setup is efficient and allows co-existence with LU.

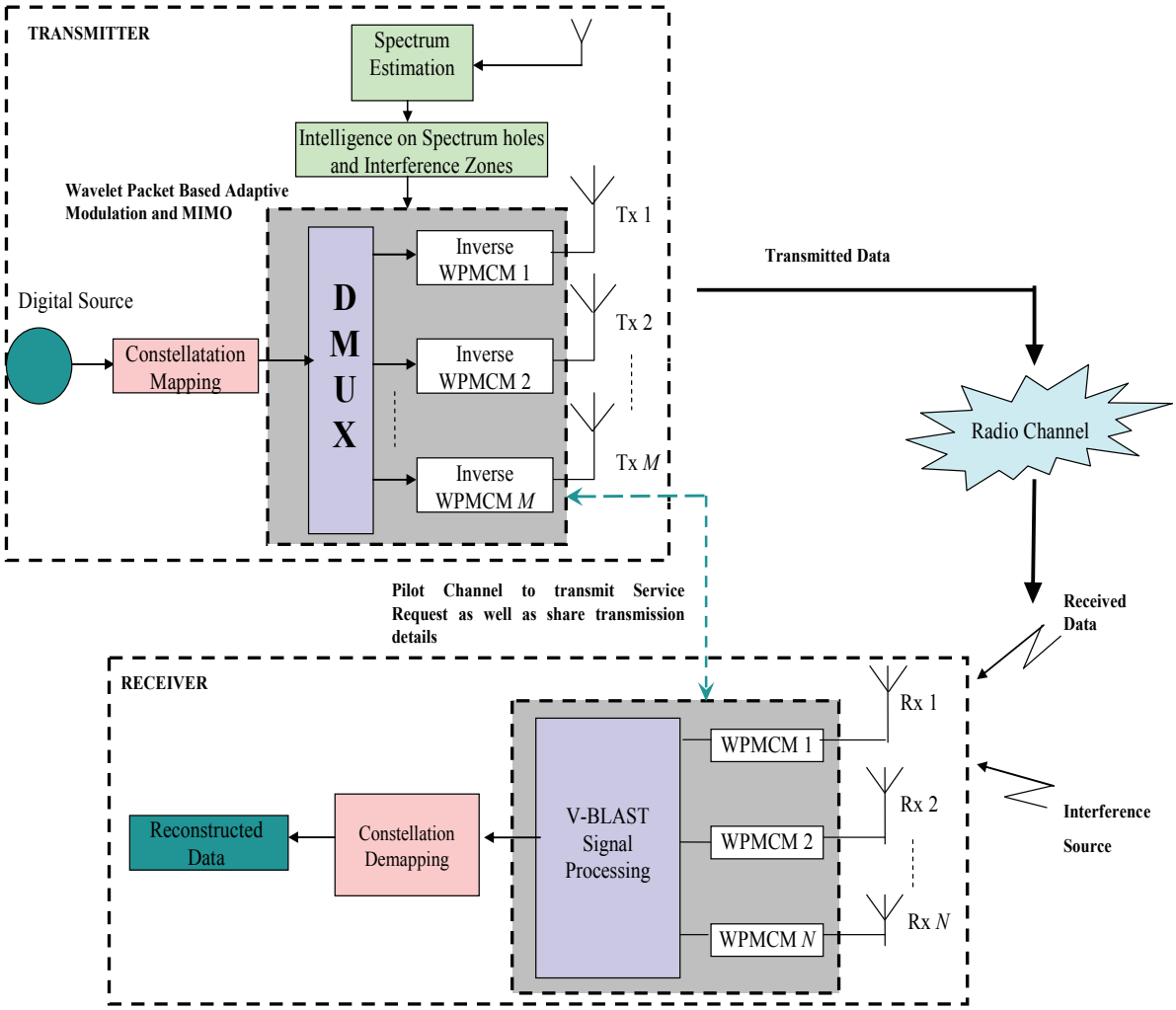

Figure 3.31: MIMO transceiver architecture for a WPMCM based spectrum pooling system

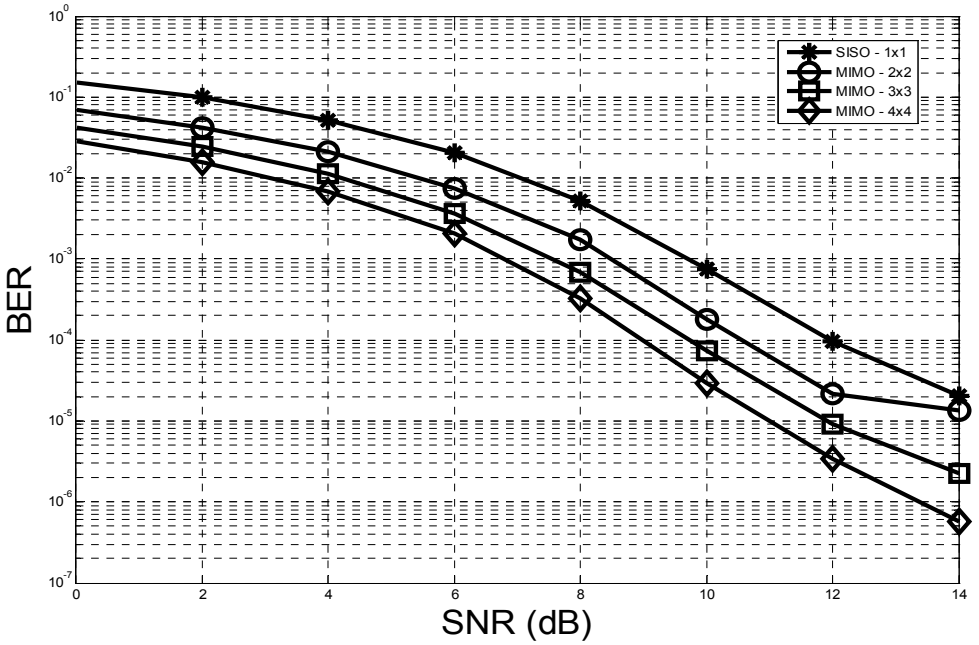
SISO - 1x1
MIMO - 2x2
MIMO - 3x3
MIMO - 4x4
BER
SNR (dB)

(a)

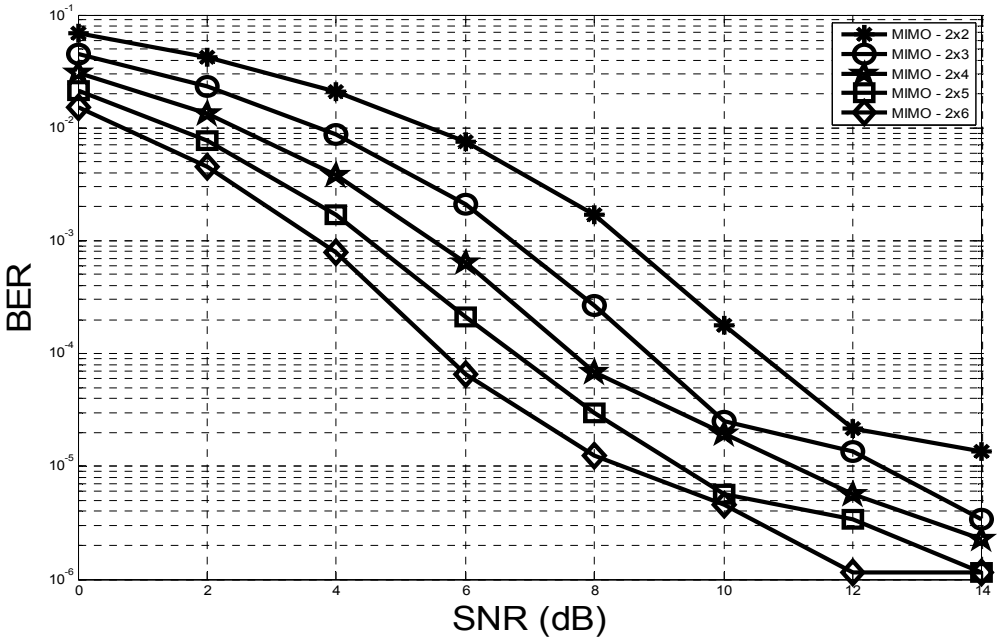
MIMO - 2x2
MIMO - 2x3
MIMO - 2x4
MIMO - 2x5
MIMO - 2x6
BER
SNR (dB)

(b)

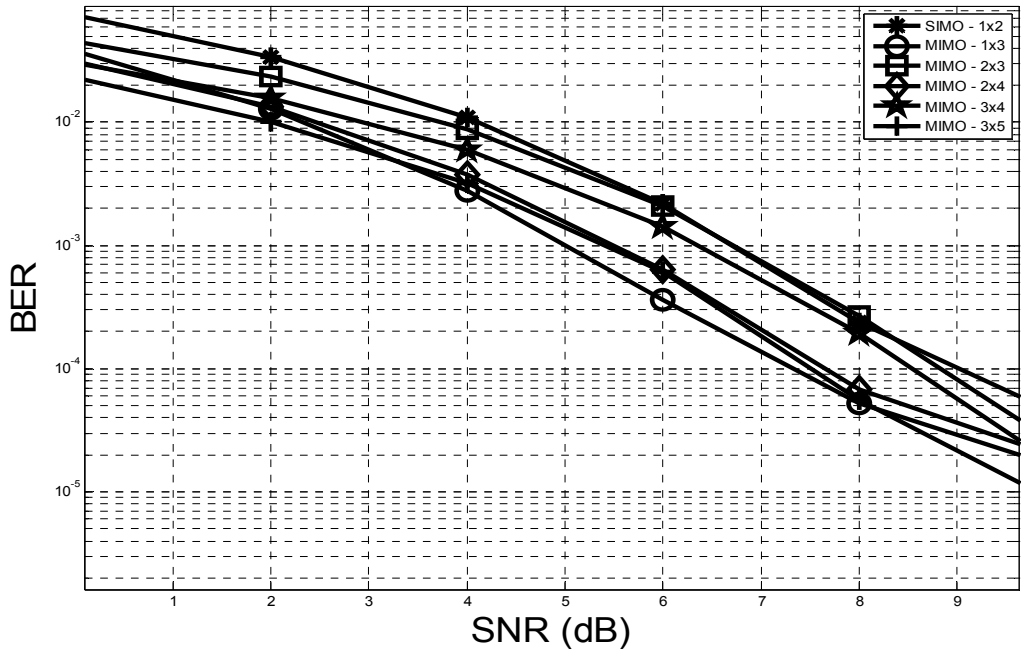

(c)

Figure 3.32: Performance of WPMCM MIMO based CR system for various combinations of transmit-receive antennas. a) Balanced Case when the number of transmit and receive antennas are the same; b) Effect of changes in the receiver configuration. c) A few other MIMO configurations; MIMO stands for Multiple input-multiple output, SISO for single input-single output and SIMO for single input-multiple output. The carriers were derived from Frequency selective filters with L=30, K=12 and B=0.1. The CR is a 2x2 MIMO

Due to the deployment of the V-BLAST architecture at the receiver, the minimum mean square error (MMSE) technique in detecting the transmitted signal is used in an optimum way. It combines the signal linearly to get an MMSE between the estimated signal and the transmitted signal. The optimum gain can be derived when the number of transmit antennas is equal or smaller than the number of receive antennas [67].

It will be interesting to see how the WP-MCM construction matches up to traditional OFDM implementations. Both the OFDM and WP-MCM scheme use the same set of transmission parameters – 128 carriers each with 40 carriers in the interference band removed. The used wavelet belongs to the family of maximally frequency selective filters. The curves (Figure 3.33) are for the MIMO configurations 1x1, 2x2 and 3x3. For all cases considered the WP-MCM setup performs comparably well with its OFDM counterpart.

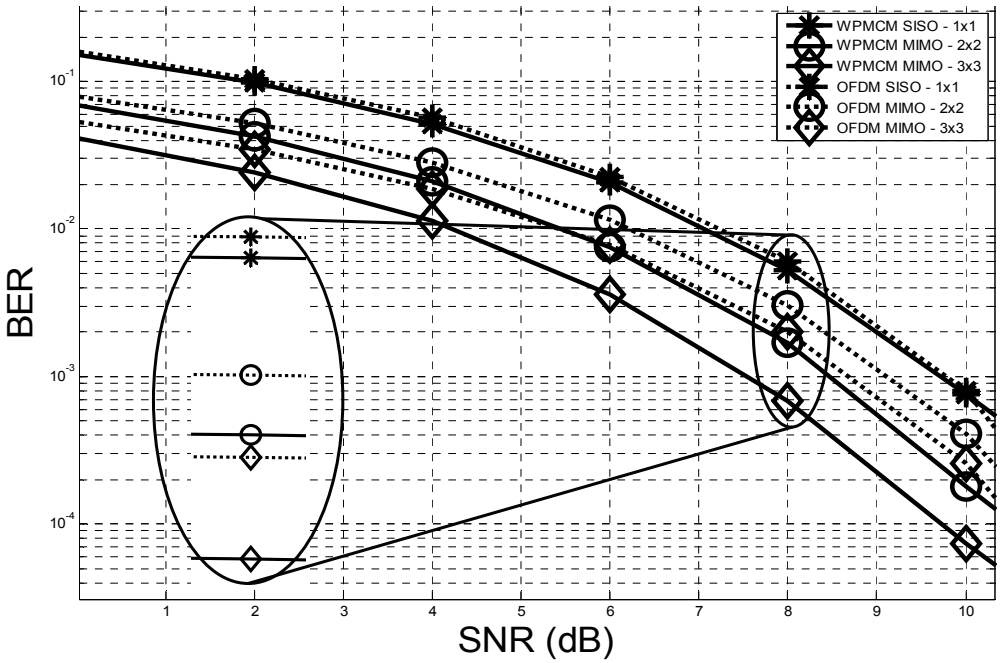

Figure 3.33:. BER performance comparison of OFDM and WP-MCM based CR systems in the presence of LU. MIMO stands for Multiple input-multiple output, SISO for single input-single output

3.4 Conclusions

This chapter has described the novel combination of CR interference avoidance technique through spectrum pooling, sidelobes reduction via combined windowing and sidelobes cancellation carriers insertion, and intelligent bit allocation in order to attain the targeted bit rate while the target BER is preserved.

Choosing the window with low sidelobes will ease the application of sidelobes cancellation carriers insertion. Due to the low sidelobes, high amplitudes of the sidelobes cancellation carriers can be avoided. In terms of BER performance, the window with low sidelobes will suppress the impact of inter carrier interference due to receiver imperfection in estimating the channel state information as an effort to remove the channel fading influence on the receive signal.

The introduced combination technique tries to solve three optimization problems. The most crucial one is the co-existence between our CR system with the LU system. We therefore design signals in such a way that the impact of CR transmission on the LU communication quality of service (QoS) is negligible. This can be accomplished physically by avoiding the band occupied by LU and suppress a part of the CR signal that smeared into the LU band.

The second one is the CR system bit rate, and the third is the CR system BER. The second and third optimization problem can be seen as the QoS aspect of the CR system. The three optimization problems will interact to each other, meaning that it will lead to a trade-off problem.

Interference (sidelobes) suppression of the CR signal in the LU band by windowing and sidelobes cancellation carriers is accomplished with the expense of the LU bitrate degradation. The application of subcarrier weighting or the use of a frequency domain additive signal in lowering the sidelobes (as described in chapter 2) will negatively affect the CR BER performance. This BER degradation however can be compensated by the application of robust channel coding techniques such as the low density parity check codes.

Another novel technique proposed in this chapter is the combination of the spectrum pooling concept with the wavelet packet multicarrier modulation (WP-MCM) using frequency selective filter wavelet basis function as replacement for the Fourier transform in the OFDM system. The signal sidelobes can be shaped by modifying the length of the wavelet filter, frequency selectivity, regularity order and the transition bandwidth of the filter.

By combining the WP-MCM concept with spectrum pooling, co-existence between the rental CR system with the LU can be achieved. Parameters (frequency selectivity, regularity order and transition bandwidth) modification will lead to a trade-off problem between the BER performance (due to the frequency selectivity option) and the sidelobe suppression.

Due to the overlapping property of the time domain WP-MCM signal, it is considered that the WP-MCM would not need the guard interval in avoiding inter symbol interference. The simulation results in the AWGN channel show that although the transmitted signal (in time domain) of one WP-MCM signal overlaps with its neighboring signals, the receiver can still reconstruct the transmitted signal.

MIMO as an effort to enhance efficient spectrum utilization has been deployed in the WP-MCM based Cognitive Radio system. The performance in an AWGN channel has been evaluated. The performance gain of MIMO in AWGN channel is derived from increasing the number of receive antennas. Spatial-Multiplexing gain on transmitting different data on different antenna can be achieved by having equal or a larger number of receive antennas compared to transmit antennas.

Further investigation on equalization for WP-MCM is required, and its deployment in a MIMO-WP-MCM system should be explored. MIMO has been evaluated in an OFDM system. The results show that MIMO with a V-BLAST receiver architecture has improved the OFDM BER performance by exploring the channel diversity. For this reason it is expected that the MIMO application will give performance improvement in WP-MCM, while equalization is required in removing the fading effect in WP-MCM. This last aspect is crucial in the application of V-BLAST in the MIMO-WP-MCM.

Chapter 4

Channel Estimation for OFDM Based Cognitive Radio

4.1 Introduction

OFDM has been considered as a robust multicarrier technique to counteract the inter symbol interference due to the multipath channel. By the insertion of the cyclic prefix or zero padding as the guard interval (GI) [68]-[69], the inter symbol interference (ISI) due to multipath channel can be avoided.

Still for coherent data detection by demapping (QAM or PSK), information about the channel state is required and therefore should be estimated by the OFDM receiver. Due to this reason the channel estimation module is a crucial element in an OFDM system as an effort to remove the fading effect in the received signal. The channel estimation can be applied blindly by utilizing the received data signal [70]-[72] or by the aid of pilots which are transmitted symbols, known by the receiver, in terms of their values and positions. Pilot insertion can be seen as a method of sampling the channel condition within the period of data transmission. Blind estimation requires extra complex computations and the results are less accurate compared to the pilot-aided channel estimation. Therefore, in this thesis we consider the pilot aided channel estimation to be applied in the OFDM system.

According to the OFDM frame duration, the pilot spacing can be arranged to cope with the channel condition. Pilot insertion in the form of training signal which is a stream of pilots dedicated to one OFDM symbol is suitable for short packet length where the frame duration is much shorter than the coherence time of the channel. Hence, one OFDM symbol dedicated as training should be sufficient to estimate the channel within the frame duration [10].

In a long frame duration the pilots are multiplexed into the data stream before transmission. The pilots will be spread among the data either in the frequency direction (within the OFDM symbol unit) or in the time direction (within the OFDM subcarrier unit). In the Cognitive Radio (CR) context, there will be de-activated carriers and some carriers which are dedicated to reduce the sidelobes of the rental OFDM based CR spectrum in the licensed user (LU)

band. This condition raises a new challenge in the design of pilot patterns in the OFDM frame.

The Wiener filter interpolation as channel estimation technique has been described in [73]-[75]. The technique directly utilizes the correlation of the channel in time and frequency based on the estimated statistical property of the channel [73]-[75]. The overview of Wiener filter channel estimation, design and criteria will be explained in section 4.2

Previously in section 2.4 we have described how the frequency hopping technique with TDD Bluetooth frame design is applied if OFDM subcarriers need to be de-activated due to the LU access. The Wiener filtering technique in this frame design including the performance evaluation will be presented in section 4.3.

Section 4.4 proposes novel works dedicated to the technique in designing optimum pilot patterns by adding the virtual pilot concept for OFDM channel estimation in the context of cognitive radio. The method in estimating the channel state information for the OFDM based CR system is described.

Further, since adding multiplexing gain to the CR system affirms one of the CR objectives [2] in improving the spectrum utilization, in section 4.4 we expand the optimum pilot pattern in SISO-OFDM-based CR system for use in to a MIMO system. Analysis and evaluations of the proposed system are reported in section 4.5.

As pilots can also be utilized for addressing other OFDM challenges such as the synchronization and peak to average power ratio (PAPR) problems, in section 4.6 we will overview how these pilots can be designed in the cognitive radio context for this purpose.

Conclusions on this chapter are given in section 4.7.

4.2 Wiener Filter Channel Estimation

In principal the Wiener filter is constructed based on the orthogonality between the estimation error and the initial channel estimates to reach the minimum mean square channel estimation error. If the estimation error $\varepsilon_{n,k}$ is defined as [75]:

$$\varepsilon_{n,k} = H_{n,k} - \breve{H}_{n,k} \tag{4.1}$$

where $H_{n,k}$ and $\breve{H}_{n,k}$ are the true and final estimated channel transfer function (CTF) (after the Wiener Filtering process) on subcarrier n of OFDM symbol k respectively, then 2 dimension (2-D) Wiener filter are obtained by applying the orthogonality principle in linear mean square estimation [75],

$$E\left\{\varepsilon_{n,k}\hat{H}^{*}_{n',k'}\right\}=0, \qquad \forall\{n',k'\}\in P \tag{4.2}$$

The symbol P in (4.2) defines the set of pilot positions within an OFDM frame while $\hat{H}_{n',k'}$ is the initial channel estimate (before filtering) on the pilot position which is derived from the least square method dividing the received signal on the pilot position with the corresponding pilot value. It is calculated from:

$$\hat{H}_{n',k'}=\frac{Y_{n',k'}}{S_{n',k'}}=H_{n',k'}+\frac{N_{n',k'}+I_{n',k'}}{S_{n',k'}}, \qquad \forall\{n',k'\}\subset P \tag{4.3}$$

Where $S_{n,k}$, $N_{n,k}$, and $I_{n,k}$ are the transmitted symbol, noise and interference components on carrier n at OFDM symbol k. The estimated (CTF) is derived from the matrix multiplication between the Wiener filter ($\boldsymbol{\omega}$) and the set of pilots. It is described in a component-wise multiplication forms by:

$$\breve{H}_{n,k}=\sum_{\{n',k'\}\in P}\omega_{n',k',n,k}\hat{H}_{n',k'} \tag{4.4}$$

Combining eqs. (4.1), (4.2) and (4.4) will lead to the so called Wiener Hopf equation [75]:

$$\underbrace{E\left\{H_{n,k}\hat{H}^{*}_{n'',k''}\right\}}_{\theta_{n-n'',k-k''}}=\sum_{\{n',k'\}\in P}\omega_{n',k',n,k}\underbrace{E\left\{\hat{H}_{n',k'}\hat{H}^{*}_{n'',k''}\right\}}_{\phi_{n'-n'',k'-k''}}, \quad \forall\{n'',k''\}\in P \tag{4.5}$$

The symbol $\theta_{n-n'',k-k''}$ is the channel time-frequency correlation function. Symbol $\phi_{n'-n'',k'-k''}$ is the autocorrelation function on the pilot positions which can be written as :

$$\phi_{n'-n'',k'-k''}=\theta_{n'-n'',k'-k''}+\frac{\sigma_I^2+\sigma_N^2}{E\{|S_{n',k'}|^2\}}\delta_{n'-n'',k'-k''} \tag{4.6}$$

The second term on the right side of eq. (4.6) is the inverse of the average OFDM frame signal to interference plus noise ratio where σ_I^2 and σ_N^2 are the interference and noise variance, respectively. By combining (4.5) and (4.6) we can find the matrix for generating the Wiener filter coefficients ($\boldsymbol{\omega}$) by multiplying the channel correlation matrix ($\boldsymbol{\theta}$) and the inverse of the autocorrelation matrix of the channel on the pilot positions ($\boldsymbol{\Phi}$) [75]:

$$\boldsymbol{\omega}^{T}=\boldsymbol{\theta}^{T}\boldsymbol{\Phi}^{-1} \tag{4.7}$$

If the receiver does not have perfect information regarding the actual channel correlation function, then the 2-D (frequency-time) Wiener filter will be generated with a mismatch correlation function. It will then produce the channel estimation mean square error also, according [75]:

$$\begin{aligned} MSE_{n,k} = E\left\{\left|\varepsilon_{n,k}\right|^2\right\} &= E\left\{\left(H_{n,k} - \tilde{\boldsymbol{\omega}}_{n,k}{}^T \hat{\boldsymbol{h}}\right)\left(H_{n,k}^* - \hat{\boldsymbol{h}}^H \tilde{\boldsymbol{\omega}}_{n,k}{}^*\right)\right\} \\ &= E\left\{\left|H_{n,k}\right|^2\right\} - E\left\{H_{n,k}\hat{\boldsymbol{h}}^H\right\}\tilde{\boldsymbol{\omega}}_{n,k}^* - \tilde{\boldsymbol{\omega}}_{n,k}^T E\left\{\hat{\boldsymbol{h}}H_{n,k}^*\right\} + \tilde{\boldsymbol{\omega}}_{n,k}^T E\left\{\hat{\boldsymbol{h}}\hat{\boldsymbol{h}}^H\right\}\tilde{\boldsymbol{\omega}}_{n,k}^* \\ &= E\left\{\left|H_{n,k}\right|^2\right\} - \boldsymbol{\theta}_{n,k}^T \tilde{\boldsymbol{\omega}}_{n,k}^* - \tilde{\boldsymbol{\omega}}_{n,k}^T \boldsymbol{\theta}_{n,k}^* + \tilde{\boldsymbol{\omega}}_{n,k}^T \boldsymbol{\Phi} \tilde{\boldsymbol{\omega}}_{n,k}^* \end{aligned} \tag{4.8}$$

where $\tilde{\boldsymbol{\omega}}_{n,k}$ is the Wiener filter coefficients matrix with the mismatch model to estimate the CTF on subcarrier n of OFDM symbol k while $\hat{\boldsymbol{h}}$ is the matrix of the initial channel estimates on the pilot positions. The term mismatch model means here the real statistical model of the channel is not equal to the estimated channel model statistics.

According to references [73]-[74] the 2-D (time-frequency) channel correlation function ($\theta_{n-n",k-k"}$) is the result of a multiplication between the time channel correlation function ($\theta^{\Delta f}_{n-n"}$) and the frequency correlation function ($\theta^{\Delta t}_{k-k"}$), i.e.

$$\theta_{n-n",k-k"} = \theta^{\Delta f}_{n-n"} \theta^{\Delta t}_{k-k"} \tag{4.9}$$

and accordingly the autocorrelation function would be derived from [75]:

$$\phi_{n'-n",k'-k"} = \theta^{\Delta f}_{n'-n"} \theta^{\Delta t}_{k'-k"} + \frac{\sigma_n^2}{E\left\{\left|S_{n',k'}\right|^2\right\}} \delta_{n'-n",k'-k"} \tag{4.10}$$

Consequence of the above considerations is that the 2-D Wiener filtering can be simplified by implementing two 1-D filters sequentially. As an example if the first filtering is applied in frequency direction, it can be followed by the time direction filtering. In this way the channel estimates after first filtering are derived from [75]

$$\breve{H}^{[1]}_{n,k} = \boldsymbol{\omega}^{[1]}_n \hat{\boldsymbol{h}}_{k'} \tag{4.11}$$

The matrix $\boldsymbol{\omega}^{[1]}_n$ is given by the first filter coefficients set and vector $\hat{h}_{k'}$ represents the subset of pilots of the initial estimates derived from (4.3) at OFDM symbol *k'*. The mean square error after this first filtering becomes:

$$MSE_{n,k}^{[1]} = E\left\{\left|H_{n,k}\right|^2\right\} - \boldsymbol{\theta}_n^T \tilde{\boldsymbol{\omega}}_n^{[1]*} - \tilde{\boldsymbol{\omega}}_n^{[1]T} \boldsymbol{\theta}_n^* + \tilde{\boldsymbol{\omega}}_n^{[1]T} \boldsymbol{\Phi} \tilde{\boldsymbol{\omega}}_n^{[1]*} \tag{4.12}$$

The final estimated CTFs are produced by the second filtering ,

$$\breve{H}_{n,k} = \breve{H}_{n,k}^{[2]} = \boldsymbol{\omega}_k^{[2]T} \hat{\boldsymbol{h}}_{n'}^{[1]} \tag{4.13}$$

The matrix $\boldsymbol{\omega}_k^{[2]T}$ is the second filter coefficients to be used for the time direction channel estimation. Vector $\hat{h}_{n'}^{[1]}$ represents the subset of pilots that are obtained from the first filtering as calculated in (4.11). Due to the second filtering the mean square error for 2x1-D filtering is obtained from (4.14).

$$MSE_{n,k} = MSE_{n,k}^{[2]} = E\left\{\left|H_{n,k}\right|^2\right\} - E\left\{H_{n,k}\hat{\boldsymbol{h}}_n^{[1]H}\right\}\tilde{\boldsymbol{\omega}}_k^{[2]*} - \tilde{\boldsymbol{\omega}}_k^{[2]T} E\left\{\hat{\boldsymbol{h}}_n^{[1]} H_{n,k}^*\right\} + \tilde{\boldsymbol{\omega}}_k^{[2]T} E\left\{\hat{\boldsymbol{h}}_n^{[1]}\hat{\boldsymbol{h}}_n^{[1]H}\right\}\tilde{\boldsymbol{\omega}}_k^{[2]*}$$

(4.14)

Simulations results in [71] show that the mean square channel estimation error (channel MSE) performances between 2-D and 2x1-D filtering are only slightly different while 2x1-D filtering gives less complexity than the to 2-D filtering.

The estimated channel correlation in time $\theta_{k-k''}^{\Delta t}$ is derived from the inverse Fourier transform of the estimated Doppler power density, while the estimated channel correlation in frequency $\theta_{n-n''}^{\Delta f}$ is derived from the Fourier transform of the estimated power delay profile. The pilots are arranged in a frame in such a way that it will fulfil the sampling theorem [75] :

$$d_t \le \frac{1}{2 f_{D_{filter}} T_S} \qquad d_f \le \frac{1}{\tau_{filter} \Delta F} \tag{4.15}$$

where $f_{D\,\text{filter}}$ and τ_{filter} are the estimated Doppler frequency and maximum channel delay filter parameters for estimating the channel correlation function in time and frequency, T_s is the OFDM symbol time including the guard interval duration, d_t is the distance between pilots in time, ΔF is the carrier spacing and d_f is the distance between pilots in frequency.

Optimum sampling can be obtained if the sampling rate of the channel in time and frequency are the same. This condition is termed as the so called balanced design. By observing (4.15), the balanced design is obtained if :

$$f_{D_{filter}} T_s \, d_t = \frac{1}{2} \tau_{filter} \Delta F \, d_f \tag{4.16}$$

This balanced design will be optimal if the power delay spectrum and power Doppler spectrum have the same shape [69]. The rectangular form of the power delay spectrum and power Doppler spectrum will then produce the frequency ($\theta_{\Delta F}$) and time ($\theta_{\Delta t}$) correlation function [75] :

$$\begin{aligned} \theta_{\Delta F}(n-n^{"}) &= \frac{\sin(2\pi\tau_{filter}\Delta F(n-n^{"}))}{2\pi\tau_{filter}\Delta F(n-n^{"})} \\ \theta_{\Delta t}(k-k^{"}) &= \frac{\sin(2\pi f_{D\,filter} T_S(k-k^{"}))}{2\pi f_{D\,filter} T_S(k-k^{"})} \end{aligned} \tag{4.17}$$

The autocorrelation (in time or frequency) between the channel in pilot positions is defined as [75] :

$$\phi_{i'-i"} = \theta_{i'-i"} + \frac{1}{\gamma_c} \tag{4.18}$$

where γ_c is the average SNR on all carriers. Correspondingly, the Wiener filter coefficients for frequency ($\omega_{\Delta F}$) and time ($\omega_{\Delta t}$) direction filtering will be derived as :

$$\omega_{\Delta F}{}^{T} = \theta_{\Delta F}{}^{T} \Phi_{\Delta F}{}^{-1}$$

$$\omega_{\Delta t}{}^{T} = \theta_{\Delta t}{}^{T} \Phi_{\Delta t}{}^{-1} \quad . \tag{4.19}$$

The pre computed filter coefficients should be designed according to the worst case channel condition that may occurs. Therefore, the estimated filter delay τ_{filter} should be chosen equal to the maximum expected excess delay of the radio channel τ_{max}, while the estimated filter Doppler frequency $f_{D\ filter}$ should be chosen equal to the maximum expected mobile radio channel Doppler frequency [73],[75]. Optimum channel estimates will be derived if all available pilots in time or frequency direction filtering are used to estimate one CTF. The filter will require a lot of memory due to the large size of filter coefficients. Another approach is to use some parts of pilots in estimating CTF and refers to the so called sliding window method. The window will slide until all CTFs on one direction filtering are estimated. An example of the sliding window frame for filtering in frequency direction is depicted in Figure 4.1.

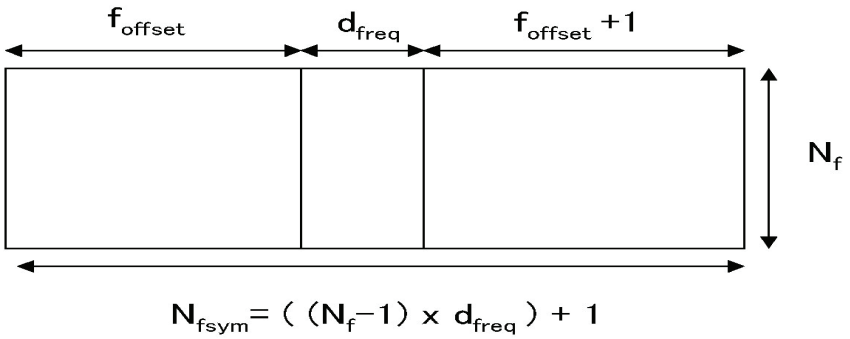

Figure 4.1: Frequency direction filtering sliding window format [76]

The symbol f_{offset} is the distance that define the position of filter coefficients that gives the Minimum Mean square error (MMSE) (filter region with strongest correlation values), d_{freq} is the distance between pilots in frequency, N_f is the number of pilots to be used to estimate one CTF, N_{fsym} is the maximum number of CTFs which in this case is the number of subcarriers that can estimated by the window in one slide. If an optimum channel estimation technique can be used, (which means all available pilots on one direction filtering are utilized), then N_{fsym} in Figure 4.1 will be equal to the number of total subcarriers.

Figure 4.2 depicts an example how the sliding window is applied in estimating the CTFs of one OFDM symbol. The CTFs on the low subcarriers index edge are estimated by using the filter coefficients on the sliding window within a $(f_{offset}+ d_{freq})$ x N_f region. The CTFs at the center part of the OFDM symbols are estimated by using the filter coefficients in the d_{freq} x N_f region, while the filter coefficients within (d_{freq} + $(f_{offset}+1)$)x N_f region are used to estimate the CTFs at the high subcarriers index edge. The box with the letter C contains the filter coefficients in the region of d_{freq} shown in Figure 4.1.

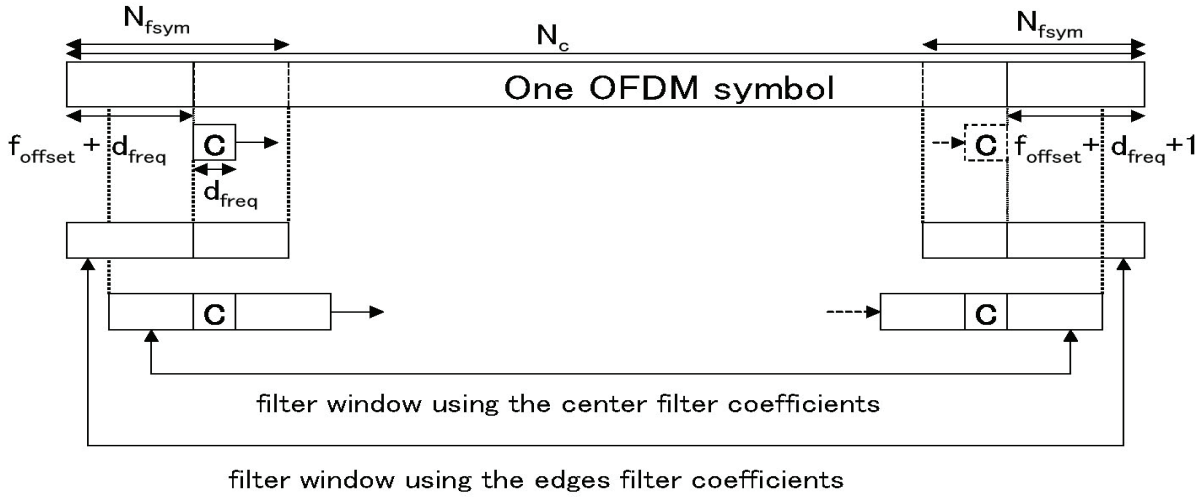

Figure 4.2: Wiener Filter channel estimation by using a sliding window [76]

4.3 Pilot Pattern for a Frequency Hopping OFDM Based Cognitive Radio

In section 2.4 we have discussed how the frequency hopping technique using the TDD Bluetooth frame is able to be applied in OFDM-based Cognitive Radio. Different possible OFDM frame configurations within this technique are given in Table 2.3.

If 2x 1-D filtering would be applied as the channel estimation technique in this OFDM system, then 2 OFDM symbols will be required for this purpose, while 1-D channel estimation requires only 1 OFDM symbol. The filtering in 1-D in this case is applied only in frequency direction. By observing Table 2.3, choosing 128 subcarriers with 11 OFDM symbols per frame is the best OFDM frame configuration option since it gives the highest throughput. The bit rate achieved with a 4-QAM constellation on each carrier for the case 2x1-D channel estimation is around 3.7 Mbits/sec without channel coding. The frame design itself is depicted in Figure 4.3 where the frame is considered as a short package. The symbol Δf refers to the carrier spacing of the OFDM symbol while T_s is the OFDM symbol duration including the guard interval duration. For the case of 1-D channel estimation only one training/pilot symbol is required, hence it gives a higher throughput compared to 2x-1D, but there might be a BER degradation. We evaluate both filtering techniques through simulations.

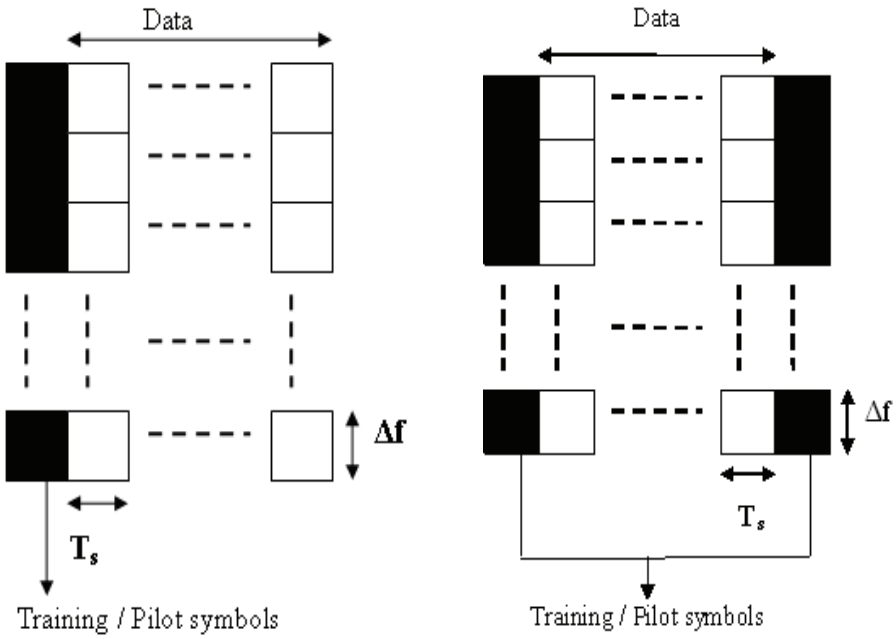

Figure 4.3: OFDM frame design for short packet transmission with (a) 1D channel estimation, and (b) 2x1D channel estimation

The channel model used in the simulations is a WSSUS (wide sense stationary uncorrelated scattering) channel [77], with a power delay profile based on the GSM channel model for rural and urban area [36] provided in Table 2.1 and 2.2. A frequency hopping channel is added by updating the Doppler frequency of the channel each time after transmitting an OFDM frame. The carrier frequency used is between 800-900 MHz. The hopping distance is at multiples of 10 MHz. The number of subcarriers is 128, the guard interval length is 6.4 μs, and 16 QAM is chosen as modulation. A frame consists of 11 OFDM symbols, and the vehicular speed is 120 km/h. Since the frame duration is constrained to be 366 μs , the distance between pilot / training symbols even fulfils a 4 times oversampling assuming a vehicular speed of 300 km/h and f_c 900 MHz. The frame duration with those parameters are also much shorter than the coherence time of the channel. Rural and urban area propagation models are examined. For the sake of simplicity of simulations, it is assumed that the synchronization is perfect. Two scenarios are examined, updated and non updated Wiener filters. In the updated Wiener filter scenario, the transceiver will update its filter coefficients while knowing the current operating carrier frequency which means that the correlation matrix in time will be updated automatically. The update will only affect the performance of 2x1-D Wiener filter since in the 1D channel estimation only the correlation matrix in frequency is required.

Updating the correlation matrix in time will add computation cost and extra processing time since the new correlation matrix has always to be saved in memory. Figure 4.4 shows that 2x1-D Wiener filter performs about 1 dB better than 1-D Wiener filter. Updating the correlation matrix in time in the range 800 – 900 MHz hopping distance does not improve the BER performance of 2x1-D Wiener filter significantly as shown in Figure 4.5. Updating the correlation matrix in time refers to updating the estimated normalized maximum Doppler frequency ($f_{D_{filter}} T_s$). Due to the OFDM duration of the system and the vehicular speed, the deviation error between the updated $f_{D_{filter}} T_s$ and a non updated $f_{D_{filter}} T_s$ is not significant, therefore the performance degradation is also not significant. By assuming a constant speed 120 km/h, and T_s= 32μs the deviation of the maximum Doppler happens if the real f_c is 900 MHz while the estimated $f_{D_{filter}} T_s$ still uses 800 MHz as the carrier frequency, hence the deviation of $f_{D_{filter}} T_s$ will be $((f_{c1} - f_{c2})v/c)T_s$ =((900MHz-800MHz)120km/h / 3.10^8 m/s)32 μs =0.00035 which is quite small. Figure 4.6 shows that 1-D Wiener filter gives a slight BER degradation (around 0.5 dB) compared to the updated 2x1-D Wiener Filter. Therefore 1-D Wiener filter is preferable compared to the 2x1-D Wiener Filter. The 1-D Wiener filtering according to Figure 4.3 is applied in frequency direction only. It estimates the CTFs on one OFDM symbol and assumes that these CTFs will not change significantly for the period of an OFDM frame. Meanwhile in the 2x1-D the whole CTFs in one OFDM frame must be estimated. The Wiener filtering in frequency direction is applied first by the sliding window technique applied onto two OFDM training symbols. Further the time direction filtering is applied on each subcarrier position. The window slides from the first OFDM symbol until the last one. It is obvious that the estimation process using 2x1-D filtering is much more complex

than estimation based on the 1-D Filtering. According to the complexity and performance results the 1-D filtering is the promising channel estimation technique in the OFDM frame with short durations. Furthermore by having the 1-D channel estimation, the last OFDM training symbol can be replaced by data. In this way the bitrate will be higher compared to the 2x1-D channel estimation. The BER performance is lower bounded by the filter matched to the power delay profile and power Doppler Spectrum of the GSM channel model. In case the CR system can access the spectrum longer than the TDD frame duration, the distance between training symbols can be increased. Figure 4.7 shows that the BER gap between the 1-D Wiener filter and the 2x1D filter for longer frame duration is larger compared to the case of short frame duration as depicted in Figure 4.6. The distance between training symbols in long frame duration is increased by a factor of 2 of the one in short packet duration. The 1-D Wiener filter can not cope with the change of the channel in time. This is the reason why the 1-D channel estimation is applied only to the system with frame duration which is shorter than the channel coherence time.

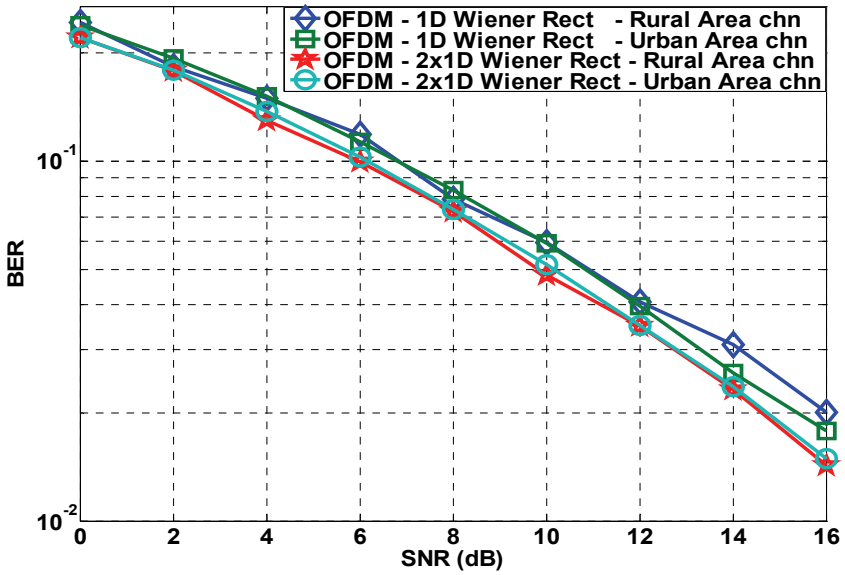

Figure 4.4: BER performance of OFDM with 1-D and 2x1-D non-updated Wiener filter

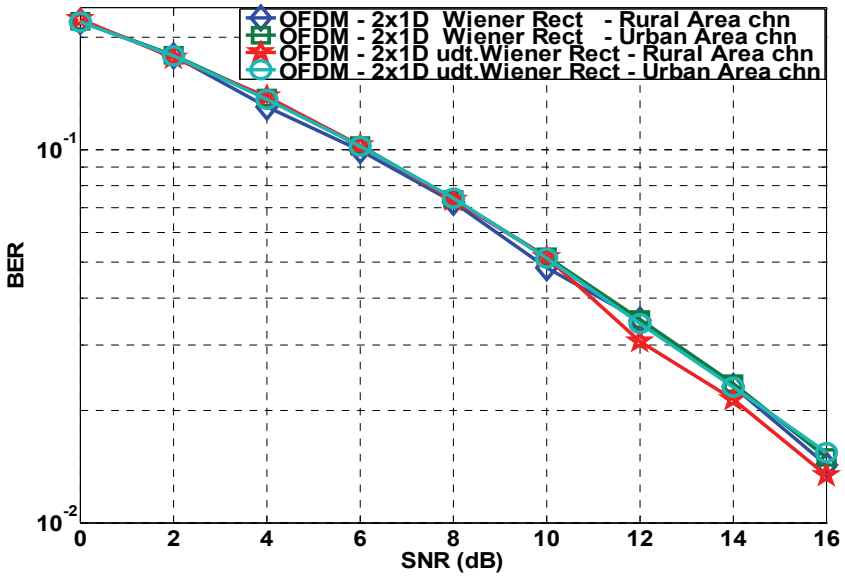

Figure 4.5: BER performance of OFDM with 2x1-D updated and non updated Wiener filter

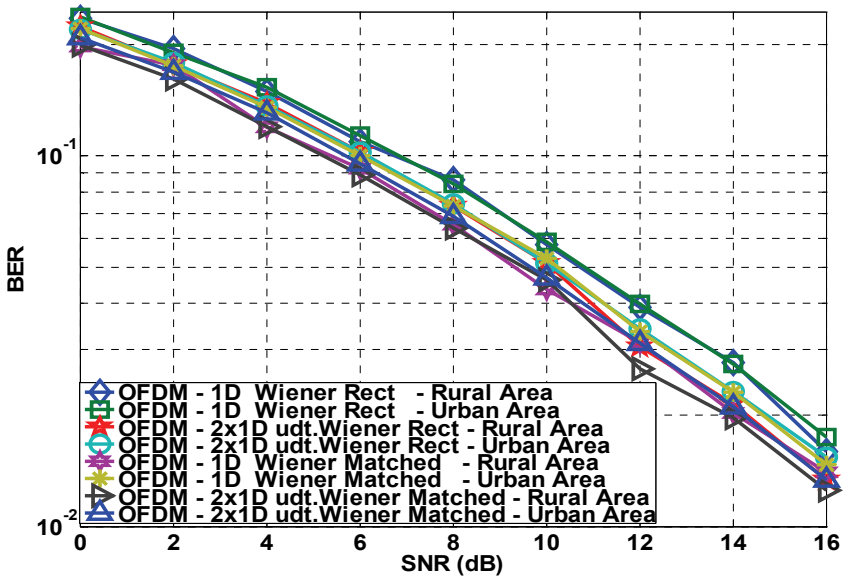

Figure 4.6: BER performance of OFDM with 1-D and updated 2x1-D Wiener filter

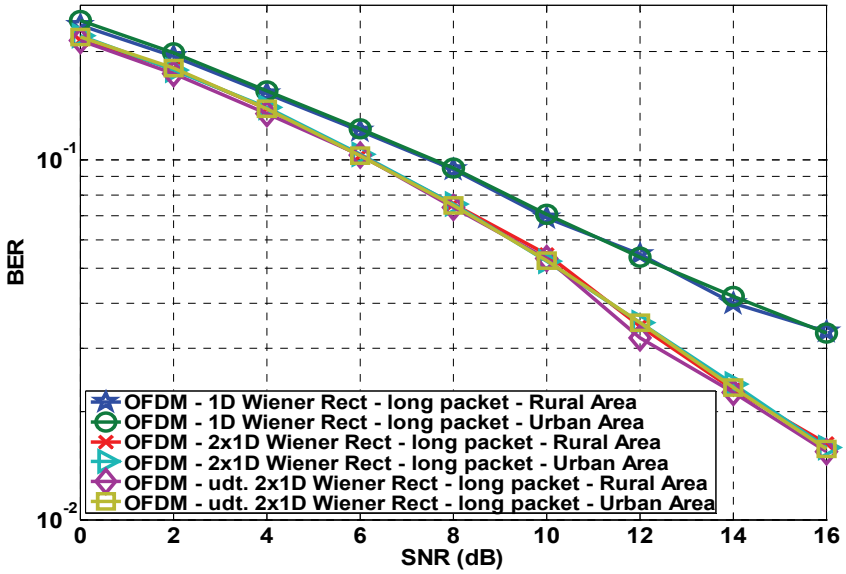

Figure 4.7: BER performance of OFDM with 1-D, 2x1-D, and updated 2x1-D Wiener filter while assuming long packet duration

4.4 Combined an Optimum Pilot Pattern and Virtual Pilots for OFDM-Based Cognitive Radio

The main concern in estimating the channel by using pilot symbols in the context of Cognitive Radio environment is where to place the pilot symbols if there is a frequency band that is occupied by the LU. The main requirement of the pilot pattern design is that the designed pilot pattern will still be able to estimate the channel optimally with the presence of LU; meanwhile the performance of LU in its spectrum band should not be deteriorated by the presence of these pilot symbols. The arrangement of the pilot symbols within an OFDM frame themselves still has to satisfy the criterion as given in eq. (4.15).

In spectrum sharing for CR, the interference is avoided by de-activating subcarriers falling in the Licensed User's band and further interference reduction is applied by de-activating more sub-carriers adjacent to LU band, complemented with time domain windowing and long symbol duration. These interference reduction methods have already been presented in chapter 2 and 3.

In this work we assume that the transmitter and receiver of our system have the knowledge of the presence of LU via the information obtained from spectrum sensing. Our receiver and transmitter will receive the information about the frequency bands that are occupied by the

LU or in the context of OFDM modulation, the subcarriers that are to be de-activated in order not to interfere with the Licensed User.

The approach to solve this problem is dea-ctivating several subcarriers (including the pilot symbols) that overlap with the frequency bands used by the LU. Most degradation in the estimation occurs where the de-activated band edges are at the pilot positions. This is because the channel estimates at the position after these pilots depend on the pilots which are further away in frequency and therefore less correlated. In order to solve this problem we shift the pilot that supposed to be on the edge of the de-activated subcarriers to one subcarrier position most nearby.

This can be applied by simply exchanging the position of the pilot symbols with selected data symbols. This process is done by exchanging the pilot subcarrier with the data subcarrier which lies either previous or next to the original pilot subcarrier. By doing this we can still be able to keep the pilot symbols to be used in the channel estimation process and to sample the channel up to the border with the LU band; however we will have to sacrifice one data subcarrier and losing some throughput. The proposed pilot pattern for the case of wideband interference is depicted in Figure 4.8.

We assume that extra effort in mitigating the Cognitive Radio system sidelobes (by adding sidelobes cancellation carriers as described in Chapters 2 and 3) can be accommodated by treating them on the positions of the de-activated carriers. In this way the shifted pilots will not be on those positions. The CTFs on sidelobes cancellation carrier positions will not be estimated.

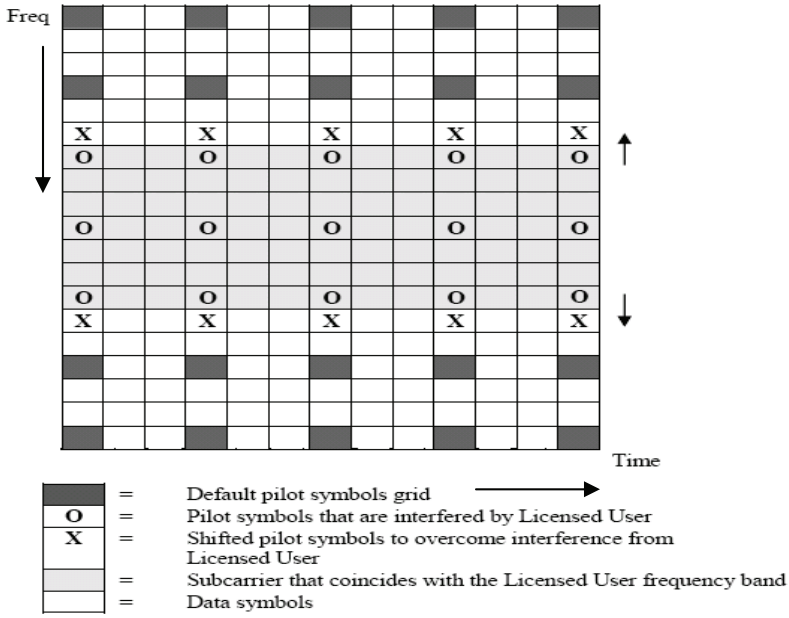

Figure 4.8: Comb/rectangular pilot pattern in the presence of a wideband licensed user

By observing Figure 4.8, we can see that the filtering by a sliding window can be done in two regions, above the LU region and below LU region. Examining eqs. (4.18), (4.19) and Figure 4.1 we know that the filter is generated by assuming constant distances between pilots. However, due to the pilot shifting shown in Figure 4.8, the distance between shifted pilot and the regular pilot is changed; therefore two extra filters should be designed. One to estimate the CTFs in the vicinity of the shifted pilots in the region above the LU band and the other one for the CTFs in the vicinity of the shifted pilots in the region below the LU band.

A hexagonal sampling pattern is considered to be the most efficient two-dimensional sampling scheme. This scheme requires 13.4% fewer samples than the rectangular sampling to represent the same circularly band limited continuous signal [78]. In [79] and [80] the application of a hexagonal pilot pattern in OFDM was evaluated and the simulations revealed that the hexagonal pattern gives a better BER compared to the Rectangular pilot pattern. In [81] the analysis was made in designing the optimum pilot pattern for OFDM channel estimation. Through simulations it was verified that the hexagonal pilot pattern is BER indeed outperformed the rectangular pilot pattern. The complete design requirements for the hexagonal pilot pattern can be found in [81].

There is another consideration assuming that the channel estimation will be optimum if the pilots are allocated in a random scattered way i.e. putting them only on the subcarrier and OFDM symbol positions that have really good SNR. In this way, the channel estimation mean square error can be reduced. The disadvantage is that if the sliding window technique is applied, this pattern randomness will require several sliding window filters, because a sliding window filter requires an invariant pilot distance. Therefore, in this dissertation the hexagonal pilot pattern is preferable compared to the random pattern despite we know that optimum filtering (using a complete set of pilots) will favour the application of the random pilot pattern since in that case, only one filter is used to do channel estimation. However, using a complete set of pilots in estimating one channel transfer function results into extra computational complexity.

If the hexagonal pilot pattern is adopted in the Cognitive Radio system combined with the pilot shifting method, then we will have the pattern as depicted in Figure 4.9.

Still in the form shown in Figure 4.9 there will be a non-constant distance between pilots, and due to the hexagonal pilot pattern and de-activated carriers in some OFDM symbols, there will be no pilots at the edges. Therefore several filters are required to estimate the CTFs.

In order to counteract this problem we propose to include the virtual pilot concept to simplify the filtering process by only utilizing one Wiener filter set. Inserting the virtual pilots between two pilots will give a two-times pilot oversampling effect to the channel estimates. The new pattern becomes as depicted in Figure 4.10.

The virtual pilot concept has been previously introduced in [82]. Virtual pilots are no pilots

allocated by the transmitter to the OFDM frame for the purpose of channel estimation, but rather are imaginary pilots located at certain data positions. Through a signal processing technique these virtual pilots will give almost the same impact as the real pilots in providing initial channel estimates. These estimates will further be utilized by the filtering or channel estimation process in producing the final channel estimates. Virtual pilots are located in between 2 consecutive pilots, which are actually at the data positions. It should be emphasized that no actual pilots are transmitted at these positions, but the received data at those locations are used for generating virtual pilots to enhance the channel estimation performance. The initial channel estimates at the virtual pilot positions are derived by interpolating linearly the pairs of the initial estimates at the actual pilots position (derived from eq. (4.3)) close to the position of the virtual pilots. The interpolation is carried out by assuming that the channel does not change significantly (slowly changed) between a pair of pilots, which denotes that the pilot spacing in frequency direction should be smaller than the channel coherence bandwidth while in time the pilot spacing is smaller than the channel coherence time.

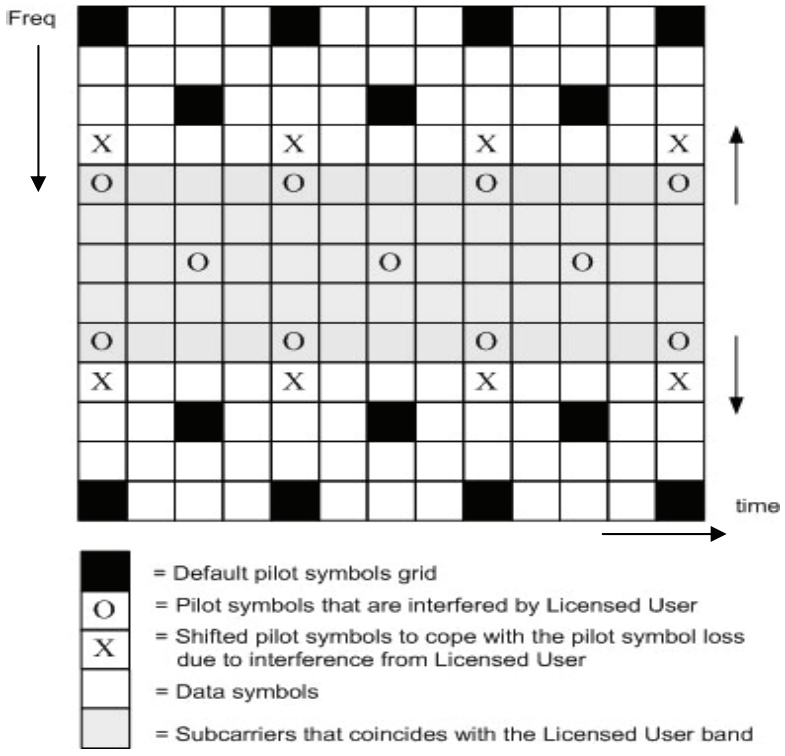

Figure 4.9: Hexagonal pilot pattern in the presence of wideband licensed user

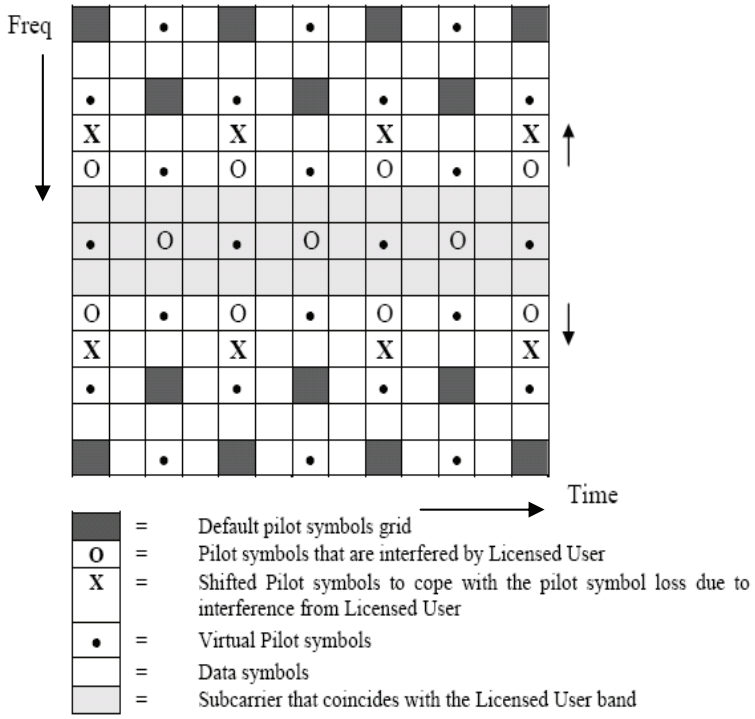

Figure 4.10: Hexagonal pilot pattern with integrated virtual pilot concept in the presence of a wideband licensed user

Based on these assumptions we try to predict the value of the initial channel estimates in between two neighboring pilot symbols that can be seen as the initial channel estimates at the virtual pilot symbol positions. The application of virtual pilots starts from the initial estimate of the channel derived from (4.3). The value of preliminary initial channel estimates on a virtual pilot position is obtained from a simple linear interpolation method, described by:

$$\hat{H}_{n',k'} = \frac{1}{2}\left[\hat{H}_{n',k'-1} + \hat{H}_{n',k'+1}\right] \text{ or } \hat{H}_{n',k'} = \frac{1}{2}\left[\hat{H}_{n'-1,k'} + \hat{H}_{n'+1,k'}\right] \tag{4.20}$$

where $\hat{H}_{n',k'-1}$, and $\hat{H}_{n',k'+1}$ indicate the initial estimates of the previous and the next pilot symbols in time, meanwhile $\hat{H}_{n'-1,k'}$, and $\hat{H}_{n'+1,k'}$ indicate the initial estimates of the previous and next pilot symbols in frequency. The virtual pilots located at the edge of the frame are estimated by extrapolating pair of pilots in the vicinity of the virtual pilot position; it can be expressed as:

$$\hat{H}_{n',k'} = \frac{1}{2}\left[\hat{H}_{n'+1,k'} + \hat{H}_{n',k'+1}\right] = \frac{1}{2}\left[H_{n'+1,k'} + H_{n',k'+1}\right] + \frac{1}{2}\left[\frac{N_{n'+1,k'} + I_{n'+1,k'}}{S_{n'+1,k'}} + \frac{N_{n',k'+1} + I_{n',k'+1}}{S_{n',k'+1}}\right]. \tag{4.21}$$

Adding the concept of virtual pilots resembles twice oversampling of the initial pilot pattern. The block diagram of the OFDM with channel estimation using virtual pilots at the receiver is depicted in Figure 4.11. The decision directed method will estimate the initial channel estimates at virtual pilot positions by predicting the transmitted symbol at those virtual pilot positions utilizing the results from eq. (4.20) or eq. (4.21). The aim of the decision directed method is to reduce the effect of interpolating the noisy initial channel estimates derived from eq. (4.20) or eq. (4.21). The process is described in Figure 4.12. $\hat{X}_v$, $\hat{X}'_v$, Y_v, $\hat{H}_v$ and $\hat{H}'_v$ are the estimated transmitted symbol before de-mapping, estimated transmitted symbol after using the decision directed method (after mapping), the received symbol, the preliminary initial channel estimate from simple linear interpolation/extrapolation and the final initial channel estimate at the virtual pilot position v after using the decision directed method, respectively. It is worth mentioning that we assume that the virtual pilot positions be always constant in between two real pilots or at the edges while in reference [82] the virtual pilot position varies according to the minimum Euclidean distance between the results before using the decision directed method and after, and the threshold selection. Our method has the advantage that by having constant virtual pilot positions the filtering process especially in the application of a sliding window, can be greatly simplified.

In the case the decision directed estimation module can perfectly estimate the transmitted symbol at the position of the virtual pilots, the initial estimates at the virtual pilot positions will be the same as if the transmitter sends the real pilots at those positions (virtual pilots). Extra deviation from the initial channel estimates at the virtual pilots comes from the decision errors in estimating the transmitted symbol at the virtual pilot positions. The received signal in frequency domain at the virtual pilot positions can be envisioned as:

$$\begin{aligned} Y_v &= \frac{H_v \cdot X_v}{\hat{H}_v} + \frac{N_v + I_v}{\hat{H}_v} = X_v \cdot \left(1 + \frac{H_v - \hat{H}_v}{\hat{H}_v} \right) + \frac{N_v + I_v}{\hat{H}_v} \\ &= X_v + \left\{ \frac{H_v - \hat{H}_v}{\hat{H}_v} \cdot X_v + \frac{N_v + I_v}{\hat{H}_v} \right\} \end{aligned} \tag{4.22}$$

where H_v, N_v and I_v are the respective CTF, noise and interference on virtual pilot position v. The decision error in estimating $\hat{X}'_v$ occurs when:

$$\left\| \frac{H_v - \hat{H}_v}{\hat{H}_v} \cdot X_v + \frac{N_v + I_v}{\hat{H}_v} \right\| > \frac{D}{2} \quad , \tag{4.23}$$

with D as the minimum distance between the constellation points of symbol X_v. The deviation

error increases as ($H_v - \hat{H}_v$) is significant and the constellation size of X_v increases. The maximum deviation takes place at the largest constellation point $X_{v,max}$. The effect of a decision error in estimating the symbol at the virtual pilot position will be an additional deviation beside noise and interference contribution to the final initial channel estimates compared to eq. (4.3),

$$\begin{aligned}\hat{H}'_v &= \frac{H_v \cdot X_v}{\hat{X}'_v} + \frac{N_v + I_v}{\hat{X}'_v} = H_v \cdot \left(1 + \frac{X_v - \hat{X}'_v}{\hat{X}'_v}\right) + \frac{N_v + I_v}{\hat{X}'_v} \\ &= H_v + \left\{\frac{X_v - \hat{X}'_v}{\hat{X}'_v} \cdot H_v + \frac{N_v + I_v}{\hat{X}'_v}\right\}.\end{aligned} \tag{4.24}$$

If the channel state between two pilots is slowly varying and assuming the noise plus interference averaging advantage in estimating $\hat{H}_v$ (as described in eq. (4.21)), then most likely ($H_v - \hat{H}_v$) will be close to zero. Moreover, in a dynamic spectrum access concept the sub-carriers in the interference band, which in this context is the LU band, will be de-activated. The sidelobe of the interferer signal will distort the CR signal, but the impact will be decreased because of the larger distance between the OFDM based CR sub-carrier to the LU band. By applying the mechanism of de-activating more carriers adjacent to LU band, or by inserting the cancellation carriers as described in chapters 2 and 3, the interference effect to the CR signal will become very low and perhaps negligible. Therefore, according to eq. (4.23), the decision error in estimating the transmitted symbol at the virtual pilot position will be dominated by the influence of the noise term N_v and interference term I_v which are divided by $\hat{H}_v$. If $\hat{H}_v$ is large, the decision error probability in estimating $\hat{X}'_v$ will be reduced. If the decision directed method can estimate the transmitted symbol accurately, the initial channel estimates at the virtual pilot position described by eq. (4.24) will be equal to eq. (4.3) because then $X_v = \hat{X}'_v$. This condition will be comparable to the scheme where real pilots are inserted at the virtual pilot positions, and the initial channel estimates are derived by the least square method (dividing the received pilot symbols by the reference pilot symbols). This analysis will be further validated in the performance evaluations in section 4.4.1.

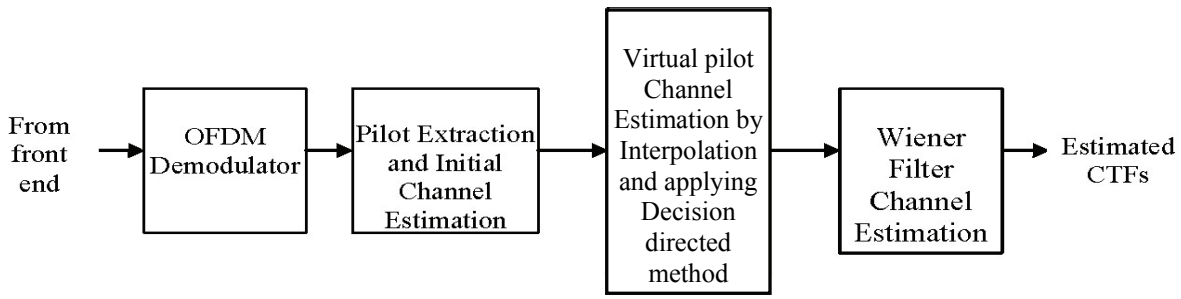

Figure 4.11: OFDM channel estimation with virtual pilots processing in the receiver

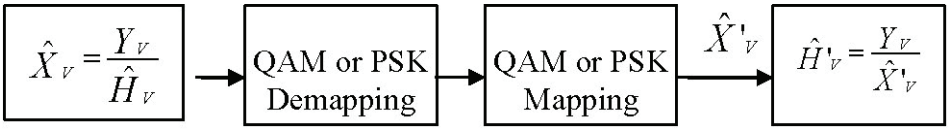

Figure 4.12: Decision directed method in estimating the virtual pilots

The additional complexity in the inclusion of the virtual pilot concept to an OFDM system is comparable to the number of virtual pilots included to the OFDM frame. Since the virtual pilots normally exist in between two real pilots, the number of extra computations required in a free environment (without LU access or de-activated carriers) equals:

$$O = \underbrace{\left(\left\lceil \frac{N_c}{d_f} \right\rceil - 1\right)}_{a}.\underbrace{\left(\left\lceil \frac{N_s}{d_t} \right\rceil - 1\right)}_{b} + \underbrace{\left(\left\lceil \frac{N_c}{d_f} \right\rceil - 1\right).\left(\left\lceil \frac{N_s}{d_t} \right\rceil - 1\right).M}_{c} + \underbrace{\left(\left\lceil \frac{N_c}{d_f} \right\rceil - 1\right).\left(\left\lceil \frac{N_s}{d_t} \right\rceil - 1\right)}_{d}, \qquad (4.25)$$

where O is the number of computations, N_c is the number of active subcarriers, N_s is the number of OFDM symbols per frame, d_f is the distance between pilots in frequency, d_t is the distance between pilots in time, and M is the constellation size of the data at the virtual pilot positions. The term a in eq. (4.25) indicates the number of virtual pilots in frequency, b is the number of virtual pilots in time. The multiplication between a and b refers to the number of interpolation/extrapolation required. The term c is the number of mathematical operations required in calculating the Euclidean distance between a symbol derived from eq. (4.22) and the reference points on the respective constellation data mapping (M-QAM or M-PSK) used at the virtual pilot positions, while the term d is the number of division operations between the received signal at virtual pilot positions and the estimated symbol after using the decision directed process as described in eq. (4.24). Since the application of the virtual pilots is to simplify the filtering process, the position of the virtual pilots should always be in the middle of two pilot positions. Therefore the distance between two pilots should be even.

If the number of de-activated sub-carriers is large enough compared to the LU band the mutual interference from or to the LU will be significantly low and can be considered negligible. It means that the interference contribution denoted by symbol I in eq. (4.3) and eqs. (4.21)-(4.24) will be close to zero. This analysis is needed in case a residual interference due to sidelobes of LU exists. The residual interference will be considered as an extra or additional noise that will degrade the SINR and will add an extra deviation into the transmitted data at the virtual pilot positions as described in eq. (4.22) and to the final initial channel estimates as depicted in eq. (4.24).

The decision directed method requires the received signal information at the virtual pilot positions. In the OFDM-based CR system sub-carriers located at the LU band and adjacent to it are de-activated for the purpose of mitigation of the mutual interference. Since the received

signal at the de-activated sub-carriers positions (LU band) is not available, the decision directed method cannot be applied to those positions. For cases where initial channel estimates located at the de-activated sub-carrier positions are required, the channel estimates will be obtained by linear interpolation / extrapolation.

By observing eq. (4.8), eqs. (4.17)-(4.19) a higher correlation value will render a lower theoretical channel estimation mean square error (MSE). By having a two-times pilot oversampling effect due to the application of virtual pilots, the Wiener filter MSE in mismatched model error case given in eq. (4.8), can be reduced. This is achieved at the cost of complexities for applying the linear interpolation/extrapolation between two real pilots with the addition of using that decision directed process.

The channel estimation is applied separately to the region before as well as after the de-activated band. If a large number of LUs exists, more sub-carriers need to be de-activated. If the positions of the LUs are scattered, then more edge effects in the channel estimation occur that will further degrade the channel estimation performance. The edge effect can be avoided if the LU band is less than the distance between pilots in frequency since the initial channel estimates at the de-activated pilot positions can still be nicely performed by the interpolation method. If many carriers need to be de-activated due to scattered LUs, then optimal filtering (using all available pilots in each filtering direction) will be feasible to be applied as long as the memory-saving capability of the Cognitive Radio device suffices.

4.4.1 Performance Evaluation and Analysis

In practice the actual power delay profile and Doppler power spectrum are not perfectly known at the receiver; the Wiener filter assumes a rectangular power delay profile and Doppler power spectrum, which creates a model mismatch. The simulations ran using a channel model based on the statistical discrete time model wide sense stationary uncorrelated scattering (WSSUS) which combines multipath fading and Doppler frequency effects [77]. The simulation parameters are provided in Table 4.1. According this Table there will be a maximum Doppler frequency of 82 Hz. No channel coding and interleaving are applied. Other channel models can be used to validate the results of the use of virtual pilots for OFDM-based CR channel estimation. Since the virtual pilot is located in between two real pilots, the virtual pilot concept will be effective for slowly varying channels. This means the coherence bandwidth and coherence time of the channel which refer to the delay spread and maximum Doppler frequency will determine the effectiveness of the virtual pilot concept. Synchronization is an important issue in every OFDM system. The problem can be solved by the aid of training symbols or the cyclic prefix characteristic of the OFDM GI. The process in the context of Cognitive Radio will be explored in section 4.6. For the simplicity of simulation, we assume perfect synchronization between transmitter and receiver.

We begin by evaluating the performance of the proposed pilot pattern according to Figure 4.8. Figure 4.13 depicts the channel mean square error (MSE) and BER results of the proposed

rectangular pilot pattern with shifted pilots due to LU access and conventional OFDM without carriers de-activation (Normal (3,3) Pilots, meaning that the distance between pilots in frequency and time is 3). Two LU widths are considered, with a 10 carriers de-activation (Modified(3,3) Pilot Pattern scheme (10 subcarriers de-activated)) and a 61 carriers de-activation (Modified(3,3) Pilot Pattern scheme (61subcarriers de-activated)). No significant performance degradation occurs related to the number of de-activated carriers. The error floor is formed due to the model mismatched used between the true power delay profile and Doppler power spectrum and the estimated ones in designing the Wiener filter. The mismatch error can be termed as the Wiener filter error.

Significant degradation can be observed if a number of wideband LU sets of carriers are scattered and therefore the filtering is applied separately in each free region (bands not occupied by LU). Due to this condition, as depicted in Figure 4.1, filters at the edges that give higher MSE compared to the middle filter (in the d_{freq} region that gives MMSE), will often be used. The simulation results depicted in Figure 4.14 show the expected behaviour, where each LU with 10 carriers de-activation is scattered in the spectrum. The results in Figures 4.13 and 4.14 have been presented in conference paper [83].

Table 4.1: Simulation parameters

Bandwidth	1.28 MHz
Number of subcarriers	213
De-activated subcarriers	61
Subcarrier spacing	5 KHz
FFT length	256
Guard interval	43.75 μs
OFDM symbol duration (inc. cyclic prefix)	$T_s^{'}$ = 243.75 μs
OFDM symbols per frame	46
Modulation for pilot symbols	BPSK
Modulation for data symbols	4-QAM
Normalized pilot spacing in frequency	d_f = 3 or d_f = 4
Normalized pilot spacing in time	d_t = 3
Fading model	*Rayleigh*
Maximum Doppler frequency	f_{Dmax} = 82 Hz
Maximum delay	τ_{max} = 9.375 μs
RMS delay spread	τ_{rms} = 3.4 μs
# of channel taps	4
Number of paths per tap	10
Power decrement per tap	1 dB
Tap spacing	3.125 μs
Channel coding and interleaver	OFF

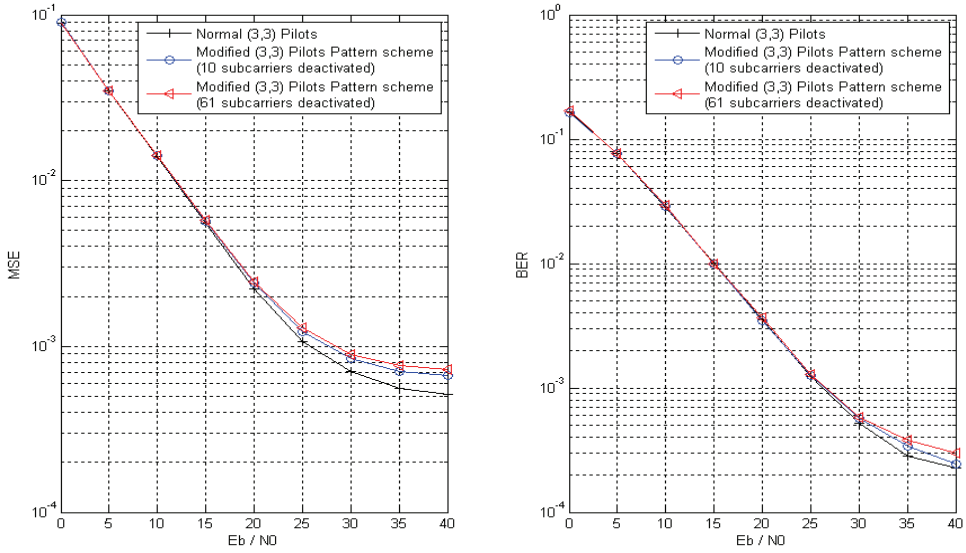

Figure 4.13: Performance of the modified pilot pattern (Eb/N0 in dB) in the presence of a wideband Licensed User (Left: MSE, Right: BER)

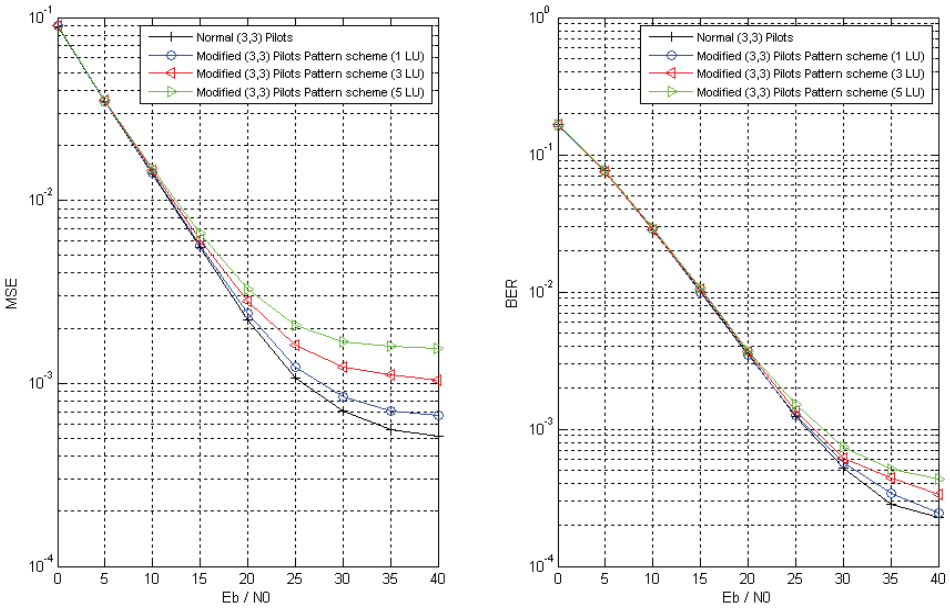

Figure 4.14. Performance of the proposed pilot pattern (Eb/N0 in dB) with an increasing number of scattered wideband Licensed Users with 10 subcarriers de-activated for each Licensed User (Left: MSE, Right: BER)

Next we evaluate the performance of the pilot pattern according to Figure 4.10 where virtual pilots are utilized to aid the channel estimation process. As a start, in order to observe the effectiveness of the virtual pilot concept, we evaluate an OFDM system without the existence of LU access. Therefore, at the beginning no carriers de-activation is applied.

Figure 4.15 shows the MSE performance comparisons of the regular rectangular, hexagonal, rectangular and hexagonal with virtual pilots from the interpolation/extrapolation process (no decision directed) in the absence of a LU band. At high SNR the hexagonal pattern with virtual pilots outperforms the other three patterns significantly. The rectangular pattern with virtual pilots outperforms the normal rectangular and hexagonal pattern at high SNR, while at low SNR their performances are close to each other. The results have been presented in reference [84].

By adding the decision directed method, the use of virtual pilots has shifted the MSE of the hexagonal pattern downwards. Both the rectangular and hexagonal pattern with decision directed virtual pilots converge close to each other as shown in Figure 4.16. At an MSE of 10^{-3} the use of the decision directed virtual pilot gives about 5 dB SNR gain compared to the use of virtual pilots from interpolation/extrapolation only. The two figures (Figure 4.15 and Figure 4.16) demonstrate that the use of the virtual pilots has reduced the Wiener filter MSE (mismatch errors) which is indicated by the reduction of the error floor for high SNR. The channel estimation MSE is thus influenced by the noise and mismatch errors.

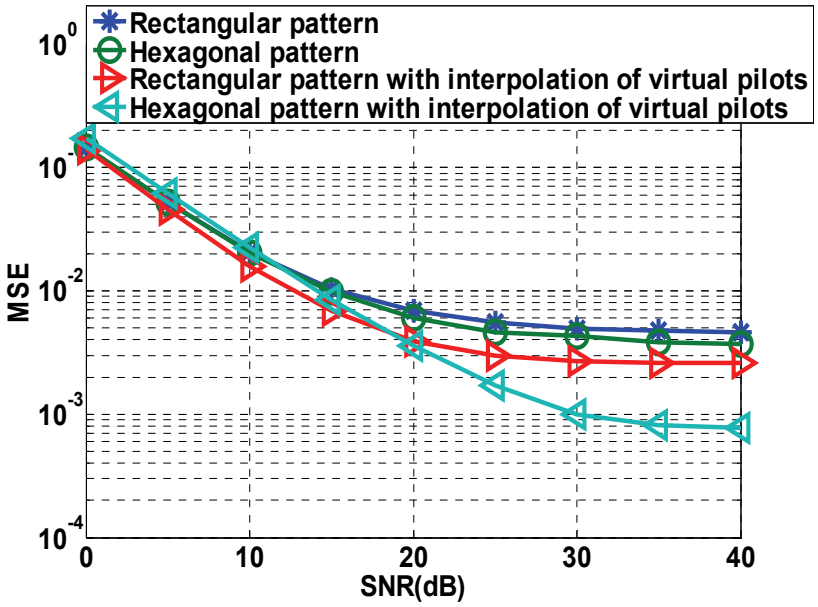

Figure 4.15: Channel estimation MSE vs SNR(dB) comparisons of regular rectangular, regular hexagonal pilot patterns, as well as rectangular and hexagonal pilot pattern with virtual pilot symbols from the interpolation/extrapolation process

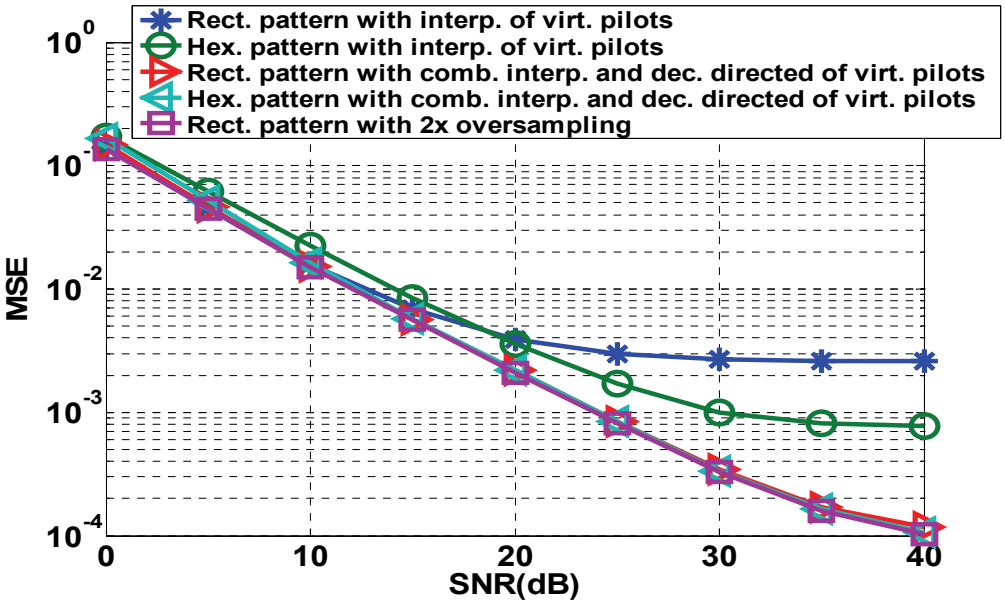

Figure 4.16: Channel estimation MSE vs SNR(dB) comparisons of rectangular, hexagonal pilot pattern with virtual pilots derived from interpolation./extrapolation, their combinations with the decision directed method and with a two-times oversampling rectangular pattern

At high SNR the noise contribution to MSE becomes negligible and only the mismatch errors contribution remains. Figure 4.17 shows the BER improvement by using virtual pilots and the decision directed method in the hexagonal pattern compared to the BER results without decision directed. As seen from this figure an 8 dB gain is derived at a BER of $2x10^{-3}$. This shows that the decision directed method improves the channel estimation performance considerably, which consequently enhances the BER performance when compared to the regular hexagonal pattern. To ensure that the combined virtual pilots with hexagonal pilot pattern is indeed powerful, we have also evaluated its performance using the low pass filtering interpolation channel estimation method [85]. The results are depicted in Figure 4.18. Although the low pass filtering exhibits a larger interpolation error compared to the Wiener filter, the application of virtual pilots has enhanced its interpolation performance.

The performance is lower bounded by the two-times oversampling rectangular pilot pattern, and they are close to each other. This means that the proposed hexagonal pilot pattern with virtual pilots and the decision directed method can perform almost the same as the two-times oversampling rectangular pilot pattern without adding more pilots. In other words, by doing under-sampling with hexagonal pilot pattern combined with virtual pilots using the decision directed method, the same channel MSE performance as without doing under-sampling pilot allocation, can be obtained while the number of pilots transmitted is reduced.

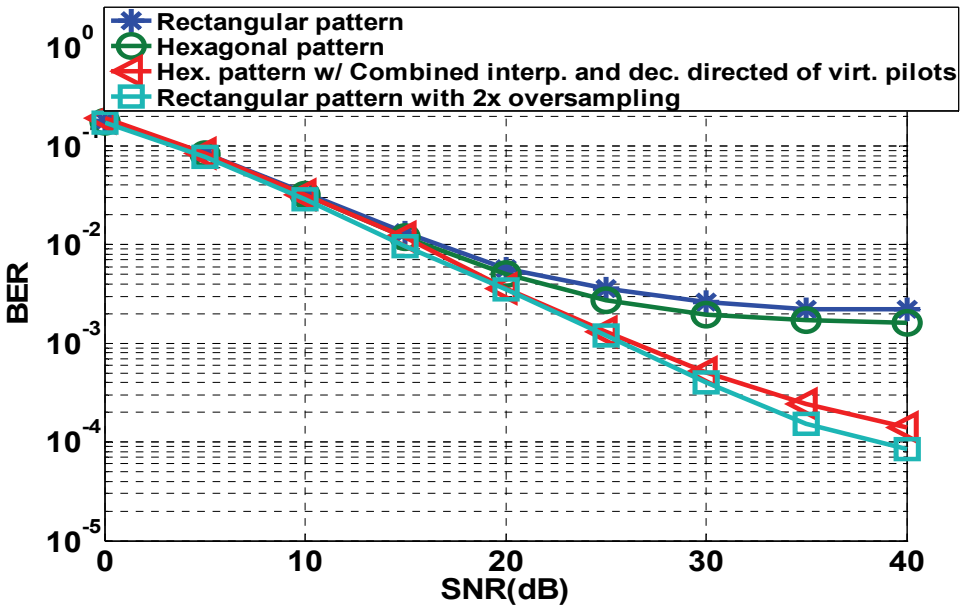

Figure 4.17: BER vs SNR(dB) comparisons of rectangular, hexagonal pattern, combined hexagonal pattern with virtual pilots from interpolation/extrapolation and decision directed method, and the two-times oversampling rectangular pattern

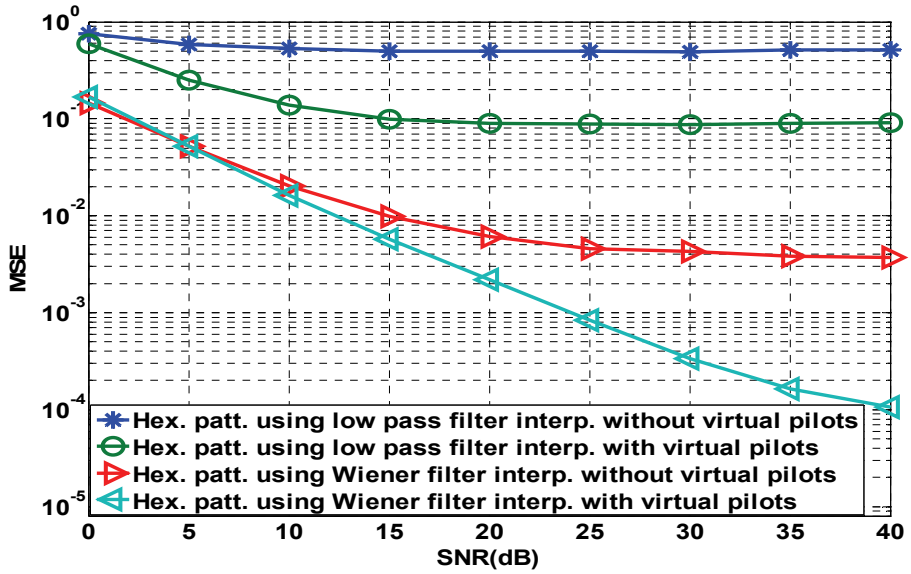

Figure 4.18: Channel estimation MSE vs SNR(dB) comparisons of hexagonal pattern, with virtual pilots from interpolation/extrapolation and the decision directed method for low pass filter interpolation and the Wiener filter channel estimation

By referring to eq. (4.22), in a slowly varying channel, the deviation of estimating the transmitted symbol on the virtual pilot positions (due to inaccurate initial channel estimates) from a simple linear interpolation/extrapolation is negligible, and the decision error is dominated by the noise component. The condition shown in Figure 4.16 where the use of the combined linear interpolation/extrapolation and decision directed virtual pilots to the hexagonal pattern has gained almost the same MSE performance as the two-times oversampling rectangular pattern refers to the circumstance that seldom decision errors occur in estimating the symbol on the virtual pilot positions. Thus eq. (4.24) will be the same as eq. (4.3) what implies the term as if we transmit real pilots on the virtual pilot positions. By also observing eq. (4.24) we have simulated the MSE performance of the use of virtual pilots to the hexagonal pattern and varying the constellation size M of the data symbols; that can be interpreted as varying the constellation size of the symbols on virtual pilot positions. According to eq. (4.24) increasing M will decrease the deviation by the noise part. Figure 4.19 confirms the analysis where at low SNR the highest M gives the lowest MSE. We have to emphasize at this point that reference [82] fails to address this issue as in that reference the pilot spacing between real pilots is decreased when allocating data with higher M.

On the contrary, the BER curve in Figure 4.20 shows that symbols with higher M are more vulnerable to noise which follows the property of QAM or PSK symbols; therefore the highest M gives the poorest BER performance. An exception is the case where the BER performance of virtual pilots M =4 outperforms M=2; this is (although the BER in $M=4$ is more vulnerable to noise compared to $M=2$) because according eq. (4.24) $M=4$ has less channel estimation deviation error. The overall errors (bit errors due to noise and channel estimation errors) for $M=4$ and $M=2$ are shown by the BER results in Figure 4.20. The virtual pilots with constellation size M=4 is more optimal when compared to M=2.

In Cognitive Radio spectrum sharing context of our simulations, there are 61 carriers de-activated (carrier no. 81 – 141) due to LU occupancy. The LU itself occupies 40 carriers in the middle; this means 10 guard bands on each side of LU are provided. In this way the mutual interference between LU and our Cognitive Radio system will be negligible. The distance between pilots in frequency is 4 sub-carriers, while in time it is 3 OFDM symbols. The sliding windows in time and frequency for CTFs estimation are designed using 4 pilots per window filter slide. Observing the frequency direction in Figure 4.9, we can see that the hexagonal pattern renders 2 sets of pilot patterns, which consequently refers to a two sets filter coefficients requirement. The proposed hexagonal pilot pattern with virtual pilot symbols simplifies the implementation of hexagonal pilot pattern filtering due to the new structure that resembles the rectangular pilot patterns structure. According to the parameters in Table 4.1 there will be 640 virtual pilots per frame required to aid the filtering. Due to the existence of de-activated carriers and pilot shifting, we cannot use eq. (4.25) to calculate the number of extra operations (interpolation/ extrapolation + decision directed) required before filtering is applied, but the number of virtual pilots in a frame and the M of the data at the virtual pilot positions suffice.

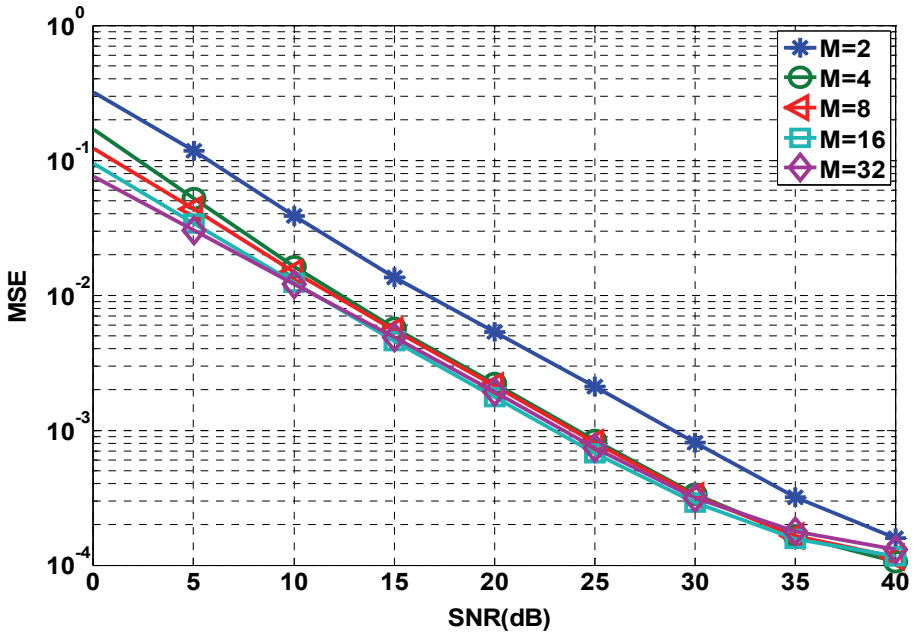

Figure 4.19: Channel estimation MSE vs SNR(dB) comparison of combined hexagonal pattern with virtual pilots from interpolation/extrapolation and the decision directed method with different constellation size (*M*) of the symbol at the virtual pilot positions

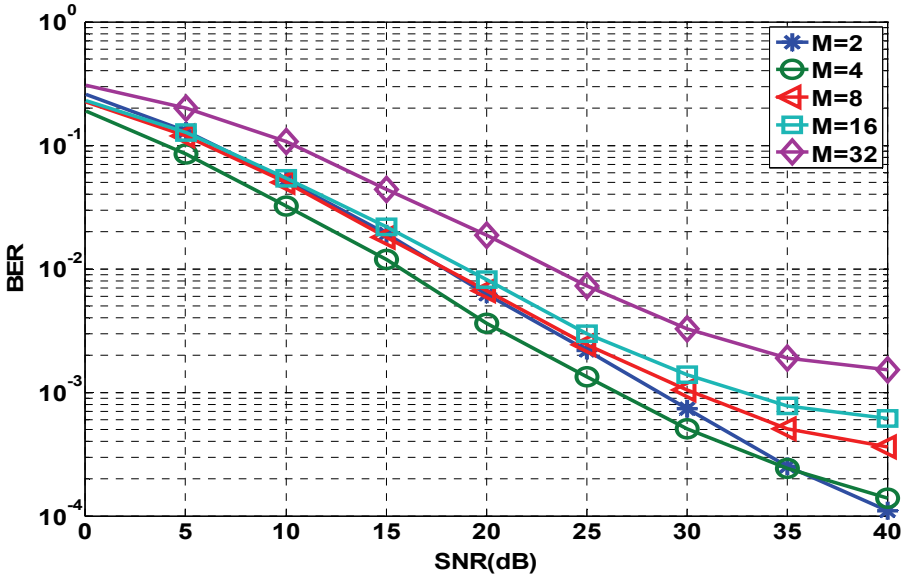

Figure 4.20: BER vs SNR(dB) comparison of combined hexagonal pattern with virtual pilots from interpolation/extrapolation and the decision directed method with different constellation size (*M*) of the symbols at the virtual pilot positions

Having *M=4* means that 3840 extra computations are required in the application of virtual pilots, where 640 computations are dedicated to linear extrapolation/interpolation, 2560 computations for calculating the Euclidean distance, and 640 division operations between received data at virtual pilot positions and the estimated symbol after the decision directed process. The performance comparison is done in the form of MSE, which is the mean square difference between the channel estimates and the real CTFs which according to reference [86] is the appropriate measure to compare the performance of different channel estimation techniques. The MSE results can not be translated directly as a one to one relationship to the bit error rate (BER) [86]. This is due to the fact that in certain cases (although MSE occurs) MSE does not deliver the decision errors onto the demapping (QAM or PSK) process. In the presence of LU, we consider the LU band 200 KHz wide which is equal to about 40 OFDM sub-carriers. Without loss of generality, the band is assumed to be located in the middle of the CR band. By de-activating 61 sub-carriers the CR system provides about 10 sub-carriers (50 KHz) guard band with respect to the LU band; hence, the mutual interference is considered to be negligible. Figure 4.21 shows the performance of the hexagonal pilot pattern with the use of virtual pilots from interpolation/extrapolation and its combination with the decision directed method in the presence of LU. The decision directed method provides at MSE of $2x10^{-3}$ about 2 dB SNR gain compared to the use of virtual pilots only derived from the interpolation/extrapolation method.

In the presence of LU, more edge effect occurs, since the estimation using the sliding window is divided into several regions. As the number of LUs increases and scattered within different spectrum regions, the edge effect will occur more often. If the sliding window technique is used as filtering method (i.e. in the situation a large number of LUs are scattered in the whole band), the channel estimation performance will be degraded. Therefore, for higher numbers of LUs the optimum Wiener filter (i.e. utilizing all pilots within an OFDM symbol) can be applied in the simulations as long as the required memory to save the filter coefficients is sufficient. Figure 4.22 shows the performance of the optimum Wiener filter with a hexagonal pilot pattern using virtual pilots derived from interpolation, or from combined interpolation and the decision directed method, and the one without virtual pilots. With the optimum Wiener filter, and adding the decision directed method it provides about 2.5 dB gain at an MSE $2x10^{-3}$ compared to estimating the virtual pilot using only interpolation, while the hexagonal pattern without virtual pilots never reaches that MSE value ($2x10^{-3}$) due to the error floor from the mismatch error between the estimated shape and the actual channel power delay profile and Doppler power spectrum shape. The optimum Wiener filter always outperforms the filtering using the sliding window, because more pilots are utilized in the estimation of one CTF. There are two factors that influence the channel estimation error, they are noise and the mismatch in estimating the channel power delay profile and Doppler power spectrum. Through all simulation results the impact of the inclusion of the virtual pilots on our system can be seen at high SNR where the mismatch error is minimized and little noise contribution exists. The impact of noise on the BER performance can be mitigated by using channel coding and interleaving. In this way the gain of the virtual pilots to our system can be

seen in the lower SNR region. The results in Figures 4.16-4.22 have been presented in reference [87].

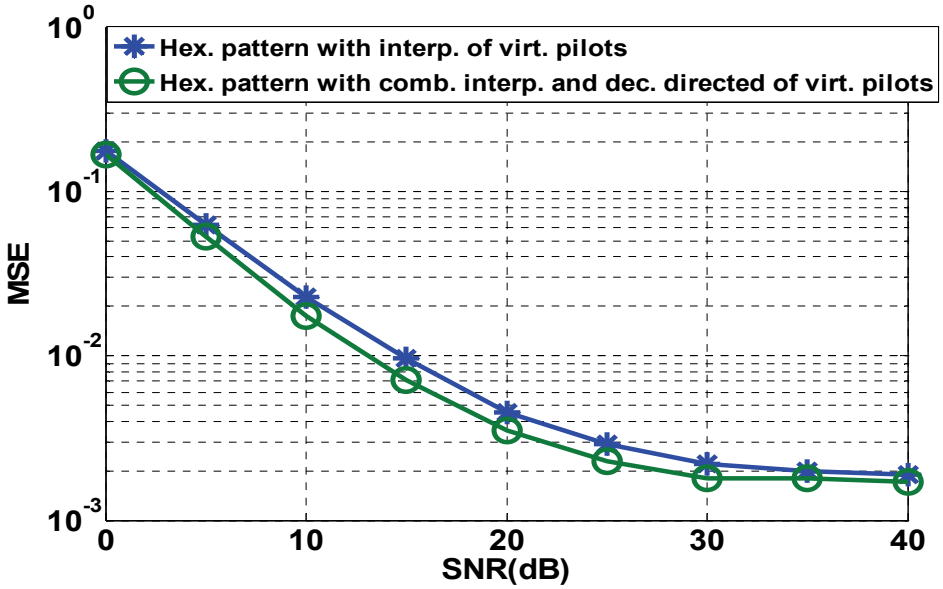

Figure 4.21: Channel estimation MSE vs SNR(dB) comparison of the hexagonal pilot pattern with virtual pilot symbols derived from interpolation/extrapolation and its combination with the decision directed method in the presence of wideband LU

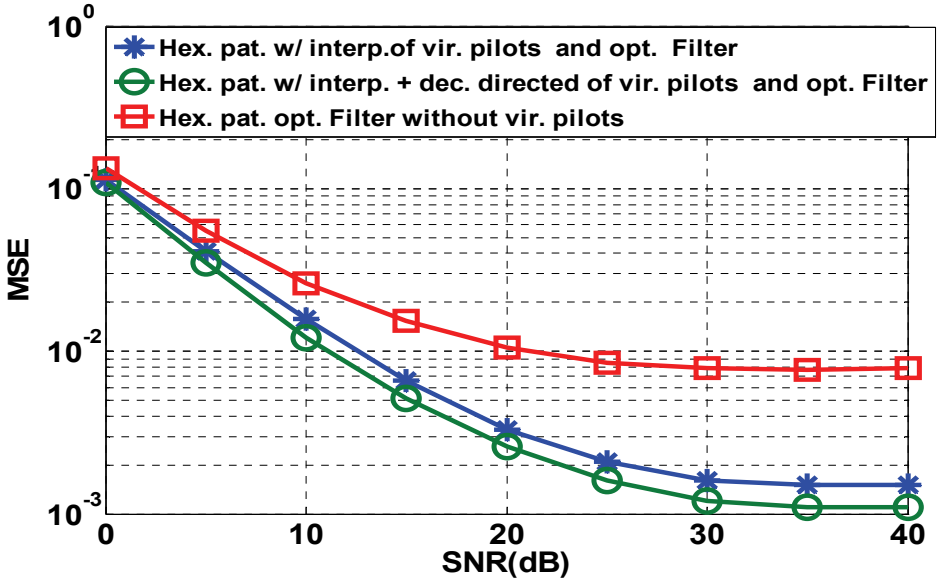

Figure 4.22: Channel estimation MSE vs SNR(dB) of the optimum Wiener Filter using the hexagonal pilot pattern and virtual pilot symbols derived from interpolation/extrapolation and its combination with the decision directed method; comparison with the one without virtual pilots in the presence of wideband LU

4.5 MIMO OFDM Based Cognitive Radio Optimum Pilot Pattern with the Virtual Pilots Concept

Since one of the major objectives in Cognitive Radio is the efficient spectrum utilization, MIMO is considered as possible technique to reach this goal [2]. Extending our previous work on single input single output (SISO) OFDM channel estimation by use of the Wiener filter and applying the optimum hexagonal pattern (in the Cognitive Radio context with the aid of virtual pilots), in this section we propose the application of this hexagonal pilot pattern with the aid of virtual pilots for the MIMO system. Without loss of generality, we consider a specific 2x2 MIMO system. The V-BLAST† algorithm is included in the receiver as the technique to separate the data from each transmit antenna, and to detect the received signal according the maximum likelihood detection. The general model of the MIMO OFDM channel estimation with the V-BLAST receiver for the Cognitive Radio system is depicted in Figure 4.23.

In our 2x2 MIMO system two spatial streams are transmitted. Due to multipath propagation the signal travels along different paths. There will be 4 independent links in the MIMO channel. The time-domain signals on the two received antennas are defined as:

$$\begin{aligned} y_1 &= s_1 * cir_{T_1R_1} + s_2 * cir_{T_2R_1} + n_1 \\ y_2 &= s_1 * cir_{T_1R_2} + s_2 * cir_{T_2R_2} + n_2 \end{aligned} \tag{4.26}$$

where y_1 and y_2 are the signals received by receive antennas *1* (R_1) and *2* (R_2) respectively. s_1 and s_2 are the symbols from transmit antennas *1* (T_1)and *2* (T_2) respectively. The $cir_{T_1R_1}$, $cir_{T_1R_2}$, $cir_{T_2R_1}$, $cir_{T_2R_2}$ are the channel impulse response (CIR) between $T_1 \& R_1$, $T_1 \& R_2$, $T_2 \& R_1$ and $T_2 \& R_2$, respectively, while n_1 and n_2 are the noise terms in each of the receive antennas which are independent of each other.

The channel transfer function (CTF) matrix will be:

$$CTF_{2X2} = \begin{pmatrix} CTF_{T_1R_1} & CTF_{T_2R_1} \\ CTF_{T_1R_2} & CTF_{T_2R_2} \end{pmatrix} \tag{4.27}$$

The CTF is derived from the Fourier transform of the CIR. Accordingly, the frequency domain received signals of the two received antennas will be:

$$\begin{aligned} Y_1 &= S_1 CTF_{T_1R_1} + S_2 CTF_{T_2R_1} + N_1 \\ Y_2 &= S_1 CTF_{T_1R_2} + S_2 CTF_{T_2R_2} + N_2 \end{aligned} \tag{4.28}$$

† V-BLAST (Vertical Bell Laboratories Space Time) algorithm is a detection algorithm on the received signals in a MIMO system. First detection is applied on the strongest signal, then it removes the contribution of the strongest signal on the received signal for the detection of the second strongest signal, and further continues the same process until the weakest signal has been detected.

where Y_1 and Y_2 are the frequency domain signals received by antennas R_1 and R_2 respectively. S_1 and S_2 are the frequency-domain symbols from transmit antennas T_1 and T_2 respectively.

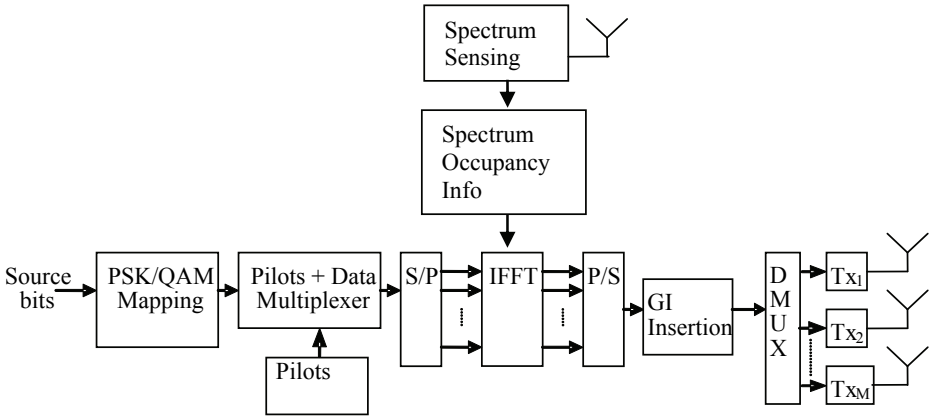

(a) Transmitter

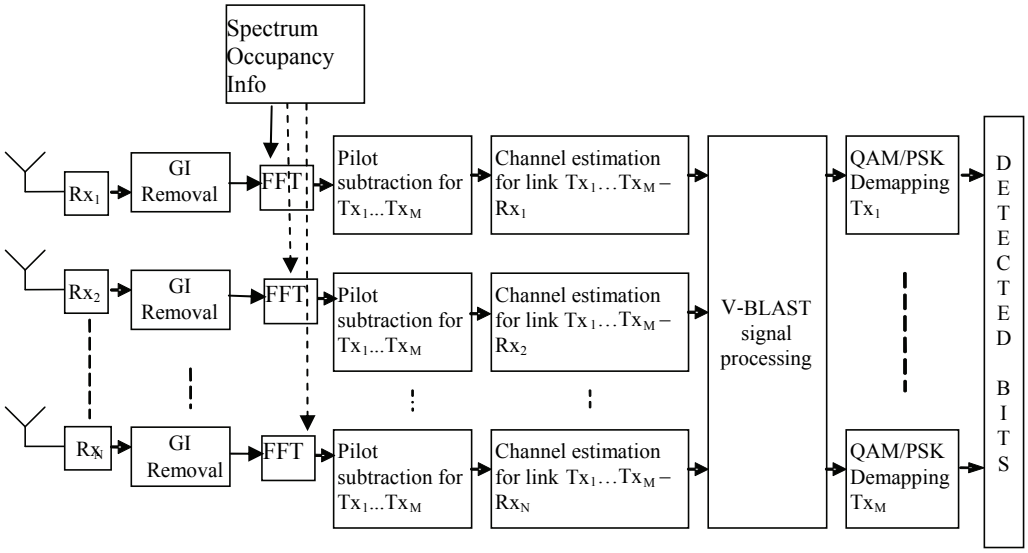

(b) Receiver

Figure 4.23: System model of the MIMO OFDM Based Cognitive Radio at (a) transmitter and (b) receiver side

We propose the pilot grid of the two transmitters. The grid must be orthogonal to each other so the channel state of each link can be properly estimated. The receiver has to recognize the pilots dedicated to each transmitter. We adopt the hexagonal pattern frame in the SISO system

[87]. The hexagonal pattern can be separated into two rectangular (comb-type) patterns. One rectangular pattern is dedicated to one transmit antenna while the other one is dedicated to the second transmit antenna. In this way at the receiver the received frame will be the combination of the two rectangular patterns which form a desired hexagonal type pilot pattern. In both patterns the pilot distance (either in time or frequency) has to fulfill the sampling theorem as described in eq. (4.15).

The pilot pattern for the first and second transmitters are depicted in Figure 4.24. The black boxes denote the pilot positions, the X boxes are virtual pilot positions, and the boxes signed by 0s are entailed to have pilot orthogonality between the first and the second transmit antenna pilot pattern. Data symbols are allocated to the white boxes. To calculate the number of pilots in a certain direction (frequency or time) we use the general formula:

$$N_p = 1 + \left(\frac{N_{sym} - A_0}{d} \right) \tag{4.29}$$

where N_p is the number of total pilots in a certain direction (frequency or time), N_{sym} is either the number of active carriers for calculating the number of pilots in frequency or the number of OFDM symbols per frame for calculating the number of pilots in time. The parameter A_0 is the position of the first pilot symbol and d is the spacing between the pilots in frequency or time. The zeros or nulling are applied to reserve those positions for the pilots of the other transmitter and thus to prevent any interference or addition of pilots while adding / combining those two frames together at the receiver.

We can notice from the pattern in Figure 4.24 that the position of the virtual pilots for both transmit antenna frames is the same. This reduces the processing complexity at the receiver.

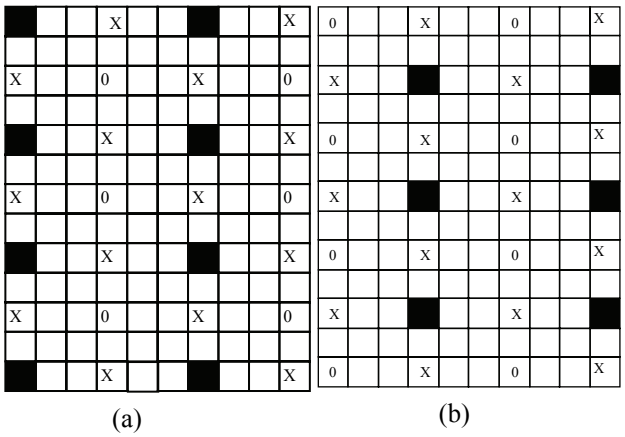

Figure 4.24: Pilot pattern for (a) the first and (b) the second transmit antennas; ‘X’ denotes the virtual pilot position, ‘0’s are inserted to preserve orthogonality between pilots dedicated to transmit antennas 1 and 2, black boxes are the pilot positions, and white boxes are data positions

The resulting received frame at the receiver is as shown in Figure 4.25. The virtual pilots are estimated from two neighboring pilots [87]. This means that virtual pilots in between two real pilots are determined by linear interpolation. This is applied based on the assumption that the channel doesn't change or changes slowly between pairs of pilots. The virtual pilots at the edges of the frame are estimated by simple extrapolation of closeby pilots. The final pattern will resemble as if twice pilot oversampling is applied. This gives a better estimate of the channel. The decision directed process applied in a SISO system [87] has not been included to the system. This is because the overlapped received signal (addition of signal from transmit antennas 1 and 2), as described in eq. (4.28), at the virtual pilot positions will lead to high decision errors.

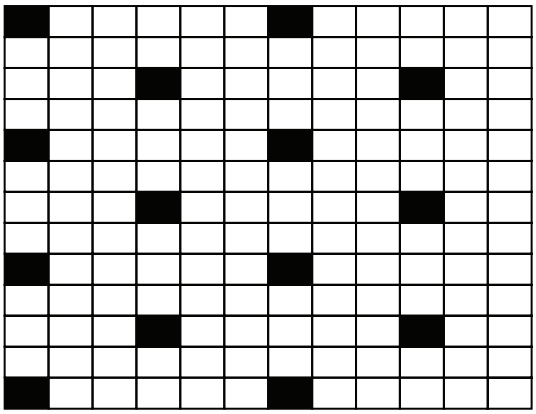

Figure 4.25: Received frame pattern on both receive antennas (Black boxes are the pilots while the white boxes are the data)

The initial channel estimate at the boxes signed by 0s are derived only from linear interpolating / extrapolating of adjacent pairs of initial estimates (i.e. previously derived initial channel estimates at virtual pilot positions), which can be seen as a linear interpolation involving 4 initial channel estimates at real pilot positions. Finally the 0 boxes will become virtual pilots as well. Due to the use of the virtual pilot concept to the proposed pilot pattern, the outcome of the final pattern will resemble the regular comb type pilot pattern. The pattern on antenna 2 (depicted in Figure 4.24(b)) so provides more virtual pilots compared to antenna 1 (depicted in Figure 4.24(a)). This regularity is important to obtain a proper and simple filtering process. The receiver of each receive antenna will separate the pilots from the data. The pilots dedicated to the first transmit antenna will be separated from the rest of the pilots which are dedicated to the other antenna. In this way the channel states of all links can be estimated.

In the case where the initial channel estimates at the virtual pilot positions derived from linear interpolation or extrapolation gives large deviation error, then there will be an additional

mismatch contribution to the filtering process. The impact can be seen as the number of filter coefficients is increasing. In this case the eq. (4.4) can be written as :

$$\begin{aligned}\breve{H}_{n,k} &= \sum_{\{n',k'\}\in P} \omega_{n',k',n,k}\hat{H}_{n',k'} + \sum_{\{v\}\in V} \omega_{n',k',n,k}\hat{H}_{v} \\ &= \sum_{\{n',k'\}\in P} \omega_{n',k',n,k}\hat{H}_{n',k'} + \sum_{\{v\}\in V} \omega_{n',k',n,k}\left(H_{v} + \Delta H_{v}\right)\end{aligned} \tag{4.30}$$

where V is the set of the virtual pilot positions. The deviation from linear interpolation or extrapolation (ΔH) comes from the noise average contribution as described by eq. (4.21) and the interpolation/ extrapolation mismatch. By observing eq. (4.30) we can see that by sliding window filtering, and increasing the filter size, due to the proposed pilot pattern, it will consequently increase the number of virtual pilots involved in estimating the CTF and that will accumulate an extra error. In addition to this error, the mismatch model used in designing the filter (**ω)** will sum up the channel estimation error. This analysis will be verified in the performance evaluation given in subsection 4.5.1. According to references [78]-[81] the hexagonal sampling pattern is considered to be the most efficient two-dimensional sampling scheme, since it requires 13.4% fewer samples than rectangular sampling in order to represent the same circularly band limited continuous signal. The previously proposed MIMO 2x2 pattern adopts the SISO hexagonal pattern.

Further we compare the results with previous MIMO pattern with the new pattern for each transmit antenna as depicted in Figure 4.26. The pattern adopts the SISO rectangular pattern as shown in Figure 4.26 (a), resulting into 2 different transmit antenna hexagonal pilot patterns depicted in Figure 4.26 (b) and (c). Zeros of the pattern are for the purpose of having orthogonality between the pilot dedicated to transmit antennas 1 and 2. It can be observed from the second MIMO pattern (pattern in Figure 4.26 (a)) that it requires more real pilots compared to the first MIMO pattern (pattern in Figure 4.25). Two virtual pilot allocation techniques have been evaluated. The first one is depicted in Figure 4.27 where the virtual pilots are only allocated on the zeros, and the second one is shown in Figure 4.28 where virtual pilots are allocated on the zeros and between the zeros and the real pilots. The first MIMO pilot pattern with the second MIMO pilot pattern will be compared in subsection 4.5.1 in terms of their channel estimation mean square error (MSE) and bit error rate (BER). The second MIMO pilot pattern includes the two virtual pilot allocation techniques.

The three MIMO pilot pattern techniques (described in Figures 4.24, 4.27 and 4.28) will be compared, and the one that gives a better performance will be chosen as pattern for the Cognitive Radio system, where some carriers will be de-activated due to the licensed user access. The three pilot pattern techniques have been simulated. The results indicate that the first pattern (described in Figure 4.24) gives a better channel estimation performance than the second pattern (Rectangular to Hexagonal) either with less virtual pilots or with more virtual pilots (Figure 4.27 and 4.28); therefore the first pattern will be utilized in the Cognitive Radio

system. The results will be further discussed in the performance evaluation and analysis in subsection 4.5.1.

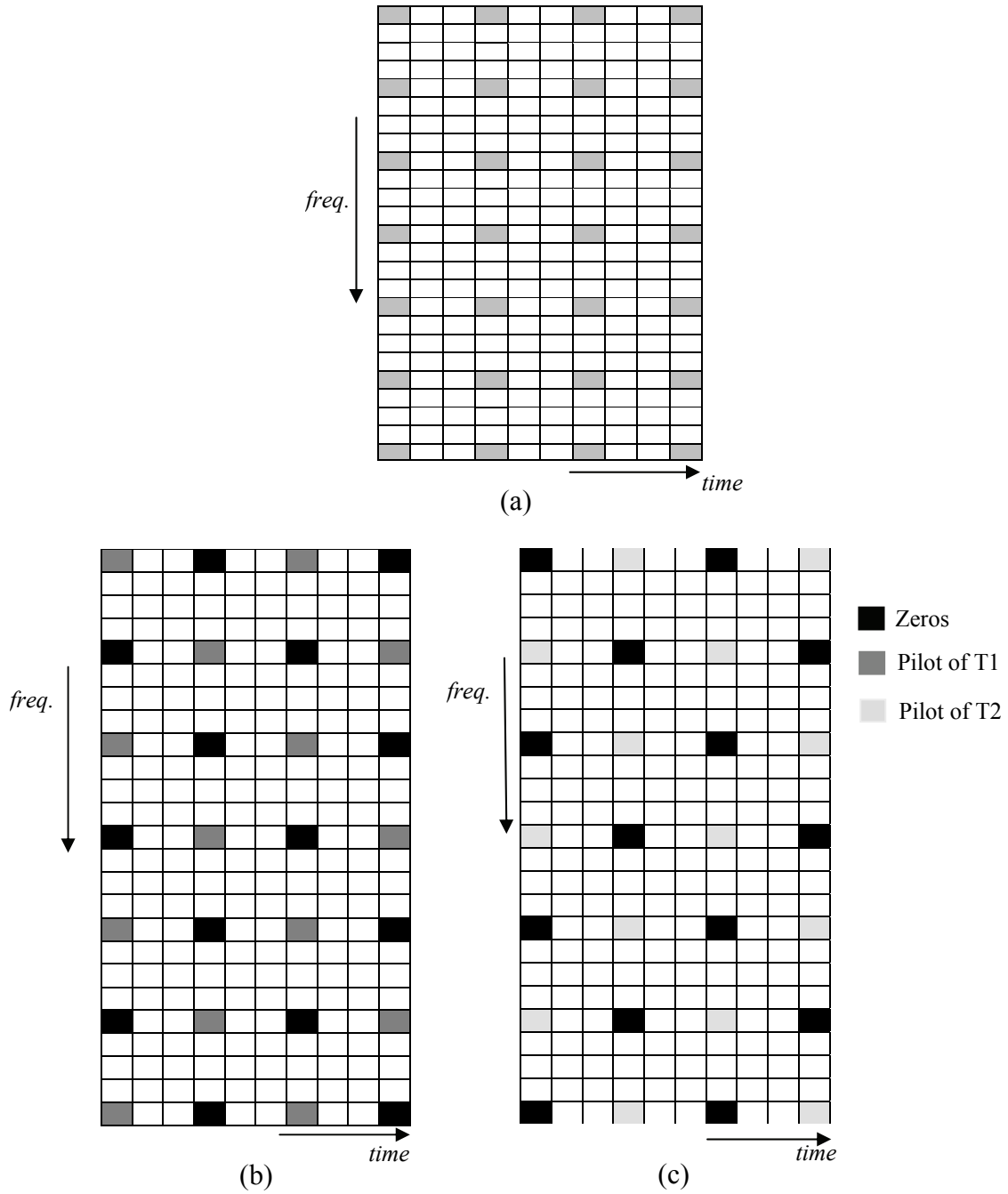

Figure 4.26: The second proposed Pilot pattern for MIMO 2x2 derived from (a) the Rectangular Comb Pilot pattern to Hexagonal Pilot pattern on (b) transmit antenna 1 (T1) and (c) transmit antenna 2 (T2)

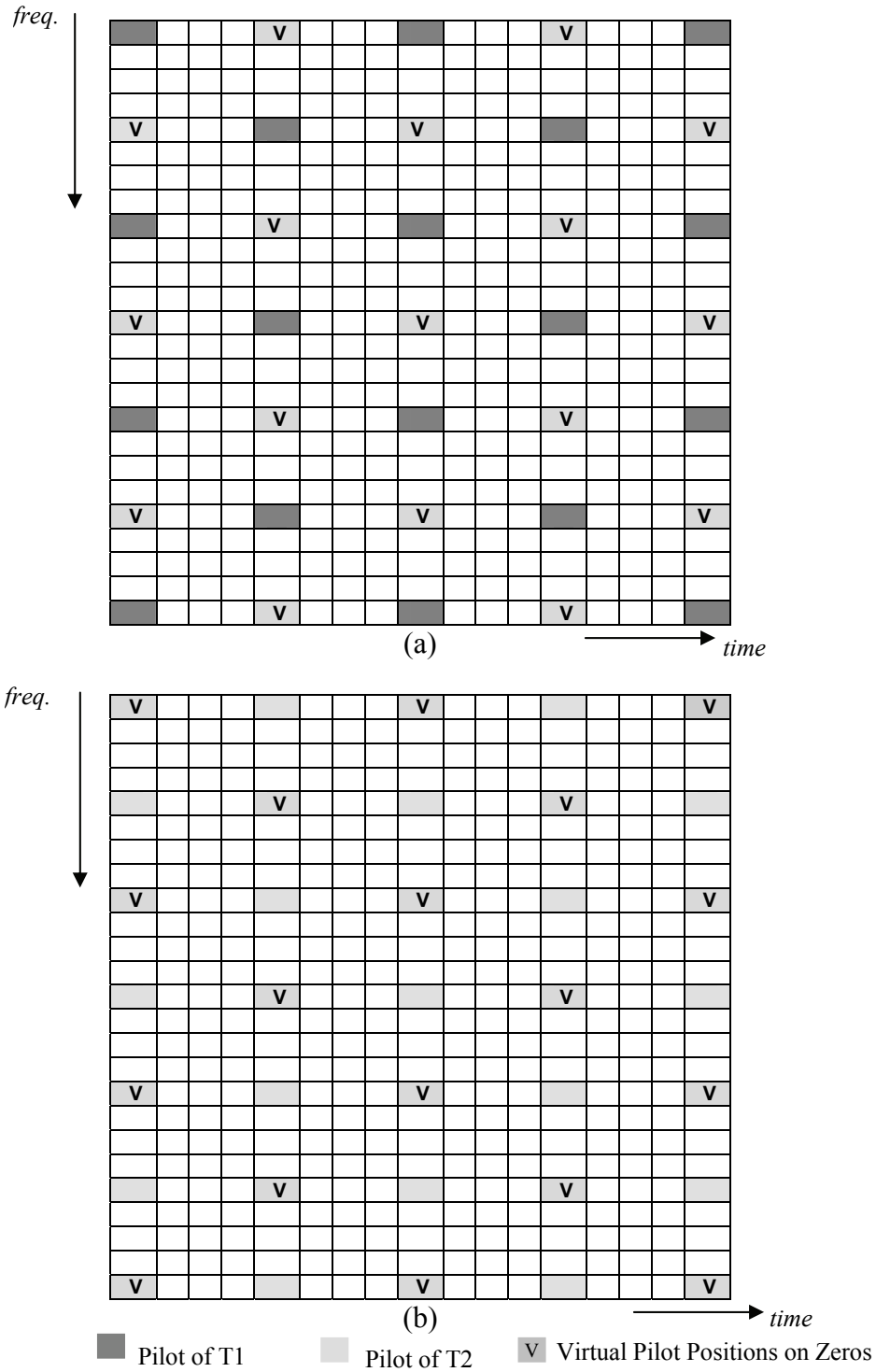

Figure 4.27: The second proposed Pilot pattern for MIMO 2x2 derived from the Rectangular Comb Pilot pattern to Hexagonal Pilot pattern with less virtual pilots on (a) transmit antenna 1 (T1) and (b) transmit antenna 2 (T2)

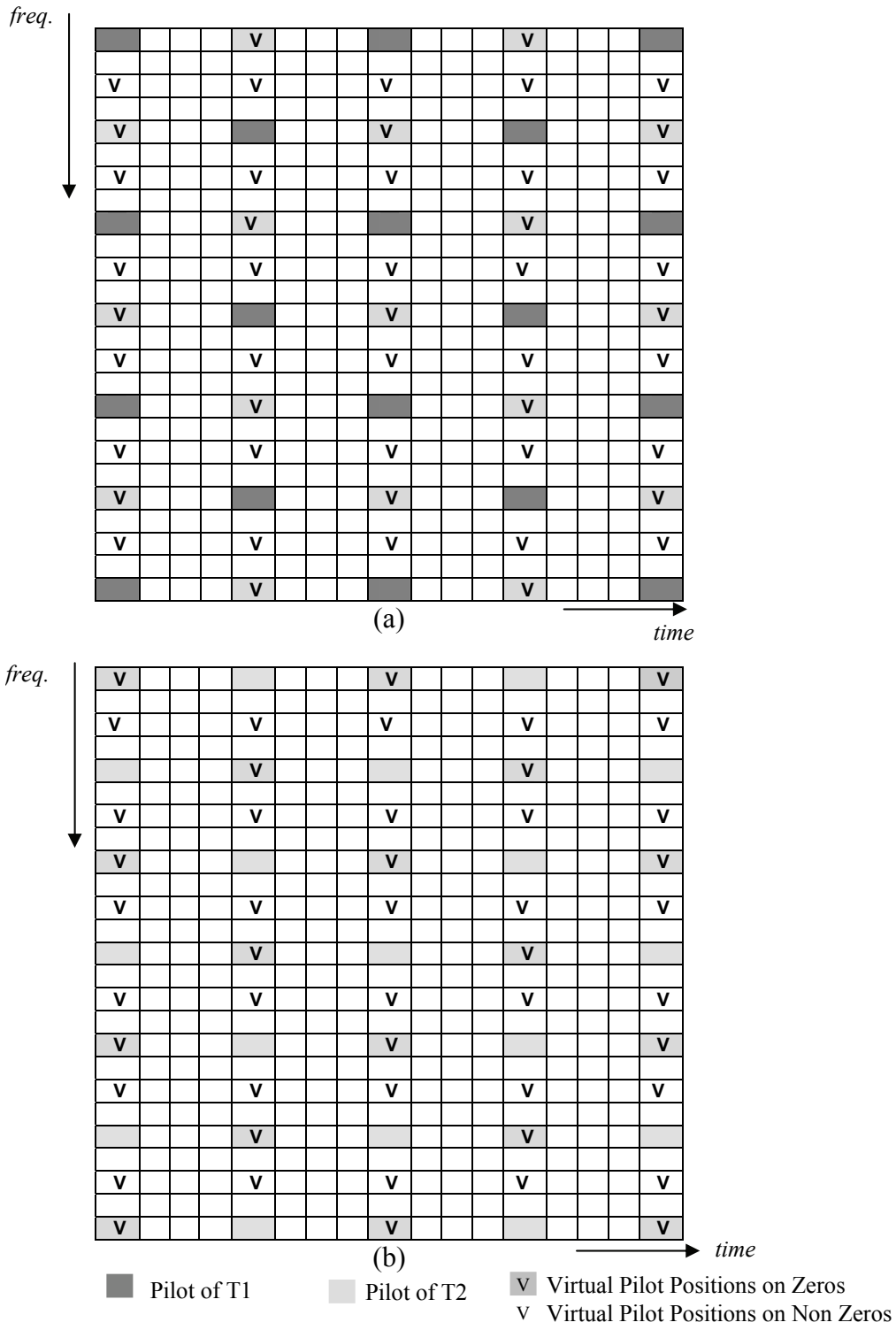

Figure 4.28: The second proposed Pilot pattern for MIMO 2x2 derived from the Rectangular Comb Pilot pattern to Hexagonal Pilot pattern with more virtual pilots on (a) transmit antenna 1 (T1) and (b) transmit antenna 2 (T2)

In the presence of licensed users, the shifted pilot scheme in Figure 4.9 will be applied, and the virtual pilot concept will be added to have a regular distance between initial channel estimate positions for the simplicity of the Wiener filtering operation. The new pattern is shown in Figure 4.29.

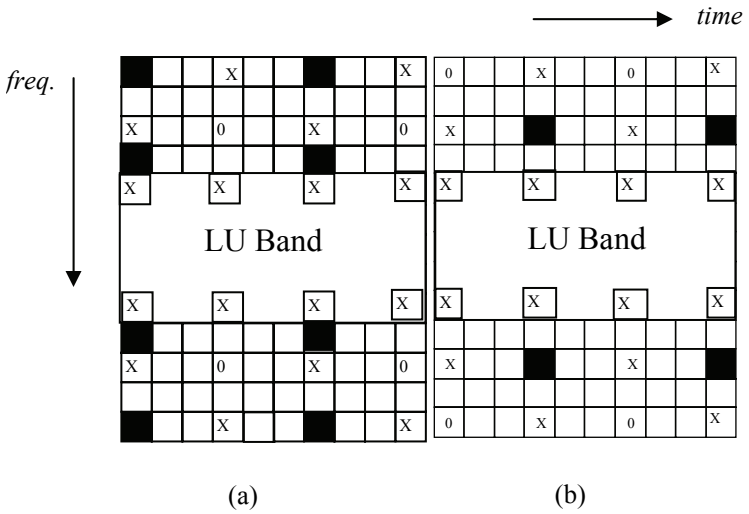

Figure 4.29: Pilot pattern for (a) the first and (b) the second transmit antenna in the presence of LU; 'X' denotes the virtual pilot position, '0's are inserted to preserve orthogonality between pilots dedicated to transmit antennas 1 and 2, the black boxes are the pilot positions, and the white boxes are data positions

4.5.1 Performance Evaluation and Analysis

We consider the wide sense stationary uncorrelated scattering (WSSUS) channel model in our simulations since it relates the power delay profile, number of multipaths, and Dopler frequency of the channel in a simple and direct way. The simulation parameters are equal to the SISO evaluation provided in Table 4.1. By adopting the hexagonal pilot pattern in the SISO system as depicted in Figure 4.25 and allocating pilots for both transmit antennas according to Figure 4.24, the distance between pilots in time is increased by a factor of two. This leads to degradation of the performance of the estimator. However applying the virtual pilots will make the effect of having the original pilots distance in time ($d_t=3$). Having more virtual pilots at the edges of the frame (edge effect) causes more performance degradation. This is because the correlation at the edges is less and each time a virtual pilot is interpolated according to eq. (4.20) or eq. (4.21) there is some interpolation error which accumulates and causes a bigger MSE. In the Wiener filtering process either in time or frequency the sliding window utilizes 4 pilots to estimate the CTFs in one slide.

Figure 4.30 shows the MSE of the four links of the first 2x2 MIMO system utilizing the virtual pilots, compared with the SISO system using a rectangular pilot pattern with $d_f=4$, $d_t=6$ and $d_f=4$, $d_t=3$ (two-times pilot oversampling in time). The SISO with $d_f=4$, $d_t=6$ forms

an MSE floor in the order of 10^{-1}, the SISO with two-times pilot oversampling in time has an error floor of around $5x10^{-2}$. The proposed MIMO 2x2 pilot pattern with the virtual pilot concept will do a two-times pilot oversampling in time and in frequency; the results in Figure 4.30 show that the proposed pattern outperforms the two-times pilot oversampling in time by obtaining an error floor 10^{-2}. Due to the deviation error from linear interpolation/extrapolation as described in eq. (4.30) the performance cannot reach the performance for the two-times pilot oversampling in time and in frequency.

Figure 4.31 depicts the advantage of the V-BLAST algorithm in exploiting the channel diversity in detecting the transmitted bits where it forms a BER floor of around $6x10^{-3}$. Meanwhile the SISO scheme with the same amount of real pilots (without virtual pilots) forms a BER floor of around $6x10^{-2}$, the SISO with two-times oversampling forms a BER floor $2x10^{-2}$, while the SISO with two-times oversampling in time and frequency forms a BER floor of around 10^{-4}. The results in Figure 4.30 and 4.31 have been disseminated in reference [88].

The impact of increasing the Wiener filter size to the channel MSE and the BER can be seen in Figure 4.32 and 4.33 respectively. Figure 4.32 shows that the MSE of the proposed MIMO pattern with 4x4, 8x8 and 16x16 form almost the same level of error floor. The deviation from the linear interpolation/extrapolation at the virtual pilot positions and the mismatched design of the Wiener filter add together into the overall channel MSE as described in eq. (4.30) and eventually impacts the BER outcome. Since in the SISO case without the presence of virtual pilots the deviation does not exist, it means that as the Wiener filter size is increased a significant performance improvement can be seen.

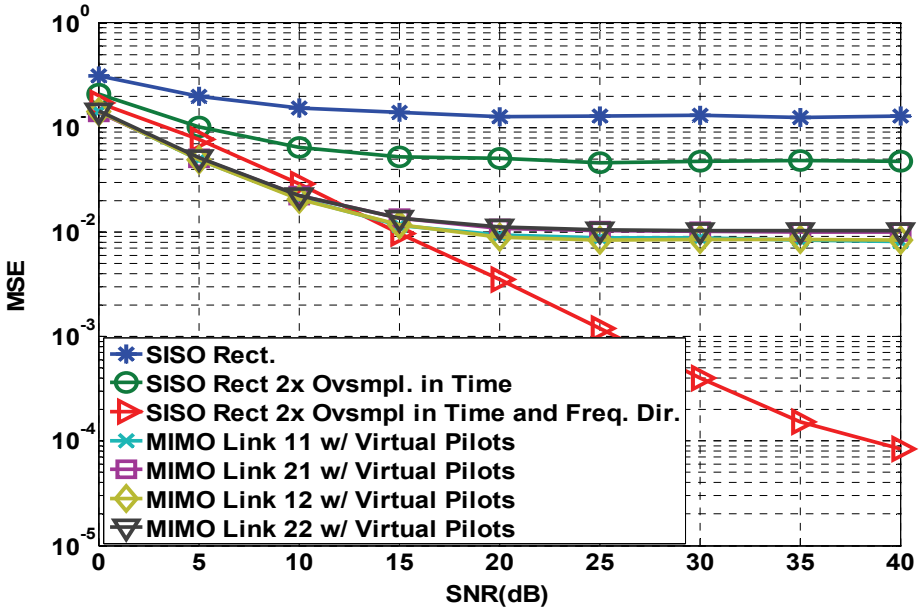

Figure 4.30: MSE vs SNR (dB) comparison between SISO Rectangular, Hexagonal and MIMO pilot patterns with a 4x4 Wiener Filter size

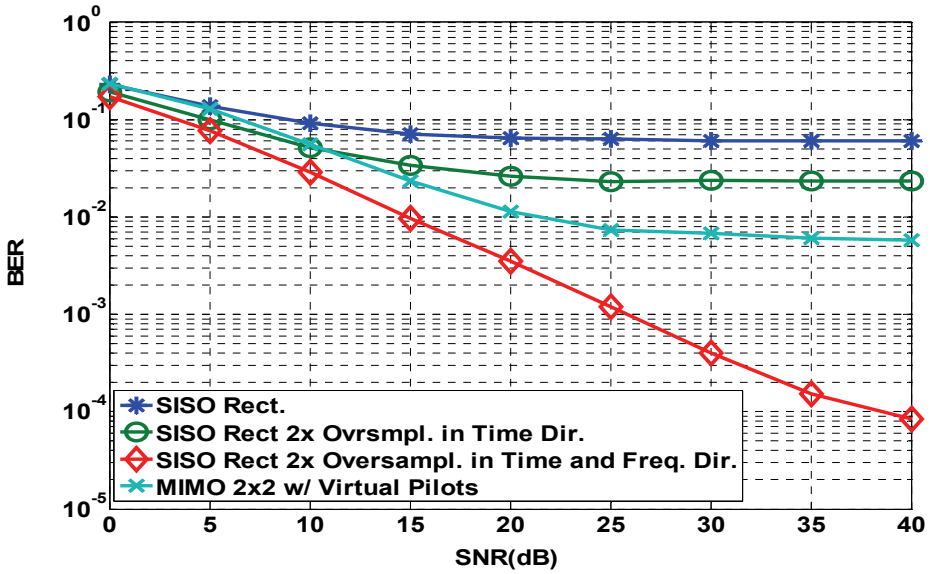

Figure 4.31: BER vs SNR (dB) comparison between SISO Rectangular, Hexagonal and MIMO pilot patterns with a 4x4 Wiener Filter size

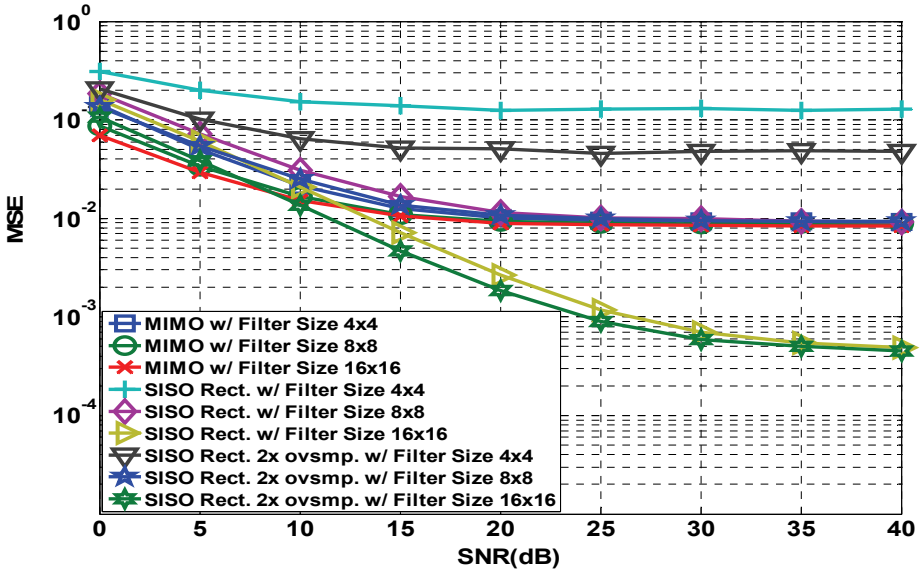

Figure 4.32: MSE vs SNR (dB) comparison between SISO Rectangular, Hexagonal and MIMO pilot patterns with increasing number of filter coefficients (number of pilots used per sliding window)

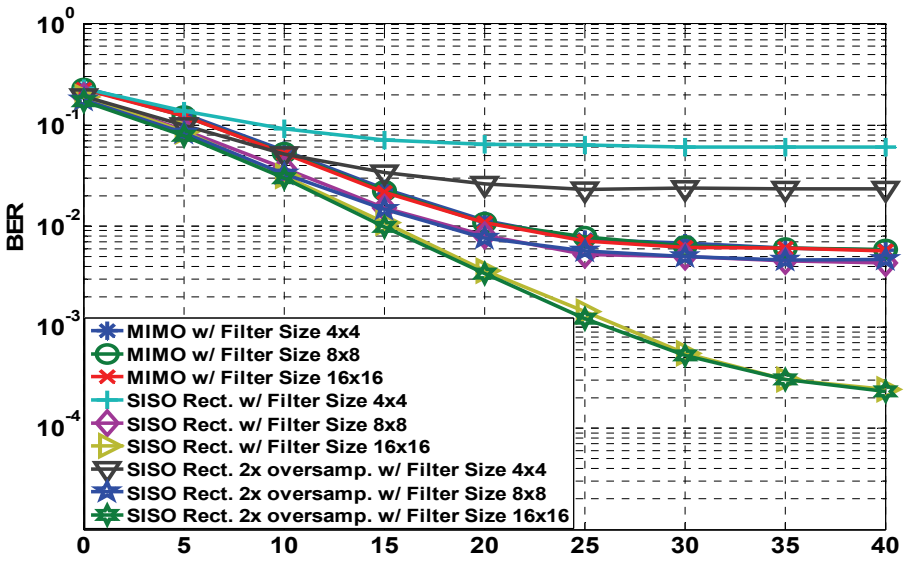

Figure 4.33: BER vs SNR (dB) comparison between SISO Rectangular, Hexagonal and the proposed MIMO pilot patterns with increasing number of filter coefficients (number of pilots used per sliding window)

The performance comparison among the first proposed MIMO pattern (Figure 4.24), the second MIMO pattern with less virtual pilots (Figure 4.27) and more virtual pilots (Figure 4.28) at a high maximum Doppler frequency (f_{Dmax} = 82 Hz) are shown in Figure 4.34 and 4.35, while the performance comparison at low Doppler frequency (f_{Dmax} = 2.05 Hz) are depicted in Figure 4.36 and 4.37.

The results in Figures 4.34 to 4.37 show that the first proposed MIMO pattern (Figure 4.24) outperforms the other two techniques (Figure 4.27 and 4.28). The first proposed MIMO pattern does not only give better channel estimation MSE but also requires less real pilots compared to the second proposed MIMO pattern. Having less pilots refers to a higher data rate. The virtual pilot concept can optimally be utilized in slowly fading channels. The comparison of the proposed MIMO pattern in high Doppler and low Doppler confirms this fact. The best performance is given by the Wiener filter 16x16 of the first proposed MIMO pattern. At high Doppler frequency this pattern forms an error floor in the order of $9\text{x}10^{-3}$ while at low Doppler frequency the error floor is in the order of $2\text{x } 10^{-3}$. The MSE performance gap between the first proposed MIMO pilot pattern (Figure 4.24) compared to the other two techniques (Figure 4.27 and 4.28) is more significant at low Doppler frequency than at high Doppler frequency as depicted in Figures 4.34 and 4.36. This phenomenon happens since the first proposed MIMO pilot pattern emphasizes the virtual pilot utilization of the first and second transmit antennas in time. Therefore, as the Doppler frequency is low the channel is slowly varying in time, and the aid of the virtual pilots in this direction will be significant. Meanwhile, in the other two techniques the virtual pilot utilization is emphasized

in frequency. Therefore, the impact of the virtual pilot utilization in the two other techniques depicted in Figure 4.27 and 4.28 becomes significant for the channel with lower delay spread.

Figure 4.38 shows for all links the MSE on the 2x2 MIMO system with three MIMO pilot patterns with an 8x8 Wiener filter for the high maximum Doppler frequency (f_{Dmax} = 82 Hz). In the first pattern (described in Figure 4.24), more pilots are allocated to the first transmit antenna compared to the second antenna; therefore the MSEs on links 11 and 12 can be better compared to links 21 and 22 respectively. The MSE performance of the second pattern with less and more virtual pilots of all links are close to each other due to the same number of allocated pilots on transmit antennas 1 and 2.

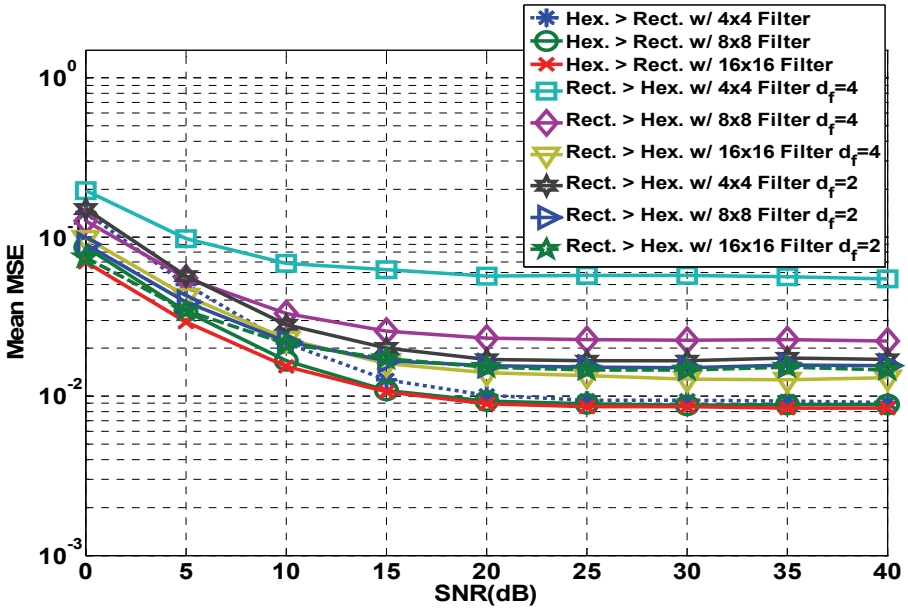

Figure 4.34: Mean MSE vs SNR (dB) comparison of all links between the first proposed MIMO pilot pattern (Hexagonal > Rectangular), and the second proposed MIMO pilot pattern (Rectangular > Hexagonal) with less virtual pilots (d_f=4) and more virtual pilots (d_f=2) for different number of filter coefficients (number of pilots used per sliding window) at high maximum Doppler (f_{Dmax} = 82 Hz)

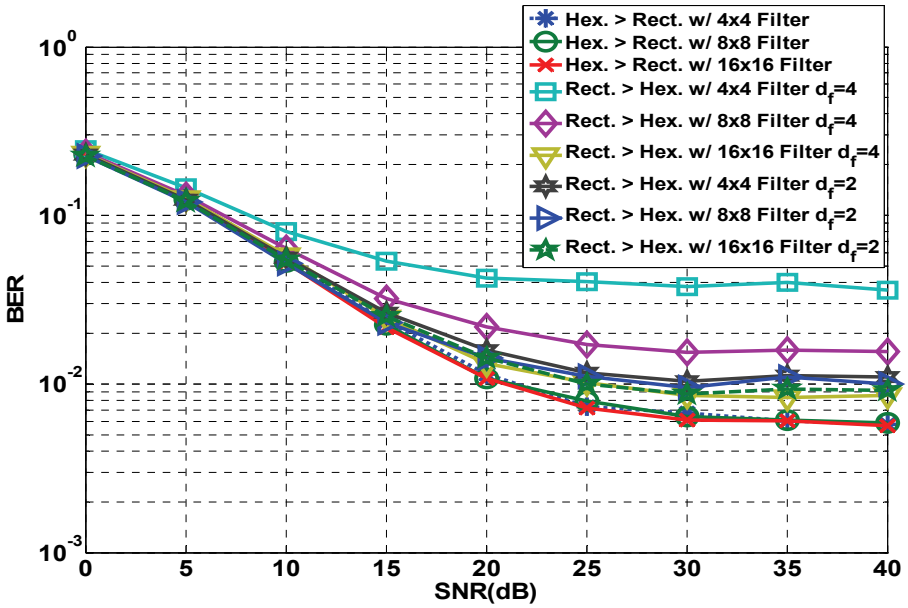

Figure 4.35: BER vs SNR (dB) comparison of all links between the first proposed MIMO pilot pattern (Hexagonal > Rectangular), and the second proposed MIMO pilot pattern (Rectangular > Hexagonal) with less virtual pilots (d_f=4) and more virtual pilots (d_f=2) for different number of filter coefficients (number of pilots used per sliding window) at high maximum Doppler (f_{Dmax} = 82 Hz)

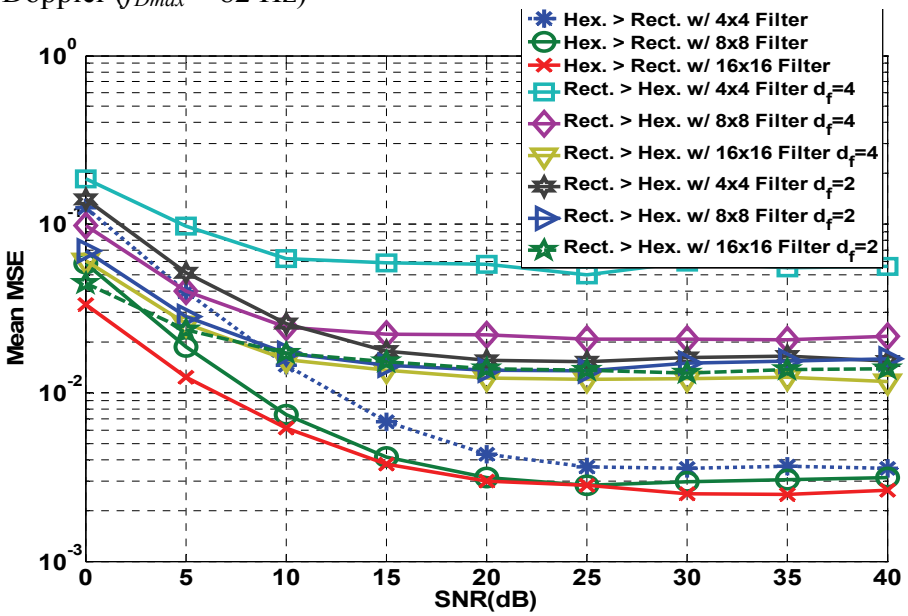

Figure 4.36: Mean MSE vs SNR (dB) comparison of all links between the first proposed MIMO pilot pattern (Hexagonal > Rectangular), and the second proposed MIMO pilot pattern (Rectangular > Hexagonal) with less virtual pilots (d_f=4) and more virtual pilots (d_f=2) for different number of filter coefficients (number of pilots used per sliding window) at low maximum Doppler (f_{Dmax} = 2.05 Hz)

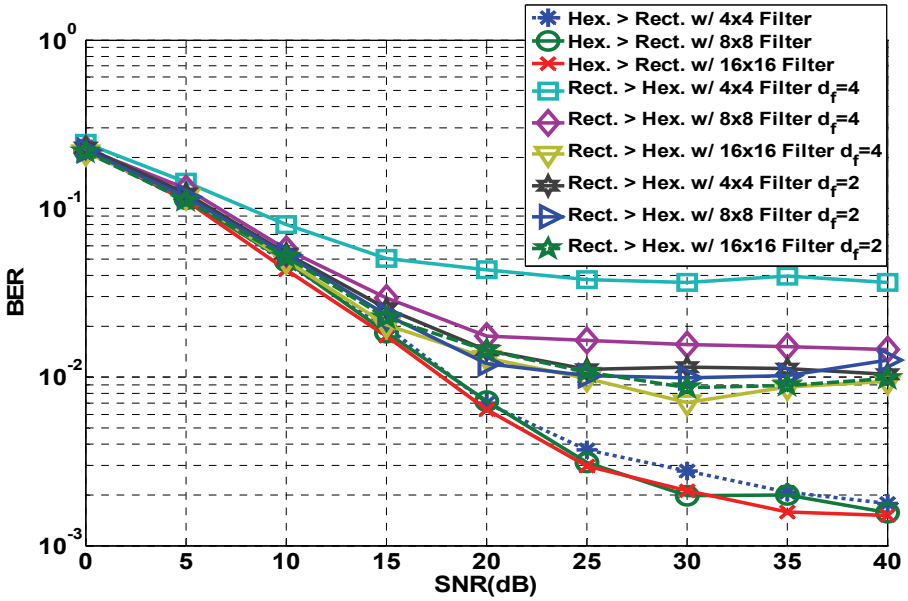

Figure 4.37: Mean MSE vs SNR (dB) comparison of all links between the first proposed MIMO pilot pattern (Hexagonal > Rectangular), and the second proposed MIMO pilot pattern (Rectangular > Hexagonal) with less virtual pilots (d_f=4) and more virtual pilots (d_f=2) for different number of filter coefficients (number of pilots used per sliding window) at low maximum Doppler (f_{Dmax} = 2.05 Hz)

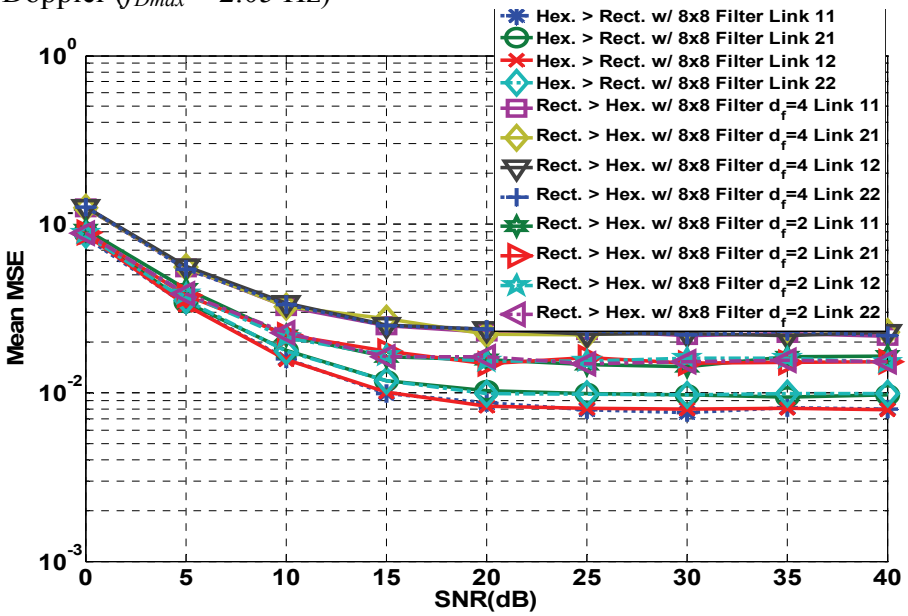

Figure 4.38: Mean MSE vs SNR (dB) comparison of each link between the first proposed MIMO pilot pattern (Hexagonal > Rectangular), and the second proposed MIMO pilot pattern (Rectangular > Hexagonal) with less virtual pilots (d_f=4) and more virtual pilots (d_f=2) for 8 filter coefficients (8 pilots are used per sliding window) in high maximum Doppler (f_{Dmax} = 80 Hz)

In the presence of the licensed user, some carriers will be de-activated. Like our evaluation in the SISO system, in this simulation scheme 61 carriers are de-activated (carrier no. 81 – 141) due to LU occupancy. The LU itself occupies 40 carriers in the middle that renders 10 guard bands on each side of the LU band. As too many carriers are de-activated the mutual interference between LU and our Cognitive Radio system becomes negligible. The distance between pilots in frequency is 4 sub-carriers, while in time it is 3 OFDM symbols. Figure 4.39 and 4.40 show the performance of the first proposed MIMO pilot pattern in the presence of LU (Figure 4.29) with a 4x4, 8x8, and 16x16 Wiener Filter size at high maximum Doppler frequency, while the performances at low maximum Doppler frequency are depicted in Figures 4.41 and 4.42.

Beside the effectiveness of the virtual pilot concept in slowly varying channel as presented in the comparisons of Figures 4.34 to 4.37, the results in Figures 4.39 to 4.42 show how the active licensed user can deteriorate the MSE performance of the proposed MIMO pilot pattern in a Cognitive Radio system. A particular result that can be observed from these Figures is that the MSE performance in the case of the proposed MIMO pilot pattern without the presence of an active licensed user (while having some carriers de-activated) is close to the MIMO system without carriers de-activation performance.

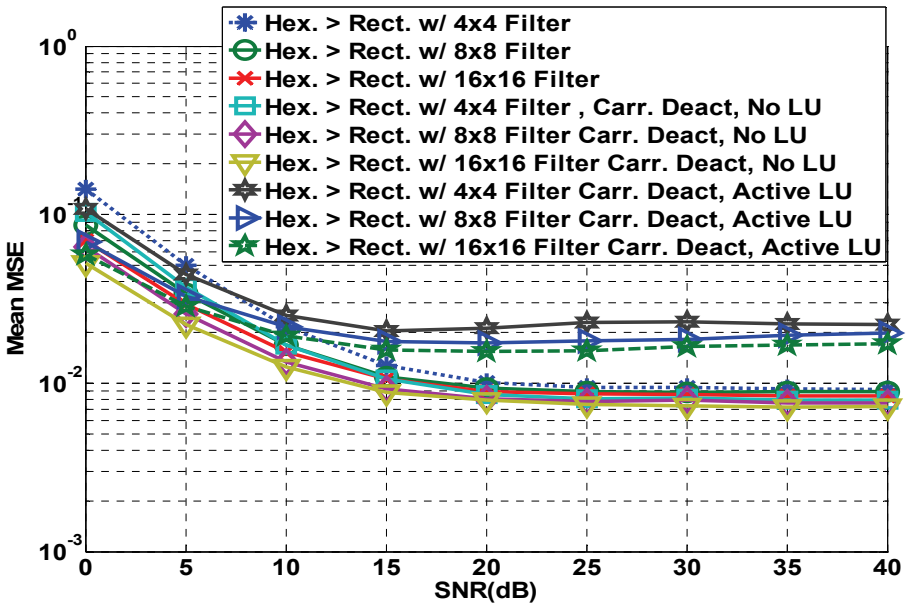

Figure 4.39: Mean MSE vs SNR (dB) of the first proposed MIMO pilot pattern (Hexagonal > Rectangular) without carriers de-activation, with carriers de-activation without the presence of a licensed user (LU), and with carrier de-activation and active LU at high maximum Doppler (f_{Dmax} = 80 Hz)

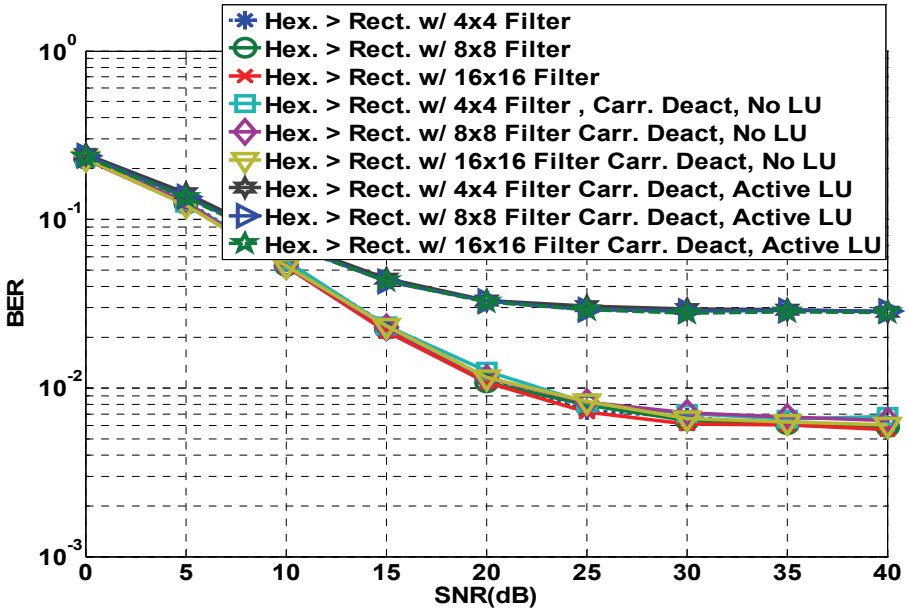

Figure 4.40: BER vs SNR (dB) of the first proposed MIMO pilot pattern (Hexagonal > Rectangular) without carriers de-activation, with carriers de-activation without the presence of a licensed user (LU), and with carrier de-activation and an active LU at high maximum Doppler (f_{Dmax} = 80 Hz)

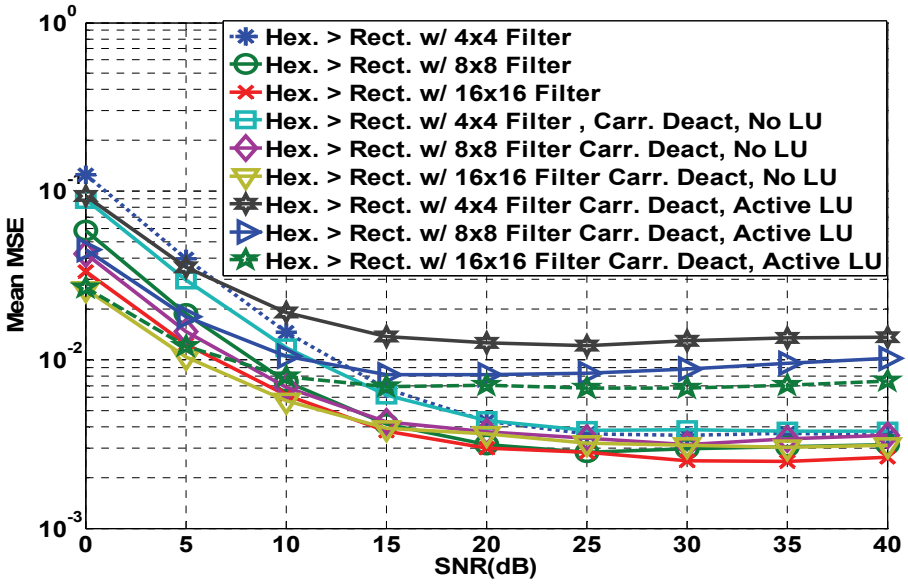

Figure 4.41: Mean MSE vs SNR (dB) of the first proposed MIMO pilot pattern (Hexagonal > Rectangular) without carriers de-activation, with carriers de-activation without the presence of a licensed user (LU), and with carrier de-activation and an active LU at low maximum Doppler (f_{Dmax} = 2.05 Hz)

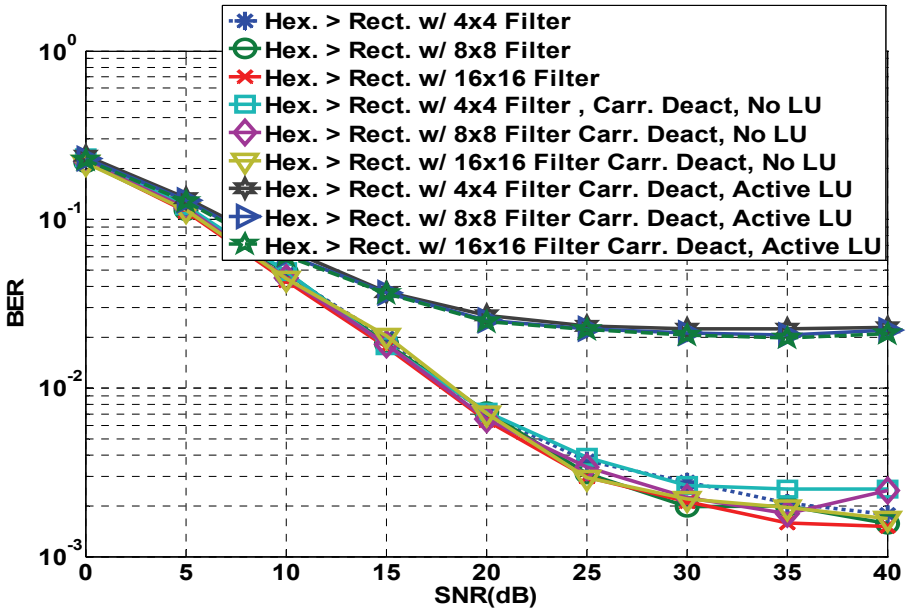

Figure 4.42: BER vs SNR (dB) of the first proposed MIMO pilot pattern (Hexagonal > Rectangular) without carriers de-activation, with carriers de-activation without the presence of a licensed user (LU), and with carrier de-activation and an active LU at low maximum Doppler (f_{Dmax} = 2.05 Hz)

There are two factors that influence the accumulation of MSE :

1) the edge effects due to the filter design according Figure 4.1 and the sliding window channel estimation technique depicted in Figure 4.2
2) the deviation error by the virtual pilots that will be accumulated, as the number of filter coefficients is increased (described in eq. (4.30)).

The MIMO system without carriers de-activation will experience less edge effects compared to the MIMO system with carriers de-activation. Depending on the size of the carriers de-activation band, the MIMO system with carrier de-activation will have less virtual pilots compared to the MIMO system without carrier de-activation. By having the current number of de-activated carriers and other simulation parameters given in Table 4.1, the curves in Figures 4.39 to 4.42 are the results of the two accumulated channel deviation errors (edge effects and virtual pilots). It means that the number of virtual pilots in the region of de-activated carriers has managed to balance the error due to the edge effects of the MIMO system with de-activated carriers.

4.6 Training and Pilot Pattern for OFDM Based Cognitive Radio Synchronization and PAPR Reduction

Beside channel estimation, synchronization and peak to average power ratio (PAPR) are common problems in an OFDM system. Therefore the Cognitive Radio system that uses OFDM as modulation technique will also face these common problems. In this section the impact of synchronization and PAPR reduction will be explored and analyzed within the Cognitive Radio context.

4.6.1 Synchronization for an OFDM-Based Cognitive Radio System

Carrier frequency, sampling frequency and frame offset are the common problems that an OFDM system normally experience. In this section we overview suitable synchronization techniques to compensate the three offset problems to be applied in an OFDM-based CR system.

A particular point to be addressed here is the impact of the carriers de-activation to the synchronization technique. The guard interval (GI) can be utilized to estimate the carrier frequency and frame offset [89]–[92]. The guard interval is a replica of the last N_{GI} time-domain OFDM symbols. In this way by using the cross-correlation method the beginning of an OFDM symbol and the carrier frequency offset can be detected. In [93] the frame offset estimation is improved by quantizing the time-domain OFDM symbol into a 4-QAM symbol constellation. The in-phase (I) or quadrature(Q) symbol values which are equal or bigger than zero are assigned by a value of 1, while the rest are -1. Further averaging the cross correlation value of the quantized time-domain OFDM symbol for the entire OFDM symbols in a frame will add to the robustness of the frame offset detection.

The frequency offset can be detected by utilizing the cross correlation amplitude between the time-domain OFDM symbol with its shifted version. The shift length is chosen as the period between the time-domain OFDM symbol with its replica, which practically in every OFDM symbol is the resemblance of the distance between the symbol on GI and its replica on the useful OFDM symbol. Beside utilizing the GI, training symbols can be inserted to the OFDM frame [94]. According to the IFFT property, half of the time-domain OFDM symbol can be replicated to the rest half of the time-domain signal by assigning zeros to the frequency domain OFDM symbols on the carriers with odd index number, while the index is starting from 0 (e.g. index $k=0,\ldots, N_{FFT}-1$). The scheme is depicted in Figure 4.43.

The replication scheme itself can be analytically proven by expanding the condition of the OFDM time domain symbol $x_n = x_{\frac{N_{FFT}}{2}+n}$ as given in eq. (4.31),

$$x_n = x_{\frac{N_{FFT}}{2}+n}$$

$$\frac{1}{N_{FFT}}\sum_{k=0}^{N_{FFT}-1} X_k e^{\frac{j2\pi kn}{N_{FFT}}} = \frac{1}{N_{FFT}}\sum_{k=0}^{N_{FFT}-1} X_k e^{\frac{j2\pi k\left(\frac{N_{FFT}}{2}+n\right)}{N_{FFT}}}$$

$$= \frac{1}{N_{FFT}}\sum_{k=0}^{N_{FFT}-1} X_k e^{\frac{j2\pi kn}{N_{FFT}}} e^{j\pi k}$$

left eq. equals to right eq., only if $e^{j\pi k} = 1$

(4.31)

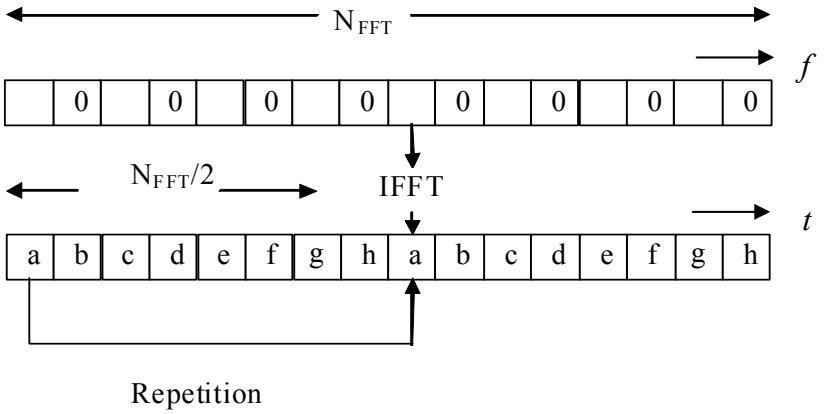

Figure 4.43: Training symbol design for synchronization purpose

According to eq. (4.31) the condition can be satisfied for any kind of symbol X_k values on even index subcarriers ($k=0,2,4,\ldots, N_{FFT}-2$), while the value of X_k on the odd index subcarriers ($k=1,3,5,\ldots, N_{FFT}-1$) must be zero. The detail proof is available in Appendix B.

In a Cognitive Radio context there are two aspects to be considered for designing the training symbols for synchronization. The first one is the requirement of having replica of the time domain training symbol within the distance of N_{FFT} /2 by assigning zeros on the odd index carriers in the frequency-domain training symbols. The second aspect concerns the application of carriers de-activation on the LU band in order to avoid mutual interference between the Cognitive radio system and the LU by putting zeros on the location of the LU band in the frequency-domain training symbols. The designed training symbol will not harm the LU transmission, and in the Cognitive Radio system itself the mutual interference can be avoided hence more accurate synchronization would be attained. By cross-correlating these training symbols with its reference at the receiver, the noise and fading effect that can degrade

the cross-correlation value will be mitigated. The cost of this technique is a reduction in bit rate due to the training symbol.

The sampling frequency offset can be estimated from the phase difference between two pilots positions in one OFDM symbol and two pilots positions in another OFDM symbol [95]. This technique is improved in reference [96] by applying equalization to mitigate the fading effect on the sampling frequency offset and by iterative averaging over all pilots. Since the synchronization problem can be solved with the insertion of pilots and training symbols, the relation with the Cognitive Radio context would only be in interference avoidance by de-activating the pilots or training symbols on the LU band. In this way the time, frequency and sampling frequency offset can be more accurately estimated.

4.6.2 Peak To Average Power Ratio Reduction for an OFDM-Based Cognitive Radio Channel Estimation

The peak to average power ratio (PAPR) reduction for an OFDM-based Cognitive Radio can be included by using a sidelobe suppression technique. This extra constraint on PAPR (see eq. (2.1) in chapter 2) means that the frequency-domain symbol composition (data and pilots) also should minimize the PAPR. The sidelobe suppression constraint becomes:

$$|X(f)|^2 = \frac{1}{N_{FFT}}\left|\sum_{n=1}^{N_{FFT}} \sqrt{p_n} X_n \int_{-(1+\alpha)T_u}^{(1+\alpha)T_u} g(t) e^{-j2\pi(f-f_n)t} dt\right|^2$$

$$subject \quad to \quad \left|X(f_{LU})\right|^2 < P_{Threshold}, \quad \sum_{n=1}^{N_{FFT}} p_n = P_T \text{ and} \tag{4.32}$$

$$\min PAPR = \min \frac{\max_{k\in\{0,\ldots,N_{FFT}-1\}}\left(\left|\sum_{n=0}^{N_{FFT}-1} X_n e^{j2\pi nk/N_{FFT}}\right|^2\right)}{E\left\{\left|\sum_{n=0}^{N_{FFT}-1} X_n e^{j2\pi nk/N_{FFT}}\right|^2\right\}}$$

In section 3.2.4 the PAPR has been analyzed and evaluated with respect to the application of adaptive bit loading and sidelobes cancellation carriers. In this section the PAPR is analyzed in relation to the pilot insertion. In reference [97] the PAPR reduction is applied by utilizing a choice of pilot values inserted in OFDM symbols in such a way that the pilots can reduce the PAPR. Pilots can be chosen from several sets of orthogonal pilot sequences. The pilots that most satisfy the constraints in eq. (4.32) will be chosen for transmission. No extra information about the pilot sequence is required. Since the pilot sequences are orthogonal to each other, the receiver can detect the transmitted pilot sequence by cross-correlating the received pilot sequence with the reference pilot sequences and choose the sequence with the highest cross

correlation value (maximum likelihood method). A drawback of this orthogonal pilot sequence is that the pilots should always be available in each OFDM symbol. Some of the carriers in each OFDM symbols will therefore be as pilots, so the data rate will be reduced.

In the Cognitive Radio context some OFDM carriers will be de-activated due to the licensed user occupancy. The scheme can be seen as non-contiguous OFDM. In reference [98] the impact of the OFDM carriers de-activation to the PAPR has been investigated. The results show that the probability of high PAPR increases with the number of total subcarriers in the case of constant active subcarriers, therefore the PAPR reduction is more important in the case of large number of de-activated subcarriers compared to conventional OFDM (without carriers de-activation).

4.7 Conclusions

In this chapter the Wiener filter has been extensively used in the Cognitive Radio application. The Wiener filter is chosen since it directly relates the index of the subcarriers and OFDM symbol to the correlation property of the channel in frequency and time. The sliding window technique is utilized to avoid a high memory requirement in storing the Wiener filter coefficients. Frequency hopping and spectrum pooling contexts have been discussed. In the frequency hopping scenario the sliding window is applied in one region, while in the spectrum pooling context one active subcarriers group will be located in a different region than another active subcarriers group (separated by subcarrier holes) because of carriers de-activation in the licensed user's band. The proposed OFDM frame design according to the Bluetooth TDD duration refers to the short frame duration; therefore a training symbol is adequate in estimating the channel transfer functions in an OFDM frame as long as the frame duration is shorter than the coherence time of the channel.

The Wiener filter interpolates the channel transfer function by utilizing a noisy channel sample at the pilot positions. The pilots are spread among an OFDM frame and fulfill the sampling theorem. The distance between pilots in frequency should be lower than the coherence bandwidth of the channel while the distance between pilots in time should be lower than the channel coherence time.

The virtual pilot concept is employed with the purpose of improving the performance of the Wiener filter by adding pilot oversampling. The virtual pilots are not real pilots, and are located between real pilots. The virtual pilots are derived from linear interpolating/extrapolating the noisy channel samples at real pilot positions. The decision directed method will enhance the accuracy of the estimated channel transfer function value at the virtual pilot positions. This method could only be applied efficiently in a SISO system. In the MIMO system the signals from all transmit antennas will contribute to the received signal of one receive antenna; therefore a direct application of the decision directed method to the estimated channel transfer function (resulting from linear interpolation/extrapolation at the virtual pilot positions) will give a higher probability of decision errors and that will lead to a

high channel estimate deviation error. An extra mechanism is thus required to separate the signal from each transmit antenna in order to make the decision directed technique properly utilized. For this reason, in this chapter the initial channel estimates at the virtual pilot positions for MIMO system are only derived from linear interpolation/ extrapolation.

A literature study has shown that the hexagonal pattern is the optimum pilot pattern to sample 2 dimensional circularly bandlimited signals. Adding the virtual pilot concept to the hexagonal pilot pattern, and combining the linear interpolation/extrapolation and the decision directed technique in predicting the initial channel estimates at virtual pilot positions for the SISO system provides a significant channel estimation improvement. It gives almost the same performance as the two-times pilot oversampling. Further, in Cognitive Radio context, the virtual pilot concept simplifies the Wiener filtering by the sliding window technique.

The three pilots allocation techniques for MIMO system have been proposed. Without loss of generality a 2 transmit antenna system was used. One pattern adopts the Hexagonal SISO pattern and separate the pilots of the first and the second transmit antenna in time. The other patterns adopt the Rectangular SISO pattern and separate the pilot allocation of the first and the second antenna with emphasis on frequency. The new pattern forms a hexagonal pattern on each of the transmit antenna. Given the channel model in Table 4.1, the simulation results show that among the three patterns the MIMO pilot pattern that adopts the SISO Hexagonal pattern outperforms the other two patterns. The impact of delay spread to the channel correlation in frequency is more accommodated by the MIMO pattern that adopts the SISO hexagonal pattern. This is due to smaller distance between the real pilots of each of the transmit antennas. The aid of virtual pilots in time becomes significant in a slowly varying fading channel. Therefore, the channel MSE performance gap between the pattern that adopts the SISO Hexagonal pattern and the ones that adopts the SISO Rectangular pattern is more significant in a channel with low Doppler frequency compared to a channel with high Doppler frequency.

With respect to the utilization of virtual pilots for MIMO channel estimation in Cognitive Radio context, the accumulated MSE comes from the deviation error in the virtual pilots and the edge effects of the Wiener filter. The more licensed users access the spectrum in a scattered manner, the more edge effects will occur. More licensed users denote more carrier de-activations that eventually reduces the number of virtual pilots; therefore there should be a trade-off between the number of edge effects and the number of de-activated carriers at those virtual pilot positions that contribute to the final channel MSE.

Peak to average power ratio (PAPR) and synchronization are common problems in the OFDM system. Literature has given solutions to these challenges in conventional OFDM systems. Combining the spectrum pooling concept (carriers de-activation) with the available synchronization and PAPR reduction techniques can accommodate these common OFDM aspects in a Cognitive Radio context.

Chapter 5

Single Carrier Cognitive Radio System

5.1 Introduction

Beside the multi-carrier approach another method of utilizing the spectrum efficiently in cognitive radio context is by shaping the waveform of a single carrier transmitted signal dynamically over a spectral region. The shaping is done so that it can adapt to a changing electromagnetic environment and it has synthesized waveform features in frequency domain which do not interfere with the occupied spectrum. The fundamental idea is to avoid a preset frequency use and operate dynamically over a chosen spectral region. The Transform Domain Communication System (TDCS) is introduced in references [99],[100] as a candidate for a single carrier technique in Cognitive Radio. In principle the transmitted signal is shaped in such a way that its bandwidth does not overlap with the LU band.

We have expanded the work in TDCS by adding an extra embedded symbol (in line with our Cognitive Radio objective) for enhancing efficient spectral utilization [2]. The scheme, analysis and performance evaluations are described in section 5.2.

In references [100] to [102] the Fourier transform as tool to shape the spectrum in TDCS is replaced by the wavelet basis function. The technique is called Wavelet Domain Communication System (WDCS). Following the extension of our research on TDCS, we also propose to implement the extra embedded symbol in the WDCS system. The scheme, analysis, limitation and evaluations are given in section 5.3.

Further, the MIMO application to the single carrier modulation Cognitive Radio system will be explored in section 5.4.

The conclusions will be drawn in section 5.5.

5.2 Transform Domain Communication System (TDCS) with Embedded Symbol

The transmitter block diagram of the TDCS system is depicted in Figure 5.1. TDCS is a single carrier transmission where its bandwidth can be divided into smaller subbands which are similar to subcarriers in an OFDM system. In this way, it is easier to locate the part of the band occupied by the LUs and subsequently not to put energy in that region. Information regarding the spectrum occupancy of the licensed users are distributed to each CR device. Upon receiving the information about the region of the LU band, a vector map $\boldsymbol{A}=[A_0,..,A_k,..,A_{NFFT}\text{-}1]$ is produced by the Spectrum Magnitude module where k defines the index of subband. Zeros are placed on the subband indexes where the LU band is located, and ones are placed on the other subband indexes. Further, the vector map $\boldsymbol{A}$ is multiplied with a random phase vector $e^{j\boldsymbol{\theta}}$ that will produce the vector $\boldsymbol{B}_{b.}$. The multiplication with scaling factor C has the purpose of realizing the desired or targeted energy used for transmitting a TDCS symbol. After multiplication with the scaling factor C, the vector $\boldsymbol{B}$ will be produced. Applying an IFFT to $\boldsymbol{B}$ will produce the time-domain TDCS basis function $b(t)$. After modulating $b(t)$ with data $d(t)$ and Guard interval (GI) insertion, followed by windowing, the to be transmitted signal $s(t)$ is formed. The GI is added to avoid inter symbol interference (ISI) due to the multipath channel effect. Windowing can be added in order to reduce the sidelobes of the transmitted signal on the LU band. TDCS gives more degrees of freedom in choosing a window to lower the sidelobes of its spectrum. Unlike in OFDM, the spectrum of the window of TDCS does not have to make a zero on the subband spacing interval as long as its sidelobes are very low, e.g a half sine window [17]. Inter-subband interference will not degrade the data detection at the receiver due to the robustness of the autocorrelation method. Windowing can be replaced by de-activating more subbands adjacent to the LU band (adding more zeros to vector $\boldsymbol{A}$ at the sub bands adjacent to the LU band) since it will not reduce the transmission bit rate.

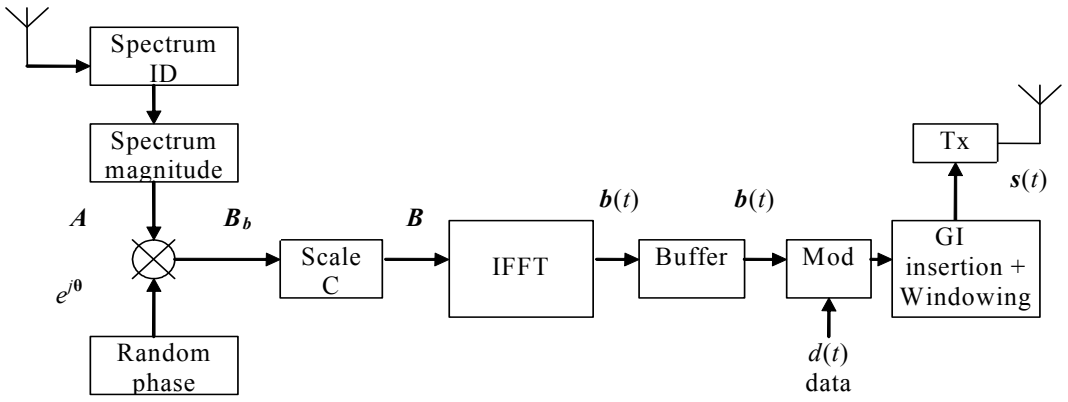

Figure 5.1: Transmitter architecture of TDCS [99]

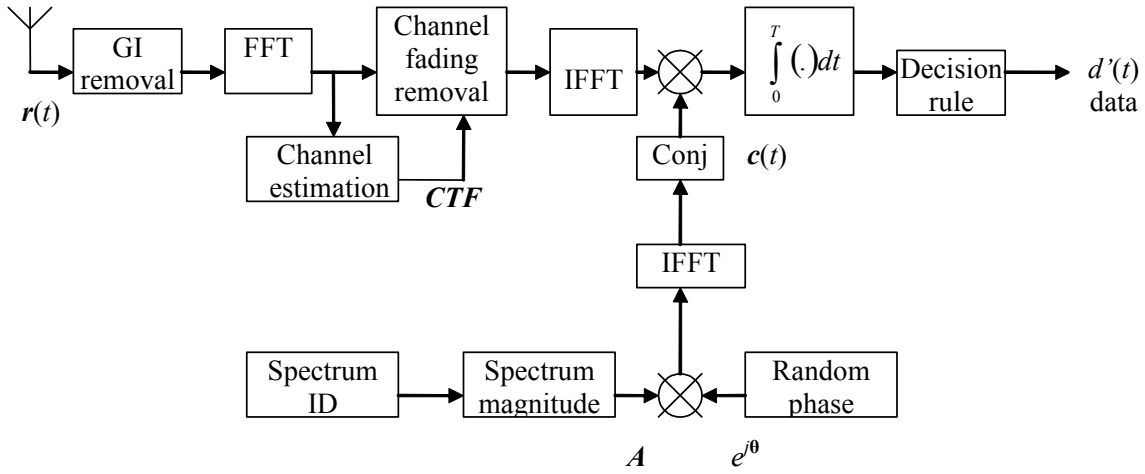

Figure 5.2: Receiver architecture of TDCS with Channel Estimation module

The impact of the zeros insertion to vector ***A*** can be observed from the TDCS power spectral density (PSD) equation,

$$PSD(f) = \left| \int_{-(1+\alpha)\frac{T}{2}}^{(1+\alpha)\frac{T}{2}} s(t) e^{-j2\pi ft} dt \right|^2 = \left| \frac{1}{N_{FFT}} \sum_{k=0}^{N_{FFT}-1} C A_k e^{j\theta_k} \int_{-(1+\alpha)\frac{T}{2}}^{(1+\alpha)\frac{T}{2}} d(t) p(t) e^{-j2\pi (f-f_k)t} dt \right|^2 \tag{5.1}$$

where T is the useful TDCS signal duration, $p(t)$ is the window function, α is the roll off factor of the window, f_k is the frequency on subband k and θ_k is the phase on subband k produced by the random phase module, C is the scaling factor, $d(t)$ is the modulated data and N_{FFT} is the number of FFT points used in the IFFT process (it can be considered as the number of subbands) [98].

If a rectangular window is used ($p(t)=1$) and α is zero, the result of the integral can be replaced by $Tsinc((f - f_k)T)$. A zero amplitude at sub-band k will remove the PSD on that sub-band position, and due to the spectrum orthogonality by this window the power contributions from the other subbands at that carrier position are also zero. Except at the frequencies not located at multiples of the subband spacing, the sidelobes coming from the sinc function of all active TDCS carriers will give power contributions. Since the sidelobes from the sinc function are deteriorated corresponding to the distance with the subband position, de-activating more subbands will lower the sidelobes. Therefore, there will be no significant signal power from

the TDCS based CR at the region of TDCS subbands which are occupied by the LUs. The time-domain signal $b(t)$ is modulated with the transmitted data $d(t)$ using a Cyclic Code Shift Keying (CCSK), Pulse Amplitude Modulation (PAM) or Pulse Position Modulation (PPM) scheme. In PAM the bits are mapped onto a real number (either positive or negative). The higher the constellation size (*CS*) of the PAM the higher will be the maximum amplitude of the PAM signal. In the context of Cognitive Radio and if PAM is applied, the PSD constraint should be taken into account and therefore a low constellation size is preferable. In CCSK the signals are cyclic shifted by the decimal number representing the composition of the bits transmitted with a length of bits equal to $\log_2 CS$. The shift length depends on *CS* and the decimal representation of the bits. The bit rate of the TDCS system with CCSK or PAM can be calculated from,

$$R_{TDCS-CCSKorPAM} = \frac{\log_2 CS}{T_s} \tag{5.2}$$

where T_S is the TDCS symbol duration including the guard interval (GI). The GI is inserted to avoid the inter symbol interference (ISI) which is introduced by the multipath channel. In the PPM the bits are mapped as shifted pulses [8]. It requires longer symbol periods for higher constellation sizes; it is therefore not advantageous to be applied in the TDCS if high rates are needed. The maximum *CS* that can be applied in CCSK is restricted to the number of subbands (N_{FFT}). The nice property of CCSK is that the BER improves as the *CS* increases [102], [103], therefore the optimum constellation size for CCSK modulation is equal to the number of subbands (N_{FFT}). Considering these facts CCSK is considered as the most optimum modulation in TDCS.

In comparison with OFDM, if the scaling factor *C* is 1 the PSD of OFDM in eq. (2.1) has larger sidelobes (with a factor of N_{FFT}) compared to the PSD of TDCS in eq. (5.1). OFDM has a factor of N_{FFT} higher bitrate compared to TDCS since the bit rate of OFDM is $\frac{N_{FFT}.\log_2 CS}{T_s}$ while the TDCS bit rate is described by eq. (5.2). Increasing the scaling factor *C* will increase the required energy to transmit the TDCS symbol but it will also increase the SNR of TDCS, hence, the TDCS BER performance will be improved.

The outputs of the random phase modules at the transmitter and at the receiver must be equal, as the latter will be used as reference at the receiver for data detection by using a correlation process. The spectrum occupancy information available at the transmitter should also be available at the receiver for accurate data detection. After the GI removal, the signal is transformed into frequency domain, followed by fading effect cancellation. In order to detect the transmitted signal, the received signal is transformed again into time-domain by the IFFT and is then de-correlated with the reference signal *c(t)*. De-correlation for symbol detection can be simplified by taking the maximum absolute value of the inverse Fourier transform of

the product of the received signal and the conjugate of the reference signal in the frequency-domain [103].

In an attempt to increase the bit rate of TDCS, we describe in this section the proposed embedded symbol to TDCS-CCSK. The embedded symbol can be derived from PAM, QAM or PSK modulation. The proposed transmitter and receiver architectures of the system are depicted in Figure 5.3.

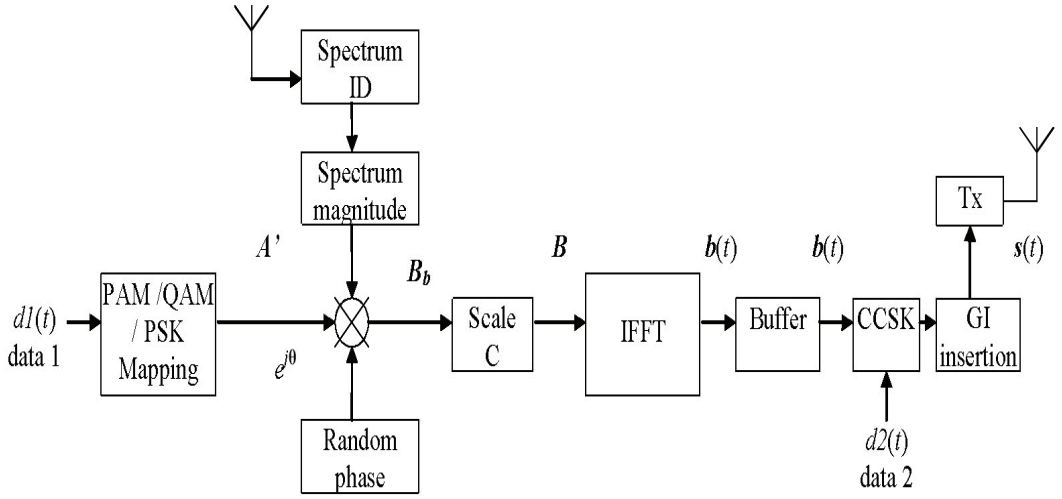

(a)

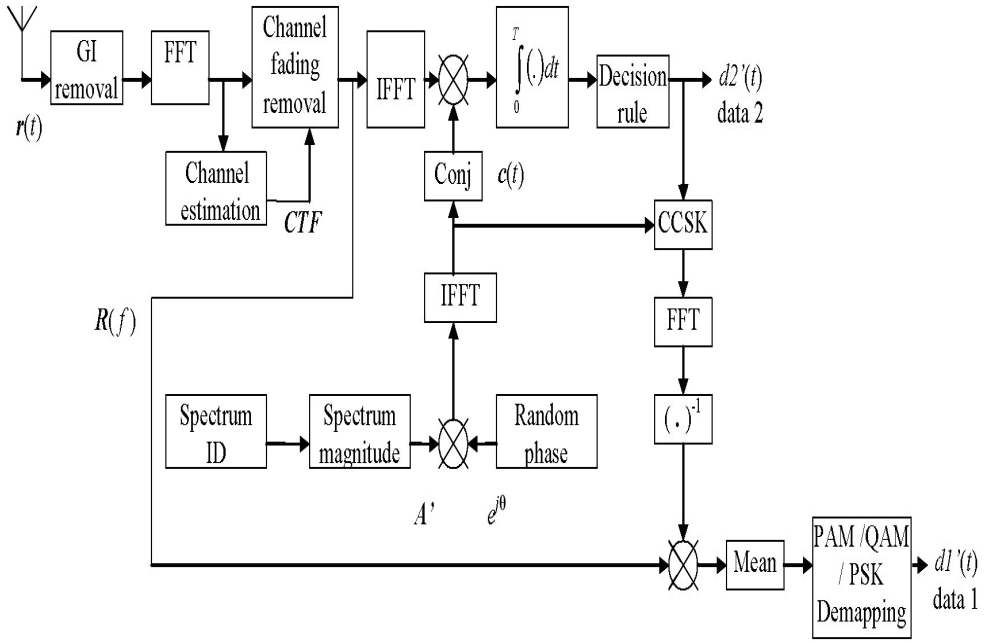

(b)

Figure 5.3: (a) Transmitter and (b) Receiver architecture of TDCS with extra embedded symbol

There are two bit sources available. The first one is for the embedded symbol, and the second one is for the CCSK modulation. We choose to have N_{FFT} as the *CS* value of the CCSK modulation since it is the optimum one, while the embedded symbol constellation size will be investigated further in the performance evaluation subsection.

At the transmitter one embedded symbol will be multiplied with a vector derived from the point to point multiplication between the vector produced by the random phase $\boldsymbol{\theta}$ and the vector produced by the spectrum magnitude $\boldsymbol{A}$. Further, legacy processes in producing the TDCS signal are applied. At the receiver, CCSK data detection is applied first. After removing the fading effect in frequency-domain, the CCSK data detection is applied by de-correlating the time-domain received signal with the time-domain reference signal. De-correlation can be simplified by taking the maximum absolute value of the inverse Fourier transform of the product of the frequency-domain conjugate received signal and the reference signal [103]. The received discrete time-domain signal y at time instant n after fading removal can be expressed as:

$$\begin{aligned} y_n &= \frac{1}{N_{FFT}} \sum_{k=0}^{N_{FFT}-1} \left[A_k e^{j\theta_k} S e^{j\varphi} e^{j\frac{-2\pi\tau k}{N_{FFT}}} + \frac{N_k}{H_k} \right] e^{j\frac{2\pi nk}{N_{FFT}}} \\ &= \frac{1}{N_{FFT}} \sum_{k=0}^{N_{FFT}-1} \left[A'_k S e^{j\varphi} e^{j\frac{-2\pi\tau k}{N_{FFT}}} + \frac{N_k}{H_k} \right] e^{j\frac{2\pi nk}{N_{FFT}}} \end{aligned} \tag{5.3}$$

where S, φ, N_k, H_k are the magnitude, phase of the embedded symbol, noise and channel gain on subband k respectively, and $A'_k = A_k e^{j\theta k}$, and τ is the data from source 2 for CCSK modulation. The reference signal c at time instant n is defined as :

$$c_n = \frac{1}{N_{FFT}} \sum_{k=0}^{N_{FFT}-1} \left[A_k e^{j\theta_k} \right] e^{j\frac{2\pi nk}{N_{FFT}}} = \frac{1}{N_{FFT}} \sum_{k=0}^{N_{FFT}-1} A'_k e^{j\frac{2\pi nk}{N_{FFT}}} \tag{5.4}$$

The correlation function R of signals y and c becomes

$$\begin{aligned} R_i &= \sum_{n=0}^{N_{FFT}-1} y_n \cdot c^*_{n-i} \\ &= \sum_{n=0}^{N_{FFT}-1} \frac{1}{N_{FFT}} \sum_{k=0}^{N_{FFT}-1} \left[A'_k S e^{j\varphi} e^{j\frac{-2\pi\tau k}{N_{FFT}}} + \frac{N_k}{H_k} \right] e^{j\frac{2\pi nk}{N_{FFT}}} \frac{1}{N_{FFT}} \sum_{l=0}^{N_{FFT}-1} A'^*_l e^{j\frac{-2\pi(n-i)l}{N_{FFT}}} \end{aligned}$$

$$= \sum_{n=0}^{N_{FFT}-1} \frac{1}{(N_{FFT})^2} \left[\begin{array}{l} \sum_{k=0}^{N_{FFT}-1} \sum_{l=0,l\neq k}^{N_{FFT}-1} \left(A'_k \, A'^{*}_l \, S e^{j\varphi} e^{j\frac{2\pi(nk-\tau k-nl+il)}{N_{FFT}}} + A'^{*}_l \frac{N_k}{H_k} e^{j\frac{2\pi(nk-nl+il)}{N_{FFT}}} \right) \\ + \sum_{r=0}^{N_{FFT}-1} \left(\left|A'_r\right|^2 S e^{j\varphi} e^{j\frac{2\pi(i-\tau)r}{N_{FFT}}} + A'^{*}_r \frac{N_k}{H_k} e^{j\frac{2\pi ir}{N_{FFT}}} \right) \end{array} \right] \tag{5.5}$$

The first term in the final eq. (5.5) is negligible due to random phase property of the TDCS [97]. Eq. (5.5) can be approximated as eq. (5.6). The complete derivation is available in the Appendix C.

$$\begin{aligned} R_i \quad &\approx \sum_{n=0}^{N_{FFT}-1} \frac{1}{(N_{FFT})^2} \left[\sum_{r=0}^{N_{FFT}-1} \left(\left|A'_r\right|^2 S e^{j\varphi} e^{j\frac{-2\pi\tau r}{N_{FFT}}} + A'^{*}_r \frac{N_r}{H_r} \right) e^{j\frac{2\pi ir}{N_{FFT}}} \right] \\ &= \frac{1}{(N_{FFT})} \left[\underbrace{S e^{j\varphi} \sum_{r=0}^{N_{FFT}-1} e^{j\frac{2\pi(i-\tau)r}{N_{FFT}}}}_{signal\ \ term} + \underbrace{\sum_{r=0}^{N_{FFT}-1} A'^{*}_r \frac{N_r}{H_r} e^{j\frac{2\pi ir}{N_{FFT}}}}_{noise\ \ term} \right] \end{aligned} \tag{5.6}$$

The derivation in eq. (5.6) fully agrees with reference [103] in doing CCSK detection. The position where the maximum correlation occurs (τ) will be selected as the estimated transmitted data on source data 2. A measure of peak power to mean sidelobe power ratio (PMR) of the basis function *b(t)* can be employed to determine the robustness of CCSK data detection [103]. The PMR is the ratio between the square of the peak cross-correlation of the basis function and the square of the average remaining cross-correlation values (termed as sidelobes). If we consider the transmitted data on source data 2 is zero (τ=0) then the PMR of the proposed TDCS will be represented by eq. (5.7), while in case TDCS-CCSK is without embedded symbol the $S e^{j\varphi}$ in eq. (5.7) is replaced by 1.

$$\begin{aligned} PMR &= \frac{E\left[R_0^2\right]}{E\left[R_{i,i\neq 0}^2\right]} = \frac{E\left[\left| \left(\frac{1}{N_{FFT}} \sum_{r=0}^{N_{FFT}-1} \left(\left|A'_r\right|^2 S e^{j\varphi} + A'^{*}_r \frac{N_r}{H_r} \right) \right) \right|^2 \right]}{E\left[\left| \left(\sum_{i=1}^{N_{FFT}-1} \frac{1}{N_{FFT}} \sum_{r=0}^{N_{FFT}-1} \left(\left|A'_r\right|^2 S e^{j\varphi} + A'^{*}_r \frac{N_r}{H_r} \right) e^{j\frac{2\pi(ir)}{N_{FFT}}} \right) \right|^2 \right]} \\ &\approx \frac{\left| S^2 e^{j2\varphi} \right| + \sigma_{N/H}^2}{\sigma_{N/H}^2} \end{aligned} \tag{5.7}$$

In eq. (5.7) it is assumed that the $\frac{N_r}{H_r}$ has a Gaussian distribution with variance $\sigma_{N/H}^2$. However, despite N_r is Gaussian distributed and if H_r is also Gaussian distributed it does not mean that $\frac{N_r}{H_r}$ is necessarily Gaussian distributed. The emphasis in giving the PMR equation is to show how the embedded symbol can enhance the PMR of TDCS-CCSK. The details and complete derivation of eq. (5.7) is provided in Appendix D.

The data from CCSK detection represents the estimated symbol cyclic shift that was taking place at the transmitter to transmit the data for CCSK modulation. This estimated shift is then further used to shift the reference signal, followed by the transformation into frequency-domain by the FFT module.

The received signal in frequency-domain (before CCSK data detection) is then divided by the shifted reference signal (in frequency-domain) which can be described as dividing the Y_r in eq. (5.6) by $A'_r e^{j\frac{-2\pi\tau r}{N_{FFT}}}$; hence, before the decision process the estimated embedded symbol $\hat{d}$ equals

$$\hat{d} = \frac{Y_r}{A'_r e^{j\frac{-2\pi\tau r}{N_{FFT}}}} = \frac{A'_r S e^{j\varphi} e^{j\frac{-2\pi\tau r}{N_{FFT}}} + \frac{N_r}{H_r}}{A'_r e^{j\frac{-2\pi\tau r}{N_{FFT}}}} = S e^{j\varphi} + \frac{N_r e^{j\frac{2\pi\tau r}{N_{FFT}}}}{A'_r H_r} \tag{5.8}$$

After taking the average value per N_{FFT} samples and detection by PAM, QAM or PSK de-mapping, the bits from source data 1 are reconstructed. Another method is by utilizing the detected data on source 2 (τ) and multiplying the product between the (in frequency-domain) received symbol and reference basis function ($U_r=FFT(\boldsymbol{y}).FFT^*(\boldsymbol{c})$ in eq. (5.6)) with $e^{j\frac{2\pi\tau r}{N_{FFT}}}$, where $r \in \{0,...,N_{FFT}-1\}$. In this way the transformation of the shifted reference basis function into frequency-domain can be avoided. In order to improve the source data 1 BER performance further, channel coding and interleaving can be applied before the mapping process, meanwhile the de-interleaving and decoding are applied after de-mapping. For simplicity these techniques will not be included here.

The new TDCS bit rate becomes:

$$R_{NEWTDCS} = \frac{\log_2 CS.CS_{EM}}{T'_s} \tag{5.9}$$

where CS_{EM} is the embedded symbol constellation size.

From spectrum point of view, the PSD of TDCS-CCSK with extra embedded symbol yields

$$PSD(f) = \left| \frac{1}{N_{FFT}} S e^{j\varphi} \sum_{k=0}^{N_{FFT}-1} A_k e^{j\theta_k} \int_{-(1+\alpha)\frac{T}{2}}^{(1+\alpha)\frac{T}{2}} p(t) e^{-j2\pi(f-f_k)t} dt \right|^2 \tag{5.10}$$

By observing eq. (5.10) it is reasonable to consider PSK as most appropriate embedded symbol modulation mode among the three mapping types (PSK, PAM, and QAM). The PSK symbols are spread over a unit circle with magnitude one. Therefore embedding the PSK symbol to the TDCS with CCSK modulation will not change the TDCS transmission power, while embedding PAM and QAM requires more power. The extra amount of power required will depend on the constellation size of the PAM/QAM embedded symbol. Moreover, the embedded symbol will affect the sidelobes of the proposed TDCS. Because PSK symbol magnitude is one, according to eq. (5.10) the sidelobes amplitude of the proposed TDCS will not change. PAM and QAM symbols with constellation size bigger than 2 have an average magnitude larger than one and therefore the sidelobes amplitude of the proposed TDCS will be affected. PAM modulation in this case will be the worse option since for the same constellation size (larger than 2) its maximum amplitude is bigger than the QAM mode. Increasing the embedded symbol's constellation size will enhance the symbol- to- noise ratio on each of the TDCS subband. According to reference[103] the symbol-to noise ratio enhancement will lead to a symbol error probability improvement and eventually to a bit error rate improvement. Increasing the constellation size means allocating more bits to the transmitted signal and as a consequence more energy is practically allocated. The amount of allocated energy is linearly dependent on the number of allocated bits. Therefore, the SNR gain obtained by increasing the CS_{EM} compared to the conventional TDCS-CCSK corresponds to

$$SNR_{Gain} = 10 \log_{10}\left(\log_2(CS_{EM})\right) dB \tag{5.11}$$

where $\log_2(CS_{EM})$ refers to the number of bits allocated to the embedded symbol.

5.2.1 Multi-User TDCS with Extra Embedded Symbol Detection Analysis

It is described in references [9],[99] that the random phase generator can be designed to support multiple user transmission. We have analyzed that the embedded symbol will not destroy the CCSK detection on each user. It can be learnt from the following derivations.

If the received signal on the receiver of user 1 is :

$$y_{n,1} = \frac{1}{N_{FFT}} \sum_{k=0}^{N_{FFT}-1} \left[A_{k,1} e^{j\theta_{k,1}} S_1 e^{j\varphi_1} e^{j\frac{-2\pi\tau_1 k}{N_{FFT}}} + \sum_{u=2}^{U} A_{k,u} e^{j\theta_{k,u}} \frac{H_k^u}{H_k^1} S_u e^{j\varphi_u} e^{j\frac{-2\pi\tau_u k}{N_{FFT}}} + \frac{N_k^1}{H_k^1} \right] e^{j\frac{2\pi nk}{N_{FFT}}}$$
$$= \frac{1}{N_{FFT}} \sum_{k=0}^{N_{FFT}-1} \left[A'_{k,1} S_1 e^{j\varphi_1} e^{j\frac{-2\pi\tau_1 k}{N_{FFT}}} + \sum_{u=2}^{U} A'_{k,u} \frac{H_k^u}{H_k^1} S_u e^{j\varphi_u} e^{j\frac{-2\pi\tau_u k}{N_{FFT}}} + \frac{N_k^1}{H_k^1} \right] e^{j\frac{2\pi nk}{N_{FFT}}} \quad (5.12)$$

where H_k^u is the channel transfer function of user u on TDCS subband k. The symbols with index attribute u in eq.(5.12) belongs to user u, while symbols with index attribute 1 belongs to user 1. U denotes the total number of users. We use the same basis reference signal c as described in eq. (5.4), but we put attribute 1 to it in order to refer it as reference signal for user 1.

The correlation on the user 1's receiver becomes:

$$R_{i,1} = \sum_{n=0}^{N_{FFT}-1} y_{n,1} \cdot c^*_{n-i,1}$$
$$= \sum_{n=0}^{N_{FFT}-1} \frac{1}{N_{FFT}} \sum_{k=0}^{N_{FFT}-1} \left[A'_{k,1} S_1 e^{j\varphi_1} e^{j\frac{-2\pi\tau_1 k}{N_{FFT}}} + \sum_{u=2}^{U} A'_{k,u} \frac{H_k^u}{H_k^1} S_u e^{j\varphi_u} e^{j\frac{-2\pi\tau_u k}{N_{FFT}}} + \frac{N_k^1}{H_k^1} \right] e^{j\frac{2\pi nk}{N_{FFT}}} \frac{1}{N_{FFT}} \sum_{l=0}^{N_{FFT}-1} A'^*_{l,1} e^{j\frac{-2\pi(n-i)l}{N_{FFT}}}$$
$$= \sum_{n=0}^{N_{FFT}-1} \frac{1}{(N_{FFT})^2} \left[\begin{array}{l} \sum_{k=0}^{N_{FFT}-1} \sum_{l=0,l\neq k}^{N_{FFT}-1} \left(A'_{k,1} A'^*_{l,1} S_1 e^{j\varphi_1} e^{j\frac{2\pi(nk-\tau_1 k-nl+il)}{N_{FFT}}} + \sum_{u=2}^{U} A'_{k,u} A'^*_{l,1} \frac{H_k^u}{H_k^1} S_u e^{j\varphi_u} e^{j\frac{2\pi(nk-\tau_u k-nl+il)}{N_{FFT}}} + A'^*_{l,1} \frac{N_k^1}{H_k^1} e^{j\frac{2\pi(nk-nl+il)}{N_{FFT}}} \right) \\ + \sum_{r=0}^{N_{FFT}-1} \left(\left| A'_{r,1} \right|^2 S_1 e^{j\varphi_1} e^{j\frac{2\pi(i-\tau_1)r}{N_{FFT}}} + \sum_{u=2}^{U} A'_{r,u} A'^*_{r,1} \frac{H_r^u}{H_r^1} S_u e^{j\varphi_u} e^{j\frac{2\pi(i-\tau_u)r}{N_{FFT}}} + A'^*_{r,1} \frac{N_r^1}{H_r^1} e^{j\frac{2\pi ir}{N_{FFT}}} \right) \end{array} \right] \quad (5.13)$$

The first term of eq. (5.13) is negligible due to the random phases and multi-user orthogonal basis function properties of the TDCS [9],[99], [100]. Therefore eq. (5.13) can be simplified ito (details are in the Appendix E),

$$R_{i,1} \approx \sum_{n=0}^{N_{FFT}-1} \frac{1}{(N_{FFT})^2} \left[\sum_{r=0}^{N_{FFT}-1} \left(\left| A'_{r,1} \right|^2 S_1 e^{j\varphi_1} e^{j\frac{-2\pi\tau_1 r}{N_{FFT}}} + \sum_{u=2}^{U} A'_{r,u} A'^*_{r,1} \frac{H_r^u}{H_r^1} S_u e^{j\varphi_u} e^{j\frac{-2\pi\tau_u r}{N_{FFT}}} + A'^*_{r,1} \frac{N_r^1}{H_r^1} \right) e^{j\frac{2\pi ir}{N_{FFT}}} \right]$$
$$\approx \frac{1}{(N_{FFT})} \left[\begin{array}{l} \underbrace{S_1 e^{j\varphi_1} \sum_{r=0}^{N_{FFT}-1} e^{j\frac{2\pi(i-\tau_1)r}{N_{FFT}}}}_{\text{signal term}} + \underbrace{\sum_{u=2}^{U} S_u e^{j\varphi_u} \sum_{r=0}^{N_{FFT}-1} A'_{r,u} A'^*_{r,1} \frac{H_r^u}{H_r^1} e^{j\frac{2\pi(i-\tau_u)r}{N_{FFT}}}}_{\text{multiple access interference term}} \\ + \underbrace{\sum_{r=0}^{N_{FFT}-1} A'^*_r \frac{N_r^1}{H_r^1} e^{j\frac{2\pi ir}{N_{FFT}}}}_{\text{noise term}} \end{array} \right] \quad (5.14)$$

According to [100], if each user has a different dedicated generator polynomial in producing the random phase then the multiple access interference term in eq. (5.11) will be small. Therefore, if the noise term does not exist, the receiver could still estimate the shift from the CCSK modulation of each user (τ_u) correctly by utilizing the reference basis function of each user ($\boldsymbol{A'}_u=[A_{0,u}\ ,\ldots,\ A_{k,u},\ldots,\ A_{N_{FFT}-1,u}\ ]$) and by choosing index i for the maximum value in correlation of each user ($R_{i,u}$).

If the receiver has a base station kind of capability, then the basis function of all users will be available at the receiver. Equation (5.14) in general form can be written as :

$$R_{i.cu} \approx \frac{1}{(N_{FFT})}\left[\begin{array}{l} S_1 e^{j\varphi_1}\sum_{r=0}^{N_{FFT}-1} A'_{r,1}A'^{*}_{r,cu}\frac{H_r^1}{H_r^{cu}}e^{j\frac{2\pi(i-\tau_1)r}{N_{FFT}}} +\ldots+ S_{cu}e^{j\varphi_{cu}}\sum_{r=0}^{N_{FFT}-1} A'_{r,cu}A'^{*}_{r,cu}e^{j\frac{2\pi(i-\tau_2)r}{N_{FFT}}} \\ +\ldots+ S_U e^{j\varphi_U}\sum_{r=0}^{N_{FFT}-1} A'_{r,U}A'^{*}_{r,cu}\frac{H_r^U}{H_r^{cu}}e^{j\frac{2\pi(i-\tau_U)r}{N_{FFT}}} + \underbrace{\sum_{r=0}^{N_{FFT}-1} A'^{*}_{r,cu}\frac{N_r^{cu}}{H_r^{cu}}e^{j\frac{2\pi ir}{N_{FFT}}}}_{noise\ \ term} \end{array}\right] \quad (5.15)$$

$$\approx \frac{1}{(N_{FFT})}\left[\psi_1 \mathrm{E}^i_{1,cu}+\ldots+\psi_{cu}\mathrm{E}^i_{cu,cu}+\ldots+\psi_u\mathrm{E}^i_{u,cu}+\ldots+\psi_U\mathrm{E}^i_{U,cu}+\eta^j_{cu}\right]$$

where $R_{i,cu}$ is the cross correlation between the received signal after fading removal with the shifted basis function of user cu on shift distance i and where $\psi_u = S_u e^{j\varphi_u}$, $E^i_{u,cu}=\sum_{r=0}^{N_{FFT}-1} A'_{r,u}A'^{*}_{r,cu}\frac{H_r^u}{H_r^{cu}}e^{j\frac{2\pi(i-\tau_u)r}{N_{FFT}}}$ and $\eta^i_{cu}=\sum_{r=0}^{N_{FFT}-1} A'^{*}_{r,cu}\frac{N_r^{cu}}{H_r^{cu}}e^{j\frac{2\pi ir}{N_{FFT}}}$.

By utilizing the basis function of all users and calculate $R_{i,cu}$ of all users, τ_u of all users wil be derived. The vector-matrix form of eq. (5.15) is

$$\mathbf{R}^{cu}{}_{N_{FFT}\,\mathrm{x}\,1}=\mathbf{E}^{cu}{}_{N_{FFT}\,\mathrm{x}\,U}\boldsymbol{\Psi}^{cu}{}_{\mathrm{U\,x\,1}}+\boldsymbol{\eta}^{cu}{}_{N_{FFT}\,\mathrm{x}\,1} \quad (5.16)$$

The matrix $\mathbf{E}^{cu}$ is derived by utilizing the obtained τ_u of all users and the basis function vectors $\boldsymbol{A'}_u$ of all users. Accordingly, the value of embedded symbols of all users before decision by QAM/PSK/PAM de-mapping (maximum likelihood) can be derived by

$$\bar{\boldsymbol{\Psi}}=\frac{1}{U}\sum_{cu=1}^{U}\left(\mathbf{E}^{cu\ -1}\boldsymbol{R}^{cu}\right)=\frac{1}{U}\sum_{cu=1}^{U}\left(\boldsymbol{\Psi}^{cu}+\mathbf{E}^{cu\ -1}\boldsymbol{\eta}^{cu}\right) \quad (5.17)$$

where $\bar{\boldsymbol{\Psi}}=\left[\bar{\psi}_1,\ldots,\bar{\psi}_U\right]=\left[\bar{S}_1 e^{j\bar{\varphi}_1},\ldots,\bar{S}_U e^{j\bar{\varphi}_U}\right]$ are the estimated embedded symbols of all users.

5.3 Wavelet Domain Communication System (WDCS) with Embedded Symbol

A variant of TDCS is the wavelet domain communication system (WDCS) [100]-[102] where the Fourier transform operation in TDCS is replaced by a wavelet transformation. The wavelet transform has been known having lower sidelobes compared to Fourier based modulation. Wavelets are used in this scheme to identify and establish an interference-free spectrum. The advantages of using wavelet are [100]:

1. Increased adaptation over a larger class of interfering signals,
2. Finer high-frequency resolution,
3. Allow implementation of *CS*-ary orthogonal signaling

The WDCS uses a packet-based transform to estimate the electromagnetic spectrum [93]. Through the use of adaptive thresholds and notches, sub-bands containing the interference are effectively canceled. From this estimate, a unique communication basis function $\boldsymbol{A}$ in the transform domain is generated so that no (or very little) energy-bearing information is contained in the areas occupied by primary users. These functions are then multiplied with a pseudo-random(PR) phase vector $e^{j\boldsymbol{\theta}}$ to generate $\boldsymbol{B}_b$. The PR code is used to randomize the phase of the spectral components. The resulting complex spectrum is then scaled with C to provide the desired energy in the signal spectrum. A time domain version $b(t)$ of the basis function is then obtained by performing an inverse wavelet transfom. The wavelet basis function can be a Coifflets, Daubechies, Haar, Symlets or Remez filter as applied earlier in WP-MCM. Finally, the basis function is modulated with data using PAM, or PPM, or CCSK modulation and then transmitted. The block diagram of the WDCS transmission process is shown in Figure 5.4.

At the receiver the detection is preceded by correlating the received signal with the reference signal in-time domain. The receiver structure of WDCS is almost similar to the TDCS, the differences are the FFT and IFFT modules in TDCS that are replaced by discrete wavelet transform (DWT) and inverse discrete wavelet transform (IDWT), respectively.

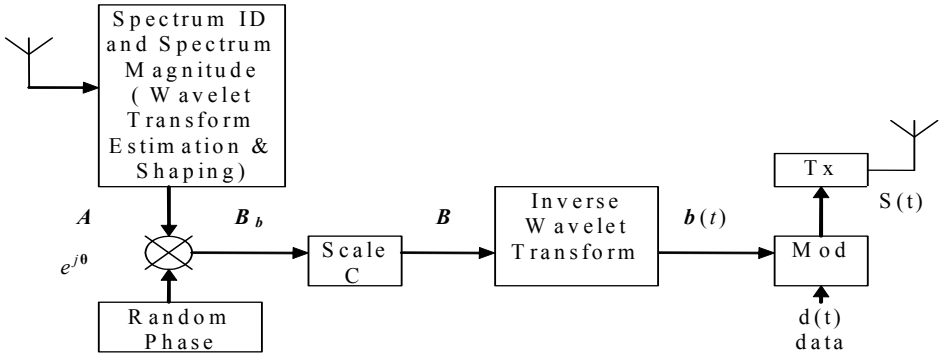

Figure 5.4: WDCS Transmitter blocks [100]

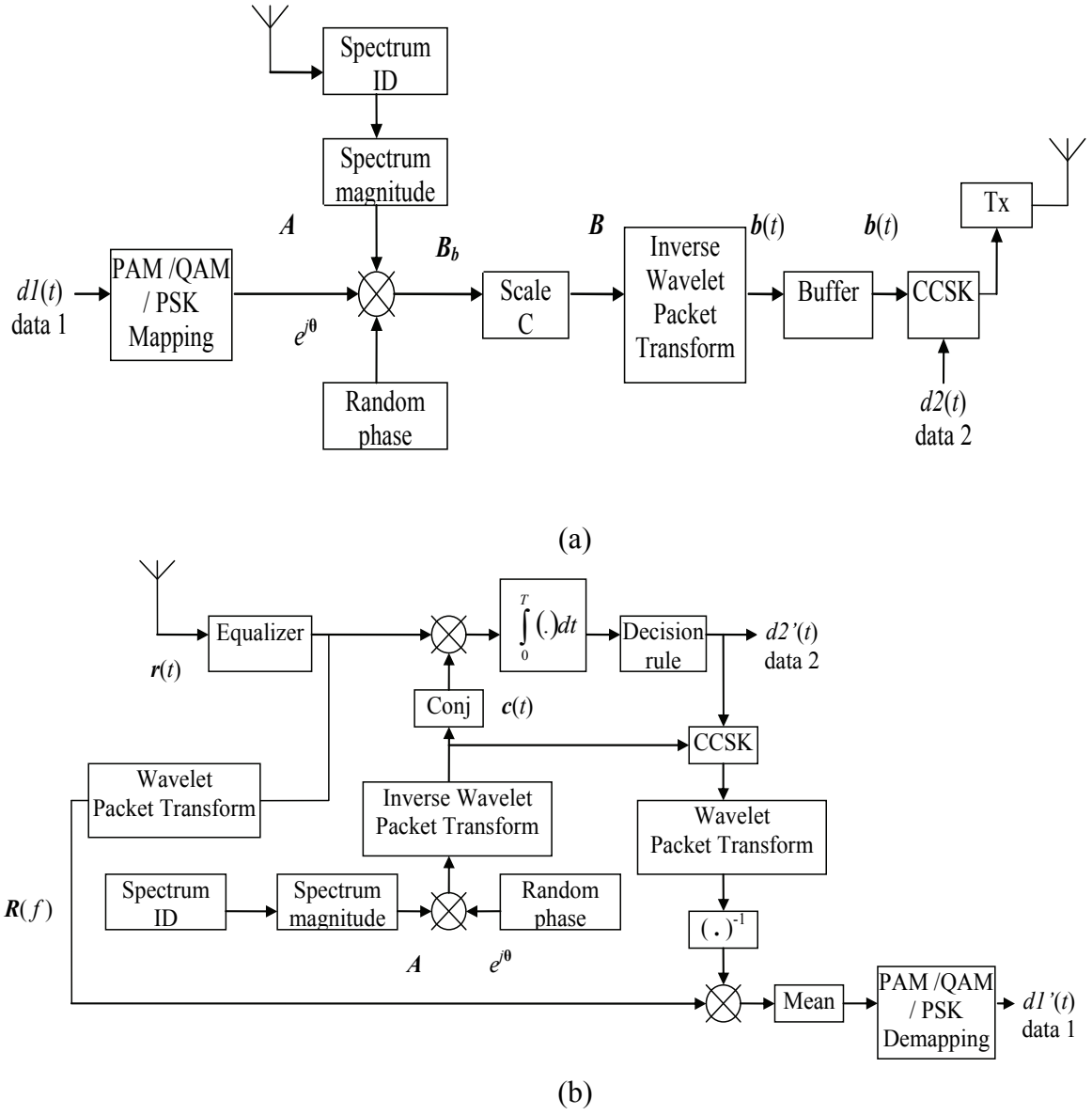

Figure 5.5: (a) Transmitter and (b) Receiver architecture of WDCS with extra embedded symbol

The application of the embedded symbol to WDCS is presented in Figure 5.5. According to reference [52] the impact of fading in the modulation technique using the wavelet basis function would be properly removed by time-domain equalization. Therefore, different with the TDCS scheme (Figure 5.3) the frequency-domain channel estimation and fading removal is replaced by time-domain equalization. Further, the CCSK detection in WDCS with extra embedded symbol system is applied in time-domain, while the embedded symbol detection

remains conducted in frequency-domain. The frequency domain embedded symbol detection is done due to the interference avoidance reason. By neglecting the signal at the LU band position (Spectrum Pooling technique), the embedded symbol will not be affected by the interference from the LU signal.

5.4 MIMO Application in a Single Carrier Cognitive Radio System

Following the gain of applying the MIMO system with V-BLAST receiver architecture in the TDCS system and using our experience reported in [105] we here extend the work by adding to the TDCS-CCSK an extra embedded symbol for higher rate transmission. The comparison in performance of the MIMO V-BLAST and the conventional TDCS will be described in next section. The MIMO system with V-BLAST receiver has been proven to be robust in counteracting the fading channel. It exploits channel diversity to improve the system BER performance through space time-coding of the estimated channel state information on all channel links. Furthermore, MIMO also increases the system bit rate. In the CR context the bit rate and BER enhancement by adding MIMO with V-BLAST receiver to our TDCS-CCSK with an extra embedded symbol refer to an efficient spectrum utilization improvement. In this way our proposed system tries to fulfill the CR objectives of highly reliable communications and efficient spectrum utilization [2] with extra complexity as a consequence.

The transmitter and receiver architectures of the proposed system are depicted in Figure 5.6, where M is the number of transmit antennas and N is the number of the receive antennas. At the transmitter after the guard interval (GI) insertion, the transmitted signal is de-multiplexed to be transmitted to a selected transmit antenna. The transmitted signal on each transmit antenna is different to each other; as a result the data rate increases M times compared with the single antenna rate. In order to preserve the amount of power used for transmission, the total power is distributed among transmit antennas. For the sake of simplicity, in our system we apply an equal distribution. The power spectral density (PSD) of the TDCS-CCSK with embedded symbol in a MIMO system becomes

$$PSD(f) = \left| \frac{1}{N_{FFT}} \sum_{m=1}^{M} \frac{1}{\sqrt{M}} S_m e^{j\varphi_m} \sum_{k=0}^{N_{FFT}-1} A_k e^{j\theta_{k,m}} \int_{-(1+\alpha)\frac{T}{2}}^{(1+\alpha)\frac{T}{2}} p(t) e^{-j2\pi(f-f_k)t} dt \right|^2 \tag{5.18}$$

where S_m and φ_m are the magnitude and phase of the embedded symbol on transmit antenna m; T is the useful signal duration; $p(t)$ is the window function; α is the roll off factor of the window; A_k and $\theta_{k,m}$ are the spectrum occupancy info (0 if it is occupied by LU, and 1 if it is available) and the phase produced by the random phase module on sub-band k of antenna m

respectively. A factor $\frac{1}{\sqrt{M}}$ is included in eq. (5.18) because the total power is distributed equally to all M transmit antennas. All transmit antennas have the same spectrum occupancy info $\boldsymbol{A}$.

If a rectangular window is used ($p(t)=1$) and α is zero, the result of the integral can be replaced by $Tsinc((f-f_k)T)$. A zero amplitude at sub-band k will remove the PSD at that carrier position, and due to the spectrum orthogonality of this window the power contributions from the other carriers on frequency f_k are also zero. Since all transmit antennas utilize the same spectrum occupancy info $\boldsymbol{A}$, there will be no signal power from the TDCS based CR in the region of TDCS sub-bands which are occupied by the LUs. The overall sidelobes will be the average of the total sum of each transmit antenna sidelobes.

The data rate of the TDCS with embedded symbol in MIMO system becomes

$$R_{EM_TDCS_MIMO}=\frac{M.\log_2(CS.CS_{EM})}{T_s} \tag{5.19}$$

where CS is the constellation size of CCSK modulation, CS_{EM} is the embedded symbol constellation size and T_s is the TDCS symbol duration including the GI.

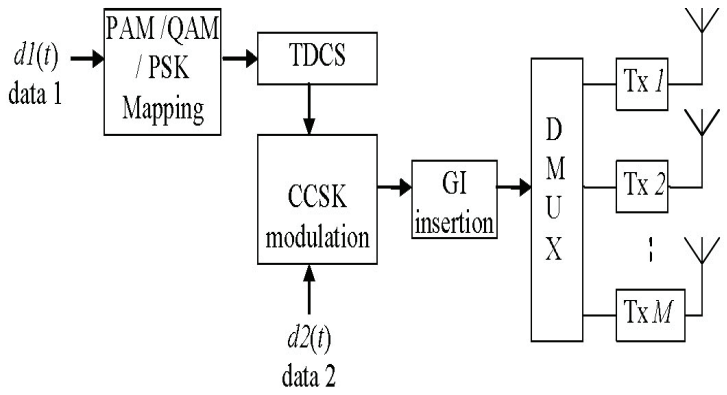

(a)

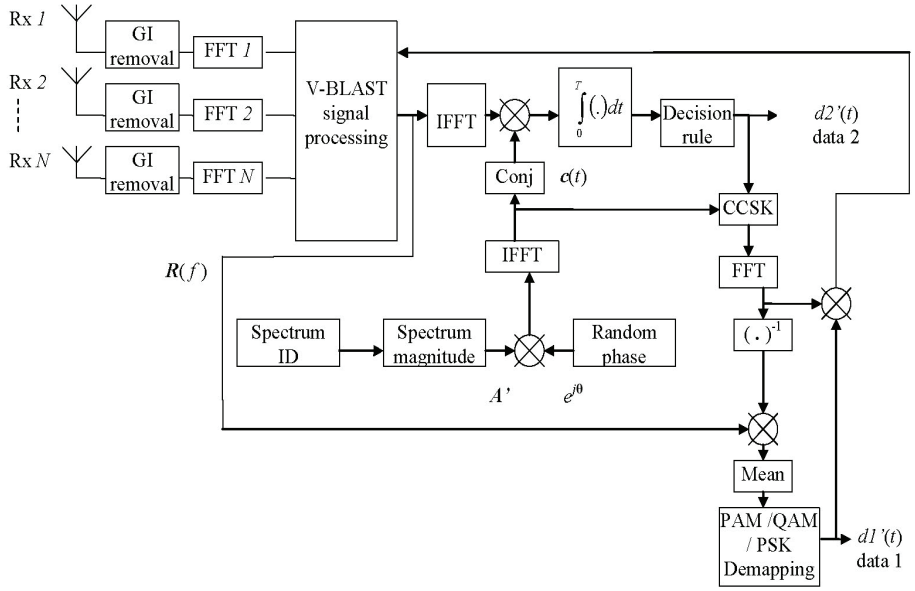

(b)

Figure 5.6: (a) MIMO Transmitter and (b) V-BLAST Receiver architecture of TDCS with extra embedded symbol

At the receiver, the received signal of each receive antenna is transformed into frequency-domain by using an FFT and then processed by the V-BLAST signal processing module where its fading effect will be removed, space-time coded and later the correlation is performed for the detection of data from the data2 source. The results from the data2 source detection will be used to detect the transmitted data from source data1.

V-BLAST is a promising implementation of a multiple input and multiple output (MIMO) system [61],[62]. At each symbol the V-BLAST algorithm detects the strongest layer of the transmitted signal, cancels the effects of this strongest layer from each of the received signals, then continue to detect the strongest on the remaining layers, until the weakest one is detected. The V-BLAST algorithm reconstructs the transmitted signal by removing the fading effect of the channel in frequency domain. The received signal at each receiver antenna n from each of the transmit antenna m equals [105]:

$$Y_n = \sum_{m=1}^{M} H_{nm} X_m + \eta_n \cdot \tag{5.20}$$

In matrix form the received signal vector is derived as :

$$\boldsymbol{Y} = \boldsymbol{HX} + \boldsymbol{\eta} \ , \tag{5.21}$$

where $\boldsymbol{Y}=[y_1,y_2,...y_N]$ is the received signal vector, $\boldsymbol{X}= [x_1,x_2,...x_M]$ is the transmitted signal vector, M is the number of transmit antennas, N is the number of receive antennas, $\boldsymbol{\eta}=[\eta_1, \eta_2,...,$

$\eta_N]$ is the noise vector and the channel matrix **H** has coefficients H_{nm}, where each coefficient describes the channel link between transmit antenna *m* and receive antenna *n* [105].

$$\begin{bmatrix} H_{11} & H_{12} & \cdots & H_{1M} \\ H_{21} & H_{nm} & \cdots & H_{2M} \\ \vdots & \vdots & \ddots & \vdots \\ H_{N1} & H_{N2} & \cdots & H_{NM} \end{bmatrix} \tag{5.22}$$

With the assumption that the information about the channel transform functions (CTFs) are available at the receiver, the channel matrix **H** can be obtained. The V-BLAST algorithm detects the signals from all the transmit antennas sequentially according to the signal strength. The V-BLAST implementation is described in Appendix F.

5.5 Performance Evaluation and Analysis

5.5.1 TDCS Evaluation

Table 5.1: Simulation parameters

TDCS Parameters	
Carrier Frequency	5.5 GHz
Number of Subcarriers	128
Carrier Spacing	31.25 KHz
Guard Interval Duration	5.25 μs
Channel coding	OFF
Channel Parameters	
Maximum Channel Delay	5 μs
Number of Taps	6
Distance between Taps	1 μs
Number of Paths	12
Power decay between Taps	1 dB
Vehicular speed	100 Km/hr
Fading Model	Rayleigh Fading

The TDCS and channel parameters are provided in Table 5.1. The fully loaded signal bandwidth is 4 MHz. In the beginning the simulations ran in a system with one transmitter and one receiver (no multiple access). In the simulations with a Rayleigh fading channel, the delay spread is 1.6282 μs. If we use the criteria for determining the coherence bandwidth as the bandwidth over which the signal envelope correlation function be larger than 0.5, the channel coherence bandwidth will be about 123 KHz. The requirement to have flat fading on each subband (carrier) is fulfilled by having a subband spacing of 31.25 kHz . The LU band is assumed to be located in the middle of our TDCS band, occupying 26 subbands (equal to a

bandwidth of 812.5 kHz); we also assume that this information is available at the transmitter and the receiver. Here we will not explore the effect of windowing, therefore we de-activated 40 subbands (1.25 MHz) which are considerably wider than the LU band so that the sidelobes to the LU's band and also the interference from LU to the TDCS system are negligible. We have simulated and compared the CCSK performance of conventional TDCS-CCSK with *CS=128* for different number of phase points to be used by the random phase generator in generating the phase vector $\boldsymbol{\theta}$. The phase is derived from a unit circle with uniform space. The comparison is depicted in Figure 5.7. The choice of *CS=128* is made with the objective of obtaining an optimum TDCS bit rate and BER according to the number of available subband/carriers, which is 128.

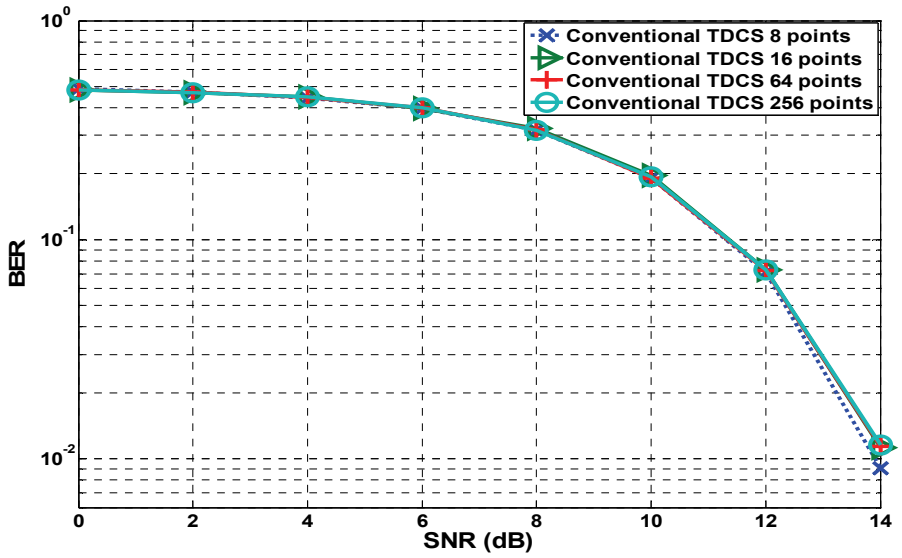

Figure 5.7: BER vs SNR (dB) comparison of the conventional TDCS-CCSK with different number of phase points on a unit circle in the AWGN channel

Table 5.2: Bit rate OF TDCS-128CCSK with different kind embedded symbols constellation size

Embedded symbol modulation mode	# of bits / TDCS symbol	Bit rate (Kbps)
BPSK	8	215
QPSK	9	242
16-PSK	11	295
64-PSK	13	349
256-PSK	15	403

The simulation results show that there is no performance difference as the number of points in the unit circle is increased, therefore in our next simulation results the random phase will be generated from the constellation of 8 phase points of a unit circle with uniform space of 45 degrees between one point to the next point. Table 5.2 shows the total bitrate of the proposed TDCS-CCSK with different embedded symbol's constellation size.

A. Analysis in AWGN Channel

We examine the BER of the embedded symbol (data1) and the data for CCSK modulation (data2) separately. The overall BER is derived by adding the sum of bit error from data1 and data 2 divided by the total number of bits. In the context of dynamic spectrum access we do not want to interfere the LU system, therefore we apply PSK mapping as the embedded symbol so the power spectrum density of TDCS-CCSK with extra embedded symbol will not be changed

Figure 5.8 shows the BER performance of the embedded symbol which refers to the detection of data from source 1 in an AWGN channel. According to the theoretical properties of PSK [106], higher constellation size is more vulnerable to noise, therefore the BER performance will be degraded. The exception of embedded BPSK detection shown in Figure 5.8 could be explained after reviewing the BER results on CCSK detection because the embedded symbol detection is applied after CCSK detection. This means that the accuracy of the CCSK detection will also influence the embedded symbol detection. Further, by observing Figure 5.9 we can see that the TDCS with 128 CCSK BER performance has almost the same curve pattern as the embedded BPSK BER performance shown in Figure 5.8.

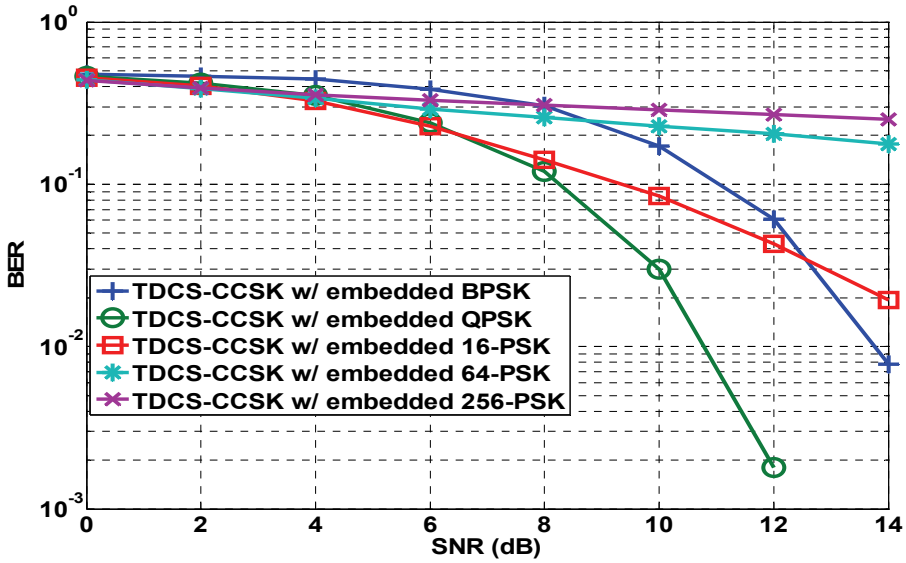

Figure 5.8: BER vs SNR (dB) performance on data1 source (embedded symbol) of the combined TDCS-CCSK with PSK embedded symbol in an AWGN channel

This symptom occurs because this embedded BPSK detection is equal to the data detection of TDCS with binary antipodal PAM modulation (without CCSK) that previously has been investigated in reference [98]; the results show that its performance is slightly better than the TDCS with 128 CCSK.

Figure 5.9 shows the effect of the embedded symbol to the CCSK detection of the TDCS system. At a BER of 10^{-2} the SNR gain of increasing the constellation size of the embedded symbol derived from the simulation results agrees with SNR gain defined in eq. (5.11). The CCSK detection SNR gain with 4, 16, 64, and 256 PSK are 3, 6, 7.8, and 9 dB ($(10.log_{10}(log_2[4,16,64,256])$ dB) respectively.

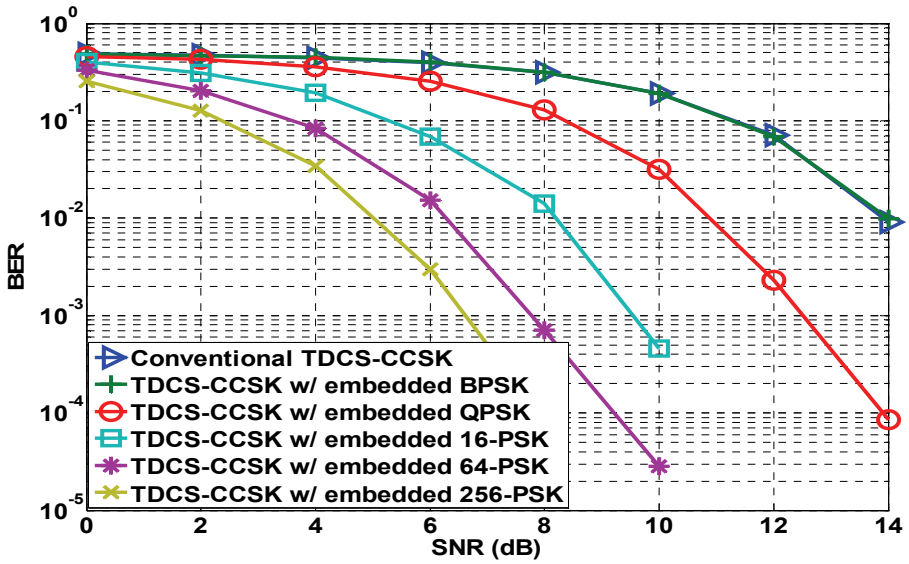

Figure 5.9: BER vs SNR (dB) performance on data2 source (CCSK symbol) of the combined TDCS-CCSK with PSK embedded symbol in an AWGN channel

As described in Figure 5.3(b), due to a system design where the CCSK detection is applied before the embedded symbol detection, the accuracy of the CCSK detection will influence the BER performance of the embedded symbol detection. Upon the perfect detection of the CCSK symbol, the embedded symbol BER performance will resemble its theoretical error probability (PSK, QAM or PAM) where lower modulation modes refer to a better BER performance. If the CCSK detection is not perfect then the CCSK BER performance shown in Figure 5.9 where higher modulation modes gives lower BER, will have impact on the BER performance of the embedded symbol; hence, the theoretical properties of PSK, QAM or PAM embedded symbol will be changed.

Therefore, the results in Figure 5.8 denotes a degradation of the theoretical BER performance of the PSK modulation modes due to imperfectness of the CCSK detection that delivers

QPSK as the most optimum embedded symbol modulation mode applied in the TDCS-CCSK system.

By considering the advantage/weakness of one modulation mode in term of BER at source data1 and data 2, Figure 5.10 shows the overall BER of the TDCS system with the PSK embedded symbol. For a SNR below 11 dB the BER of TDCS with embedded 64 PSK still outperforms the conventional TDCS-CCSK. For a SNR higher than 13 dB the TDCS-CCSK with embedded 64 PSK is outperformed by the conventional TDCS-CCSK; therefore, in this region the constellation size limit of the embedded symbol using QAM and PSK mapping is 16. The embedded symbol with 4 PSK gives the best overall BER performance at high SNR, while for low SNR 16 PSK is a better alternative. These facts will be compared with the results in case a Rayleigh fading channel is assumed.

We have observed the performance of the TDCS with QPSK embedded symbol in multi user AWGN environment. For simplicity reasons we have considered 2 users in the simulations. Figure 5.11 depicts the BER performance of both users at the source1detector, source2 detector and the overall BER. The BER performance curves of both users have the same behaviour as shown in Figures 5.8 to 5.10 for the TDCS-CCSK with embedded QPSK case. This means that the embedded symbol does not destroy the CCSK symbol detection in a multi user AWGN environment.

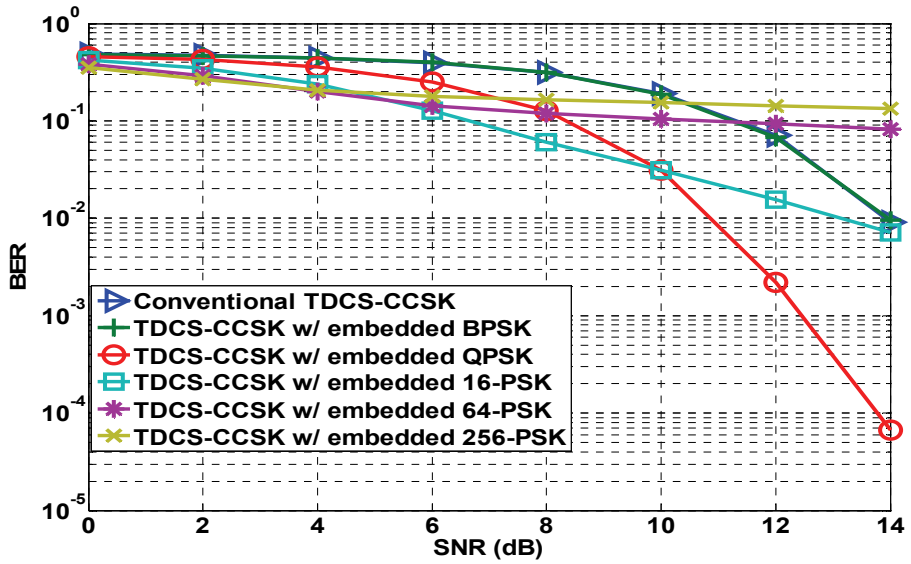

Figure 5.10: Overall BER vs SNR (dB) performance of the Combined TDCS-CCSK with PSK embedded symbol in an AWGN channel

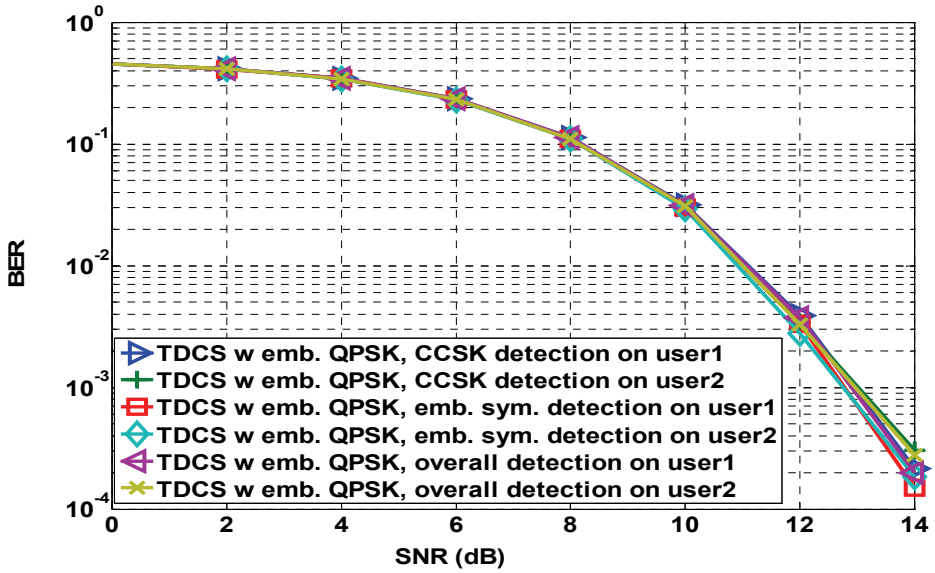

Figure 5.11: BER vs SNR (dB) performance of the Combined TDCS-CCSK with QPSK embedded symbol in a 2 users environment assuming an AWGN channel

B. Analysis in case of a Rayleigh Fading Channel

The Rayleigh fading channel model is derived according to the wide sense stationary uncorrelated scattering (WSSUS) model [73] using parameters given in Table 5.1. The Doppler effect is included in the model. We assume that the transmitter and receiver are perfectly synchronized, and the channel transfer functions (CTFs) of all links are perfectly known at the receiver. For simplicity the frequency-domain equalization for all simulations used zero-forcing equalization.

Figure 5.12 shows how Rayleigh fading has severely destroyed the overall BER performance of TDCS-CCSK with embedded symbol. Although we assume perfect knowledge of CTFs in the simulation, the division between the noise and CTF has altered the correlation property of the TDCS basis function, because we use zero forcing equalization technique; hence, a BER degradation occurs as depicted in Figure 5.12. Therefore, we add MIMO with the V-BLAST receiver architecture to the system to mitigate the fading effect.

In a multi-user environment with Rayleigh fading channel the overall performance of the TDCS-CCSK with embedded symbol degrades. According to eq. (5.14) and eq. (5.15) the fading channel gain can disturb the correlation property of the TDCS basis function that eventually has an impact on the CCSK detection and further on the embedded symbol detection. Figures 5.12 and 5.13 show how the fading channel destroys the TDCS performance. The performance in a MIMO system with V-BLAST receiver architecture (which will be explored later) gives a clear view on the BER degradation of TDCS-CCSK with embedded symbol in a multi-user environment with a Rayleigh fading channel.

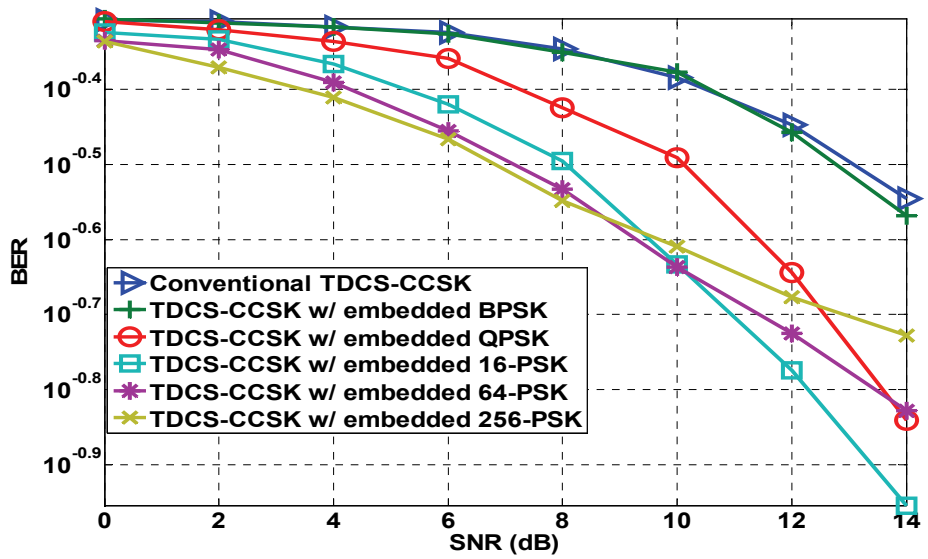

Figure 5.12: Overall BER vs SNR (dB) performance of the combined TDCS-CCSK with PSK embedded symbol in a Rayleigh fading channel

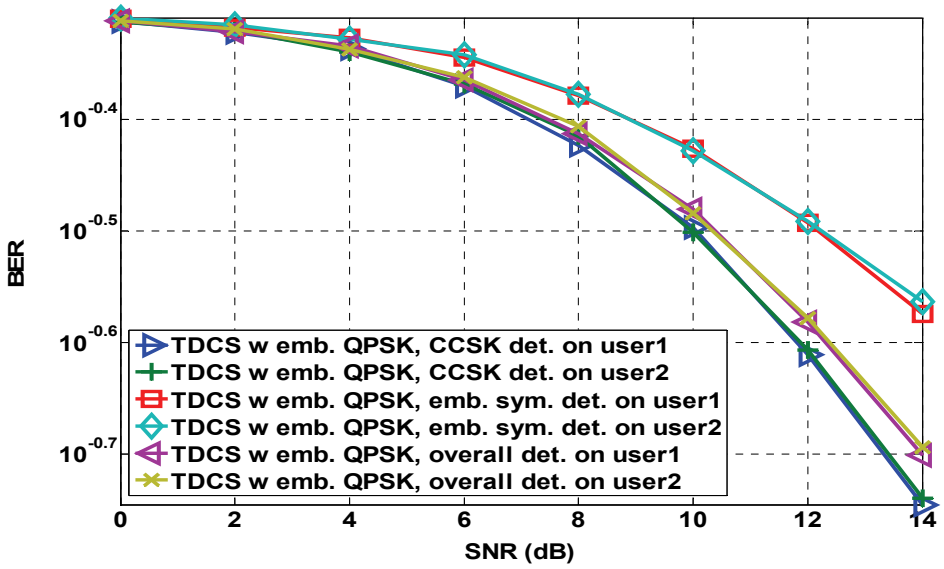

Figure 5.13: BER vs SNR (dB) performance of the Combined TDCS-CCSK with QPSK embedded symbol in a 2 users environment and a Rayleigh fading channel

In an earlier phase we searched for the optimum configuration of MIMO system with the most promising modulation mode for the extra symbol to be embedded to the MIMO TDCS-CCSK system. For this purpose we have selected QPSK as the embedded symbol modulation mode, as the results in Figure 5.10 show, this mode gives the best overall BER.

In reference [105] we investigated the influence of MIMO V-BLAST to the conventional TDCS-CCSK where the embedded symbol was not included, and we compared their performance with MIMO OFDM with the V-BLAST receiver architecture. For a scaling factor *C=1*, figures 5.14 to 5.16 depict some of the results given in reference [105]. According to that reference MIMO with a ratio between transmit and receive antennas of ½ and lower gives optimum BER results. Further simulation results show that OFDM MIMO architecture gives a better SNR gain as compared to the application of adaptive bit loading in OFDM. In subsection 3.2.4 we found out that the adaptive bit loading with the Fischer algorithm in OFDM and perfect channel estimates provides a 5 dB SNR gain. From Figure 5.14 we learn that in order to have a BER of 10^{-2}, conventional OFDM requires 14 dB SNR while in Figures 5.15 and 5.16 (by increasing the number of receive antenna compared to the transmit antenna) will give more than 6 dB SNR gain.

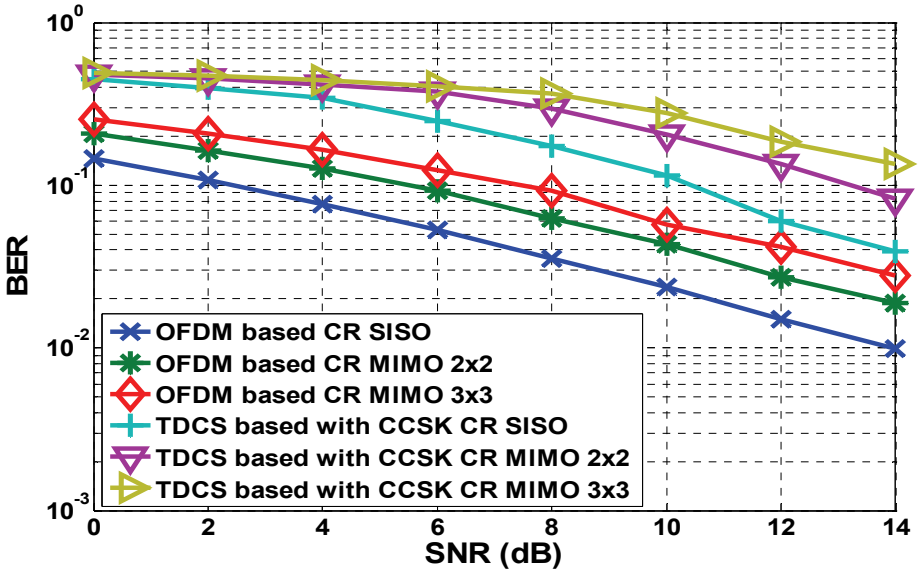

Figure 5.14: BER vs SNR (dB) performance of CR TDCS with CCSK, and OFDM-based with BPSK, in a MIMO V-BLAST architecture with a balanced antenna design

Figures 5.15 and 5.16 show that having a ratio of ½ between transmit and receive antenna gives a significant performance improvement to TDCS. It even outperforms OFDM at high SNR.

Now we investigate the TDCS-CCSK with embedded QPSK and different MIMO compositions. Figure 5.17 depicts the overall BER of the scheme. The notation *m* x *n* denotes the MIMO system with *m* transmit antennas and *n* receive antennas. The results show that the configuration with more receive antennas than transmit antennas gives more promising results, especially when the ratio between transmit and receive antennas is ½ and lower.

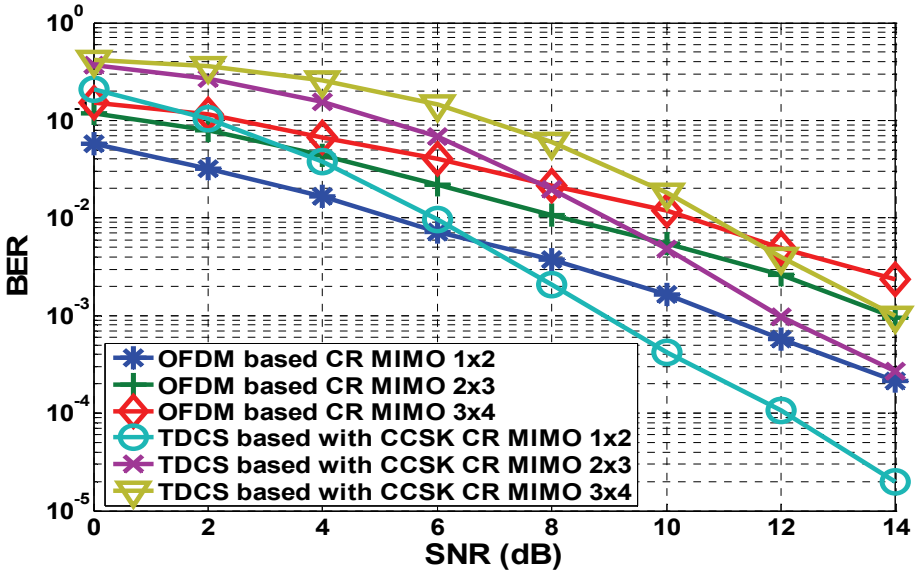

Figure 5.15: BER vs SNR (dB) performance of CR TDCS with CCSK, OFDM-based with BPSK, in a MIMO V-BLAST architecture and a difference of one between the number Tx and Rx antennas

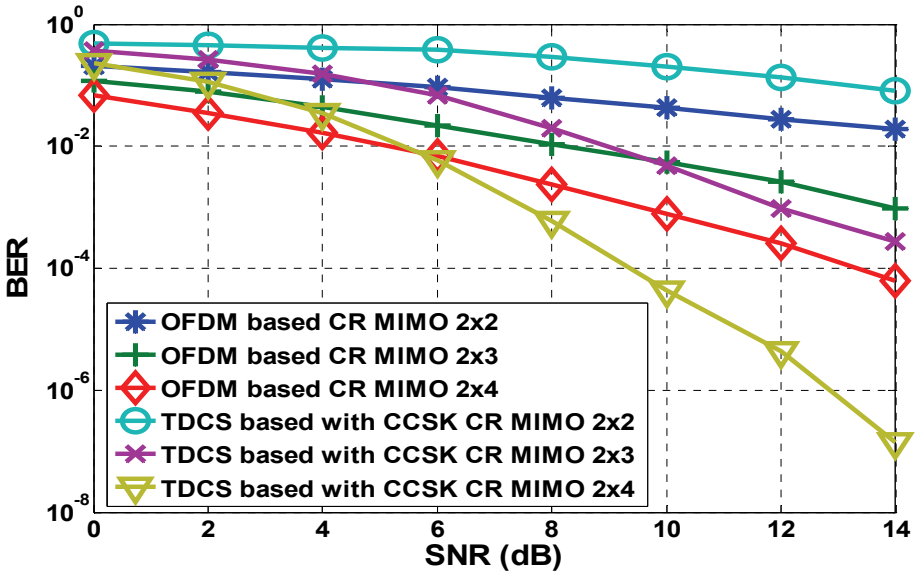

Figure 5.16: BER vs SNR (dB) performance of CR TDCS with CCSK, OFDM-based with BPSK, in a MIMO V-BLAST architecture with 2 Tx antennas and equal or higher number of Rx antennas

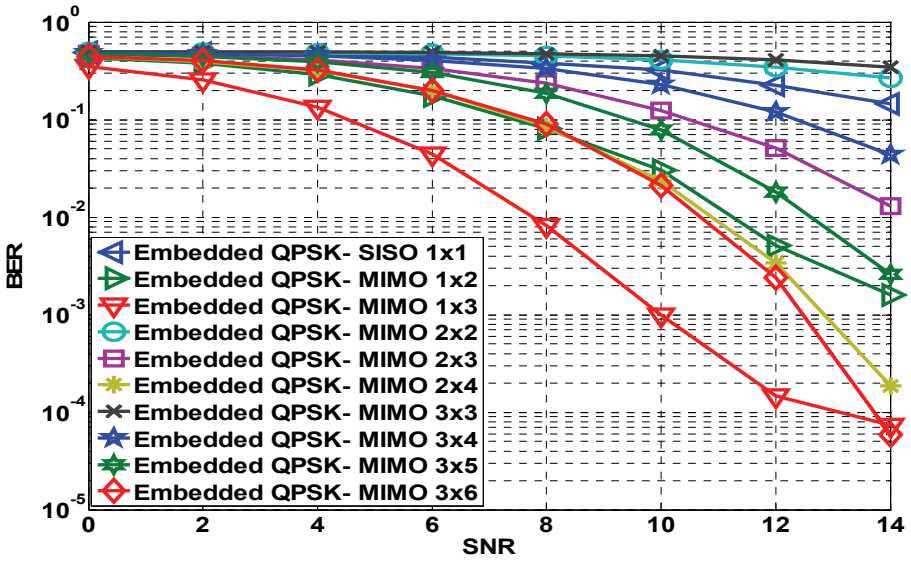

Figure 5.17: Overall BER performance vs SNR (dB) of the SISO and MIMO TDCS-CCSK with embedded QPSK in a Rayleigh fading channel and several Tx-Rx antennas configuration

Next we made simulations for the MIMO 2x4 antennas configuration. Figure 5.18 shows QPSK as most optimum embedded system modulation mode, in terms of BER performance. The BER tendency and characteristics of the results of the MIMO 2x4 TDCS-CCSK with PSK embedded symbol in a Rayleigh fading channel shown in Figure 5.18 resemble the performance in an AWGN channel, as depicted in Figure 5.10. Therefore, we investigate the BER performance on source data 1 and source data 2 separately.

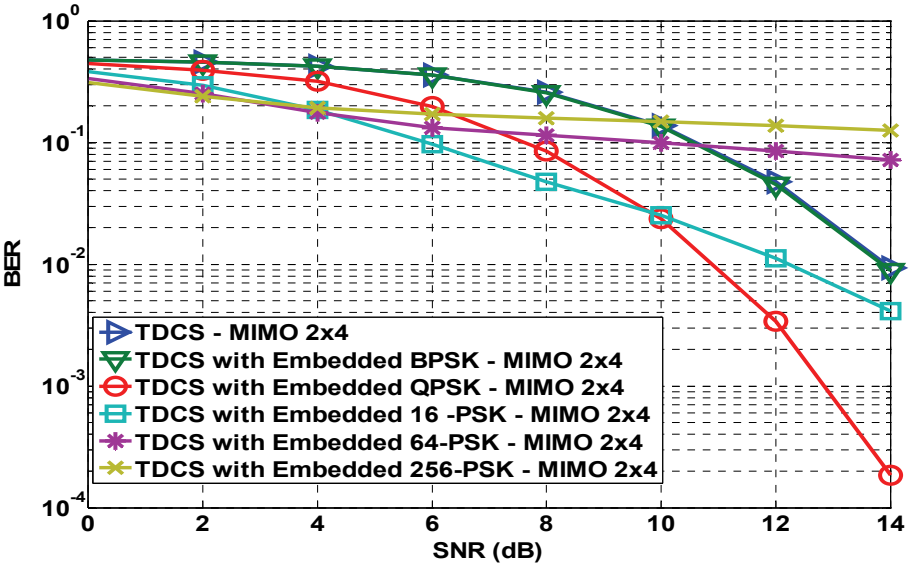

Figure 5.18: Overall BER performance vs SNR (dB) of the MIMO 2x4 TDCS-CCSK with embedded PSK and assuming a Rayleigh fading channel

Figure 5.19 shows that the performance of the CCSK detection in MIMO 2x4 TDCS-CCSK with PSK embedded symbol is in line with the finding we had in the AWGN channel. As the embedded symbol constellation size increases the CCSK correlation property is enhanced. The embedded symbol detection results in Figure 5.20 show similar BER characteristics as the BER results we have found in the AWGN channel, depicted in Figure 5.8.

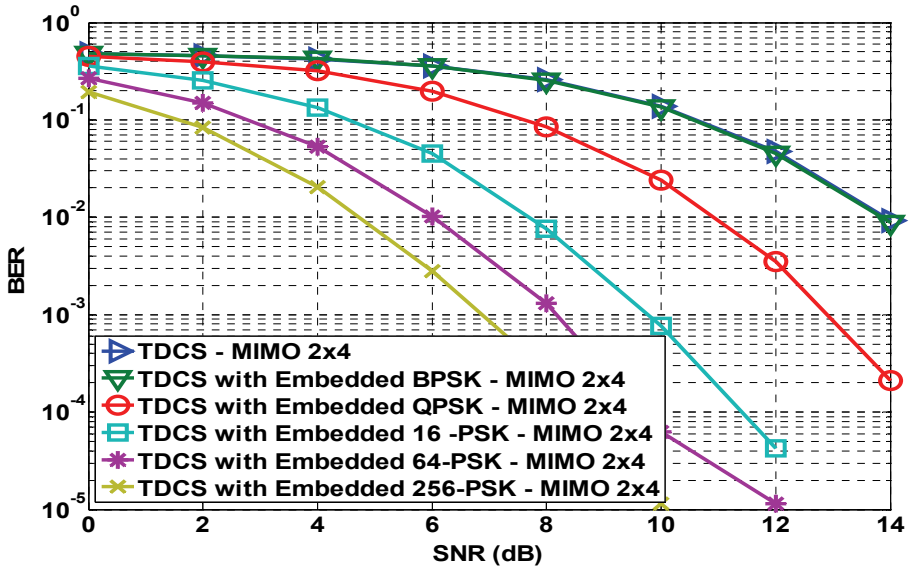

Figure 5.19: BER performance vs SNR (dB) on source data2 (CCSK symbol) of the MIMO 2x4 TDCS-CCSK with embedded PSK symbol in a Rayleigh fading channel environment

In Figure 5.19, at a BER of 10^{-2} of the CCSK detection in 2x4 MIMO TDCS-CCSK, the SNR gain achieved by increasing the embedded symbol constellation size in a Rayleigh fading channel environment is equal to the SNR gain obtained by increasing the embedded symbol in an AWGN channel (3, 6, 7.8, and 9dB for 4-,16-,64- and 256-PSK respectively).

Considering the trade-off between the overall bit rate and overall BER performance (that can be observed from Table 5.2, Figures 5.10 and 5.18), we come to the conclusion that 16 PSK is the optimal embedded symbol modulation mode.

The BER results of MIMO 2x4 TDCS-CCSK with QPSK embedded symbol in a 2 user environment with Rayleigh fading (Figure 5.21) indicate how the channel fading can change the cross correlation detection robustness of the TDCS basis function in a multi-user environment. If we compare the CCSK detection performance at BER 10^{-3} , the single user MIMO 2x4 TDCS-CCSK with QPSK requires about 13 dB SNR (Figure 5.19) while the multi-user part requires 14 dB SNR (Figure 5.21). That means that the multi-user environment in a Rayleigh fading channel gives 1 dB SNR degradation. Another observation is that the overall TDCS-CCSK (with QPSK embedded) performance in a single user Rayleigh fading channel at BER 10^{-2} requires 11 dB SNR (Figure 5.18), while in the multi-user case it requires about 12 dB SNR (Figure 5.21).

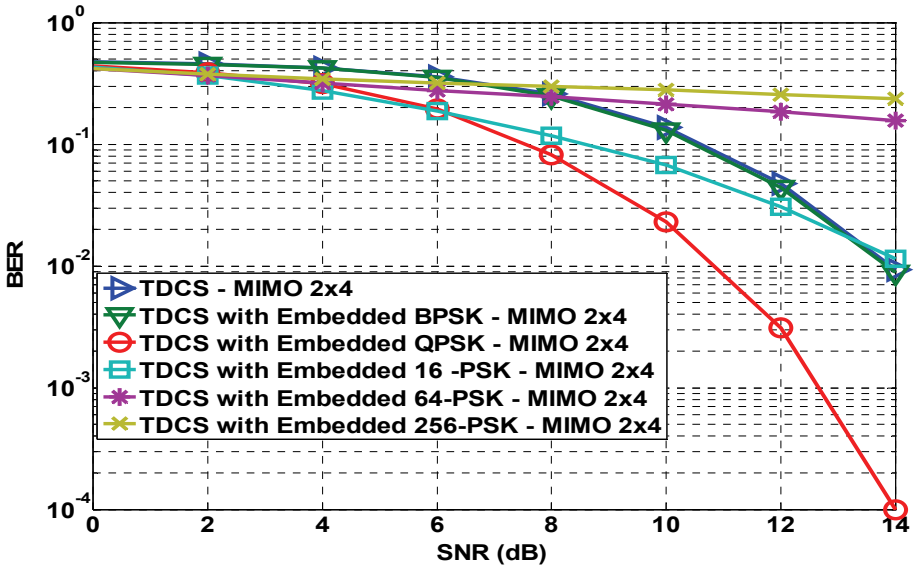

Figure 5.20: BER performance vs SNR (dB) on source data1 (embedded symbol) of the MIMO 2x4 TDCS-CCSK with embedded PSK symbol in a Rayleigh fading channel environment

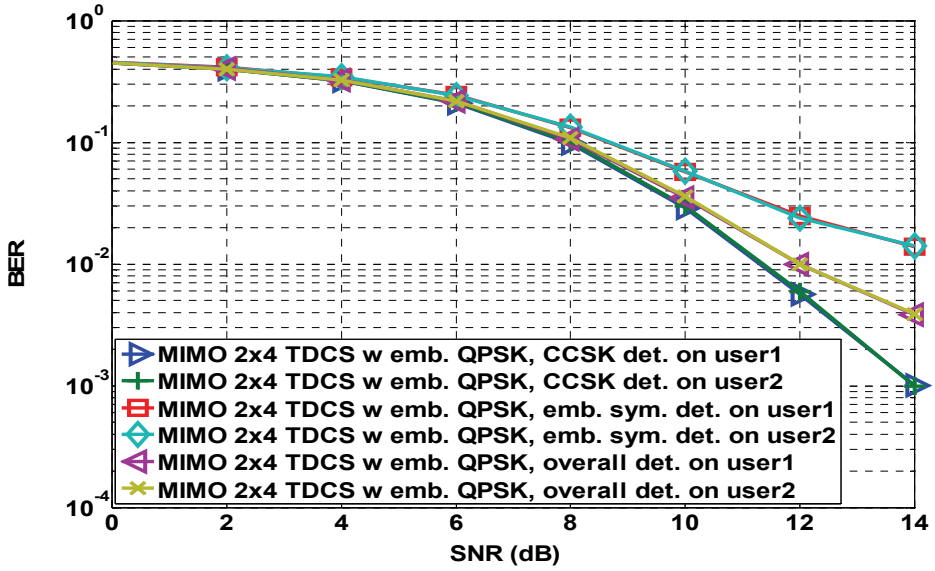

Figure 5.21: BER performance vs SNR (dB) on source data1 (embedded symbol) of the MIMO 2x4 TDCS-CCSK with embedded QPSK symbol in a 2 users environment experiencing Rayleigh fading

5.5.2 WDCS Evaluation

As applied in the TDCS evaluation, in the WDCS with embedded symbol system we also examine the BER of the embedded symbol (data1) and the data for CCSK modulation (data2) separately. The overall BER is derived by adding the sum of bit errors from data1 and data 2 divided by the overall number of bits. For the same reason as in the TDCS system, in the context of dynamic spectrum access we do not want to interfere the LU system; therefore we apply the PSK mapping as the embedded symbol; so the power spectrum density of WDCS-CCSK with extra embedded symbol will not be changed. The "Frequency Selective Wavelet" that has been used as basis function for WPMCM in section 3.3 is also employed as basis function in this WDCS. The Frequency Selective Wavelet is more flexible compared to other wavelet basis function since its parameters such as filter length, regularity order and the transition bandwidth can be varied according the desired targeted performance. In this evaluation we consider a filter length of 30, regularity order of 12 and transition bandwidth of 0.1. We evaluate the performances only for the AWGN channel. The synchronization between transmitter and receiver is considered to be perfect.

Figure 5.22 shows the BER performance of the embedded symbol. Different from Figure 5.8, the property of PSK mapping is clearly seen in the embedded symbol BER results. BPSK gives the best BER performance, while increasing the constellation size will deteriorate the BER performance. This difference will be explained after analysis of the CCSK detection results.

The CCSK detection BER performances are depicted in Figure 5.23. The BER tendency has the same behaviour for TDCS-CCSK detection as depicted in Figure 5.9. As the embedded symbol constellation size increases, the CCSK BER improves. The 9 dB gain for 256-PSK as embedded symbol compared to BPSK and depicted in the TDCS case in Figure 5.9 is also shown in Figure 5.23.

By observing Figure 5.9 and 5.23 we see that the CCSK detection in the WDCS system outperforms the CCSK detection in TDCS system. It requires 14 dB SNR for the conventional TDCS-CCSK to reach the BER 10^{-2} while for the WDCS-CCSK system with a frequency selective wavelet it requires only 10.2 dB SNR. It has been explained in the TDCS evaluation that the performance of the CCSK detection will influence the embedded symbol detection. Therefore due to its better BER performance property, the frequency selective WDCS-CCSK could preserve the embedded symbol BER performance according to its error probability behaviour (i.e. BER degrades as the constellation size increases).

The overall BER is shown in Figure 5.24. The overall BER is derived from dividing the total number of errors on the embedded symbol detection and the CCSK detection divided by the total number of transmitted bits.

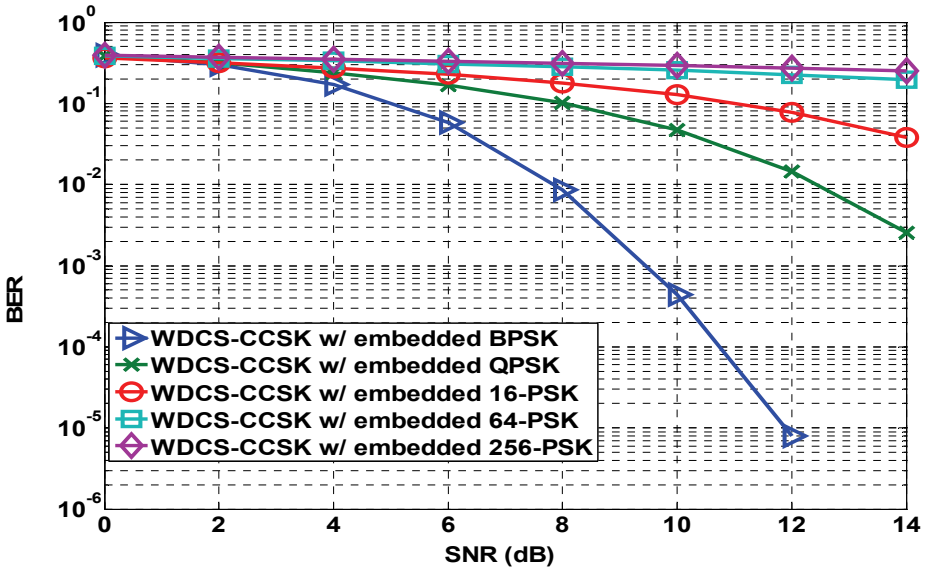

Figure 5.22: BER vs SNR (dB) performance on source 1 (embedded symbol) of the combined WDCS-CCSK with PSK embedded symbol assuming an AWGN channel environment

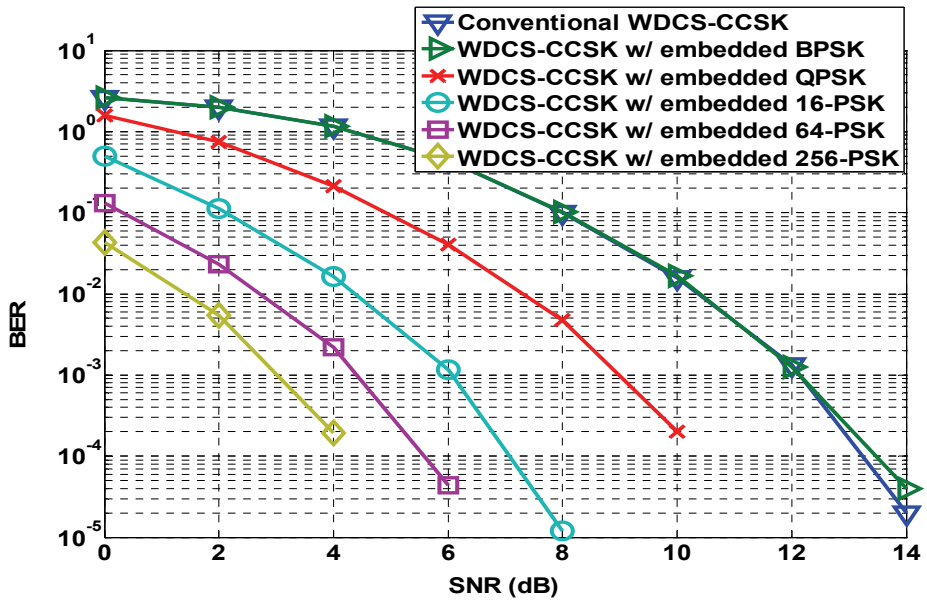

Figure 5.23: BER vs SNR (dB) performance on source 2 (CCSK symbol) of the combined WDCS-CCSK with PSK embedded symbol assuming an AWGN channel environment

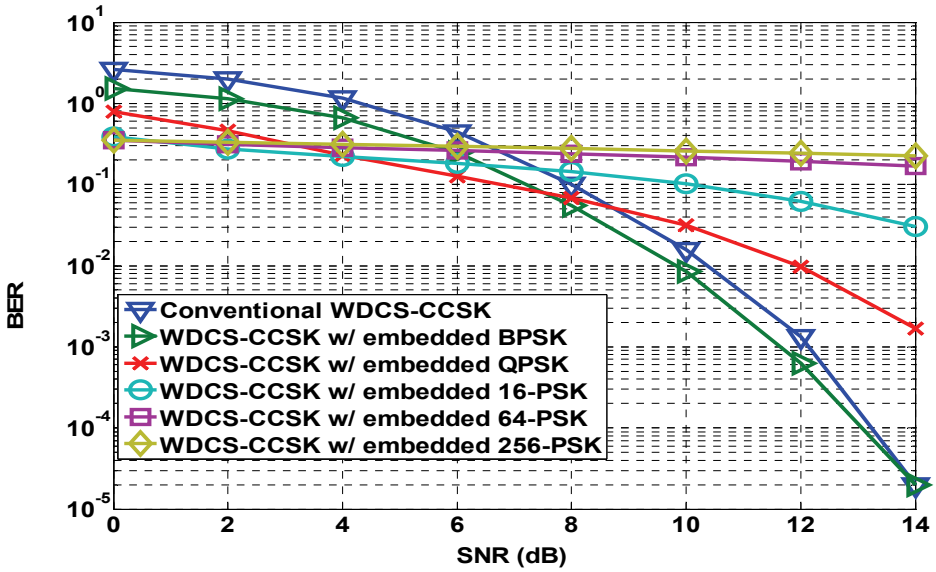

Figure 5.24: Overall BER vs SNR (dB) performance of the combined WDCS-CCSK with PSK embedded symbol assuming an AWGN channel environment

5.6 Conclusions

In this chapter the feasibility of the transform domain communications sytem (TDCS) as single carrier modulation technique for Cognitive Radio system has been studied. An effort to combat the TDCS bit rate limitation has been employed. A novel application of an embedded symbol as extra data source has been proposed.

In the Cognitive Radio context sidelobes refer to the amount of interference to the LU access. The sidelobe level of a signal are found in its power spectrum density (PSD). According to PSD observations, OFDM gives a factor of ($1/ N_{FFT}$) larger sidelobes compared to TDCS, if the TDCS scaling factor C is 1. If the scaling factor C is equal to $\sqrt{N_{FFT}}$ TDCS sidelobe will have the same magnitude as OFDM sidelobes. The TDCS BER performance will be improved but the TDCS bitrate remains and it is lower than the OFDM bitrate. Increasing the scaling factor C denotes stepping up the SNR of TDCS, hence, the TDCS BER performance will be improved.

Therefore, by putting the power spectrum density constraint as criterion in selecting the embedded symbol modulation mode, the PSK modulation is considered as the appropriate mode since embedding the PSK symbol will not increase the sidelobes of the TDCS signal.

The impact of the embedded symbol to the multi user data detection has been analyzed. The embedded symbol does not deteriorate the CCSK multi-user detection in an AWGN channel. However, the Rayleigh Fading channel disturbs the orthogonality property of each user's TDCS basis function. Therefore, the CCSK BER performance on each user degrades.

Following the successful application of the embedded symbol in the TDCS-CCSK system, the application of the embedded symbol in WDCS-CCSK system has also been explored. Based on the good performance of the frequency selective wavelet basis function in the Multi-carrier wavelet packet modulation, in this chapter we evaluated the application of the frequency selective wavelet in WDCS-CCSK. The results have shown that the WDCS-CCSK with frequency selective wavelet outperforms the TDCS-CCSK system.

In the design of TDCS-CCSK or WDCS-CCSK with embedded symbol, the CCSK detection is applied prior to the embedded symbol detection. Therefore the CCSK detection accuracy will influence the accuracy of the embedded symbol detection. Results have shown that increasing the constellation size of the embedded symbol will improve the CCSK detection, while the property of the PSK modulation denotes that the BER will be deteriorated as the constellation size decreases. Imperfections in CCSK detection will disturb the error probability property of PSK (increased BER as constellation size increased). Since the WDCS-CCSK gives a better CCSK detection accuracy, it could preserve the BER property of the PSK modulation mode.

MIMO V-BLAST has been well known as an effective technique in utilizing channel diversity to enhance the BER performance of a wireless system. In addition to this MIMO increases the bit rate of a wireless system. We evaluate the feasibility and the effectiveness of the MIMO V-BLAST in the proposed TDCS-CCSK with embedded symbol system. The results have shown a significant improvement in data detection for a multi-user environment experiencing Rayleigh fading.

Chapter 6

AAF Project Cognitive Radio Demonstrator in IRCTR TU Delft

6.1 Introduction

The goal of AAF is: "Research and demonstration of a Cognitive Radio system, which continuously adapts its communications scheme to the available resources". The focus of the research is on identification of free resources in the frequency domain and adaptive OFDM-based transmission. Important challenges include stability of the system, identification of interference to other systems and meta-communications. All are addressed as part of the research. A verification platform will prove the consistency and comprehensiveness of the solution. The available demonstrator allows us to investigate the potentials of co-existence between the licensed system and the rental Cognitive Radio based system.

In this chapter, the design and implementation of a Cognitive Radio test bed is proposed. The test bed can be used to validate to which degree the Cognitive Radio system is non-interfering to primary users. The system can emulate primary and secondary users and accordingly the performance of various adaptive radio transmission schemes can be evaluated. The CR test bed comprises two basic parts, the radio (to generate, transmit, receive and process wireless signals) and a cognitive brain which learns from the environment and performs rational processes and predicts probable consequences and remembers past successes and failures. The baseband processing in this thesis itself is the radio that generate, transmit, receive and process the wireless signals.

The AAF requirements are considered in creating a working hardware demonstrator. Accordingly the hardware requirements are specified. Based on the requirements, criteria have to be developed to enable of making decision on selection of the vendors and the boards.

In this chapter the Cognitive Radio development verification platform in IRCTR TU Delft[§] within the AAF project will be described. Section 6.2 gives the insight into the hardware

[§] The works on the verification platform at IRCTR TU Delft were performed by student assistants : Shreyas Bhargav Raghunathan, Maarten v. d. Oever, Zhen Qin, R. D. Mohammady under the author's guidance and Przemysław Pawełczak, as well as technician Fred v. d Zwan and Faculty members Dr. H. Nikookar, Dr. R. Hekmat and Prof. Dr L. P. Ligthart.

selection according to the hardware specification that fulfils the desired Cognitive Radio requirements. Among several available boards we come up with the decision of choosing P25-M and USRP as the development boards for the IRCTR TU-Delft Cognitive Radio verification platform.

Section 6.3 describes the observed scheme configuration involving the collaboration of USRP and P25M. The adaptive spectrum selection will be shown, and the proposed future expected scenario is presented. Summary of this chapter is given in section 6.4.

6.2 The Hardware Requirements for Baseband Transmission

A digital signal processing (DSP) board for the processing of the signals is required in a Cognitive Radio verification platform. A DSP board is required because a regular computer would not be able to process the high bandwidths. The DSP board must be able to fulfill various applications required.

The most important parts on the board are the decoding and encoding of the analogue signal. The encoding and decoding are done by Digital to Analogue Converters (DAC) and Analogue to Digital Converters (ADC). If these components are too slow then it is impossible to decode or encode the desired bandwidth for the transmission.

According to [34] the requirements in Table 6.1 can be distilled.

Table 6.1: The AAF project parameter requirements

Parameter	**Value**
Topology	Multi-hop
Modulation scheme	ODFM
Minimum frequency (RF) $f_{\min}$	400 MHz
Maximum frequency (RF)$f_{\max}$	900 MHz
Transmit power	30 dB(m)
Minimum channel SNR	15 dB
Minimum bandwidth $B_{\min}$	1 MHz
Maximum bandwidth $B_{\max}$	10 MHz
Maximum number of carriers	128
Maximum Doppler frequency f_d	15 Hz (at 900MHz, 18 km/h) 125 Hz (at 900 MHz, 150 km/h) 250 Hz (at 900MHz, 300 km/h)

The desired total bandwidth is set to 10 MHz. Figure 6.1 depicts an illustration of the system output, where [C_1, $C_{1,...,}C_{NFFT}$] are the position of each subcarrier.

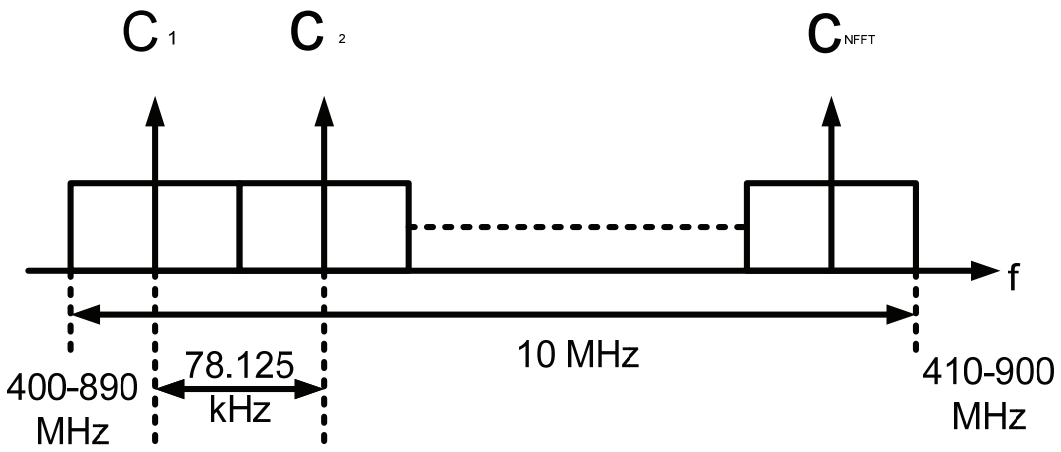

Figure 6.1: OFDM subcarriers with 10 MHz bandwidth

The 10 MHz bandwidth (B) delivers a minimum sample rate (f_s) for the analogue to digital converter of 20 MHz. The relation between B and f_s is defined as :

$$B = \frac{f_s}{2} \tag{6.1}$$

Modern filter techniques allow for generation a smooth signal with a low output frequency. The DAC must be able to pre-form a digital to analogue conversion at the same rate as the ADC.

The performance of ADCs can be measured by its Figure of merit (FoM). The FoM takes into account the converter's power dissipation P[W], its resolution (specified in Effective Number of Bits (ENOB)) and its sampling rate f_s [Hz]. This FoM is given as [34]:

$$FoM = \frac{P}{2^{ENOB}.f_s}[\text{pJ / conversion - step}] \tag{6.2}$$

Nowadays, having a FoM of 2pJ/conversion-step for an ADC is considered to be reasonable. The ENOB that an ADC must support can be estimated by the dynamic range of the band of interest i.e., Δ_{dB}.

Assuming a 6 dB per bit dependence for AD converters, the minimum number of desired bits can be determined from this dependence and the dynamic range Δ_{dB}. Next formula is used especially for OFDM Systems [34]

$$b \cong \frac{\Delta dB + 4.77}{6.02} \tag{6.3}$$

where b is the effective number of bits. The dynamic range is determined from the carrier spacing Δf , and the minimum channel frequency $f_{\min}$.

$$\Delta dB = 20\log(1 + \frac{f_{min}}{\Delta f}) \tag{6.4}$$

The carrier spacing is defined as :

$$\Delta f = \frac{1}{N_{FFT}\frac{1}{B}} \tag{6.5}$$

where B is the signal bandwidth and N_{FFT} is the total number of subcarriers. By using the maximum bandwidth (B_{max}) 10 MHz, the carrier spacing would be,

$$\Delta f = \frac{1}{128 \cdot \frac{1}{10 \cdot 10^6}} = 78.125 \text{ kHz} \tag{6.6}$$

Therefore, the dynamic range value equals:

$$\Delta_{dB} = 20\log(1 + \frac{890 \cdot 10^6}{\frac{1}{128 \cdot \frac{1}{10 \cdot 10^6}}}) = 81.13 \text{ dB} \tag{6.7}$$

Putting this dynamic range Δ_{dB} value in eq. (6.4) will yield minimal number of desired bits of the AD converter

$$b = \frac{81.13 + 4.77}{6.02} = 14.26 \text{ bits} \tag{6.8}$$

Therefore, a minimum of 14 bits converter would be suitable to fulfil the 10 MHz signal bandwidth. To assure that each OFDM subcarrier will experience flat fading, the carrier spacing should be much larger than the Doppler frequency (f_D) [34]

$$f_D << \Delta f \tag{6.9}$$

By referring to Table 6.1, having an 78.125 KHz carrier spacing will satisfy eq. (6.9). It will accommodate the expected 250 Hz maximum Doppler frequency. Further, the requirement according to [34] described in (6.10)

$$N_{FFT} << \frac{B}{f_D} \tag{6.10}$$

will be fulfilled as because

$$128 << \left(\frac{10 \cdot 10^6}{250} \right) = 40 \text{ x } 10^3 \tag{6.11}$$

The evaluation boards have Field Programmable Gate Arrays (FPGA) on board. An FPGA is a device with programmable connections and logic. The FPGA can be used for the signal processing. The FPGA is programmed in Very High Speed Digital Hardware Description Language (VHDL).

The FPGA must be able to process the data and transfer it to the DSP chip. The FPGA capability depends on the number of available gates and clock rate. The maximum data rate of the samples that is offered to the FPGA is 25 MHz of data. It is offered by the ADC. The FPGA is able to process the data pipelined there, with a required minimum clock speed of 25 MHz.

Some of the boards also have a DSP processor on it. The DSP processor is a processor dedicated for digital signal processing. The FFT is going to be implemented on the DSP processor. This is a major advantage over the FPGA. The processors can be programmed using C/C++. The available memory on the DSP processors is important, and also the number of bits the DSP can handle. Usually the number of bits of the DSP is equal or bigger than the number of bits of the ADC. If the DSP processor is used for the FFT, then the result matrixes need to be stored. The required memory is quantified as :

$$FFT\ table = 2 \cdot 20 \cdot 128 \cdot 16 \cdot 2 = 163840 \text{ bits} \tag{6.12}$$

The FFT table size consists of an FFT table and the invFFT table (this is the reason for the factor of 2 in eq. (6.12)), with 20 symbols for each of the 128 carriers that consist of 16 bits real and 16 bits imaginary numbers. The result in eq. (6.12) denotes that 163.840 bits memory space is required to save the FFT tables.

A dedicated control channel is required to provide information about the state of the link. This is necessary when a node experiences a lot of interference and receives corrupted data. A

proposed solution for the control channel is Tmotes[**]. The disadvantage of Tmotes (or standard 802.15.4) is its short distance communications. For the demonstrator it would be convenient if the board has a Multiple Input Multiple Output (MIMO) capability. MIMO provides a higher bitrate. MIMO requires an additional ADC and DAC installed on the Board. The extra ADC and DAC can be used as side channel. If a board contains only one additional ADC or DAC then they will be used for side channel.

For the boards implementation usually a computer and programming software is necessary. For the programming of the FPGAs a JTAG connector is required. The FPGA needs to be programmed because the ADC and DAC is usually connected to the FPGA. When a board is selected, it is preferable that the board supports 32 or 64 bit PCI, because these standards are supported by common computers. When it comes to varying the number of subcarriers and the signal bandwidth, Table 6.2 and 6.3 show the expected hardware requirements that have to be satisfied. Table 6.2 shows the required hardware specification if the signal bandwidth is 10 MHz and the number of subcarriers is 128.

Table 6.2: Hardware specifications if B= 10 MHz and N_{FFT}=128

Variable	**value**
Samples frequency	25 MHz[††]
ΔdB	81.13 dB
Inter frequency spacing	78125 Hz
ADC resolution[‡‡]	14,26 bits
Doppler shift tests	Passed
FFT tables memory	163.840 bits

Table 6.3: Hardware specifications if B= 10 MHz and N_{FFT}=64

Variable	**value**
Samples frequency	25 MHz[§§]
ΔdB	75.11 dB
Inter frequency spacing	156250 Hz
ADC resolution[***]	13,26 bits
Doppler shift tests	Passed
FFT tables memory	81.920 bits

[**] Tmotes are small embedded devices which are capable of measuring several features in the surrounding environment such as temperature and light. In addition to this they are equipped with a radio transmitter which can be used to communicate between Tmotes.
http://www.daimi.au.dk/~spony/adv_courses/NPaI/report/node4.html
[††] 20MHz + 5MHz over sampling
[‡‡] The ADC resolution is also valid for the DAC
[§§] 20MHz + 5MHz over sampling
[***] The ADC resolution is also valid for the DAC

Lowering the FFT size on the same signal bandwidth will reduce the required number of ADC bits therefore the required memory size will be reduced. Table 6.4 shows the hardware specification if the signal bandwidth is 2.5 MHz and the number of carriers is 128.

Table 6.4: Hardware specifications if B= 2.5 MHz and N_{FFT}=128

Variable	**value**
Samples frequency	6 MHz[†††]
ΔdB	93.17 dB
Inter frequency spacing	19531 Hz
ADC resolution[‡‡‡]	16,26 bits
Doppler shift tests	+[§§§]
FFT tables memory	163.840 bits

From Table 6.4 it can be concluded that the sample frequency has decreased but the number of required bits has increased. This means that the processing speed can be a lot slower.

After excluding some high end boards, other options needed to be taken into consideration. The selection of another high end board was not preferred. After browsing the Innovative Integration site the P25M board was the closest one which fits with the requirements given in Table 6.1. Therefore P25M has been selected [107]. The development board is depicted in Figure 6.2.

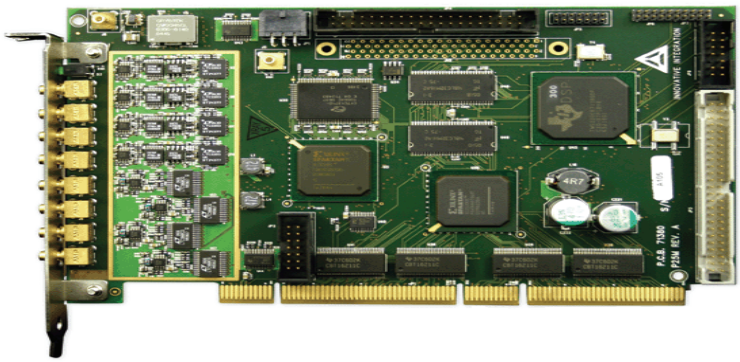

Figure 6.2: P25M development board

[†††] 5MHz + 1MHz over sampling
[‡‡‡] The ADC resolution is also valid for the DAC
[§§§] + means passed the Doppler shift tests

The specifications of the P25M are listed in Table 6.5. With these specifications the device is capable to meet the requirements concerning the ADC and DAC.

Table 6.5: Specifications of Innovative Integration P25M

ADC component		**DAC component**	
Number of channels	4	Number of channels	4
Sample rate	25 MSPS	Max generation rate	50 MSPS
Max Bandwidth	12 MHz	Max Bandwidth	25MHz
Bits width	16	Bits Width	16
Connection	To FPGA	Connection	To FPGA
Power dissipation	unknown	Power dissipation	unknown

The onboard FPGA is a Xilinx Spartan 3 with 1 million gates. The DSP chip of the P25M is a Texas Instruments with clock speed of 300 MHz and 32 Mega Bytes of RAM memory. The processor is a 32 bit floating point processor.

The TMS320C6413 DSP processor takes about 500 clock cycles to calculate an FFT. This means that the TMS320C6413 can process 6000 FFT`s per second. That is not enough for the demonstrator.

The P25M fits in a standard PCI slot. The PCI slot is a 64 bit slot. This means a 64 bit computer needs to be used in for the project.

The P25M is capable to meet the bandwidth requirements. By having 4 channels, the P25M can support MIMO as well. Besides the results of the DSP processor the P25M can keep up with the requirements and is relatively low priced. That makes the P25M to be a serious candidate for the use in the demonstrator.

6.3 Spectrum Scanner Module

In scanning the spectrum, the universal software radio peripheral (USRP[****]) is chosen as the suitable device. USRP is a software radio device, connected to a host computer via the USB port with 480 Mb/s data rate. It can send and receive signal up to 16 MHz of RF bandwidth. The USRP contains an FPGA that can be reprogrammed, 4 high speed ADCs, 4 high speed DACs, and lot of auxiliary analog and digial IO to do integration into a larger system.

USRP can accommodate up to 2 transceiver daughterboards, therefore it is capable of having 2x2 MIMO. Table 6.6 describes the specifications of the USRP.

Table 6.6: USRP Specifications

ADC		**DAC**	
Number of channels	4	Number of channels	4
Sample rate	64 MSPS	Max generation rate	128 MSPS
Max Bandwidth	16 MHz	Max Bandwidth	16MHz
Bits width	12	Bits Width	14
SFDR	85 dB	SFDR	83 dB

SFDR stands for Spurious Free Dynamic Range. SFDR is defined as the ratio of the RMS value of the carrier frequency (maximum signal component) at the input of the ADC or DAC to the RMS value of the largest noise or harmonic distortion component at its output.

USRP is equipped with 4 digital downconverters with programmable decimation rates, 2 digial upconverters with programmable interpolation rates, high speed USB 2.0 interface (480 Mb/s); modular architecture supports wide variety of RF daughterboards; auxiliary analog and digital I/O support complex radio controls such as RSSI and AGC.

High sample rate processing takes place in the FPGA, while the lower sample rate processing happens in the host computer. The two onboard digital downconverters (DDCs) mix , filter, and decimate (from 64 MS/s) incoming signals in the FPGA. Two digital upconverters (DUCs) interpolate baseband signals to 128 MS/s before translating them to the selected output frequency. The DDCs and DUCs combined with the high sample rates also greatly simplify analog filtering requirements.

The baseband processing for transmission and reception is applied in a host computer connected to the USRP through the USB interface. The spectrum sensing itself would be considered as reception processing, and it is performed based on energy detection.

[****] Information about USRP is available at http://www.ettus.com/

The USRP mainboard can be connected to several daughterboard options. Daughterboards are the front end sub system part that will transmit or receive the signal on the desired operating carrier frequency.

Figure 6.3 depicts the USRP development board including its daughterboard.

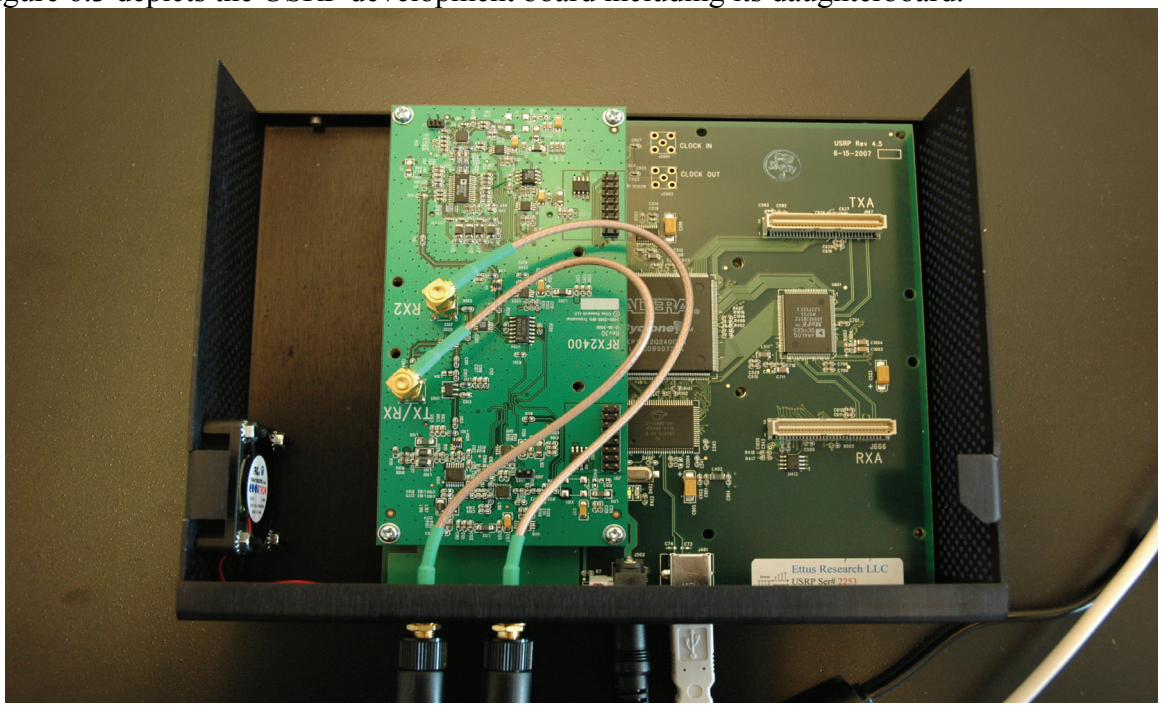

Figure 6.3: Inside the USRP

6.4 Cognitive Radio Nodes Demonstrator Design

The basic single node Cognitive Radio configuration is depicted in Figure 6.4. The evaluation system involves 2 USRP modules, 2 laptop PCs as host computers for the USRP, and a desktop computer with the P25M board installed. The results of the configuration according Figure 6.4 has been presented as a demonstrator paper in reference [108].

The system applied cooperative sensing, the spectrum sensing from USRP1 is combined with spectrum sensing result from USRP2 through a Samba Linux network. USRP1 acts as server that will give the decision about final spectrum occupancy information, and further sends this information to the baseband processing module on the P25M. Until now, the P25M is not connected to any front end interface for transmitting the signal to air. But the final goal of such a demonstrator is transmitting of adaptive CR signals in air.

The demonstrator aims to be a proof-of-concept Dynamic Spectrum Access (DSA) system. Specifically, a simple multi-carrier OFDM-based CR system with Spectrum Pooling (SP) has

been implemented in the P25M platform. SP is applied by windowing and carriers de-activation, where cancellation carriers can be inserted. Channel estimation has been applied by using the Least Squares method. In a later phase the developed Wiener filter with optimum pilot pattern and virtual pilot concept will be implemented. In the Least Squares method several OFDM symbols are transmitted as pilots.

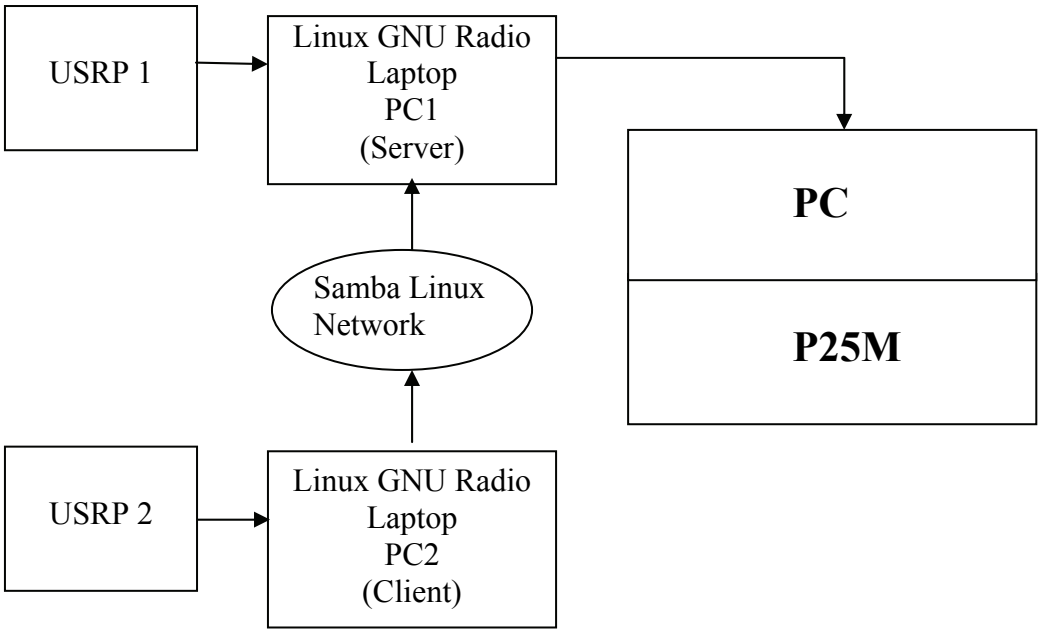

Figure 6.4: Single Cognitive Radio unit with 2 spectrum sensing elements (USRPs) and one baseband processing sub-unit

The block design of P25M is represented in Figure 6.5. In the beginning we implement a simple OFDM-based cognitive radio scheme with spectrum pooling. The spectrum pooling will be simply the time domain windowing combined with adaptive de-activation of carriers located in the occupied licensed user's band. The Block diagram of the OFDM demonstrator is depicted in Figure 6.6. Figure 6.7 shows the algorithm of TDCS at the transmitter side, while the receiver side is depicted in Figure 6.8.

The P25M performs the following tasks;

- Implementation of Adaptivity by the Adaptive bit loading algorithm.
- Baseband transmission and reception of the data bits (coding and modulation).

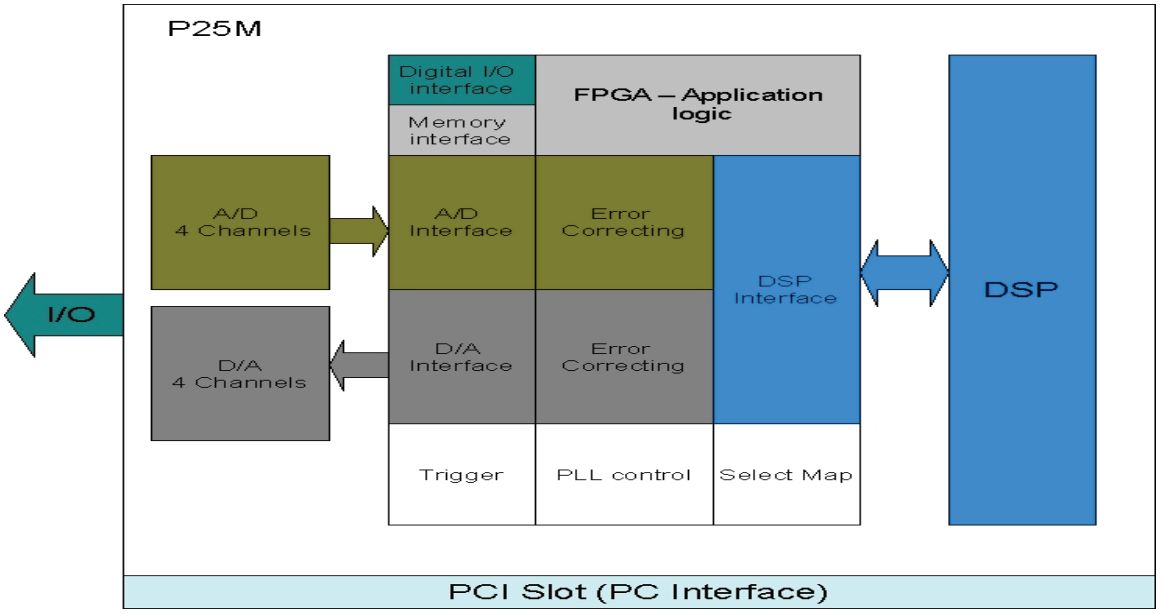

Figure 6.5: P25M Block design

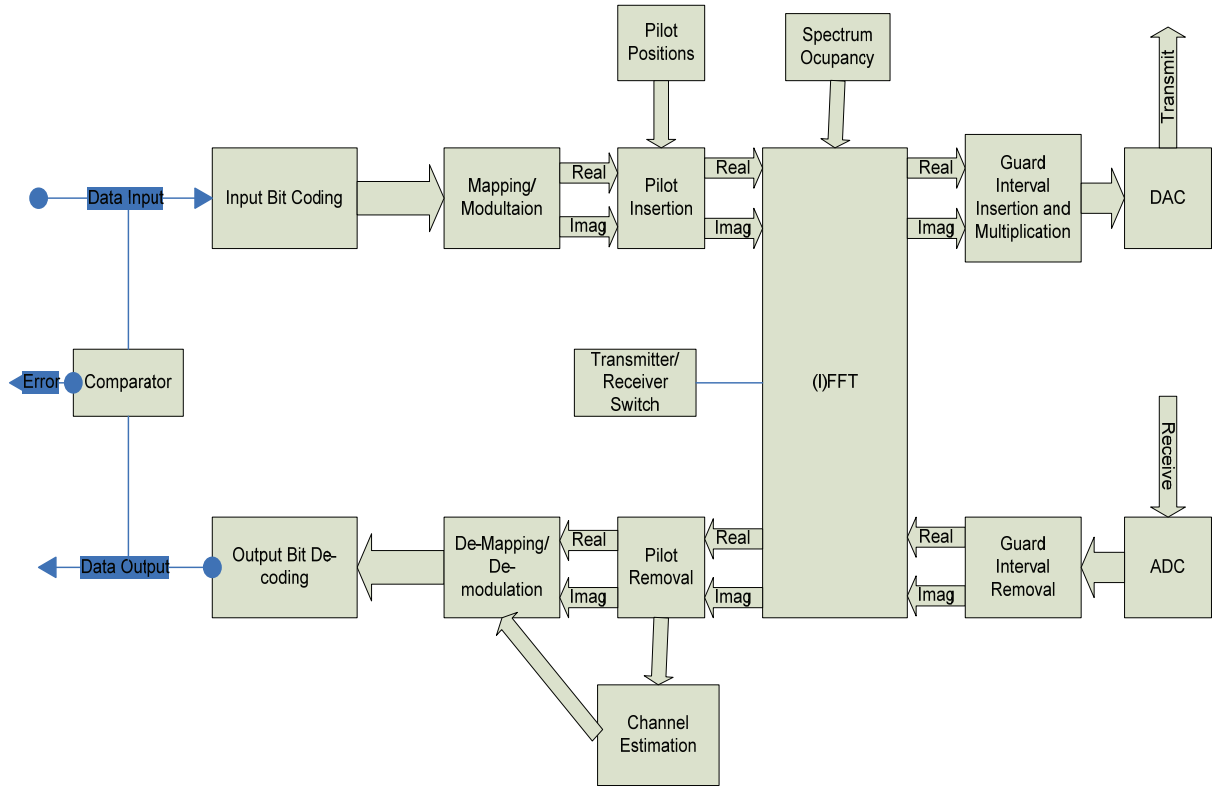

Figure 6.6: Signal flow of IRCTR-AAF Cognitive Radio Demonstrator

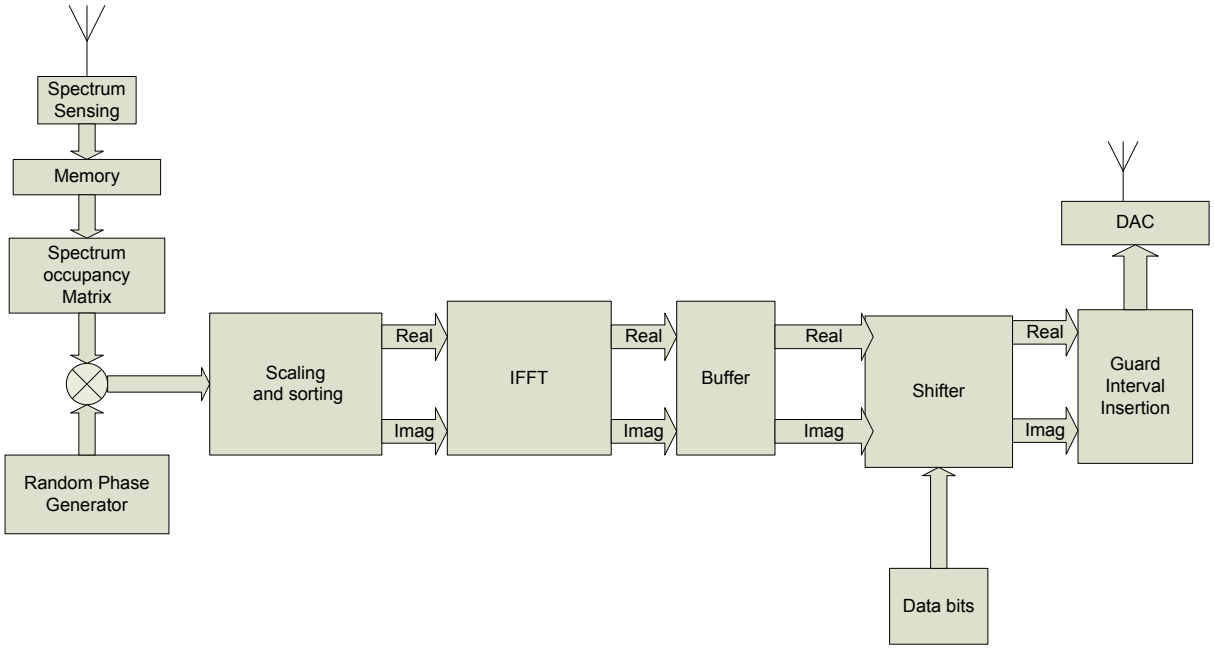

Figure 6.7: Transmitter architecture of TDCS

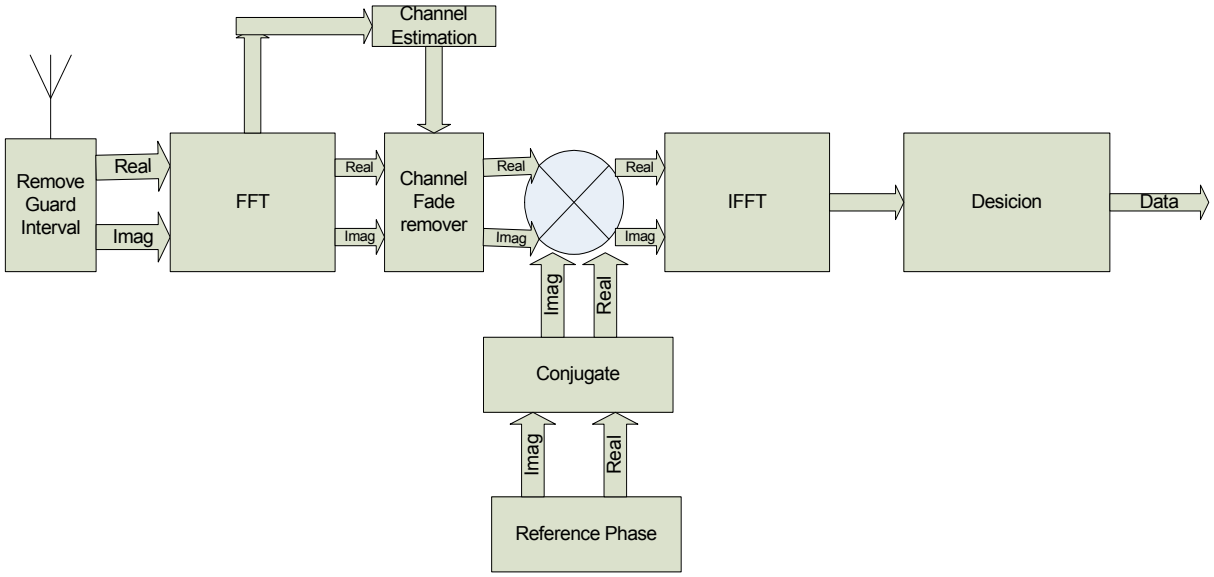

Figure 6.8: Receiver architecture of TDCS with Channel Estimation module

An example of cooperative spectrum sensing results is shown via a graphical user interace (GUI) on a linux computer, depiced in Figure 6.9.

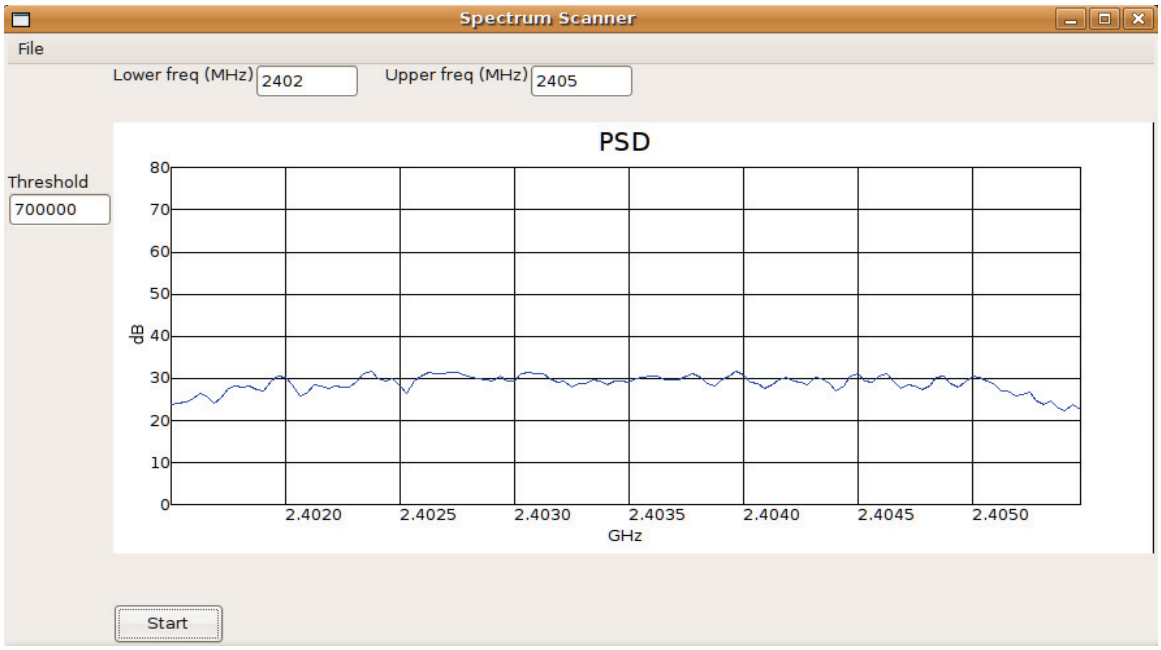

Figure 6.9: An example of GUI spectrum scanner with 3 MHz bandwidth , frequency range 2.402-2.405 GHz

We have implemented the spectrum pooling technique described in section 2.2 to the baseband processing in P25M. The window is rectangular, 128 subcarriers were designed. Figure 6.10 (a) shows the subcarrier occupied by the Cognitive Radio (CR) system using P25M baseband processing, and accordingly Figure 6.10 (b) gives the power spectrum density of the CR OFDM signal.

The VHDL simulation results of P25M are presented in Figure 6.11. There is a timing offset between the results before IFFT module (data[5:0] in Figure 6.11) and after FFT module (data_out[5:0] in Figure 6.11) on the simulations due to FFT and IFFT processing time. Each symbol is represented by 6 bits ([5:0]).

Figure 6.12 depicts the expected future observation of a Cognitive Radio networks with three nodes. Each node will have its own spectrum scanning capability. A node will act as the server that gives a decision about the spectrum occupancy information. This information will be distributed to the three nodes.

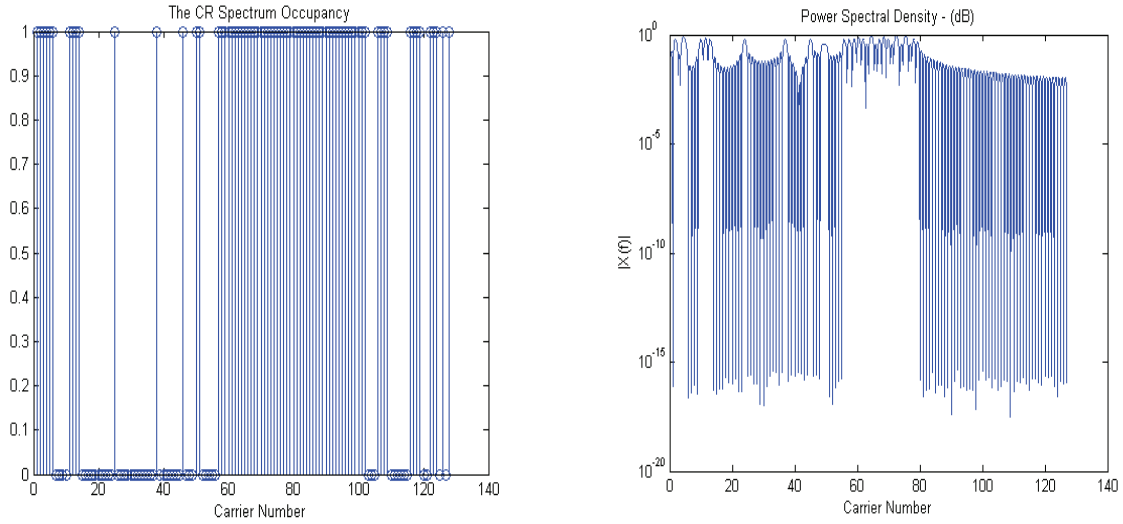

(a) (b)

Figure 6.10: (a) Carriers occupied by the Cognitive Radio System; (b) Cognitive Radio power spectral density

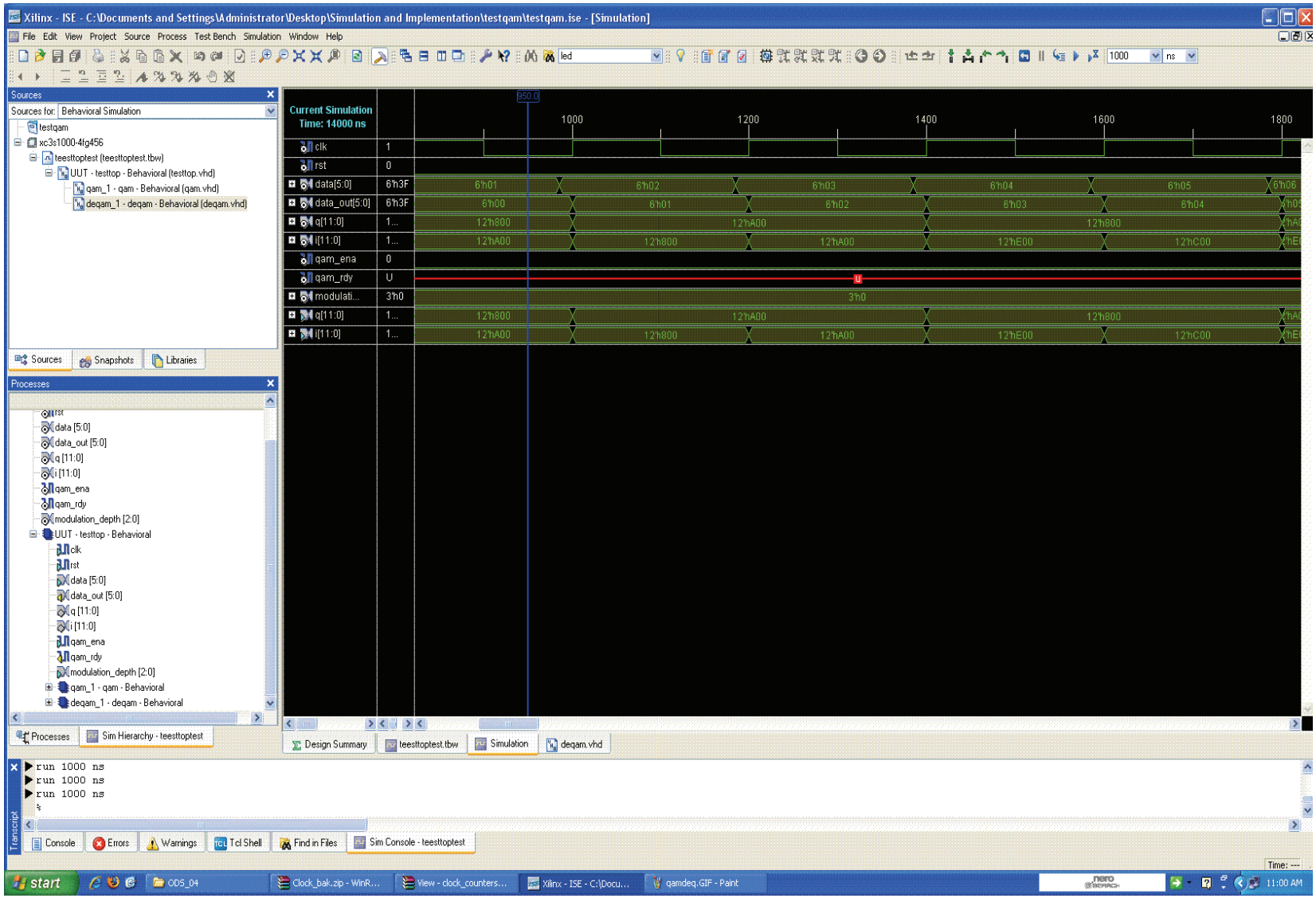

Figure 6.11: VHDL simulation results of the OFDM based Cognitive Radio System on FPGA

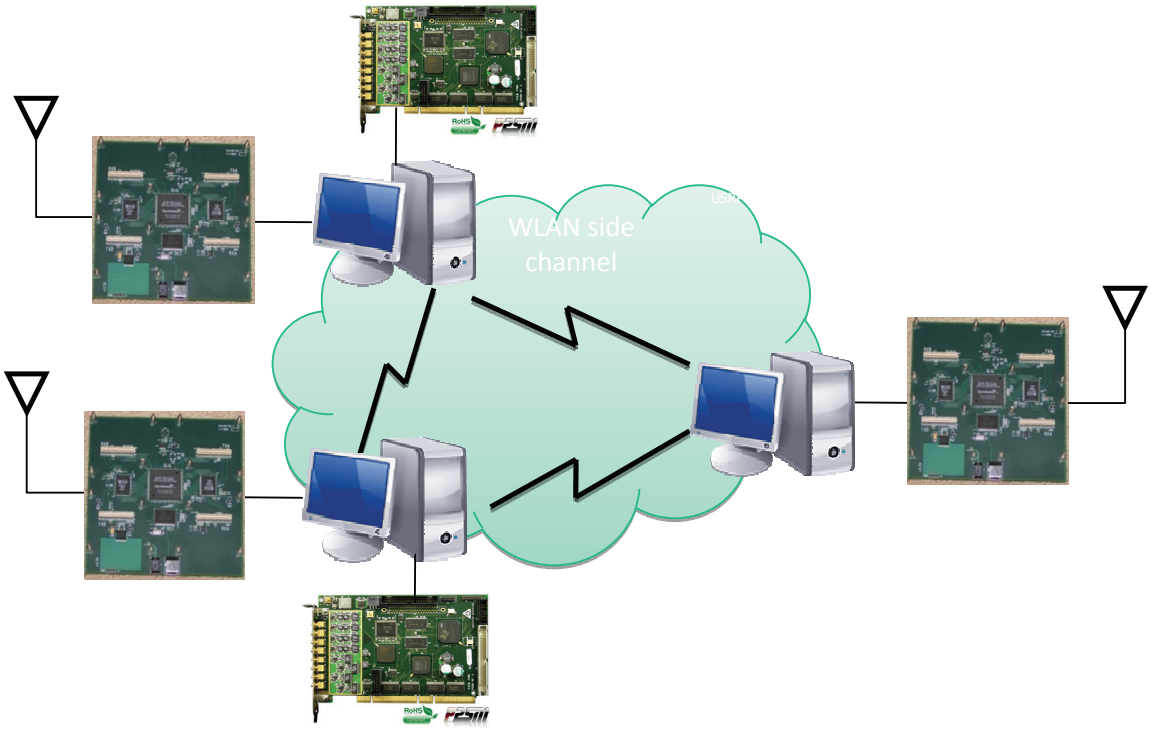

Figure 6.12: Outlook of three Cognitive Radio nodes with spectrum sensing capability on each node

The following conditions of the network should be satisfied :

- Each SU (Secondary User) is a PC equipped with an USRP and a P25M DSP board.
- The RFX400 transceiver daughter boards are installed on the USRP main board and are in charge of the dynamic spectrum access.
- P25M runs the OFDM transmission and adaptive bit loading algorithms under PC's control.
- A dedicated control channel based WLAN is used for SU's to cooperate with each other.
- An SU communicates with other SU's by sending its result of spectrum sensing.

The USRP block design is depicted in Figure 6.13. The PC-based USRP is a device which allows us to create a software radio and can be programmed for the following tasks:

- Gathering local spectrum sensing data. Each node listens to the activities in the currently designated band via an RF interface built on and controlled by the USRP. The data is then processed by the USRP and awaiting for P25M access.

- Networking. Meta communication has been investigated by using an Ultra Wide Band Technique [109]. In this demonstrator the meta communications is carried out by an WLAN side channel, to exchange spectra availability information. Real data communication between nodes is taken care of by USRP's with a wireless interface.

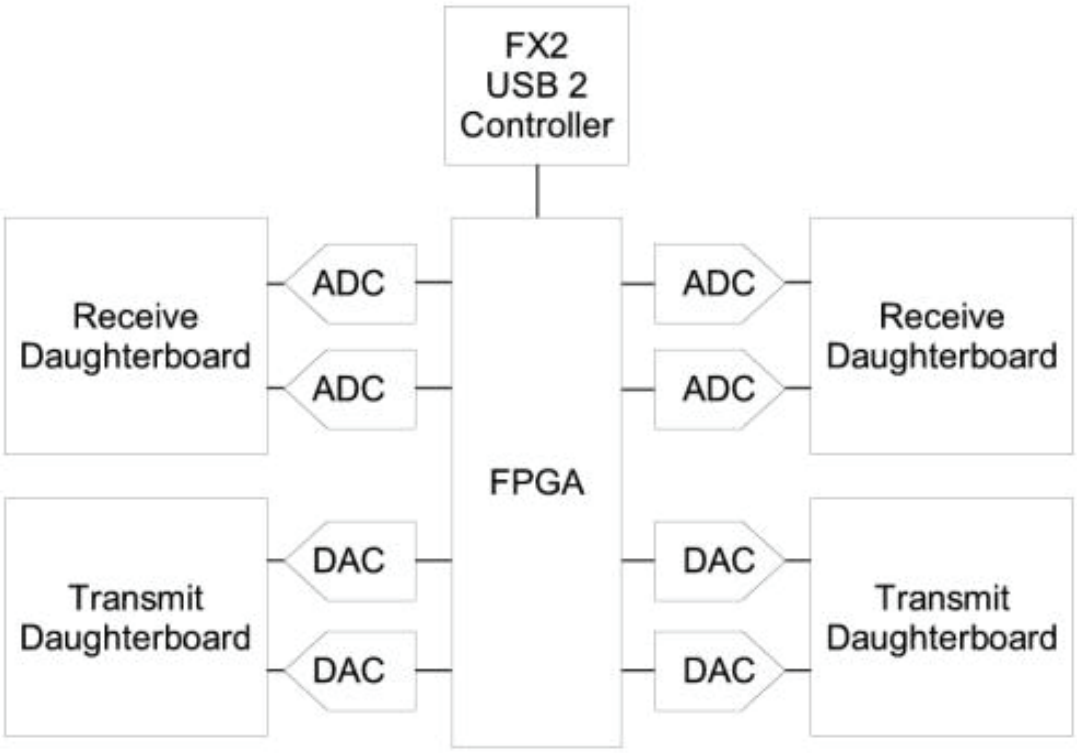

Figure 6.13: USRP block design

6.5 Conclusions

In this chapter a demonstrator as verification platform of a Cognitive Radio system has been proposed. The sensing is conducted by the Universal Software Radio Peripheral (USRP) device, while the signal processing for transmission is applied in an P25M evaluation board.

The initial system has been build by combining 2 USRP devices as sensing module. Each of the USRP is connected to a computer for sensing the signal processing purpose. One computer will act as server that will do cooperative sensing by combing the sensing information from the 2 USRP devices.

It is expected that the system can work with 10 MHz signal bandwidth. The ADC and the DAC component of the transceiver module should fulfil the nowadays FoM of 2pJ per conversion step. Accordingly, among several available evaluation boards on the market, the P25M board is selected.

At the initial stage, the minimum baseband processing i.e. the spectrum pooling and windowing have been implemented in the P25M. It is foreseen that complex algorithms such as channel estimation, synchronization and PAPR reduction can be incorporated in the platform.

The information about the spectrum occupancy is circulated through the WLAN channel. It is expected that in a real application this information should be broadcasted to each Cognitive Radio node in a side channel i.e. UWB.

Extra evaluation and design are required. It is expected that in future the P25M will be connected to the front end (RF) module. The feasibility of the USRP as front end module and the possibility of USRP to be applied as transceiver module are still under investigation.

Chapter 7

Conclusions and Recommendations

Cognitive Radio is an intelligent communication system. It has the capability to learn from its environment and react accordingly by changing its transmission parameters to obtain reliable communications and efficient spectrum utilization. Since one of the Cognitive Radio objective is to obtain efficient utilization of the radio spectrum, and the focus of our Adaptive Ad-hoc Freeband (AAF) project is on identification of free resources in the frequency domain, the specific scope of Cognitive Radio is the effective spectrum use. The intelligence and learning process by observing and analyzing the channel and spectrum conditions and further react to it by adjusting the transmission parameters will aid the radio system to access the spectrum effectively while reliable communications can still be achieved. In this thesis, special attention has been given to efficient spectrum utilization in the Cognitive Radio context by having the co-existence between the rental (Cognitive Radio) system with the legacy (licensed) system side by side while each of the systems has their quality of service (QoS) preserved.

7.1 Conclusions

The successful co-existence between the rental system with the legacy system side by side can be realized by having low mutual interference between the two systems. Chapter 2 introduces Orthogonal Frequency Division Multiplexing (OFDM) as a proper modulation technique to be applied in the Cognitive Radio system due to its flexibility in the notching part of its spectrum on the licensed user band by de-activating some of its carriers. In order to apply the carrier de-activation, spectrum occupancy information is required to locate the position of de-activated carriers in frequency-domain. In this dissertation, this information is assumed to be available. The spectrum occupancy information is obtained from the spectrum sensing module which is not the focus of this thesis. Spectrum sensing is another critical research issue and requires a proper attention. Simple sensing can be applied by energy detection in a certain frequency band. The project partner in Twente university conducted the spectrum sensing related research issue. The principal investigator is Marnix Heskamp. In order to have really accurate spectrum occupancy information, a special mechanism is required to gather spectrum information from all available cognitive radio devices. This issue is even more critical especially in the case that the LU's geographical position is close to one RU so that it is easily

detected by the corresponding RU while that LU is far from other RUs that probably cannot detect its presence. A simple mechanism would be the application of the logical 'OR' operation to the spectrum information vector of all RU transceivers. In the AAF project the spectrum information is planned to be distributed to all RU (Cognitive Radio) transceivers through a dedicated control channel. Techniques for mutual interference reduction between the OFDM-based rental (Cognitive Radio) system and the licensed system has been studied in this thesis. Among them are combined windowing and guard band handling (adjacent carriers de-activation), sidelobes cancellation carriers, frequency-domain additive signal, adaptive transition symbol, multiple choice sequence and constellation expansion. If due to the licensed user access, too many carriers of the OFDM-based Cognitive Radio system need to be de-activated, then the available carrier resources cannot accommodate the targeted Cognitive Radio system QoS. In this case frequency hopping is suggested. Ultra Wide Band could be an alternative due to its signal power property below the noise level hence it can be overlapped with the LU signal it self. Because the demand of the Cognitive Radio service is to provide high data rate at long distance transmission, the use of frequency hopping scheme is preferable. The frequency hopping has to collaborate with the spectrum sensing module. As the spectrum scanning module indicates that a certain amount of bandwidth is available at a certain carrier frequency (f_c), then the front end module will hop to that frequency, stabilizes itself and then transmits data.

Following the objectives of Cognitive Radio to obtain reliable communications and the emphasis of efficient spectrum utilization on the co-existence between the rental system with the legacy system, in chapter 3 we have proposed OFDM with adaptive bit loading, as the technique to preserve the rental system QoS, to be combined with the sidelobes reduction technique using windowing and cancellation carriers as a means to reduce the mutual interference between the rental and the legacy systems. Simulation results have shown that with perfect channel estimation, a 5 dB SNR gain could be achieved by applying the adaptive bit loading with the Fischer algorithm compared to the conventional OFDM; the combination of a raised cosine window with roll off factor 0.2 and 2 cancellation carriers on each side resulted into more than 30 dB sidelobes reduction. The possibility of peak to average power ratio (PAPR) growth due to the sidelobes cancellation carriers insertion has been analyzed. The evaluation shows that the sidelobes cancellation carriers give insignificant impact to the PAPR growth. Furthermore, the Fourier transform in OFDM can be replaced by the wavelet basis function. Literature has indicated that as wavelet basis functions give lower sidelobes compared to Fourier-based OFDM; in this thesis we proposed the use of a frequency selective wavelet basis function instead of the Fourier transform in OFDM combined with the spectrum pooling concept (de-activation of carriers in the licensed user band) for Cognitive Radio application. The technique is termed as the wavelet packet multicarrier modulation (WPMCM). The parameters of the frequency selective wavelet basis function such as the filter length, regularity order and the transition bandwidth can be set to fulfill the desired performance outcome i.e. the sidelobe amplitude. The results in an AWGN channel showed that at certain frequency selective wavelet parameters the WPMCM based Cognitive Radio outperforms the OFDM based Cognitive Radio in term of BER performance. As MIMO has

been well known as technique to increase specral efficiency, its advantage in the Cognitive Radio application was observed. The combination technique between windowing, cancellation carriers and adaptive bit loading will give a spectral efficiency enhancement but at the expense for extra complexity in the implementation.

Channel estimation is crucial and is considered as the most stringent module in the OFDM system. The channel estimation module is even more important in the Cognitive Radio context. The channel estimation would be the Cognitive Radio awareness element on the changing channel environment and its fading condition. An example of its use is in the application of adaptive bit loading. In adaptive bit loading the bits are allocated to each subcarrier according to the estimated fading state on the corresponding subcarrier. In this thesis the pilot-aided channel estimation is chosen to be applied in the Cognitive Radio system due to its better performance and less complex implementation compared to the blind channel estimation. A Wiener filter utilizes the distance between pilots in time and frequency in an OFDM frame and relates them with the channel correlation function in time and frequency to design the filter coefficients for channel estimation purpose in a straightforward way. Therefore, without loss of generality, in this thesis this filter was chosen for the Cognitive Radio system. In the application of frequency hopping, the OFDM frame design according to the Bluetooth TDD duration was proposed. Bluetooth was evaluated, as this technology uses frequency hopping technology in its transmission. Through simulations the frame design was evaluated in 900 MHz in a rural area and urban area. The results showed that one training symbol can effectively accommodate the channel estimation on one frame. The 900 MHz channel was explored due to the available information regarding its channel power delay profile characteristics in the ETSI documentation. Adopting the efficient implementation of a hexagonal pilot pattern in a conventional OFDM system, in chapter 4 we proposed the combination of hexagonal pilot pattern, pilot shifting and virtual pilots concept to be applied in the Cognitive Radio context, where some of the carriers will be de-activated due to the licensed user access. The proposed virtual pilot concept itself takes advantage of the slowly varying channel condition between two real pilot positions and accordingly predicts the initial channel estimates at the virtual pilot positions by linear interpolating/extrapolating the initial channel estimates at the real pilot positions combined with the decision directed method. The results showed that the utilization of the virtual pilots in a hexagonal pilot pattern within the Cognitive Radio context increased the channel estimation performance by more than 10 dB compared to the Hexagonal pattern without virtual pilots. Extensive work was done with respect to the optimal pilot pattern for a Cognitive Radio system by adopting the optimum single input single output (SISO) Hexagonal pilot pattern combined with the virtual pilot concept for Cognitive Radio system into its multiple input multiple output (MIMO) system version. Without loss of generality a 2x2 MIMO system was considered. Since the received signal at each of the receive antenna gets contributions from signals of all transmit antennas, the application of the decision directed method in the virtual pilot concept could lead to a severe decision error. Therefore the decision directed method was removed from predicting the initial channel estimates at the virtual pilot position. The stresses of two virtual pilot utilization concept was made to the

MIMO pilot pattern for the Cognitive Radio system. The first pattern utilizes the virtual pilots at a longer distance between pilots in time. The impact of the virtual pilots will be significantly caught at low maximum Doppler frequencies. The second pattern emphasizes the use of the virtual pilots at a longer distance between pilots in frequency. Therefore, a significant impact of the virtual pilots could be seen on the channel model with low delay spread. Further, the second pattern could be extended to have more virtual pilots for the intention of having an oversampling gain. Given the simulation parameters with fixed power delay profile, and different maximum Doppler frequency, the first pattern outperformed the second pattern including the one with more virtual pilots. The gap between them was even larger at low maximum Doppler frequencies.

In chapter 5 an attempt was made to increase the single carrier transform domain communications system (TDCS) bit rate by embedding an extra symbol as another bit source. The embedded symbol has not only increased the TDCS bit rate but also improved the cyclic code shift keying (CCSK) detection as the legacy data source depending on the constellation size of the embedded symbol. As the embedded symbol constellation size increases the CCSK BER reduces. Analysis and simulations showed that the embedded symbol does not destroy the multiple access capability of TDCS in an AWGN channel environment. A Rayleigh fading channel disturbs the cross correlation of the TDCS multi-user basis function. Simulation results indicated how the CCSK and embedded symbol BER were degraded. A further attempt to enhance the TDCS performance was made by employing MIMO. The results displayed how MIMO TDCS could combat the fading effect. The simulation results indicated, by having a ratio of ½ between the transmit and receive antenna, the BER performance of TDCS-CCSK with embedded symbol in a Rayleigh fading channel resembles a performance as in an AWGN channel. Due to the system design, the embedded symbol detection was applied after CCSK detection. Therefore, the error in CCSK detection propagated to the embedded symbol detection. For to this reason, the BER on the embedded symbol was influenced by the tendency that a higher embedded symbol constellation sizes gave a better CCSK detection while the embedded symbol detection was deteriorated. These two tendencies put a trade-off to the final embedded symbol error rate. The results showed that in the TDCS system the embedded symbol QPSK detection performs better than the BPSK detection. The application of the embedded symbol was also evaluated in the wavelet domain communication system (WDCS). In the WDCS the Fourier transform that forms the basis function into time domain signal is replaced by the wavelet packet basis function. In this thesis, we proposed the usage of the frequency selective wavelet in the WDCS with an embedded symbol. The results demonstrated that the CCSK detection in WDCS is more accurate than in TDCS. For this reason, the WDCS could preserve the PSK modulation behavior (higher constellation renders higher BER) in the embedded symbol detection. In terms of power spectral density, and scaling factor 1 the single carrier TDCS/WDCS based Cognitive Radio has a factor $1/N_{FFT}$ lower sidelobes compared to multi carrier OFDM/WPMCM counterpart. Increasing the scaling factor of TDCS/WDCS increases its sidelobes and also its SNR at the expense of a larger amount of required transmit power.

In chapter 6 a prototype Cognitive Radio verification platform was presented. The P25M was selected for the development board, while USRP was considered to aid the P25M in providing the spectrum occupancy information. The initial platform includes 2 USRP as a means to provide the cooperative sensing effect. Each of the USRPs is connected to a computer that conducts the signal processing, while the P25M is embedded also to a computer. One USRP-computer node acts as a server where the decision about the final spectrum occupancy information is made. The connection between the two USRP-computers and the computer (which contains the P25M board for the spectrum occupancy information transfer) is employed through a local area network (LAN). Progress on this prototype is still ongoing. It is planned that the developed baseband processing in this thesis will be implemented in the development board (P25M). Furthermore the transceiver front end component will be appended to the P25M and the system will be evaluated from the signal on air.

7.2 Recommendations for Future Work

In this thesis research has been done on Fourier-based modulation such as OFDM and TDCS based Cognitive Radio. Sidelobes reduction techniques in OFDM have been overviewed. Without loss of generality the sidelobes reduction and fading mitigation applied to OFDM could also be applied to the TDCS system. Channel estimation in OFDM-based Cogntive Radio has been explored. The same channel estimation technique in OFDM is expected to be applied in the TDCS system too. Bit rate enhancement in OFDM is applied intelligently by adaptive bit loading, while in TDCS extra embedded symbol is the proposed technique.

Limited subjects have been explored to the Fourier-based modulation counterpart, which is wavelet based modulation such as WPMCM and WDCS. The evaluations have been limited to the AWGN channel. Literature describes that time domain equalization is a suitable technique to remove the fading effect in the wavelet based modulation technique (WPMCM and WDCS).

Our evaluations have shown that frequency domain equalization is not feasible to be applied to WPMCM system. We predict that this problem is caused by the overlapping property of the transmitted WPMCM signal. It seems like the time domain equalization is the realistic solution in counteracting the channel fading effect to the signal.

By applying a suitable equalization technique the use of frequency selective wavelet in WPMCM and WDCS based Cognitive Radio system could be explored further in a Rayleigh fading channel, including the embedded symbol application to the WDCS. The work can further be extended to MIMO applications since the channel state information will be provided by the equalization module.

Another possible future work with respect the WPMCM implementation is the application of the tree extension on the subcarriers with good channel conditions to compensate the loss of

data source due to de-activated carriers. It is expected that extending the tree on a subcarrier with good channel condition will give higher rate and good BER. The scheme is depicted in Appendix G.

Appendix A

OFDM based Cognitive Radio Frame Design for Frequency Hopping Scenario

A frame design is chosen with small bandwidth, and the frame duration is based on the TDD Bluetooth frame. The TDD Bluetooth system is depicted in Figure A.1. Only about half a duration of the slot can be used for transmission. After the system transmits the bits, it hops to a free (unoccupied) frequency band and it needs time to stabilize itself in that band. The frame duration must not exceed 366 μs.

According to [34] in order to fulfil 2 pJ(pico joule) per conversion step *Figure of Merit* of the analog to digital converter (ADC), the signal bandwidth must not exceed 5 MHz. Since the sampling frequency is twice the signal bandwidth, the sampling time must not be less than 0.1 μs.

As the spectrum scanning module indicates a 5 MHz bandwidth (available in a certain carrier frequency (f_c) e.g. between 800 -900 MHz), the front end module will hop to that frequency, stabilizes itself and then transmits data. Depending on the cognitive radio device capability, and assuming that the scanning process and transmitting data are independent of each other, the scanning can be conducted in parallel to the front end's oscillator stabilization and data transmission process. After data transmission, the information on the free 5 MHz bandwidth (provided by the spectrum scanning module) will be available to each CR transceiver through a common control channel [11]. Upon receiving the f_c information, the front end will set the oscillator to the corresponding f_c. This algorithm can obviously only be applied to the device which has parallel processors. In this way, the scanning and transceiver are done separately and parallel to each other. In this thesis, the device configuration is realized by combining the USRP as spectrum scanning module with the P25M development board as transceiver module. USRP can also be used as transceiver module. More about these two platforms and demonstrator are presented in chapter 6.

Time required for the transmitter's front end to transmit the data and stabilizing itself to the new carrier frequency is about 625 μs; during this period also the spectrum scanner module senses the frequencies. The process flow of the frequency hopping including spectrum scanning and data transmission is described in Figure A.2.

For the devices without having the capability to scan and transmit data in parallel, a certain time slot is required for dedicating the processor to only scan the spectrum and then proceed the transmission process at the cost of a bit rate degradation.

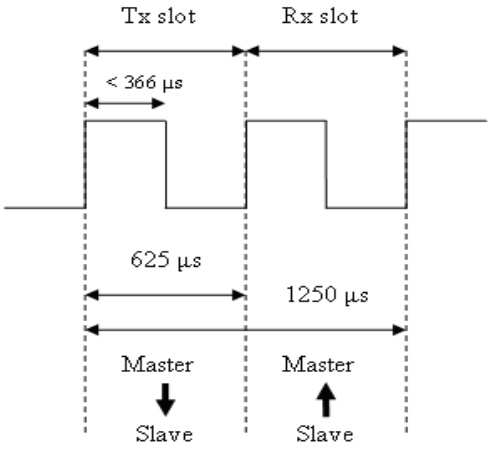

Figure A.1: TX/RX cycle of the Bluetooth system

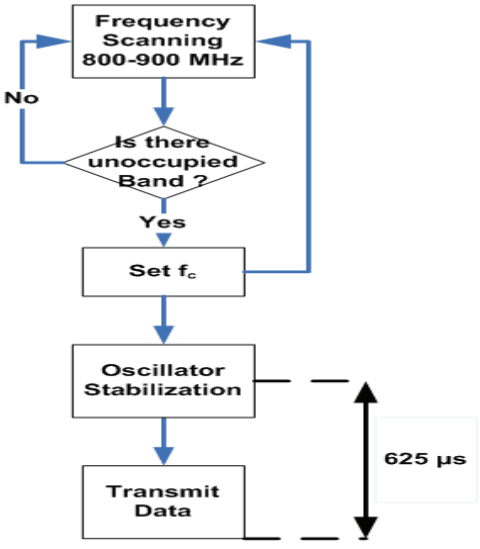

Figure A.2: Process flow of hopping and data transmission for a CR system, OFDM based with a Bluetooth TDD frame design

The advantage of having the capability to scan and transmit in parallel is the following. In the time a cognitive radio device does its transmission in a certain frequency band and an LU in between that period also transmits its signal in that band, the spectrum scanning module of

that cognitive radio device will detect the LU presence and commands the transmission module to stop its transmission. Then it scans for a new frequency in a different band. An extended capability will be attained if the cognitive radio has two scanning module that can work in parallel. One scans in the own band where it transmits data, and the other one scans a different band to find an alternative if a sudden LU access appears in the band where the cognitive radio system transmits data.

With respect to this mechanism, the spectrum sensing module of that cognitive radio device should have knowledge about the data transmitted by the transmission module , e.g. in terms of a pilot or training symbol, then should subtract this known data from the received signal at that frequency band, and further apply LU signal detection. In the cooperative sensing mechanism (where the logical OR operation is applied), the decision by one device in claiming one spectrum region is occupied will be enough to notch the spectrum of all cognitive radio devices within its network in that occupied spectrum region. In this work, we assume that this sensing mechanism is available.

Appendix B

Training Symbol Repetition Period Mathematical Proof by Zeros Insertion

To validate the zero insertion on the odd index of subcarriers, we can observe the following equations.

The first one is if the zeros are inserted on the odd index of subcarriers.

$$x_n = \frac{1}{N_{FFT}} \sum_{k=0}^{N_{FFT}-1} X_k e^{\frac{j2\pi kn}{N_{FFT}}} = \underbrace{\frac{1}{N_{FFT}} \sum_{k=0}^{\frac{N_{FFT}-2}{2}} X_{2k} e^{\frac{j2\pi(2k)n}{N_{FFT}}}}_{\text{even index of subcarriers}} + \underbrace{\frac{1}{N_{FFT}} \sum_{k=0}^{\frac{N_{FFT}-2}{2}} X_{(2k)-1} e^{\frac{j2\pi((2k)-1)n}{N_{FFT}}}}_{\substack{0 \\ \text{odd index of subcarriers,} \\ \text{where values of the component } X_{2k-1} \text{ are zeros}}}$$

$$= \frac{1}{N_{FFT}} \sum_{k=0}^{\frac{N_{FFT}-2}{2}} X_{2k} e^{\frac{j2\pi(2k)n}{N_{FFT}}}$$

$$x_{\frac{N_{FFT}}{2}+n} = \frac{1}{N_{FFT}} \sum_{k=0}^{N_{FFT}-2} X_k e^{\frac{j2\pi k\left(\frac{N_{FFT}}{2}+n\right)}{N_{FFT}}} = \underbrace{\frac{1}{N_{FFT}} \sum_{k=0}^{\frac{N_{FFT}-2}{2}} X_{2k} e^{\frac{j2\pi(2k)\left(\frac{N_{FFT}}{2}+n\right)}{N_{FFT}}}}_{\text{even index of subcarriers}} +$$

$$\underbrace{\frac{1}{N_{FFT}} \sum_{k=0}^{\frac{N_{FFT}-2}{2}} X_{(2k)-1} e^{\frac{j2\pi((2k)-1)\left(\frac{N_{FFT}}{2}+n\right)}{N_{FFT}}}}_{\substack{0 \\ \text{odd index of subcarriers,} \\ \text{where values of the component } X_{2k-1} \text{ are zeros}}}$$

$$= \frac{1}{N_{FFT}} \sum_{k=0}^{\frac{N_{FFT}-2}{2}} X_{2k} e^{\frac{j2\pi(2k)n}{N_{FFT}}} e^{j2\pi k} = \frac{1}{N_{FFT}} \sum_{k=0}^{\frac{N_{FFT}-2}{2}} X_{2k} e^{\frac{j2\pi(2k)n}{N_{FFT}}} \tag{B.1}$$

Since $e^{j2\pi k}$ is always 1 for every integer value of k, then if zeros are inserted on the component of x_k for every odd values of k, $x_n = x_{\frac{N_{FFT}}{2}+n}$.

The following equation depicts if zeros are inserted on the even index of subcarriers.

$$x_n = \frac{1}{N_{FFT}} \sum_{k=0}^{N_{FFT}-1} X_k e^{\frac{j2\pi kn}{N_{FFT}}} = \underbrace{\frac{1}{N_{FFT}} \sum_{k=0}^{\frac{N_{FFT}-2}{2}} X_{2k} e^{\frac{j2\pi(2k)n}{N_{FFT}}}}_{0} + \underbrace{\frac{1}{N_{FFT}} \sum_{k=0}^{\frac{N_{FFT}-2}{2}} X_{(2k)-1} e^{\frac{j2\pi((2k)-1)n}{N_{FFT}}}}_{\text{odd index of subcarriers,}}$$

even index of subcarriers,
where values of the component X_{2k} are zeros

$$= \frac{1}{N_{FFT}} \sum_{k=0}^{\frac{N_{FFT}-2}{2}} X_{(2k)-1} e^{\frac{j2\pi((2k)-1)n}{N_{FFT}}}$$

$$x_{\frac{N_{FFT}}{2}+n} = \frac{1}{N_{FFT}} \sum_{k=0}^{N_{FFT}-2} X_k e^{\frac{j2\pi k\left(\frac{N_{FFT}}{2}+n\right)}{N_{FFT}}} = \underbrace{\frac{1}{N_{FFT}} \sum_{k=0}^{\frac{N_{FFT}-2}{2}} X_{2k} e^{\frac{j2\pi(2k)\left(\frac{N_{FFT}}{2}+n\right)}{N_{FFT}}}}_{0} +$$

even index of subcarriers,
where values of the component X_{2k} are zeros

$$\underbrace{\frac{1}{N_{FFT}} \sum_{k=0}^{\frac{N_{FFT}-2}{2}} X_{(2k)-1} e^{\frac{j2\pi((2k)-1)\left(\frac{N_{FFT}}{2}+n\right)}{N_{FFT}}}}_{\text{odd index of subcarriers}}$$

$$= \frac{1}{N_{FFT}} \sum_{k=0}^{\frac{N_{FFT}-2}{2}} X_{(2k)-1} e^{\frac{j2\pi((2k)-1)\left(\frac{N_{FFT}}{2}+n\right)}{N_{FFT}}} = \frac{1}{N_{FFT}} \sum_{k=0}^{\frac{N_{FFT}-2}{2}} X_{(2k)-1} e^{\frac{j2\pi((2k)-1)n}{N_{FFT}}} e^{j\pi((2k)-1)}$$

$$= -\frac{1}{N_{FFT}} \sum_{k=0}^{\frac{N_{FFT}-2}{2}} X_{(2k)-1} e^{\frac{j2\pi((2k)-1)n}{N_{FFT}}}$$

(B.2)

Since $e^{j\pi((2k-1))}$ is always -1 for every integer value of k, then if zeros are inserted on the component of x_k for every even values of k, $x_n = -x_{\frac{N_{FFT}}{2}+n}$.

Appendix C

Single User CCSK Detection in TDCS with an Embedded Symbol

The CCSK detection by cross correlating the received signal after fading removal with the reference basis signal according to (5.5) is as follows:

$$
\begin{aligned}
R_i \quad &\approx \sum_{n=0}^{N_{FFT}-1} \frac{1}{(N_{FFT})^2}\left[\sum_{r=0}^{N_{FFT}-1}\left(\left|A'_r\right|^2 S e^{j\varphi} e^{j\frac{-2\pi\tau r}{N_{FFT}}} + A'^{*}_r \frac{N_r}{H_r}\right) e^{j\frac{2\pi i r}{N_{FFT}}}\right] \\
&= \frac{1}{(N_{FFT})}\sum_{r=0}^{N_{FFT}-1}\left(\left|A'_r\right|^2 S e^{j\varphi} e^{j\frac{-2\pi\tau r}{N_{FFT}}} + A'^{*}_r \frac{N_r}{H_r}\right) e^{j\frac{2\pi i r}{N_{FFT}}} \\
&\approx \frac{1}{(N_{FFT})}\sum_{r=0}^{N_{FFT}-1}\left(\underbrace{\underbrace{\left(A'_r S e^{j\varphi} e^{j\frac{-2\pi\tau r}{N_{FFT}}} + \frac{N_r}{H_r}\right)}_{Y_r} A'^{*}_r}_{U_r}\right) e^{j\frac{2\pi(ir)}{N_{FFT}}} \qquad \text{(C.1)} \\
&\approx \frac{1}{(N_{FFT})}\left[S e^{j\varphi}\sum_{r=0}^{N_{FFT}-1}\left|A'_r\right|^2 e^{j\frac{2\pi(i-\tau)r}{N_{FFT}}} + \sum_{r=0}^{N_{FFT}-1} A'^{*}_r \frac{N_r}{H_r} e^{j\frac{2\pi(ir)}{N_{FFT}}}\right] \\
&= \frac{1}{(N_{FFT})}\left[\underbrace{S e^{j\varphi}\sum_{r=0}^{N_{FFT}-1} e^{j\frac{2\pi(i-\tau)r}{N_{FFT}}}}_{signal\ \ term} + \underbrace{\sum_{r=0}^{N_{FFT}-1} A'^{*}_r \frac{N_r}{H_r} e^{j\frac{2\pi ir}{N_{FFT}}}}_{noise\ \ term}\right] \qquad \text{(C.2)}
\end{aligned}
$$

By observing (C.1) we can come to the vector of cross-correlation value:

$$\mathbf{R} = IFFT\left[FFT(\mathbf{y}).FFT^{*}(\mathbf{c})\right] \qquad \text{(C.3)}$$

Appendix D

The Power to Mean Sidelobe Power Ratio (PMR) of TDCS basis function

In conventional TDCS-CCSK if we assume the transmitted CCSK data is 0, and by observing (C.2) the peak of the correlation detection using the reference basis function will occur when the received signal is cross-correlated with the unshifted reference basis function (0 shift). The peak term in this case is defined as :

$$R_0 = \frac{1}{N_{FFT}}\left[\underbrace{Se^{j\varphi}\sum_{r=0}^{N_{FFT}-1} e^{j\frac{2\pi 0 r}{N_{FFT}}}}_{signal\ \ term} + \underbrace{\sum_{r=0}^{N_{FFT}-1} A'^{*}_{r}\frac{N_r}{H_r}e^{j\frac{2\pi 0 r}{N_{FFT}}}}_{noise\ \ term}\right] = \frac{1}{N_{FFT}}\left[Se^{j\varphi} + \sum_{r=0}^{N_{FFT}-1} A'^{*}_{r}\frac{N_r}{H_r}\right] \tag{D.1}$$

Accordingly based on the derivation for eq. (5.7), the peak power to mean sidelobe power ratio (PMR) of the TDCS basis function with extra embedded symbol is derived as :

$$PMR = \frac{E\left[R_0^2\right]}{E\left[R_{i,i\neq 0}^2\right]} = \frac{E\left[\left|\frac{1}{N_{FFT}}\sum_{r=0}^{N_{FFT}-1}\left(Se^{j\varphi} + A'^{*}_{r}\frac{N_r}{H_r}\right)\right|^2\right]}{E\left[\left|\sum_{i=1}^{N_{FFT}-1}\frac{1}{N_{FFT}}\sum_{r=0}^{N_{FFT}-1}\left(Se^{j\varphi} + A'^{*}_{r}\frac{N_r}{H_r}\right)e^{j\frac{2\pi(ir)}{N_{FFT}}}\right|^2\right]}$$

$$= \frac{\left|E\left[\left(\frac{1}{N_{FFT}}\sum_{r=0}^{N_{FFT}-1}\left(Se^{j\varphi}\right)\right)^2\right] + E\left[\left(\frac{1}{N_{FFT}}\sum_{r=0}^{N_{FFT}-1}\left(A'^{*}_{r}\frac{N_r}{H_r}\right)\right)^2\right]\right|}{\left|E\left[\left(\underbrace{\sum_{i=1}^{N_{FFT}-1}\frac{1}{N_{FFT}}\sum_{r=0}^{N_{FFT}-1}Se^{j\varphi}e^{j\frac{2\pi(ir)}{N_{FFT}}}}_{=0}\right)^2\right] + E\left[\left(\sum_{i=1}^{N_{FFT}-1}\frac{1}{N_{FFT}}\sum_{r=0}^{N_{FFT}-1}A'^{*}_{r}\frac{N_r}{H_r}e^{j\frac{2\pi(ir)}{N_{FFT}}}\right)^2\right]\right|} \tag{D.2}$$

$A'_r = A_r e^{j\theta_k}$ with $A_r \in \{0,1\}$. $|A'_r|$ will then be either 0 or 1. It is assumed that $\frac{N_r}{H_r}$ has a Gaussian distribution with variance $\sigma_{N/H}^2$. Hence (D.2) becomes [103]:

$$PMR = \frac{\left| S^2 e^{j2\varphi} + E\left[\left(\frac{1}{N_{FFT}} \sum_{r=0}^{N_{FFT}-1} A'^*_r \frac{N_r}{H_r} \right)^2 \right] \right|}{\left| E\left[\sum_{i=1}^{N_{FFT}-1} \left(\frac{1}{N_{FFT}} \sum_{r=0}^{N_{FFT}-1} A'^*_r \frac{N_r}{H_r} e^{j\frac{2\pi(ir)}{N_{FFT}}} \right)^2 \right] \right|} \tag{D.3}$$

$$\approx \frac{\left| S^2 e^{j2\varphi} \right| + \frac{1}{N_{FFT}} N_{FFT} \sigma_{N/H}^2}{\frac{1}{N_{FFT}} N_{FFT} \sigma_{N/H}^2} = \frac{\left| S^2 e^{j2\varphi} \right| + \sigma_{N/H}^2}{\sigma_{N/H}^2}$$

Appendix E

Multi User CCSK Detection in TDCS with an Embedded Symbol

In a multi-user environment CCSK detection, by cross correlating the received signal after fading removal with the reference basis function at user 1 according to eq. (5.13), we derive

$$
\begin{aligned}
R_{i,1} &\approx \sum_{n=0}^{N_{FFT}-1} \frac{1}{(N_{FFT})^2}\left[\sum_{r=0}^{N_{FFT}-1}\left(\left|A'_{r,1}\right|^2 S_1 e^{j\varphi_1} e^{j\frac{-2\pi\tau_1 r}{N_{FFT}}} + \sum_{u=2}^{U} A'_{r,u}\, A'^{*}_{r,1} \frac{H^u_r}{H^1_r} S_u e^{j\varphi_u} e^{j\frac{-2\pi\tau_u r}{N_{FFT}}} + A'^{*}_{r,1}\frac{N^1_r}{H^1_r}\right) e^{j\frac{2\pi ir}{N_{FFT}}}\right] \\
&\approx \frac{1}{(N_{FFT})}\sum_{r=0}^{N_{FFT}-1}\left(\left|A'_{r,1}\right|^2 S_1 e^{j\varphi_1} e^{j\frac{-2\pi\tau_1 r}{N_{FFT}}} + \sum_{u=2}^{U} A'_{r,u}\, A'^{*}_{r,1} \frac{H^u_r}{H^1_r} S_u e^{j\varphi_u} e^{j\frac{-2\pi\tau_u r}{N_{FFT}}} + A'^{*}_{r,1}\frac{N^1_r}{H^1_r}\right) e^{j\frac{2\pi ir}{N_{FFT}}} \\
&\approx \frac{1}{(N_{FFT})}\sum_{r=0}^{N_{FFT}-1}\left(\left(A'_{r,1} S_1 e^{j\varphi_1} e^{j\frac{-2\pi\tau_1 r}{N_{FFT}}} + \sum_{u=2}^{U} A'_{r,u}\frac{H^u_r}{H^1_r} S_u e^{j\varphi_u} e^{j\frac{-2\pi\tau_u r}{N_{FFT}}} + \frac{H^u_r}{H^1_r}\right) A'^{*}_{r,1}\right) e^{j\frac{2\pi(ir)}{N_{FFT}}}
\end{aligned}
\tag{E.1}
$$

$$
\approx \frac{1}{(N_{FFT})}\left[\begin{aligned}
&S_1 e^{j\varphi_1}\sum_{r=0}^{N_{FFT}-1}\left|A'_{r,1}\right|^2 e^{j\frac{2\pi(i-\tau_1)r}{N_{FFT}}} + \sum_{u=2}^{U} S_u e^{j\varphi_u}\sum_{r=0}^{N_{FFT}-1} A'_{r,u}\, A'^{*}_{r,1}\frac{H^u_r}{H^1_r} e^{j\frac{2\pi(i-\tau_u)r}{N_{FFT}}} \\
&+\sum_{r=0}^{N_{FFT}-1} A'^{*}_{r,1}\frac{N^1_r}{H^1_r} e^{j\frac{2\pi ir}{N_{FFT}}}
\end{aligned}\right]
$$

$$
\approx \frac{1}{(N_{FFT})}\left[\begin{aligned}
&\underbrace{S_1 e^{j\varphi_1}\sum_{r=0}^{N_{FFT}-1} e^{j\frac{2\pi(i-\tau_1)r}{N_{FFT}}}}_{\text{signal term}} + \underbrace{\sum_{u=2}^{U} S_u e^{j\varphi_u}\sum_{r=0}^{N_{FFT}-1} A'_{r,u}\, A'^{*}_{r,1}\frac{H^u_r}{H^1_r} e^{j\frac{2\pi(i-\tau_u)r}{N_{FFT}}}}_{\text{multiple access interference term}} \\
&+\underbrace{\sum_{r=0}^{N_{FFT}-1} A'^{*}_{r}\frac{N^1_r}{H^1_r} e^{j\frac{2\pi ir}{N_{FFT}}}}_{\text{noise term}}
\end{aligned}\right]
\tag{E.2}
$$

The inner bracket represents the received signal on user 1 after removal of its own fading. By observing (E.1) we can come to the vector of cross-correlation value :

$$\mathbf{R}_1 = IFFT\left[FFT(\mathbf{y}_1).FFT^*(\mathbf{c}_1) \right] \tag{E.3}$$

where $\mathbf{R_1}$, $\mathbf{y_1}$ and $\mathbf{c_1}$ are the cross-correlation vector , the received signal vector, and the reference basis signal vector for user 1 respectively.

Appendix F

V-BLAST Algorithm

The V-BLAST algorithm is implemented as [105] :

1. Build a Moore pseudo inverse matrix of **H**
   $$\mathbf{G} = \mathbf{H}^{+} = (\mathbf{H}^{*}\mathbf{H})^{-1}\mathbf{H}^{*}$$

2. Find the row of **G** where its Euclidean norm is the smallest one
   $$k = \arg\min_{j} \| \mathbf{G}_j \|$$
   and j is the column of matrix **G**. In TDCS system the sum is applied for N_{FFT} samples since one transmitted symbol is represented by N_{FFT} samples

3. Take the row *k* of **G** as the nulling vector **w** in TDCS **w** will be in the form of a matrix since we want to estimate the whole N_{FFT} samples
   $$\mathbf{w} = (\mathbf{G})_k$$

4. Obtain the strongest transmit signal
   $$\boldsymbol{r}_k = \mathbf{w} \,.\, \boldsymbol{Y}$$
   in the TDCS system $\mathbf{r}_k$ will be a vector of size N_{FFT}.

5. The vector $\mathbf{r}_k$ is the output from the V-BLAST signal processing module. It is in frequency-domain. The vector $\mathbf{r}_k$ will be transformed into time domain by IFFT, then decorrelated by the reference signal to obtain the estimated symbol *d2'* from the source data 2. The vector $\mathbf{r}_k$ will be used also to detect the transmitted data on source data 1 by multiplying it with the inverse of the frequency-domain form of the shifted reference signal. The shift depends on the result derived from the detection of data from source data2. Later after averaging the signal over N_{FFT}, symbol demapping is proceed to have the estimated symbol *d1'* on source data 1.

6. After detection of the strongest transmitted signal, its effect must be cancelled from the received signal vector to reduce the detection complexity of the remaining transmit signals. The symbol *d2'* is mapped again into its TDCS with CCSK representation in frequency-domain, and then multiplied with *d1'*. Later the results of this multiplication are fed back to the V-BLAST signal processing module. The cancellation is applied as

   $$\boldsymbol{Y} = \boldsymbol{Y} - (\mathbf{H})_k * d1' * \text{FFT}(\text{Mapping}(d2'))$$

where k is the column index. The k-th column of channel matrix $\mathbf{H}$ is then zeroed for the purpose of detection of the strongest transmitted signal on the next layer. The algorithm returns to step 1 untill the transmitted symbols on all layers have been detected.

Appendix G

Future Work in Wavelet Packet Multicarrier Modulation Based Cognitive Radio System

The application of the tree extension on the subcarrier with good channel condition to compensate the loss of data source due to de-activated carriers is depicted in Figure G.1. In the figure an example of de-activated carrier is signed by the cross, and implemented by allocating zero symbol to the carrier.

At this stage the design of the wavelet basis functions used in this thesis cannot accommodate the notching part of its spectrum on a LU band by itself. Notching can only be applied by de-activating carriers located at the LU band.

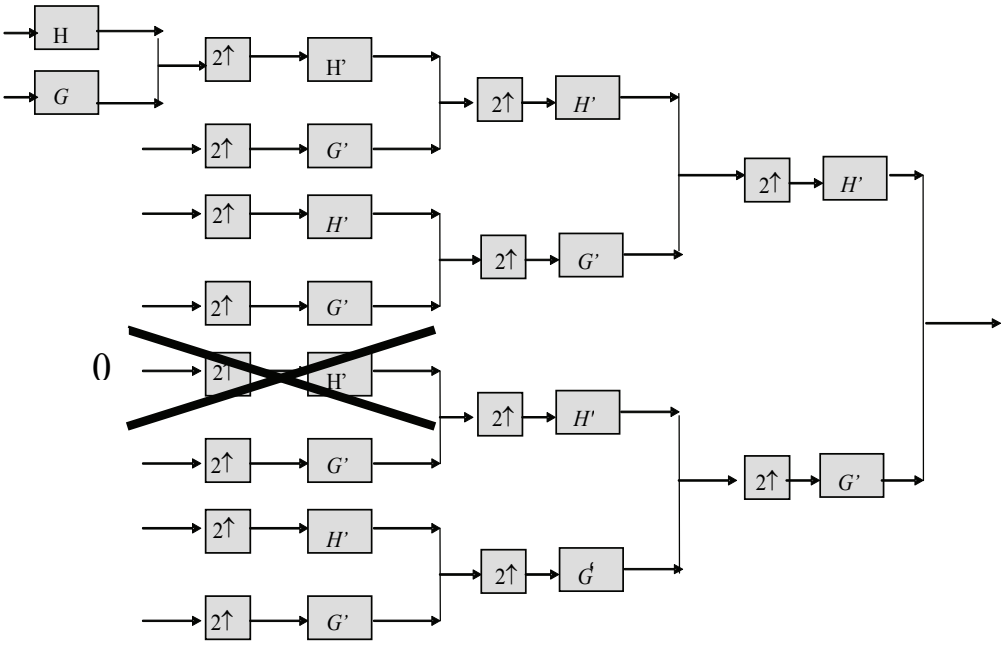

Figure G.1: Proposed future work on WPMCM to compensate the loss of data source due to de-activated carriers by extending the tree on a subcarrier with good channel condition

Bibliography

[1] Joseph Mitola III, *Cognitive Radio An Integrated Agent Architecture for Software Defined Radio*, PhD thesis, Dept. of Teleinformatics, KTH Royal Institute of Technology, Stockholm, Sweden, 2000.

[2] S. Haykin, "Cognitive Radio: Brain Empowered Wireless Communications", in *IEEE Journal on Selected Areas In Communications*, vol. 23, no.2, pp. 201-220, Feb. 2005.

[3] B. Fette, "Technical Challenges and Opportunities", presented at the Conference Cognitive Radio, Las Vegas, NV, Mar. 2004.

[4] M. Dillinger, K. Madani and N. Alonistioti, Eds., *Software Defined Radio : Architectures, Systems and Functions*, Wiley, New York, 2003.

[5] M. A. Fischler and O. Firschein, *Intelligence: The Brain, and the Computer*, ser. MA. Reading: Addison-Wesley, pp. 81, 1987.

[6] I. Budiarjo, M. K. Lakshmanan, and H. Nikookar, "Cognitive Radio Dynamic Access Techniques", in *International Journal on Wireless Personal Communications-Springer*, vol. 45, no. 3, pp. 293-324, Feb. 2008.

[7] R. W. Brodersen, A. Wolisz, D. Cabric, S. M. Mishra and D. Wilkomm, "CORVUS : A Cognitive Radio Approach for Usage of Virtual Unlicensed Spectrum, White Paper, Dept of electrical Engineering and Computer Science University of Berkeley, July, 2004. http://bwrc.eecs.berkeley.edu/Research/ MCMA/CR_White_paper_final1.pdf.

[8] M.G. Di Benedetto and G. Giancola, *Understanding Ultra Wide Band*, Upper Saddle River, NJ, Prentice Hall, 2004.

[9] V.D. Chakravarthy, A. K. Shaw, M. A. Temple, and J. P. Stephens, "Cognitive Radio – An Adaptive Waveform with Spectral Sharing Capability", in *Proc. IEEE Wireless Communications and Networking Conference*, vol 2, pp. 724- 729, Mar. 2005.

[10] R. van Nee and R. Prasad, *OFDM for Wireless Multimedia Communications*, Artech House Publishers, Boston, London, UK, 2000.

[11] T. Weiss and F. Jondral, "Spectrum Pooling - An Innovative Strategy for the Enhancement of Spectrum Efficiency", in *IEEE Communications Magazine,* vol. 42, no. 3, pp. S8-14, March 2004.

[12] I. Budiarjo et al., “D3.31 Radio System : First Phase Verification and advances in architecture and algorithms”, Adaptive Ad-hoc Freeband (AAF) wireless communications, Netherland, Sci. Rep. P1.0.06, 2006.

[13] T. Weiss, J. Hillenbrand, A. Krohn, and F. K. Jondral, ”Mutual Interference in OFDM-based Spectrum Pooling Systems”, in *Proc. IEEE Vehicular Technology Conference*, Milan, Italy, pp. 1873- 1877, 17-19 May 2004.

[14] H. Nikookar and R. Prasad. “Wave Shaping of Multicarrier Signal for Data Transmission Over Wireless Channels”, in *Proc. 6 th IEEE International Conference on Universal Personal Communications Record (ICUPC)*, pp. 173–177, 1997.

[15] P. Tan and N. C. Beaulieu. “Reduced ICI in OFDM Systems Using the Better than Raised – Cosine Pulse”. in *IEEE Communications Letter,* vol. 8, no. 3, pp. 135 – 137, March 2004.

[16] A. Assalini and A. M. Tonello,”Improved Nyquist Pulses”, in *IEEE Communications Letters,* vol. 8*,* no.2*,* pp. 87-89, 2004.

[17] C. Muschalik , “Improving An OFDM Reception Using An Adaptive Nyquist Windowing”, in *IEEE Transactions on Consumer Electronics*, vol. 42, no.3, pp. 259-269, 1996.

[18] K. Witrisal, “*OFDM Air Interface Design for Multimedia Communications*”, Ph.D. Thesis, Dept. Electrical Eng. Mathematics and Computer Science, Delft University of Technology, Apr. 2002.

[19] H.Nikookar and R.Prasad," Optimal Waveform Design for Multicarrier Transmission Over a Multipath Channel", in *Proc. 47th IEEE Vehicular Technology Conference*, Phoenix, Arizona, USA, May 4-7, pp. 1812-1816, 1997.

[20] F. Harris, E. Kjeldsen, “A Novel Interpolated Tree Orthogonal Multiplexing (ITOM) Scheme with Compact Time-Frequency Localization: an Introduction and Comparison to Wavelet Filter Banks and Polyphase Filter Banks”, in *Proc. Software Defined RadioTechnical Conference and Product Exposition*, Orlando, Florida, USA, Nov. 2006.

[21] H. Yamaguchi, “Active Interference Cancellation Technique for MB-OFDM Cognitive Radio”, *Proc. 34 th European Microwave Conference*, Amsterdam, The Netherlands, vol. 2, pp. 1105-1108, Oct. 2004.

[22] S. Brandes, I. Cosovic, and M. Schnell, “Sidelobe Suppression in OFDM Systems by Insertion of Cancellation Carriers”, *Proc. 62nd IEEE Vehicular Technology Conference (VTC)*, Fall, Dallas, USA, Sept, 2005.

[23] S. Brandes, I. Cosovic, and M. Schnell, "Reduction of Out of Band Radiation in OFDM Systems by Insertion of Cancellation Carriers", in *IEEE Comunications Letters*, vol. 10, no. 6, pp. 420-422, June 2006.

[24] S. Brandes, I. Cosovic, and M. Schnell**, "**Reduction of Out-of-Band Radiation in OFDM Based Overlay Systems**",** in *Proc. First IEEE International Symposium New Frontiers in Dynamic Spectrum Access Networks (DySPAN)*, Baltimore, Maryland, USA, pp. 662 – 665, Nov. 2005.

[25] U. Berthold, F. K. Jondral, S. Brandes and M. Schnell, "OFDM Based Overlay Systems: A Promising Approach for Enhancing Spectral Efficiency" in *IEEE Communications Magazine*, vol. 45, no. 12, pp. 52-58, Dec. 2007.

[26] I. Cosovic, S. Brandes, and M. Schnell, "A Technique for Sidelobe Suppression in OFDM System", in *Proc. IEEE GLOBECOM*, vol. 1, pp. 204-208, Nov. 2005.

[27] I. Cosovic, S. Brandes, and M. Schnell, "Subcarrier Weighting : A Method for Sidelobe Suppression in OFDM Systems", in *IEEE Communications Letters*, vol. 10, no. 6, pp. 444-446, June 2006.

[28] H.Nikookar and R.Prasad," Weighted OFDM for Wireless Multipath Channels", in *IEICE Transactions on Communications*, vol. E83-B, no. 8, pp. 1864-1872, Aug. 2000.

[29] I. Cosovic and T. Mazzoni, "Suppression of Sidelobes in OFDM systems by multiple choice sequences", in *European Transactions on Telecommunications Special Issue on Multi carrier – Spread Spectrum Wiley InterScience*, pp. 623-630, June 2006.

[30] H. A. Mahmoud and H. Arslan, "Sidelobe Suppression in OFDM –Based Spectrum Sharing Systems by Using Adaptive Symbol Transition", in *IEEE Communications Letters*, vol. 12, no. 2, pp. 133-135, Feb. 2008.

[31] I. Cosovic and T. Mazzoni, "Sidelobe Suppression in OFDM Spectrum Sharing Systems via Additive Signal Method", in *Proc. 65th IEEE Vehicular Technology Conference (VTC)*, Dublin, Ireland, pp. 2692-2696, Apr. 2007.

[32] S. Pagadarai, R. Rajbanshi, A. M. Wyglinski, and G. J. Minden, "Sidelobe Suppression for OFDM-Based Cognitive Radios Using Constellation Expansion", in *Proc. IEEE Wireless Communicaitons and Networking Conference (WCNC)*, Las Vegas, Nevada, USA, pp. 888-893, Apr. 2008.

[33] S. Pagadarai, A. M. Wyglinski, R. Rajbanshi, "A Novel Sidelobe Suppression Technique for OFDM-Based Cognitive Radio Transmission", in Proc. *IEEE Symposia*

on New Frontiers Dynamic Spectrum Access Networks (DySPAN), Chicago, USA, Oct. 2008.

[34] F.W. Hoeksema, M. Heskamp, R. Schiphorst, and C.H. Slump. A Node Architecture for Disaster Relief Networking, in *Proc. 1st IEEE Int. Symposium on new Frontiers in Dynamic Spectrum Access Networks (DySPAN'05)*, pp. 577-584, Nov 2005.

[35] I. Budiarjo, H. Nikookar, and L.P. Ligthart, "Performance Evaluation of OFDM Based Cognitive Radio System With Wiener Filter Channel Estimation Using Frequency Hopping GSM Channel Model at 900 MHz", in *Proc. 10th European Conference on Wireless Technology (ECWT)*, Munich, Germany, pp. 74-77, Oct. 8-12, 2007.

[36] ETSI. Digital cellular telecommunications system (phase 2+). Technical Specification ETS 300 910 GSM 05.05 version5.3.1, 1997.

[37] T. Keller and L. Hanzo, "Adaptive Multicarrier Modulation: A Convenient Framework for Time-Frequency Processing in Wireless Communications", in *Proceeding of the IEEE,* vol . 88, no. 5, May 2000, pp 611–640, May 2000.

[38] L. Hanzo, C. H. Wong, and M. S. Yee, *Adaptive Wireless Transceivers*, John Wiley and Sons Ltd, Baffins, Chichester, 2002.

[39] T. Keller and L. Hanzo, "Blind-Detection Assisted Sub-band Adaptive Turbo-Coded OFDM Scemes", in *Proc. IEEE Vehicular Technology Conference (VTC)*, vol. 1, Houston, TX, pp. 489-493, July 1999.

[40] S. B. Reddy, T. Yucek, and H. Arslan, "An Efficient Blind Modulation Detection Algorithm for Adaptive OFDM Systems", in *Proc. IEEE Vehicular Technology Conference (VTC)*, vol. 3, Orlando, USA, Oct. 2003,.

[41] P. S. Chow, J. M. Cioffi, and J. A. C Bingham, "A Practical Discrete Multitone Transveiver Loading Algorithm for Data Transmission over Spectrally Shaped Channels", in *IEEE Transactions On Communications,* no. 2, vol. 43, pp. 773–775, Feb. 1995.

[42] R. F. H. Fischer and J. B. Huber, "A New Loading Algorithm For Discrete Multitone Transmission", in *Proc. IEEE GLOBECOM '96*, pp. 724–728, Nov. 1996.

[43] A. N. Barreto and S. Furrer, "Adaptive Bit Loading for Wireless OFDM Systems", in *Proc. IEEE Int. Sym. Personal, Indoor, Mobile Radio Commun.*, vol. 2, pp. 88–92, 2001.

[44] R. Gruenheid, E. Bolinth, and H. Rohling, “A Blockwise Loading Algorithm for The Adaptive Modulation Technique in OFDM Systems”, in *Proc. Veh. Technol. conf.*, vol. 2, pp. 948–951, Fall 2001.

[45] R. Gruenheid, E. Bolinth, H. Rohling, and K. Aretz, “Adaptive Modulation for the HIPERLAN/2 Air Interface”, in *Proc. 5th Int. OFDM Workshop* Hamburg,Germany, 2000.

[46] M. Lei and P. Zhang,”Subband Bit and Power Loading for Adaptive OFDM”, in *58th IEEE Vehicular Technology Conference*, vol. 3, pp. 1482-86, Oct. 200.

[47] I. Budiarjo, H. Nikookar and L. P. Ligthart, “Performance Evaluation of Adaptive Bit Loading for OFDM With Channel Estimation Using 2x1-D Wiener Filter”, *Proc. 9th International Symposium on Wireless Personal Multimedia Communications (WPMC)*, San Diego, USA, Sep. 2006.

[48] I. Budiarjo, H. Nikookar and L. P. Ligthart, “Combined Spectrum Pooling and Adaptive Bit Loading for Cognitive Radio OFDM Based System”, *Proc. 13th IEEE Symposium on Communications and Vehicular Technology (SCVT)*, Liege, Belgium, Nov. 2006.

[49] R. Hassun, M. Flaherty, R. Matreci and M. Taylor, “Effective Evaluation of Link Quality Using Error Vector magnitude Techniques”, *Proc. Wireless Communications Conf.*, Boulder, CO, USA, pp. 89-94, Aug. 1997.

[50] A. Jamin and P. Mahonen, “Wavelet Packet Modulation for Wireless Communications”, in *Wireless Communications & Mobile Computing Journal*, vol. 5, Issue 2, pp. 123-137, John Wiley and Sons Ltd, March 2005.

[51] B. G. Negash and H. Nikookar, “Wavelet-based Multicarrier Transmission Over Multipath Wireless Channels”, in *IEE Electronics Letters*, Vol. 36 No. 21, pp. 1787–1788, October 2000.

[52] C.V. Bouwel, J. Potemans, S. Schepers, B. Nauwelaers and A.V. Capelle, "Wavelet Packet Based Multicarrier Modulation", in *Proc. IEEE Benelux Symposium on Communications and Vehicular Technology*, Leuven, Belgium, October 2000.

[53] P. P. Vaidyanathan, *Multirate Systems and Filter Banks*, Englewood Cliffs, NJ, Prentice-Hall, Inc., 1993.

[54] I. Daubechies, *Ten Lectures on Wavelets*, SIAM, Philadelphia, 1992.

[55] M. Vetterli and I. Kovacevic, *Wavelets and Subband Coding*, Prentice Hall PTR, Englewood Cliffs, New Jersey, 1995.

[56] S. Mallat, “A Theory for Multiresolution Signal Decomposition: The Wavelet Representation”, in *IEEE Trans. Pattern Anal. Machine Intell*., vol. 11, pp. 674-693, July 1989.

[57] C. S. Burrus, R. A. Gopinath, H. Guo, *Introduction to Wavelets and Wavelet Transforms, a Primer*, Upper Saddle River, NJ (USA): Prentice Hall, 1998.

[58] B.Burke, *The World According to Wavelets: The Story of a Mathematical Technique in the Making*, Second Edition, A K Peters, May 1998.

[59] O. Rioul and P. Duhamel, "A Remez Exchange Algorithm for Orthonormal Wavelets", in *IEEE Trans. Circuits Systems - II*, vol. 41, no. 8, pp. 550-560, August 1994.

[60] O. Rioul and P. Duhamel, "Note on ‘A Remez Exchange Algorithm for Orthonormal Wavelets’," Authors note available on the internet at http://www.comelec.enst.fr/~rioul/publis/199302rioulduhamelnote.pdf.

[61] A. V. Oppenheim and R. W. Schafer, *Discrete-Time Signal Processing*, Englewood Cliffs, NJ, Prentice Hall, 1989.

[62] A. Jensen and A.L. Cour-Harbo, *Ripples in Mathematics: The Discrete Wavelet Transform*, Springer, 2001.

[63] M. K. Lakshmanan, I. Budiarjo, and H. Nikookar, “Maximally Frequency Selective Wavelet Packets Based Multi Carrier Modulation Scheme for Cognitive Radio Systems”, in *Proc. IEEE GLOBECOM*, Washington D.C., USA, pp. 4185-4189, Nov. 2007.

[64] E.R. de Lima, S.J. Flores, V. Almenar, M.J. Canet, “Performance Enhancements in OFDM-WLAN Systems Using MIMO Access Techniques”, in *Proc. International Workshop on Telecommunications*, Santa Rita do Sapucai, MG, Brazil, August, 2004.

[65] P.W. Wolniansky, G.J. Foschini, G. D. Golden, and R. A. Valenzuela, “V-BLAST: An Architecture for Realizing Very High Data Rates Over the Rich Scattering Wireless Channel”, in *Proc. International Symposium on Signals Systems and Electronics (ISSE)*, Pisa, Italy, pp 295-300, Oct 1998.

[66] M. K. Lakshmanan, I. Budiarjo, and H. Nikookar, “Wavelet Packet Modulation MIMO Based Cognitive Radio System with V-BLAST Receiver Architecture”, in *Proc. IEEE Wireless Communications and Networking Conference*, Las Vegas, USA, pp. 705-710, March 2008.

[67] H. Che, *Adaptive OFDM and CDMA Algorithms for SISO and MIMO Channels,* Ph.D. Thesis, Dept. Electrical Eng. Mathematics and Computer Science, Delft University of Technology, May. 2005.

[68] B. Muquet, Z. Wang, G. B. Giannakis, M. de Courville, and P. Duhamel, "Cyclic Prefixing or Zero Padding for Wireless Multicarrier Transmissions?", in *IEEE Transactions on Communications*, vol. 50, no. 12, pp. 2136-2148, Dec. 2002.

[69] N. Wang and S. D. Blostein, "Adaptive Zero-Padding OFDM over Frequency-Selective Multipath Channels", in *EURASIP Journal on Applied Signal Processing*, no. 10, pp. 1478-1488, 2004.

[70] N. Chotikakamthorn and H. Suzuki, "On Identifiability of OFDM Blind Channel Estimation", in *Proc. 50 th IEEE Vehicular Technology Conference (VTC)*, Amsterdam, The Netherlands, vol. 4, pp. 2358-2361, Sept. 1999.

[71] K. Amleh, H. Li and R. Wang, "Blind Channel Estimation, Equalisation and CRB for OFDM with Unmodelled Interference", in *IET Communications* , vol. 1, no. 3, pp. 489-495, June 2007.

[72] M. C. Necker and G. L. Stuber, " Totally Blind Channel Estimation for OFDM over Fast Varying Mobile Channels", in *Proc. IEEE International Conference on Communications (ICC)*, vol. 1, New York, USA, pp. 421-425, Apr. 2002.

[73] P. Hoeher, S. Kaiser and P. Robertson, "Pilot-symbol aided channel estimation in time and frequency," in *Proceedings IEEE GLOBECOM*, Phoenix, USA, pp. 90–96, Apr. 1997.

[74] P. Hoeher, S. Kaiser and P. Robertson, "Two-Dimensional Pilot Symbol Aided Channel Estimation by Wiener Filtering", in *Proc. IEEE International Conference on Accoustics, Speech, and Signal Processing (ICASSP)*, vol. 3, Munich, Germany, pp. 1845-1848, Apr. 1997.

[75] S. Kaiser, *Multi-Carrier CDMA Mobile Radio Systems – Analysis and Optimization of Detection, Decoding and Channel Estimation,* VDI Verlag Gmbh, Dusseldorf, Germany, 1998.

[76] I. Budiarjo, *OFDM Channel Estimation by Adaptive Filtering*, MSc Thesis Report, Munich University of Technology, 2003.

[77] P. Hoeher, "A Statistical Discrete-Time Model for The WSSUS Multipath Channel*", IEEE Transactions on Vehicular Technology*, vol.41, No.4, pp. 461-468, November, 1992.

[78] D.E. Dudgeon, and R.M. Mersereau, *Multidimensional Signal Processing*, Prentice-Hall, 1983.

[79] M. J. Fernandez - Gettino Garcia, J.M Paez-Borallo and S. Zazo, " Efficient Pilot Patterns For Channel Estimation in OFDM Systems Over HF Channels," in *IEEE Vehicular Technology Conference Fall 99*, Amsterdam, The Netherlands, September 1999.

[80] M. J. Fernandez - Gettino Garcia, J.M Paez-Borallo and S. Zazo, "Pilot Patterns For Channel Estimation in OFDM", in *Electronic Letters*, vol. 36, no. 12, June 2000.

[81] J. L. Choi and Y. H. Lee, "Optimum Pilot Pattern for Channel Estimation in OFDM Systems", in *IEEE Transactions on Wireless Communications*, vol. 4, no. 5, Sept. 2005.

[82] J. Zhu and W. Lee, "Channel Estimation with Power-Controlled Pilot Symbols and Decision Directed Reference Symbols", in *Proc. IEEE 58th Vehicular Technology Conference (VTC),* vol. 2, pp. 1268-1272, Oct. 2003.

[83] I. Rashad, I. Budiarjo, and H. Nikookar, "Efficient Pilot Pattern for OFDM based Cognitive Radio Channel Estimation – Part 1", in *Proc. 14 th IEEE Symposium on Communications and Vehicular Technology (SCVT)*, Delft, The Netherlands, Nov. 2007.

[84] I. Budiarjo, I. Rashad, and H. Nikookar, "Efficient Pilot Pattern for OFDM based Cognitive Radio Channel Estimation – Part 2", in *Proc. 14 th IEEE Symposium on Communications and Vehicular Technology (SCVT)*, Delft, The Netherlands, Nov. 2007.

[85] S. Sand, A. Dammann, and G. Auer, "Adaptive Pilot Symbol Aided Channel Estimation for OFDM Systems", in *Proc. 4 th International Workshop on Multi Carrier Spread Spectrum & Related Topics (MC-SS 2003)*, Oberpfaffenhofen, Germany, pp. 227-234, Sept. 2003.

[86] G. Auer, "Modelling of OFDM Channel Estimation Errors", in *Proc. 10 th International OFDM Workshop* , Hamburg, Germany, Aug. 2005.

[87] I. Budiarjo, I. Rashad, and H. Nikookar, "On the Use of Virtual Pilots with Decision Directed Method in OFDM Based Cognitive Radio Channel Estimation Using 2x1-D Wiener Filter ", in *Proc. IEEE International Conference on Communications (ICC)*, Delft, The Netherlands, pp. 703-707, Nov. 2007.

[88] I. Budiarjo, H. A. Sulaiman, and H. Nikookar, "On The Use of Virtual Pilots for 2x2 MIMO V-BLAST OFDM Channel Estimation with Wiener Filter in Hexagonal Pilot

Pattern", in *Proc. IEEE 15th Symposium on Communications and Vehicular Technology (SCVT)*, Antwerp, Belgium, Nov. 2008.

[89] M. Sandell, J. J. V. D. Beek, and P. O. Boerjesson, "Timing and Frequency Synchronization in OFDM Systems Using the Cyclic Prefix", in *Proc. International Symposium on Synchronization*, Essen, Germany, pp. 16-19, Dec. 1995.

[90] J. J. V. D. Beek, M. Sandell, and P. O. Boerjesson, "ML Estimation of Time and Frequency Offset in OFDM Systems", in *IEEE Transactions on Signal Processing*, vol. 45, pp. 1800-1805, July 1997.

[91] B. Y. Prasetyo, F. Said, A. H. Aghvami, "On The Guard Band-Based Coarse Frequency Offset Estimation Technique for Burst OFDM Systems", in *Proc. IEEE 51st Vehicular Technology Conference*, Tokyo, Japan, pp. 220-224, May 2000.

[92] T. Lu, J. Chen and H. Li, "Low –Complexity Blind Symbol Timing Offset Estimation in OFDM Systems", *in EURASIP Journal on Applied Signal Processing*, pp. 532-540, 2005.

[93] J. J. van de Beek et. al.,"Low Complex Frame Synchronization in OFDM Systems", in *Proc. International Conference on Universal Personal Communications (ICUCC)*, Tokyo, Japan, pp. 982-986, Nov. 1995.

[94] T. Weiss, A. Krohn, and F. Jondral, "Synchronization Algorithms and Preamble Concepts in Spectrum Pooling Systems", in *Proc. IST Mobile and Wireless Telecommunications Summit*, June 2003.

[95] M. Sliskovic, "Carrier and Sampling Frequency Offset Estimation and Correction in Multicarrier Systems", in *Proc. IEEE GLOBECOM*, San Antonio, Texas, USA, pp. 285-289, Nov. 2001.

[96] K. B. Png et. al., "Two-Dimensional Iterative Sampling Frequency Offset Estimation for MB-OFDM System", in *Proc. IEEE 63rd VTC*, Melbourne, Australia, pp. 1344-1348, May 2006.

[97] M. J. Fernandez-Getino Garcia, O. Edfors, and J. M. Paez-Borallo, "Peak Power Reduction for OFDM Systems with Orthogonal Pilot Sequences", in *IEEE Transactions on Wireless Communications*, vol. 5, no. 1, pp. 47-51, Jan. 2006.

[98] R. Rajbanshi, A. M. Wyglinski, and G. J. Minden, "Peak to Average Power Ratio Analysis for NC-OFDM Transmissions", in *Proc. IEEE 66 th Vehicular Technology Conference*, Baltimore, USA, pp. 1351-1355, Oct. 2007.

[99] V. Chakravarthy, A. S. Nunez, J. P. Stephens, A. K. Shaw and M. A. Temple, "TDCS, OFDM, and MC-CDMA: A Brief Tutorial", in *IEEE Communications. Magazine*, vol 43, no. 9, pp S11 –S16, Sept. 2005.

[100] M. J. Lee, *Wavelet Domain Communication System (WDCS): Packet-Based Wavelet Spectral Estimation And M-ary Signaling*, Master thesis, Air Force Institute of Technology, Ohio, USA, Mar. 2002.

[101] M. J. Lee, M. A. Temple, R. L. Claypoole Jr., R. A. Raines, J. P. Stephens, "Wavelet Domain Communication System: Bit Error Sensitivity Characterization for Geographically Separated Transceivers", in *Proc. MILCOM*, Anaheim, CA, vol. 2, pp. 1378–82, Oct. 2002.

[102] M. J. Lee, "*Wavelet Domain Communication System (WDCS): Packet- Based Wavelet Spectral Estimation and M-ARY Signaling*", Master thesis, AFIT/GE/ENG/02M-14, Graduate School of Engineering and Management Air Force Institute of Technology Wright – Patterson Air Force Base, Ohio, USA, Mar. 2001, DTIC:ADA401433, approved for public release.

[103] G.M. Dillard, M. Reuter, J. Zeidler and B. Zeidler, "Cyclic Code Shift Keying: A Low Probability of Intercept Communication Technique", in *IEEE Trans. on Aerospace and Electronic Systems*, vol.39, no.3, pp. 786-798, July 2003.

[104] A. S. Nunez, *Interference Suppression in Multiple Access Communications Using M-Ary Phase Shift Keying Generated Via Spectral Encoding*, M.Sc Thesis Report, Air Force Institute of Technology, Ohio, USA, 2004.

[105] I. Budiarjo, H. Nikookar, and L.P. Ligthart,"Cognitive Radio with Single Carrier TDCS and Multicarrier OFDM Approach with V-BLAST Receiver in Rayleigh Fading Channel", in *Proc. 2nd International Conference on Cognitive Radio Oriented Wireless Communications (CrownComm)*, Orlando,USA, Aug. 2007.

[106] J. G. Proakis and M. Salehi, *Communication Systems Engineering*, Upper Saddle River, NJ, Prentice Hall, 2002.

[107] M. v. d. Oever, *A Cognitive Radio Demonstrator*, Thesis Report, Technische Hochschule Rijswijk, Rijswijk, The Netherlands , June, 2007.

[108] S. B. Raghunathan, M. v. d. Oever, R. D. Mohammady, P. Pawełczak, I. Budiarjo, M. Heskamp, Q. Zhang, A. Kokkeler, H. Nikookar, Z. Qin, R. Hekmat, and L. P. Ligthart, "Dynamic Spectrum Access AAF Platform", in *IEEE Symposia on New Frontiers in Dynamic Spectrum Access Networks (DySPAN)*, Oct 14-17, 2008, Chicago, Illinois, USA.

[109] I. Budiarjo, M. Heskamp, Q. Zhang, and F.W. Hoeksema, ”*D.3.31Radio System: First Phase Verification and Advances in Architecture and Algorithms*”, Adaptive Ad-hoc Freeband (AAF), August, 2006, The Netherlands.

List of Abbreviations

AAF	Adaptive Adhoc Freeband
ADC	Analog to Digital Converter
AWGN	Additive White Gaussian Noise
BER	Bit Error Rate
BPSK	Binary Phase Shift Keying Modulation
BTRC	Better Than Raised Cosine
CCDF	Complementary Cumulative Distribution Function
CCSK	Cyclic Code Shift Keying
CIR	Channel Impulse Response
CSI	Channel State Information
CTF	Channel Transfer Function
CR	Cognitive Radio
DAC	Digital to Analog Converter
ETSI	European Telecommunications Standard Institute
FDD	Frequency Division Duplex
FFT	Fast Fourier Transform
FoM	Figure of Merit
GSM	Global System for Mobile Communications
ICI	Inter Carrier Interference
IDWPT	Inverse Discrete Wavelet Packet Transform
IFFT	Inverse Fast Fourier Transform
ISI	Inter Symbol Interference
LS	Licensed System
LU	Licensed User
MCM	Multicarrier Modulation
MCS	Multiple Choice Sequence
MIMO	Multiple Input Multiple Output
MMSE	Minimum Mean Square Error
MSE	Mean Square Error
OFDM	Orthogonal Frequency Division Multiplexing
PAM	Pulse Amplitude Modulation
PAPR	Peak to Average Power Ratio
PDF	Probability Density Function
PMR	Peak Power to Mean Sidelobe
PSD	Power Spectral Density
QAM	Quadrature Amplitude Modulation
QoS	Quality of Service
QPSK	Quadrature Phase Shift Keying
QMF	Quadrature Mirror Filter
RDS	Root mean square Delay Spread

rms	Root mean square
RS	Rental System
RU	Rental User
SBLA	Simple Blockwise Loading Algorithm
SISO	Single Input Single Output
SINR	Signal to Interference plus Noise Ratio
SNR	Signal to Noise Ratio
TDCS	Transform Domain Communication System
TDD	Time Division Duplex
V-BLAST	Vertical-Bell Laboratories -Layered -Space-Time
WDCS	Wavelet Domain Communication System
WP-3	Work Package 3
WPMCM	Wavelet Packet Multicarrier Modulation
WPT	Wavelet Packet Transform
WSSUS	Wide Sense Stationary Uncorrelated Scattering
ZF	Zero Forcing

List of Symbols

α	Window roll off factor
$\varepsilon_{n,k}$	Channel estimate mismatch error on subcarrier n of OFDM symbol k
γ_{margin}	System performance margin (in dB) that defines the maximum allowable noise quantity on the system
Γ	SNR gap (in dB) which is a constant which estimates the difference between channel capacity and the actual capacity usage by the transmission scheme
$\varphi_m[k]$	Complex basis wavelet function
$\boldsymbol{\Pi}(l)$	Permutation matrix that will do the interleaving
σ_I^2	Interference variance
σ_n^2	Noise variance
τ_{filter}	Estimated maximum delay of the channel for filter design
τ_{max}	Maximum delay of the channel
θ_n	Random phase on subband n of TDCS
$\theta_{n-n",k-k"}$	Channel time frequency correlation function
$\boldsymbol{\theta}$	Random phase vector
$\phi_{n'-n",k'-k"}$	Autocorrelation function on pilot positions
$\boldsymbol{\omega}$	Wiener filter coefficients matrix
ccN	Total number of sidelobes cancellation carrier
d_f	Distance between pilots in frequency direction
d_t	Distance between pilot in time direction
e_m	Decision directed error energy between the ideal constellation phasor positions and the received phasors
f_D	Doppler frequency
$f_{Dfilter}$	Estimated Doppler frequency for filter design
f_n	Frequency on carrier n
f_{LU}	Frequency in the range of LU band,
$\boldsymbol{F_{LU}}$	Fourier transformation matrix for the signal in LU band
$g(t)$	Window function
$H_{n,l}$	Actual channel state on subcarrier n of OFDM symbol l
$\breve{H}_{n,k}$	Final estimated value of the frequency-domain channel transfer function (CTF) at subcarrier n of OFDM symbol k
$\hat{H}_{s,n}$	Estimated value of signaling subcarriers
$I_{n,l}$	Interference term on subcarrier n of OFDM symbol l
$\boldsymbol{I}$	Signal part of the cognitive radio signal in LU band
$\hat{I}_{n,l}$	Estimated interference on subcarrier n of OFDM symbol l

N_{FFT}	Number of FFT points which refers to the possible number of total OFDM/TDCS subcarriers,
$N_{n,l}$	Noise term on subcarrier n of OFDM symbol l
$\hat{N}_{n,l}$	Estimated noise on subcarrier n of OFDM symbol l
P_{budget}	Total allocated power per OFDM symbol
p_n	Allocated power on carrier n
$p_s(\gamma)$	Probability of a signaling error given SNR γ
$P_{Threshold}$	Limit of interference power that is still tolerable by the LUs
$Q(x)$	Area covered by the normal distribution function from x to infinity
R_n	Number of allocated bits in subcarrier n
$R_{s,n}$	Received symbols in the signaling subcarriers
R_{target}	Target total bits per OFDM symbol
T_{GI}	OFDM guard interval duration
T_S	OFDM symbol duration including the guard interval
T_u	Useful OFDM symbol duration
X_n	Modulated data on subcarrier n of OFDM symbol l
$X^P_{n,l}$	Modulated pilot on subcarrier n of OFDM symbol l
$\boldsymbol{X}$	Symbol vector
$\boldsymbol{y}^m$	The mth time domain OFDM symbol including the guard interval

Publications by the Author

Book Chapters

1. I. Budiarjo, M. K. Lakshmanan, and H. Nikookar, "Cognitive Radio Dynamic Access Techniques for Mutual Interference Reduction and Efficient Spectrum Utilization", submitted for a chapter in book "Cognitive Radio Systems", IN-TECH, ISBN 978-953-7619-25-1.

2. M. K. Lakshmanan, I. Budiarjo, and H. Nikookar, "Robust Bases for Spectrum Pooling Cognitive Radio Systems on Wavelet Packet Multi-carrier Modulation MIMO Architecture", submitted for a chapter in book "Cognitive Radio Systems", IN-TECH, ISBN 978-953-7619- 25-1.

Journal Papers

3. I. Budiarjo, M.K. Lakshmanan, and H. Nikookar, "Cognitive Radio Dynamic Access Techniques", in *Springer International Journal on Wireless Personal Communications special issue on Cognitive Radio Technologies*, vol. 45, no. 3, pp. 293-324, Feb. 2008.

4. I. Budiarjo, H. Nikookar and L.P. Ligthart, "Cognitive Radio with Single Carrier TDCS and Multicarrier OFDM Approach with V-BLAST Receiver in Rayleigh Fading Channel", in *ACM / Springer Mobile Networks and Application (MONET) Journal special issue on Cognitive Radio Oriented Wireless Networks and Communications,* vol. 13, no. 5, pp. 416-423, July 2008.

5. I. Budiarjo, H. Nikookar and L. P. Ligthart, "Cognitive Radio Modulation Techniques Reducing Mutual Interference", in *IEEE Signal Processing Magazine special issue on Signal Processing for Cognitive Radio Networks*, vol. 25, issue 6, pp. 24-34, Nov. 2008.

6. I. Budiarjo, H. Nikookar and L. P. Ligthart, "Combined Spectrum Pooling, Adaptive Bit Loading and Sidelobes Cancellation Carriers : An Advanced Technique for OFDM-Based Cognitive Radio in Overlay Spectrum Sharing Access", to be submitted to *IEEE Wireless Communications*.

7. I. Budiarjo, H. Nikookar, and L.P. Ligthart, "MIMO TDCS with Extra Embedded Symbol and V-BLAST Receiver Architecture for Higher Data Rate Dynamic Spectrum Access", submitted to *IEEE Transactions on Mobile Computing*.

Conference Papers

8. I. Budiarjo, H.Nikookar, and L.P. Ligthart,"Overview of Adaptive OFDM in the Context of Cognitive Radio", in *Proc. 12th Annual Symposium of IEEE on Communications and Vehicular Technology (SCVT) in the Benelux*, Enschede, The Netherlands, pp. 1-5, Nov. 3, 2005.

9. I. Budiarjo, H. Nikookar, and L.P. Ligthart,"Performance Evaluation of Adaptive Bit Loading For OFDM With Channel Estimation Using 2x 1-D Wiener Filter", in *Proc. 9th Annual International Symposium on Wireless Personal and Multimedia Communications (WPMC)*, San Diego, USA, pp. 1138-1142, Sept. 17-20, 2006.

10. I. Budiarjo, H. Nikookar, and L.P. Ligthart, "Combined Spectrum Pooling and Adaptive Bit Loading for Cognitive Radio OFDM Based System", in *Proc. 13th Annual Symposium of IEEE on Communications and Vehicular Technology (SCVT) in the Benelux*, Liege, Belgium, pp. 73-76, Nov. 23, 2006.

11. I. Budiarjo, H. Nikookar, and L.P. Ligthart, "Techniques for Cognitive Radio", *invited paper on the 2nd Center for TeleInfrastruktur (CTIF) Workshop*, Aalborg, Denmark, May 22-23, 2007.

12. I. Budiarjo, H.Nikookar, L.P. Ligthart,"Cognitive Radio with Single Carrier TDCS and Multicarrier OFDM Approach with V-BLAST Receiver in Rayleigh Fading Channel", in *Proc. 2nd International Conference on Cognitive Radio Oriented Wireless Networks and Communications (CROWNCOM),* Orlando, Florida, USA, pp. 140-146, August 1-3, 2007. (*Note : This paper has been selected by the CrownCom 2007 TPC Co-Chairs for publication in a special issue of ACM / Springer Mobile Networks and Applications (MONET) journal*)

13. I. Budiarjo, H. Nikookar, and L.P. Ligthart, "Performance Evaluation of OFDM Based Cognitive Radio System With Wiener Filter Channel Estimation Using Frequency Hopping GSM Channel Model at 900 MHz", in *Proc. 10th European Conference on Wireless Technology (ECWT)*, Munich, Germany, pp. 74-77, Oct. 8-12, 2007.

14. M. K. Lakshmanan, I. Budiarjo and H. Nikookar, "Maximally Frequency Selective Wavelet Packets Based Multicarrier Modulation Scheme for Cognitive Radio Systems", in *Proc. 50th IEEE Global Communications (GLOBECOM) Conference*, Washington, DC, USA, pp. 4185-4189, Nov. 26-30, 2007.

15. I. Rashad, I. Budiarjo and H. Nikookar, "Efficient Pilot Pattern for OFDM based Cognitive Radio Part I", in *Proc. 14th IEEE Symposium on Communications*

and Vehicular Technology (SCVT), Delft, The Netherlands , pp. 1-5, Nov. 15, 2007.

16. I. Budiarjo, I. Rashad and H. Nikookar, "Efficient Pilot Pattern for OFDM based Cognitive Radio Part II", in *Proc. 14th IEEE Symposium on Communications and Vehicular Technology*, Delft, The Netherlands, pp. 1-5, Nov. 15, 2007.

17. M. K. Lakshmanan, I. Budiarjo and H. Nikookar, "Wavelet Packet Multi-carrier Modulation MIMO Based Cognitive Radio Systems with VBLAST Receiver Architecture", in *Proc. IEEE Wireless Communications and Networking Conference (WCNC)*, Las Vegas, USA , pp. 705-710, March 31 – April 3, 2008.

18. I. Budiarjo, I. Rashad and H. Nikookar, "On The Use of Virtual Pilots with Decision Directed Method in OFDM Based Cognitive Radio Channel Estimation Using 2x1-D Wiener Filter", in *Proc. IEEE International Conference on Communications (ICC)*, Beijing, China , pp. 703-707, May 19-23, 2008.

19. I. Budiarjo, H. Nikookar, and L.P. Ligthart," On the Utilization of Embedded Symbol for CCSK BER Improvement in TDCS Dynamic Spectrum Access", in *Proc. IEEE European Wireless Technology Conference*, Amsterdam, The Netherlands, pp. 123-126, Oct. 28-29 2008.

20. I. Budiarjo, H. Abdulrahman Sulaiman, and H. Nikookar, "On the Use of Virtual Pilots for 2x2 MIMO V-BLAST OFDM Channel Estimation with Wiener Filter in Hexagonal Pilot Pattern", in *Proc. 15th IEEE Symposium on Communications and Vehicular Technology* (SCVT), Antwerp, Belgium, Nov. 2008.

21. I. Budiarjo and H. Nikookar, "MIMO TDCS with Extra Embedded Symbol for Higher Data Rates in Overlay Spectrum Sharing System", in *Proc. IEEE Wireless Communications and Networking Conference (WCNC)*, Budhapest, Hungary, pp. 1-6, April 5-8, 2009.

Demonstrator Paper

22. S. B. Raghunathan, M. v. d. Oever, R. D. Mohammady, P. Pawełczak, I. Budiarjo, M. Heskamp, Q. Zhang, A. Kokkeler, H. Nikookar, Z. Qin, R. Hekmat, and L. P. Ligthart, "Dynamic Spectrum Access AAF Platform", in *IEEE Symposia on New Frontiers in Dynamic Spectrum Access Networks (DySPAN)*, Oct 14-17, 2008, Chicago, Illinois, USA.

Reports

23. I. Budiarjo, H. Nikookar,"*D.3.12 Adaptive Baseband Processing : State of the Art*", Adaptive Ad-hoc Freeband (AAF), May, 2005, The Netherlands.

24. M. Heskamp, I. Budiarjo, Q. Zhang and A. Kokkeler, "*D.3.22 First Phase Radio System Architecture, Algorithms and Mappings*", Adaptive Ad-hoc Freeband (AAF), October, 2005, The Netherlands.

25. I. Budiarjo, M. Heskamp, Q. Zhang, and F.W. Hoeksema, "*D.3.31Radio System: First Phase Verification and Advances in Architecture and Algorithms*", Adaptive Ad-hoc Freeband (AAF), August, 2006, The Netherlands.

26. I. Budiarjo, M. Heskamp, Q. Zhang, H. Nikookar , A. J. Kokkeler, "*D.3.41 Radio system: Second phase verification and advances in architecture and algorithms*", Adaptive Ad-hoc Freeband (AAF), July 2007, The Netherlands.

Publication Cross-reference Table

The thesis is based, in part, on the publications listed in the previous sections. The following table indicates the relevance of the publications to the chapters within the thesis.

Publication	Ch. 1	Ch. 2	Ch. 3	Ch. 4	Ch. 5	Ch. 6
1		◙	◙		◙	◙
2			◙		◙	
3		◙	◙		◙	◙
4				◙	◙	
5		◙			◙	◙
6			◙			
7					◙	
8	◙	◙	◙			
9			◙	◙		
10		◙	◙			
11	◙	◙	◙		◙	◙
12				◙	◙	
13		◙		◙		
14			◙		◙	
15				◙		
16				◙		
17			◙		◙	
18				◙		
19					◙	
20				◙		
21					◙	
22						◙
23	◙	◙	◙	◙		◙
24	◙	◙	◙	◙		◙
25	◙	◙	◙	◙		◙
26	◙	◙	◙	◙	◙	◙

Samenvatting

Adaptive Baseband Verwerkingstechnieken voor Cognitieve Radio Systemen

Cognitieve Radio is een nieuw paradigma in de draadloze communicatie. Het voegt intelligentie en een dimensie van 'bewustzijn' toe aan het radiocommunicatiesysteem. Een cognitief systeem is zich bewust van veranderingen in zijn omgeving. Het 'bewustzijn' dat in dit proefschrift beschreven wordt heeft betrekking op het spectrum en de kanaalkeuze. Door op een intelligente manier te leren en de omgeving te begrijpen kan een cognitief systeem zijn transmissieparameters aanpassen aan de veranderende omgeving. Het doel van een cognitief systeem is betrouwbare communicatie en efficiënt spectrumgebruik.

Alhoewel het grootste deel van het radiospectrum al gelicentieerd is, hebben studies en metingen aangetoond dat het spectrum niet druk bezet is. Sommige banden worden zelfs nauwelijks gebruikt. Congestie treedt op als gevolg van een slechte spectrumtoegangstechniek. Hierdoor ontstaat de mogelijkheid om spectrum te 'huren' of te gebruiken als de gelicentieerde gebruiker niet actief is, danwel in combinatie met een gelicentieerd systeem een extra gebruiker toe te laten door middel van een cognitief systeem waarbij gebruik gemaakt wordt van de gaten in het spectrum. Op deze manier wordt het spectrum efficiënter gebruikt. De uitdaging is om een win-win co-existentie te bereiken tussen het cognitieve radiosysteem (het huursysteem) en het gelicentieerde systeem. In de literatuur is Spectrum pooling voorgesteld als een techniek waarmee het spectrum gedeeld kan worden met het gelicentieerde systeem, door gebruik te maken van Orthogonal Frequency Division Multiplexing (OFDM) als modulatietechniek. Sommige OFDM-carriers die zich in de gelicentieerde band bevinden worden ge-deactiveerd zodat deze draaggolven niet interfereren met het gelicentieerde systeem. Door deze flexibiliteit wordt OFDM beschouwd als een geschikte techniek voor cognitieve radio. Interferentie op het signaal van de gelicentieerde gebruiker kan verder beperkt worden door meer carriers te de-activeren, door windowing en door verschillende signaal-bewerkingstechnieken. Deze technieken worden in dit proefschrift bestudeerd en de resultaten worden gepresenteerd. De techniek om spectrum te delen kan alleen werken als er nauwkeurige informatie over de bezetting van het spectrum beschikbaar is. Deze informatie is afkomstig uit een spectrum sensing module. Voor spectrum sensing is een geavanceerde module nodig, welke veel aandacht vraagt. Dit proefschrift richt zich niet op de spectrum sensing module, maar gaat er vanuit dat de informatie over de bezetting van

het spectrum beschikbaar en nauwkeurig is. Onze onderzoekspartner bij de Universiteit Twente[†] behandelt het onderwerp van spectrum sensing.

Om het doel van cognitieve radio, namelijk betrouwbare communicatie, te realiseren, is het belangrijk om niet alleen stil te staan bij de techniek aan de kant van de gelicentieerde gebruiker, maar ook bij die van de huurgebruiker. Naast het veiligstellen van betrouwbare communicatie op het gelicentieerde systeem moet de gewenste kwaliteit en Quality of Service (QoS) van het cognitieve systeem worden gehaald. De praktische parameters waarnaar gekeken moet worden zijn de Bit Error Rate (BER) en de bitrate van het systeem. Het toepassen van OFDM met spectrum shaping met als doel de bijdrage van interferentie in het gelicentieerde systeem te beperken, kan alleen gedaan worden ten koste van de 'eigen' QoS. Onderzoeksresultaten in de literatuur hebben aangetoond dat door toepassing van Adaptive Bit Loading de BER van een OFDM-systeem kan worden verbeterd. Bij Adaptive Bit Loading worden afhankelijk van de kanaalkwaliteit de bits op een intelligentie manier toegewezen aan elke afzonderlijke OFDM-carrier en worden de als doelgestelde BER en bitrate van het hele systeem aangepast. In de thesis stellen we voor om Adaptive Bit Loading toe te passen in combinatie met Spectrum Shaping, met als doel de QoS van het cognitieve systeem te behouden. De impact van deze combinatie op de toename van de OFDM Peak to Average Power Ratio (PAPR) wordt geëvalueerd door simulaties.

Er bestaat een groeiende interesse om de Fourier-transformatie in OFDM te vervangen door Wavelet Basis functions. Deze techniek wordt ook wel Wavelet Packet Multi Carrier Modulation (WPMCM) genoemd. In de literatuur zijn onderzoeksresultaten gepresenteerd waarin WPMCM geëvalueerd wordt en de resultaten worden vergeleken met OFDM. Op basis van succesvolle toepassing van een Frequency Selective Wavelet in een Ultra Wide Band systeem evalueren we in dit proefschrift de geschiktheid van de Frequency Selective Wavelet in WPMCM, gecombineerd met het concept van Spectrum Pooling, om te worden toegepast in een cognitief radiosysteem. Omdat efficiënt spectrumgebruik één van de hoofddoelen is van cognitieve radio, is er voldoende reden om Multiple Input Multiple-Output (MIMO) op te nemen in het cognitieve radio systeem. In dit proefschrift wordt dit onderwerp bestudeerd en worden de prestaties van MIMO in een OFDM- en WPMCM-gebaseerd cognitief radiosysteem geëvalueerd.

Channel estimation (kanaal schatten) is de cruciale module in elk OFDM-systeem. Wij stellen een effectief channel estimation schema voor, gebaseerd op optimale piloot patronen aanwezig in conventionele OFDM en gebruikmakend van virtuele 'piloot-tonen' om te worden toegepast in cognitieve radiosystemen. De virtuele piloottonen worden afgeleid uit de combinatie van lineaire interpolatie/extrapolatie tussen twee echte piloottonen via de zogenoemde decission directed method. Zonder beperking in algemene toepasbaarheid

[†] Dit proefschrift is onderdeel van het Werkpakket 3 (WP3) in het Nederlandse Adaptive Adhoc Freeband (AAF) project. In WP3 zullen 3 proefschriften worden voltooid, één over Spectrum Sensing, één op Baseband Processing (dit proefschrift) en het derde proefschrift handelt over het in kaart brengen van Spectrum Sensing en Baseband Verwerking tot een heterogene architectuur.

gebruiken we het Wiener-filter als channel estimation techniek, vanwege zijn efficiëntie en recht-toe-recht-aan-manier waarmee de kanaalcorrelatie-eigenschappen van de afstand tussen de piloottonen en de data worden uitgenut. We werken het Single Input Single Output (SISO) op OFDM gebaseerde cognitieve radiosysteem uit en breiden het daarna uit met de MIMO-applicatie.

Naast OFDM- en WPMCM-gebaseerde cognitieve radiosystemen zijn recentelijk ook het Transform Domain Communication System (TDCS) en het Wavelet Domain Communication System (WDCS) geïntroduceerd als veelbelovende modulatietechnieken voor cognitieve radiotoepassingen. TDCS en WDCS hebben beperkingen in bitrate. In een poging om de bitrate van TDCS en WDCS te verbeteren, stellen we voor om een extra embedded symbool toe te voegen aan TDCS en WDCS. We analyseren de impact van het embedded symbool op de datadetectie in een multi-useromgeving. Deze aanpak wordt al ondersteund in conventionele TDCS en WDCS. Bovendien evalueren we de prestaties van TDCS met een embedded symbool in een MIMO-systeem.

Als een soort verificatieplatform voor cognitieve radio hebben we een praktische Demonstrator voorgesteld, die bestaat uit een spectrum scanning module en een transceiver module werkend in basisband. De spectrum sensing wordt gebruikt door de Universal Software Defined Radio Peripheral (USRP), terwijl de baseband processing transceiver module is toegepast in een FPGA development board. De huidige versie van het cognitieve radiosysteem verificatieplatform is simpel, maar heeft beperkte mogelijkheden. Verdere ontwikkelingen op dit gebied zijn nodig en details voor gerelateerd toekomstig werk zijn ook in dit proefschrift opgenomen.

Acknowledgement

This thesis is the result of a four year PhD journey with hard work. This thesis has come to its present shape due to support of many people. Therefore, I would like to acknowledge the people who have provided me with the support over the past years to complete this thesis.

First of all, I would like to thank my supervisor Dr. Homayoun Nikookar, for his guidance, discussions, reviews and strong support during my research work. Also I would like to thank Prof. Alex Yarovoy for introducing my resume to Dr Nikookar so I had the chance to pursue my PhD in Cognitive Radio.

I would like to express my deepest gratitude to my promotor Prof. Leo Ligthart for the opportunity given to me to do research in the field of Cognitive Radio, for his valuable comments on shaping the manuscript, and for guiding me with the propositions and thesis summary in Dutch.

I would like to thank the Freeband AAF project for funding my research, and also the team of researchers in a fruitful cooperation: Ir. Fokke Hoeksema, Dr. Andre Kokkeler, Dr. Qiwei Zhang, and Ir. Marnix Heskamp, all from Twente University; Dr. Ramin Hekmat and Dr. Przemyslaw Pawelczak, both from WMC TU Delft.

I am thankfull to my room-mate colleague, Ir. Madan K. Lakshmanan for the collaboration and discussion especially on the subject of wavelet based transmission and his words of wisdom. I would like to acknowledge my master students at IRCTR TU Delft : Ir. Ikhsan Rashad, Ir. Haval Abdulrahman Sulaiman, and Ir. Iman Ghaseminezhad Marandi for their contribution to this thesis. My gratitude to student assistants Ir. Shreyas Raghunathan, Ir. Maarten van de Oevers, and Ir. Rahman Doost for their effort in developing the IRCTR Cognitive Radio demonstrator platform.

I would like to thank Mrs Mia van der Voort-Kester, Laura Bauman, Dominique Meijer, Marjon Verkaik, Patricia Thoms and Rowena for their constant assistance with the administrative matters. My acknowledgement go also to all my colleagues in IRCTR, I enjoy the time in the International Research Centre for Pubs and Restaurants (IRCPR) gatherings. My gratitudes to all of my Indonesian countrymen in Delft, the Delft Christian Fellowship community, fellows in International Church Levend Water Delft for their support, and Delft Student Chaplancy as well. My gratitude to my colleague in KPN Selmar Sneider and my

friend Dirk Goedbloed from Levend Water Church in Delft for helping me shaping the Samenvatting.

I would like to dedicate this thesis to my parents Baik Ukurta Purba and Bedya Haris. I thank them for their wisdom, patience and care in shaping me the way that I am. I am really greatfull to have them, *Yesus menyertai dan memberkati mu Ayah dan Ibu*. My gratitude to my beloved brother and friend Zakaria Budiarjo for his support while I am abroad.

Finally, I would like to thank Winny Vyedrametha Sihombing for being patience in supporting and accompanying me in finishing this dissertation while she is in a different continent with 6 hours time difference, the wonderfull love and care that she brings to my life, and her wonderfull cover design for this thesis.

Curriculum Vitae

Ibrahim Budiarjo was born in 1978 in Bandung, West Java province, Indonesia. After finishing his Bachelor Study in 2001 in Bandung Institute of Technology, Indonesia with Sarjana Teknik (Bachelor of Engineering) degree in Electronics, he continued his study in Communications Engineering in Munich University of Technology, Germany and received his M.Sc degree in 2003. His M.Sc thesis was about OFDM channel estimation by adaptive filtering. The M.Sc thesis was performed at Deutsche Luft und Raumfahrt (DLR) Oberpfaffenhofen Germany and DoCoMo Eurolabs Muenchen Germany. He did a voluntary internship in Knorr Bremse AG Germany working on CAN bus system for a year (till end of 2004).

In February 2005 he became a PhD candidate at the International Research Centre for Telecommunications and Radar (IRCTR) TU Delft, the Netherlands within the Dutch Adaptive Adhoc Freeband (AAF) Project which resulted in this dissertation. The focus of his research is on the adaptive baseband processing for Cognitive Radio systems.